MECHANICS OF LONGITUDINAL ROLLING OF TUBE THROUGH THREE GROOVED ROLLS

by

KEITH BAINES

B.Sc., M.Sc., C.Eng., M.I.Mech.E., A.M.C.S.T

Submitted in fulfilment of the requirements of the Degree of Doctor of Philosophy

The University of Aston in Birmingham

Faculty of Engineering

Department of Mechanical and Production Engineering

Mechanical Engineering Division

June 1984

Supervisor: Professor D. H. Sansome

MECHANICS OF LONGITUDINAL ROLLING OF TUBE THROUGH THREE-GROOVED ROLLS

KEITH BAINES Ph.D. THESIS 1984

SUMMARY

This investigation examined the process of the longitudinal rolling of tubes through a set of three driven grooved rolls. Tubes were rolled with or without internal support i.e. under mandrel rolling or sinking conditions.

Knowledge was required of the way in which the roll separating force and rolling torque vary for different conditions of rolling. The objective of this work being to obtain a better understanding and optimization of the mechanics of the process.

The design and instrumentation of a complete experimental three-roll mill for the rolling of lead tube as an analogue material for hot steel, with the measurement of the individual roll force and torque is described. A novel type of roll load cell was incorporated and its design and testing discussed.

Employing three roll sizes of 170 mm, 255 mm and 340 mm shroud diameter, precise tube specimens of various tube diameter to thickness ratios were rolled under sinking and mandrel rolling conditions. To obtain an indication of the tube-roll contact areas some of the specimens were partially rolled. For comparative purposes the remaining tubes were completely rolled as a single pass.

The roll forces, torques and tube parameters e.g. reduction of area, D/t ratio, were collated and compared for each of the three roll diameters considered. The influence of friction, particularly in the mandrel rolling process, was commented upon.

Theoretical studies utilising the equilibrium and energy methods were applied to both the sinking and mandrel rolling processes. In general, the energy approach gave better comparison with experiment, especially for mandrel rolling. The influence of the tube deformation zones on the two processes was observed and on the subsequent modification of the tube-roll arc contact length. A rudimentary attempt was made in the theoretical sinking analysis to allow for the deformation zone prior to roll contact; some success was noted.

A general survey of the available tube rolling literature, for both the sinking and mandrel processes has been carried out.

KEY WORDS:

Tube rolling

Deformation zones

Energy Method

Three-grooved rolls

THREE-GROOVED ROLL

LONGITUDINAL TUBE ROLLING

FRONTISPIECE

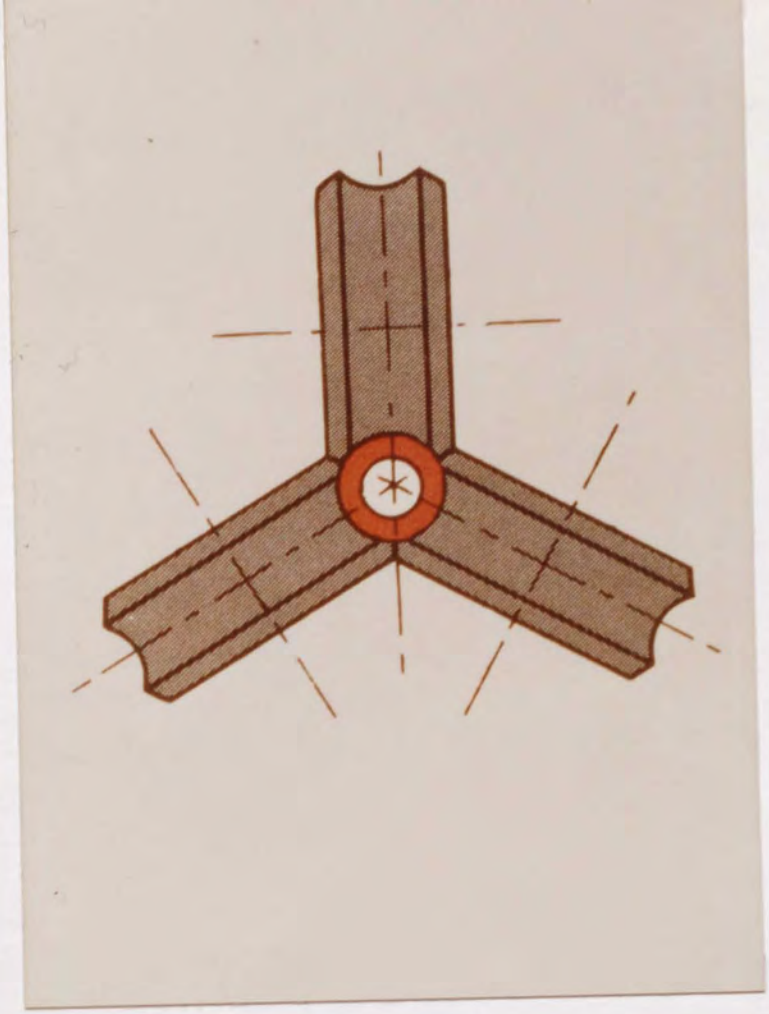

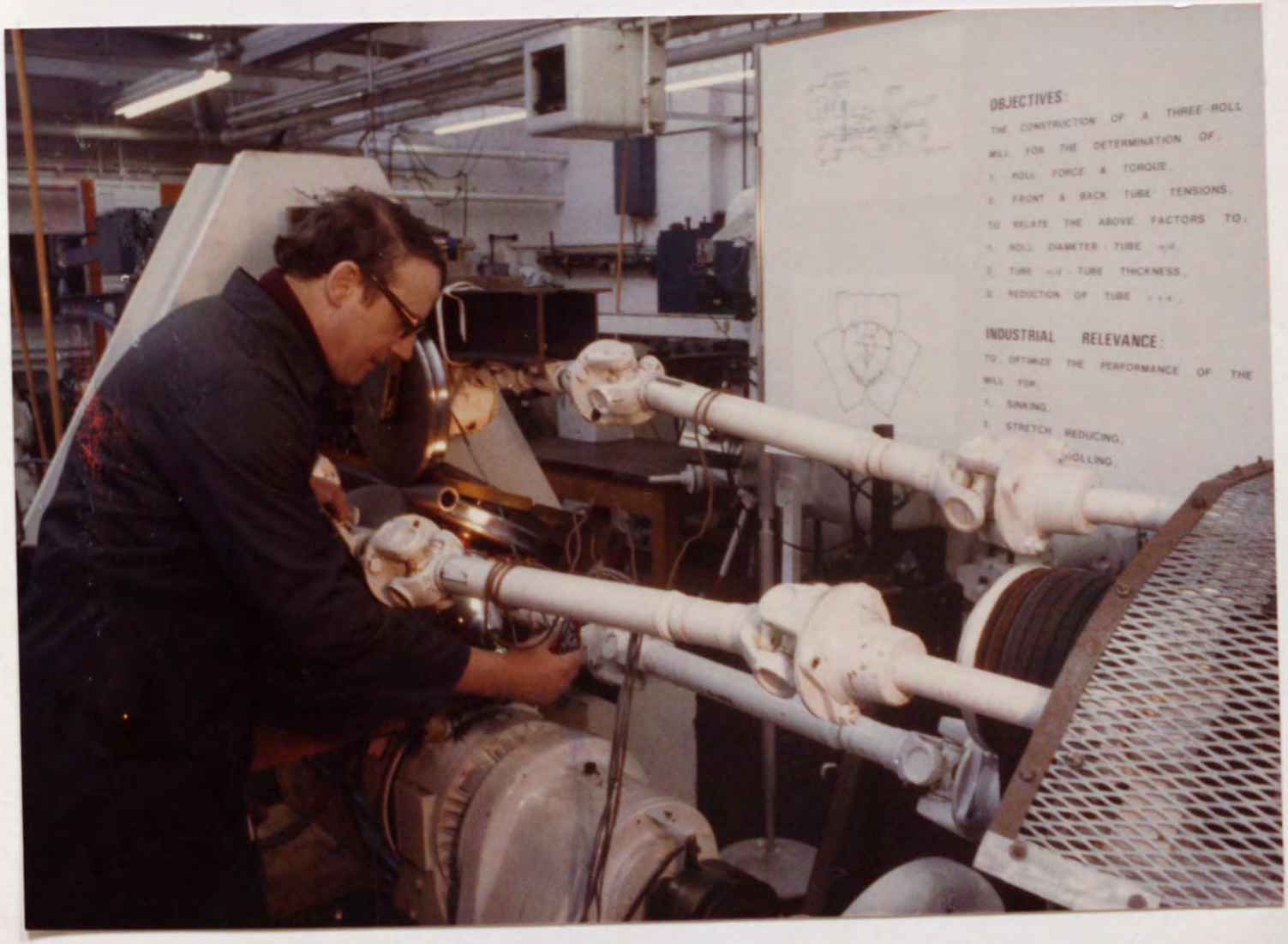
OBJECTIVES:
THE CONSTRUCTION OF A THREE-ROLL
MILL FOR THE DETERMINATION OF:
1. ROLL FORCE & TORQUE.
2. FRONT & BACK TUBE TENSIONS.
TO RELATE THE ABOVE FACTORS TO:
1. ROLL DIAMETER : TUBE
2. TUBE : TUBE THICKNESS.
3. REDUCTION OF TUBE
INDUSTRIAL RELEVANCE:
TO OPTIMIZE THE PERFORMANCE OF THE
MILL FOR:
1. SINKING.
2. STRETCH REDUCING.
3. ROLLING.

CONTENTS

LIST OF PLATES

LIST OF SYMBOLS

A_o	Cross-sectional area of tube at the entry plane
A_1	Cross-sectional area of tube at the exit plane
e_g	Groove eccentricity
h	Groove radius relative to tube axis
J	Reduction of area
L_g	Calculated length of the arc of contact
L_m	Measured length of the arc of contact
$L_{m.c}$	Measured length of the arc of contact (corrected)
m	Friction.factor
o.d.	Tube outer diameter
i.d.	Tube inner diameter
M_p	Full plastic bending moment per unit length
P	The roll separating force (RSF)
p_r	Roll pressure
P_m	Mean roll pressure
r	Tube radius
r_b	Radius of the mandrel
r_g	Radius of the groove
R_r	Radius of the roll at the root of the groove
R_s	Radius of the roll at the shroud
R	Radius of the roll at any point on the groove surface
S	Contact area between tube and roll
T_t	Total Roll torque
t	Tube wall thickness
U	Tube velocity in the direction of rolling

V	Volume of tube in the deformation zone
v	Roll velocity
v_r	Relative velocity between tube and roll
V_b	Mandrel speed
$\dot{V}$	Volume rolled per unit time
W_h	Work of homogeneous deformation per unit volume
W_r	Redundant work per unit volume
W_f	Work done against friction per unit volume
W_t	Total work done by the rolls per unit volume
W_e	Work done by the roll pressure
W_T	Total work done per unit volume
$\dot{W}$	Rate of doing work

GREEK SYMBOLS

δ	Mean draft
ε_t	Thickness strain
ε_z	Longitudinal strain
ε_θ	Circumferential strain
ε_h	Generalized homogeneous strain
ε_r	Redundant strain
$\bar{\varepsilon}_A$	Apparent strain
$\bar{\varepsilon}_m$	Total generalized strain
ε_f	Frictional strain
μ	Coefficient of friction
ϕ_m	Maximum angle of contact
ϕ	Angle of contact at any point on the line corresponding to the root of the groove
γ_c	Peripheral angle of contact between tube and mandrel
γ_{cl}	Peripheral angle of contact between tube and mandrel at the exit plane
θ	Groove angle
θ_c	Groove angle of contact
$\bar{\sigma}_y$	Mean yield stress
τ	Shear stress
$\bar{\lambda}$	Mean strain rate
ω	Angular velocity of the roll

Subscripts:

o	Entry plane condition
1	Exit plane condition
m	Mean or maximum
r	Roll groove root or relative
s	Roll groove shroud

N.B.

Other symbols used in this text are defined as they appear.

CHAPTER ONE

INTRODUCTION

1. INTRODUCTION

Tubes find extensive applications in the petro-chemical industries, in the transportation of high pressure fluids and in many arduous structural configurations.

Longitudinal tube-reducing mills are employed to hot reduce the diameter of tubes which have previously been produced by another process. The tubes are generally seamless, although welded tubes are also reduced by this method. It is more difficult to reduce smaller diameter seamless tubes by a direct hot working process since all the processes involve some form of mandrel or plug inside the tube during its manufacture. Thus the smallest diameter tubes hot rolled with an internal tool is about 25 mm. Smaller diameter seamless tubes are generally elongated by cold drawing. This also gives a better tolerance to the finished tube size.

The longitudinal rolling of tube through two or more grooved rolls is carried out in a series of roll stands. These mills generally form the last and an important sequence in the complex process of hot seamless tube manufacture.

The general arrangement of a complete tube production mill is shown in FIGURE 1.1. This incorporates a furnace for heating the billets, a piercer to produce the bloom, a mandrel mill to elongate the bloom, a mandrel extractor, a re-heating furnace and finally a tube reducing-mill.

The five main production sequences for the hot tube manufacturing processes from solid round original billets are as follows:-

THE COMPLETE TUBE PRODUCTION MILL

FIGURE 1.1

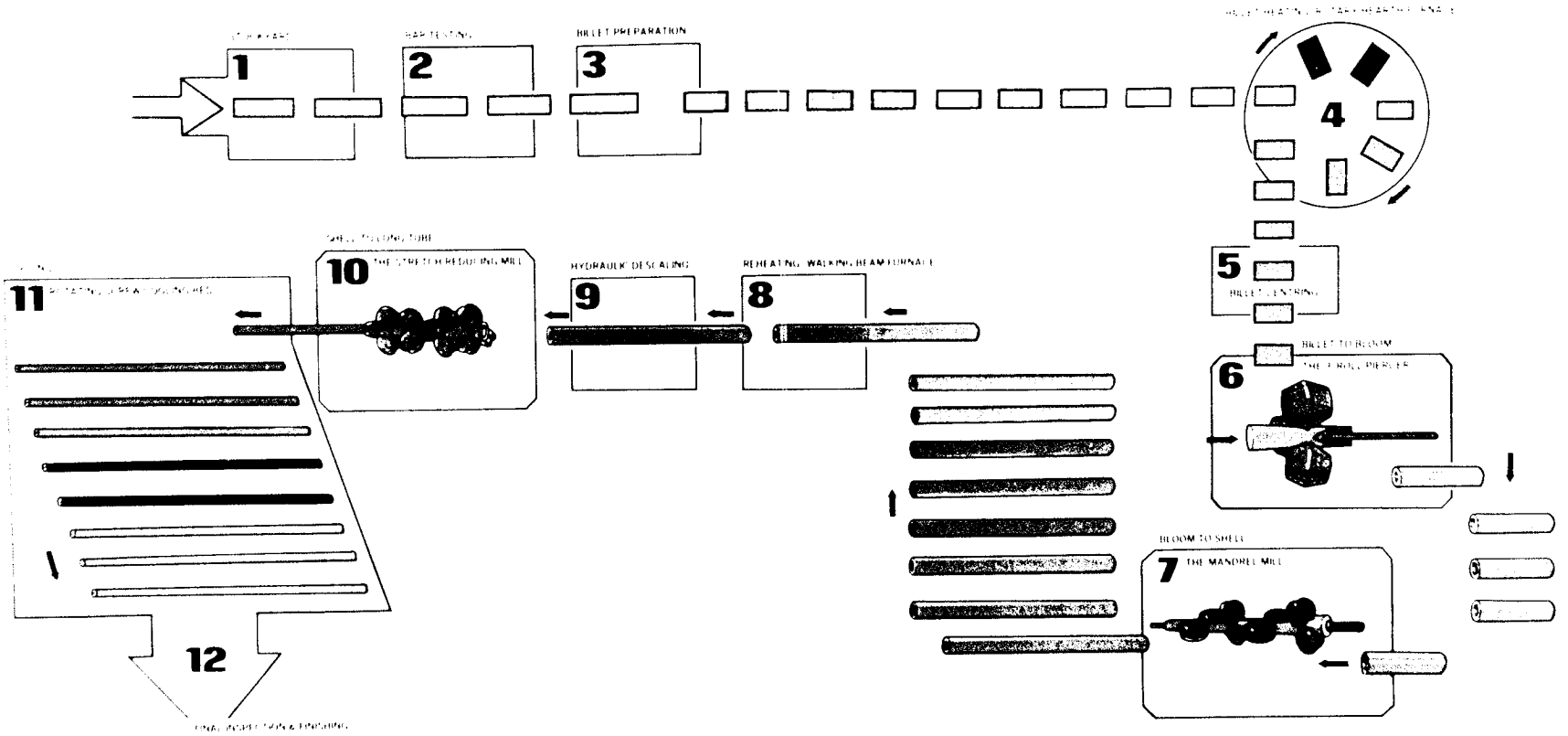
1
2
BILLET PREPARATION
3
4
5
6
7 THE MANDREL MILL
8
9 HYDRAULIC DESCALING
10
11
12

1. rotary pierce	- plug and/or mandrel mill	- reduce (stretch/sink)
2. rotary pierce	- Assel elongate	- reduce (stretch/sink)
3. rotary pierce	- Pilger	- reduce (stretch/sink)
4. punch pierce	- push bench	- reduce (stretch/sink)
5. punch pierce	- extrude	- reduce (stretch/sink)

The tube reduction mill is the final stage for all the tube manufacturing processes where the intermediate stage generally defines the specific tube production process e.g. the Assel mill.

A tube-reducing mill consists of a number of longitudinal stands, each containing a number of equi-orientated grooved rolls, presenting to the on going tube, the required pass shape. Successive sets of grooved rolls are arranged to have gradually decreasing pass size such that the initial diameter of the tube is reduced to the size finally required as it passes longitudinally down the mill. Two-grooved rolls are the more common stand arrangement but the inherent more efficient three-roll configuration (FRONTISPIECE) is becoming more prevalent in modern tube reducing mills.

If the tube diameter is reduced by rolls containing completely circular grooves the reduction per pass must be small, otherwise the tube material will be forced into the gap between the roll flanges, producing fins or at the very least marking of the tube. In industrial practice

therefore the roll groove is "oval" to encourage preferential work of the tube at the root of the groove and thereby minimise the tendency to produce fins.

Generally for the two-grooved roll configuration the full roll shape is oval with the major axis parallel to the roll axis. To maximise the reduction in tube diameter at each stand the axis of each roll in successive stands is arranged to be at an intermediate angle to the axis in adjacent stands. For the two-and three-roll mills the intermediate angle is 90^{o} and 60^{o} respectively. For the two-roll case, with consecutive roll passes having axes inclined at 90^{o} to one another, the consequence is that the major axis of the tube leaving one stand is presented to the root of the roll groove in the next stand and hence the tube is successively compressed from one oval shape to another at right angles.

This arrangement results in the angle of bite of the roll being greater than would be produced with a circular grooved roll, since, for the two-roll case, the major axis of the tube meets the succeeding roll at a point further out from the axis of the tube than it would do otherwise. Little increase in the tube reduction takes place, since the amount of work involved in compressing the tube from one oval shape to another is relatively small. Furthermore, ovaling does not result in thickening of

the tube wall for only the reduction in mean tube diameter is effective in altering the wall thickness and it is this which requires an appreciable amount of work. Therefore, in any shape of roll pass it is important to consider the mean pass diameter. This is taken as the diameter of a circular tube having the same circumference as that of the pass, considering the pass as a closed oval.

Although the aforementioned description of the ovality sequence applies to the two-grooved roll profile, the same principles, appropriately modified, apply to the three-and four-grooved roll configurations.

When a tube is continuously passed through a reducing mill, the product of the tube cross-sectional area and its linear speed, must be constant at all sections in the mill i.e. constant volume flow conditions. In addition to the change in outside diameter of the tube as it passes through the mill, there is always some change in wall thickness.

When a tube, which is unsupported internally, is rolled by a single stand without front or back tension or compression, the tube thickness and velocity often increase with the diametral reduction. Under such conditions the thickening which takes place due to the purely compressive action of the grooved rolls is said

to take place under no-pull or sinking conditions. This condition arises in a multi-stand mill when increasing roll speeds at each successive stand are adjusted to produce neither tension nor compression in the lengths of tube between each stand. Furthermore, the whole tube length will thicken by an amount dependent upon the overall reduction that takes place and the diameter of the rolls.

However, as a result of rolling an unsupported tube through a series of equiorientated two-roll stands, each containing a pair of "oval" grooved rolls, the wall thickening will not be uniform around the section of the tube, being greater on diametral planes corresponding to the "oval" pass width. Moreover, as the tube diameter decreases, the degree of non-uniformity in the wall thickness increases. As a consequence, a squaring of the tube bore will be manifest for the two-roll configuration, and for the three-and four-roll arrangement the bore will tend to become hexagonal or octagonal respectively. Hence to minimise this shaping of the tube bore, the total allowable reduction in tube diameter in sinking is restricted.

If it is arranged for each stand pass to operate at a higher speed relative to the preceding stand i.e. in excess of that which is required for the previous sinking condition, then tension in the tube is generated between

the stands and the process becomes one of stretch reducing. Such an arrangement not only reduces the tube diameter but lessens tube thickening between the stands and the roll loads are reduced as a consequence of tension. An unfortunate consequence of the application of inter-stand tension is that appreciable end lengths of the tube are not subjected to the full tensioning action. Therefore the stretch-reducing mill will produce a tube which is thinner in the middle than at the ends, the end thickness being that which would arise from sinking conditions, while the middle thickness is that arising from the full stretch-reducing process. The length of the thickened ends of the tube, which may have to be rejected as scrap, can be reduced by keeping the inter-roll stand distance to a minimum. The incorporation of the stretch reducing process in the last stage of the complete mill also increases the range of finished tube sizes manufactured from the single hollow billet.

Another variant of the process is the mandrel mill. Here a mandrel is inserted inside the tube to provide internal support to the bore whilst the tube wall is being worked between the roll grooves and the mandrel at each roll stand. As a consequence of this internal support, in contrast to the sinking process, a much greater reduction of the cross-sectional area and wall

thickness is possible at each stand, resulting in a shorter mill i.e. fewer stands. However, as a result of such large reductions, brought about in a smaller number of stands, the final tube is less uniform in cross-section and must be passed on for further processing i.e. stretch reducing. Since each tube size requires a new set of rolls or mandrels the range of tubes that can be economically produced by the mandrel mill is restricted.

Generally the mandrel mill has between seven and nine stands of two-or three-grooved rolls each. As for the sinking process the axes of adjacent sets of two-or three-rolls are set at angles of 90^{o} and 60^{o} respectively to minimise finning of the tube. Again the roll groove shape is circular for the last stand. Due to the inherent groove "ovality" a clearance between the tube and mandrel is maintained at the groove shroud. In the last stand this clearance is distributed over the whole circumference of the mandrel-tube interface. This clearance also assists the stripping of the mandrel from the tube.

The complete continuous tube mill is highly productive but the range of tube sizes it can produce is limited. Furthermore, for economic reasons, these mills are unsuitable for the manufacture of large tube sizes.

To summarise: primarily because of their mechanical simplicity, two-roll mills are often employed. However, large reductions of area and diameter are not achieveable if high dimensional control is to be maintained in such mills.

Alternatively the four-roll or Stüting mill has been used for large reductions. However, the four-roll mill is expensive, it requires a complicated drive system and roll changing can be a difficult and an expensive operation.

Consequently, although the three-roll arrangement of the process is not widely employed in the UK, it is widely used elsewhere and its use is increasing since three-roll mills possess most of the advantages associated with the four-roll design. Thus, slip between the roll and tube is minimal, there is little marking of the tube and a greater draft per stand is obtained than with the conventional two-roll mill; also it is not as expensive as a four-roll mill.

It will be noted in Chapters 2.2 and 3 from the relative paucity of references to the three-roll mill that there is at present little fundamental knowledge of the process, however since this configuration is being adopted more widely there is a considerable need for a reliable theoretical and experimental approach to the performance

and the optimisation of such a mill. Thus this investigation was planned to place the mechanics of longitudinal tube rolling through three-grooved rolls on a reliable foundation and to proceed on the following lines:

The design and construction of a single pass three-roll experimental mill in which prime consideration could be given to the determination of the:

(i) roll torque - total and individual,
(ii) roll separating force,
(iii) front and back tube tensions.

It was decided to relate the above factors to the following variables:

(i) ratio : roll diameter/tube diameter,
(ii) ratio : tube outside diameter/tube wall thickness $(\frac{D}{t})$,
(iii) percentage reduction of the tube cross-sectional area,
(iv) reduced tube strain distribution.

By maintaining the pass profile of the three-grooved rolls constant, the change in tube reduction can be controlled by varying the outside diameter of the ingoing tube consistent with an appropriate adjustment to the internal tube diameter to retain the specified

ratio of the tube outside diameter/tube wall thickness. Hence the three-rolls will present to the tube to be rolled, an unchanging pass area for any particular series of test reductions.

In mill practice the reduction of tube is normally carried out under one of three conditions:

1. No internal tube support and without tube tension; (sinking).
2. No internal tube support but with tube tension; (stretch reducing).
3. With internal tube support and with or without tube tension; (mandrel rolling).

and some of these conditions are considered in the experimental work.

The analysis of the aforementioned tube rolling processes is complex, especially for the last condition i.e. mandrel rolling. Until recently all the theories involved the classical approach by considering the equilibrium of forces acting on an element of the tube in the deformation zone together with a yield criterion. The resulting differential equations were then solved for the appropriate end conditions. As commented upon by Cole (35), these theories, many semi-empirical, appear to be only of partial validation and an alternative theoretical approach utilising the strain energy

concept was attempted by Haleem (40) with some success. Consequently, in this thesis, both the slab equilibrium method of analysis, with appropriate modifications, and the newer work energy or apparent strain approach are considered for critical comparison. Therefore this research programme relating roll separating force and torque to roll diameter, groove profile design, reduction of tube area, frictional condition at the roll-tube interface, tube yield stress and the tube dimensions, will lead to a better understanding of the mechanics of deformation and thus to an optimisation of the tube rolling process.

Optimisation of the process is defined as the production of the maximum reduction of area per stand consistent with acceptable tube quality. To verify the theoretical analysis incontrovertible data will be obtained for a wide variety of rolling conditions. Subsequently it should be possible, using the verified theory, to predict the performance of three-roll longitudinal tube-rolling mills with a minimum of further ad hoc experimental work and incidentally this approach may provide a more unified theoretical approach to more general tube rolling conditions.

CHAPTER TWO

CRITICAL REVIEW

(i) BRIEF REVIEW OF PUBLISHED WORK ON THE LONGITUDINAL ROLLING OF TUBE THROUGH TWO-GROOVED ROLLS

(ii) DETAILED REVIEW OF PUBLISHED WORK ON THE LONGITUDINAL ROLLING OF TUBE THROUGH THREE-GROOVED ROLLS

2. CRITICAL REVIEW

Publications concerning tube making mills such as sinking, stretch-reducing and mandrel mills are few in number and, indeed, there is very little emanating from English language sources, so that, at the outset, it seemed that very little was known about these processes. There is, however, a notable amount of German work but the significance of this is dwarfed by comparison with the immense amount of Soviet work which is available. Russian references in this field are extremely numerous, and it would not be appropriate to try to cover them all here. This two part critical review contains a cross-section of the Russian papers, and consideration of the references given in any of these can lead into the whole field of the Soviet literature. In view of the complexity and diversity of the topics, a chronological progression has been adopted.

2.(i). BRIEF REVIEW OF PUBLISHED WORK ON THE LONGITUDINAL ROLLING OF TUBE THROUGH TWO-GROOVED ROLLS

The first reference available dates from 1934 and is contained in a book by Evans (1) on seamless tube manufacture. In the field of longitudinal rolling there is a section on the plug mill but only a mention of the continuous mill. Photographs are reproduced of both two- and four-roll reducing mills, with the statement that the four-roll mill was more efficient than the two-roll since a greater reduction could be effected with the same number of roll stands.

A reference to Findlater's (2) work (1947) is most readily to be found in a Compendium called *Tube Mill Practice*, which was published by the American Association of Iron and Steel Engineers in 1953; it also contains the papers by Rodder (4) and Young (5). Although the paper was presented by Findlater, it was, in fact, a report of the work of the Stretch Reducing Mill Committee of the National Tube Company, Pittsburgh, and, as it is virtually the only American published information on stretch-reducing appears very frequently in Soviet bibliographies. In his article Findlater discusses the results of his studies of stretch-reducing which were made on somewhat converted equipment. The advantages to be obtained by the creation of tension conditions between the stands are enumerated, and also it is made clear that the inevitable end-thickening makes the production of long lengths of tubing an economic necessity.

An article in Stahl and Eisen reports the work by Hartjenstein (3) on a single stand reducing mill at the Deutsche Rohrenwerke,

Dusseldorf. The problem was that the Company had an eighteen stand, two-roll mill which was of obsolescent design and was no longer capable of producing tubes to the limits of accuracy demanded by the prevailing market. The roll diameter was 310 mm (12.2in.) and the inter-stand spacing was 750 mm (29.5in.). As the mill was being operated as a stretch reducer, such a large inter-stand spacing caused end wastage, due to over-tolerance of the wall thickness for a length of up to 1.5 m (5ft.), and this was a considerable proportion of the total length of the rolled tube in this case. Economic reasoning showed that the off-cut ends could not be made profitable even by being passed on to cold drawing for finishing. Hartjenstein therefore had to decide whether production should be transferred to a new mill with minimized inter-stand spacing, or, whether a volte-face should be made and the mill operated under no-tension conditions thereby obtaining a tube of uniform thickness along the length even though that thickness had been increased by the free forming operation. In order to obtain quantitative data for the tube rolling process, tubes of various ingoing diameters and wall thicknesses were rolled down to 37 mm (1.45in.) o.d. using four types of pass configuration: two-roll, round groove; two-roll, normal oval groove with incipient flank opening over an arc of 30 deg., [of the form shown in FIGURE 3.15B.]; two-roll, pronouncedly oval groove with closed flanks, the circumference of which was equal to that of the round groove, [of the form shown in FIGURE 3.15C.]; and four-roll, round groove. A single stand was used throughout the testing. A large number of results were obtained and presentation is in graphical form, concentrating in the majority of cases, on the effect of groove shape on the various parameters. Also, as tests were carried out at

temperatures of 700°C, 850°C and 1000°C, it was found that the tendency to wall thickening decreased with increasing temperature.

The paper by Rodder (4) of the Aetna-Standard Engineering Co., Ohio considers the rotary piercer-plug mill-reeler-reducing mill production sequence. The author defines the sinking process and presents empirical expressions for the calculation of roll separating forces and power requirements. The mill, while normally used for simple final sizing, had also been used as a stretch-reducer.
The author does not compare his expressions with experimental data.

A mill which was new in 1950 at the National Tube Co., Pittsburgh, is the subject of the article by Young (5). The stretch-reducing mill in this plant consisted of twelve two-roll stands, with rolls of 356 mm (14 in) dia., and having an inter-stand distance of 368 mm (14.5 in); each stand was driven individually.
It is stated that not only was the wall thickness of the tube reduced, but also it was possible to make diameter reductions in successive stands which were more than 20% greater than on a no-pull mill. The article is not fundamental in its approach, but has practical significance.

The first British reference is a series of four articles by Blair (6) published in 1950, which gives invaluable practical information on all aspects of the process. A very telling comment is quoted: "Many mills have been designed on such vague

assumptions and misconceptions with regard to the behaviour of the tube passing through them, that their subsequent performance is very different from that which had been predicted." This is still the case in spite of the large amount of work published overseas, particularly on the two-roll longitudinal tube-rolling process. Blair attempted to rectify this situation and his first article reviews roll stand designs for both two-and four-roll systems (it is stated that the three-roll configuration did not appear to be used to any extent at that time) and lists all of the process parameters. He considered the concept of 'effective radius', this being defined as the radius of a circle which, when turning at the same speed as the rolls, moves at its circumference with the same linear velocity as the outgoing tube. The effective radius, therefore, is useful in defining points on each side of the groove at which no slip take place between the roll and the workpiece. Although he utilised this concept in discussing the design of two-roll mills,he indicated that the procedure could be extended to the three-roll arrangement. He quotes for a two-roll tube rolling mill operating without interstand tension, i.e. sinking, a constant effective roll radius of approximately 91% of the pass height and suggested that this value could also be used for the three-roll system. However, for tube reducing mills employing interstand

tension, this radius could change appreciably, therefore the concept may be limited in its application.

Blair compares the three-and four-roll arrangement with the more common two-roll system and he notes the improvement in tube quality and the practicability of greater tube reductions per stand than for the two-roll arrangement. In the concluding article Blair considers groove design, roll drive, the use of idle rolls for alternate stands, relative roll speeds for stretch-reducing, and the length of end-thickening.

In 1954, Shevchenko (7) published *The Continuous Rolling of Tubes* which treated all aspects of longitudinal rolling, mandrel, sink and stretch, mainly for two-roll mills, but three-and four-roll mills are mentioned. Amidst a notable paucity of references, to come upon a whole book on the subject is unusual but it is the first pointer towards pre-eminence of the USSR in investigations in this field of interest. The emphasis is practical rather than fundamental (this was the case with Blair (6) also) and there is an extensive section on changes in wall thickness and also factors affecting diametral spread and forward slip. In all, it would seem that every possible operational variable is described without them necessarily being analysed.

Vatkin (8) used pin loadcells in a tube rolling investigation. He carried out tests in two-roll sinking in

order to compare the results with theoretical predictions. The diameter of the roll was 260 mm (10.2 in) and the groove was circular having a diameter of 35 mm (1.375 in); tubes were rolled in both the hot and cold condition. There is good correlation between the experimental work and his theoretical predictions for the maximum roll pressure.

A series of tests on tube reducing with tension at the Novotrubnyi Plant was carried out by Kaufman, Gleiberg, Nodev and Shanin (9) in 1956. They used a twenty stand mill with individual drives to each stand and quoted the interstand tension by referring to a formula by Danilov, Gleiberg and Balakin (10). Tension coefficients,[+] of 1.2%, 3.0% and 4.0% were used. A table of results shows how the thickness of the outgoing tube decreased with increasing tension. It is stated that, for a tension coefficient of 3%-4%, the main length of the tube had a reduced thickness while the thickness of the end portions was unchanged.

The authors also generated stretch conditions in a mill with group drives, apparently with some success, but

[+]The tension coefficient describes the extra stretch resulting from inter-stand tension expressed as a percentage of the tube yield stress.

conclude, obviously, that individual drives are to be preferred.

The paper by Yamada, Watake, Inoue and Tani (11) is a report of plug rolling experiments at the Nippon Tokushu Steel Co.; plug-bar force, roll separating force and roll torque were all measured by means of electrical resistance strain gauges. They obtained reasonably linear experimental relationships between roll separating force and torque and between roll separating force and plug-bar force. The authors do not reach any theoretical conclusion but base the analysis on Sachs and Klinger (12), who considered the basic configuration for the flow of metals through tools of circular contour.

Chekmarev and Gulyaev (13), at the All-Union Institute for Tube Research, studied roll groove design for two-roll sink and stretch-reducing mills, but the amount of stretch involved was only small. The paper gives a detailed method of analysis for the sequential calculation of passes through the stands and for determination of the desirable degrees of ovalization; the condition for filling the groove was a major concern. The authors attempted to avoid a pass design which would cause either over- or under-filling.

Gulyaev and Yurgelenas (14) studied "certain basic technological parameters" for tube reducing with tension and their paper has sections on:

(i) the measurement of the mean wall thickness of a rolled tube, in which they present a nomogram for the calculation of thickness change for sinking in two-roll, oval grooves, and also present information showing that the main position in a groove where thickening takes place is between the angles of 60^{o} and 90^{o} from the root of the groove,

(ii) the maximum extension of a tube in which expressions are developed on the basis of constancy of volume and on the method of analysis of Neumann and Hancke. (This paper is considered in Chapter 2.2),

(iii) the capacity of a given reducing mill to provide a particular extension of a tube, in which a number of empirical formulae are quoted,

(iv) the magnitude of interstand stress required to produce a given tube extension. The authors state that their formulae have been verified completely by tests on a two-roll mill with individual drive to each stand and on a three-roll mill with group drives. The nomogram appears to be useful.

Shveikin and Gun (15) at the Ural Polytechnic Institute, were also concerned with the change in wall thickness caused by rolling and derived formulae for the thickening or thinning of a tube due to pure sinking by using the theory of shells. These theoretical results are compared with experimental values quoted from Danilov, Gleiberg and Balakin (10) and by Matveev and Vatkin; the agreement is very good being of the order of $\pm$ 2% for the majority of cases.

A Hungarian paper by Torma and Hantos (16) (1958), *'An examination of the theories of tube reduction'* is mentioned here merely to make it clear that this is not a major fundamental work but rather another paper which is concerned with pass design and work per stand.

In 1958, there was a review by Vater (17) of the field of work of tube reducing mills. He reviewed the design of drive systems for two-and three-roll mills and the operation of stretch-reducers.

An extensive review and comparison of expressions for the calculation of wall thickening for sinking without any tension on mills with individual drives was published by Gulyaev and Yurgelenas (18) in 1961. The formulae discussed are those by Gleiberg (19), Kraev (20), Shevchenko (7), Shveikin and Gun (15), Kolmogorov and Gleiberg (21), and Blair (6), and the range of sizes for which each formula is applicable is listed.

Two papers of the first-order significance were published by Kirichenko (22) and (23) in 1964, both are fundamental

theoretical treatments for two-roll sinking, the first for torque and the second for pressure distribution, and both will be considered in Chapter 3 on theoretical approaches.

It may also be worth mentioning at this stage that the longitudinal tube reducing processes figure largely in the textbook entitled *The Hot Rolling of Tubes* by Danilov, Gleiberg and Balakin (10), in marked contrast with English language books in which the subject is hardly, if ever, mentioned.

The textbook serves as a useful summary of the U.S.S.R. work in the field of longitudinal tube rolling with two-, three- and four-roll mills. In one section they state the advantages for the three-(and four-)roll arrangements relative to the basic two-roll system, e.g. improvement in rolled tube quality and an increase in the reduction per stand.

This book is also informative on the effect of the profile on the deformation of the tube but does not relate the design of the profile to the fundamental mechanics of the process.

The mandrel rolling process is the subject of a descriptive paper by Shevchenko and Chekmarev (24) also in 1964. The mill had three stands, each fitted with pairs of roll separating force loadcells, and graphs show the variation of force and velocity parameters with time for various conditions of large and small tension between stands I and II, and III.

The Matveev and Lavrov (25) paper, is also concerned with mandrel rolling and the effect of tension between the stands on the way in which the grooves are filled. Lead, aluminium and steel tubes were rolled in a single stand, with the front and back tensions applied by hydraulic means. The authors draw the rather obvious conclusion that longitudinal compression assists in filling the groove and this may be complete when this compression is as low as 10 per cent of the yield stress.

A paper which should also be mentioned, in passing, is by Fomichev and Kirichenko (26) in which the Kirichenko approach of references (22) & (23) is applied to the plug rolling process.

Further work on mandrel rolling was done by Shevchenko and Chekmarev (27) (1965) who carried out tests on a seven-stand continuous mill with group drives. Reproduced in FIGURE 2.1. is a diagram of the way in which the tube cross-section changes in passing through the stands. A detailed analysis for the roll pass design of the mill is given.

Ivshin and Shveikin (28) also contribute a theory for the prediction of the torque required in a stretch-reducing mill and they predict the thickness change due to stretch-reducing and make comparisons with calculations from the work of Gulyaev and Yurgelenas (29) and Shevchenko and Zimin (30).

Fomichev and Kirichenko (31) consider the limiting inter-stand tensions for the continuous rolling of bars and tubes.

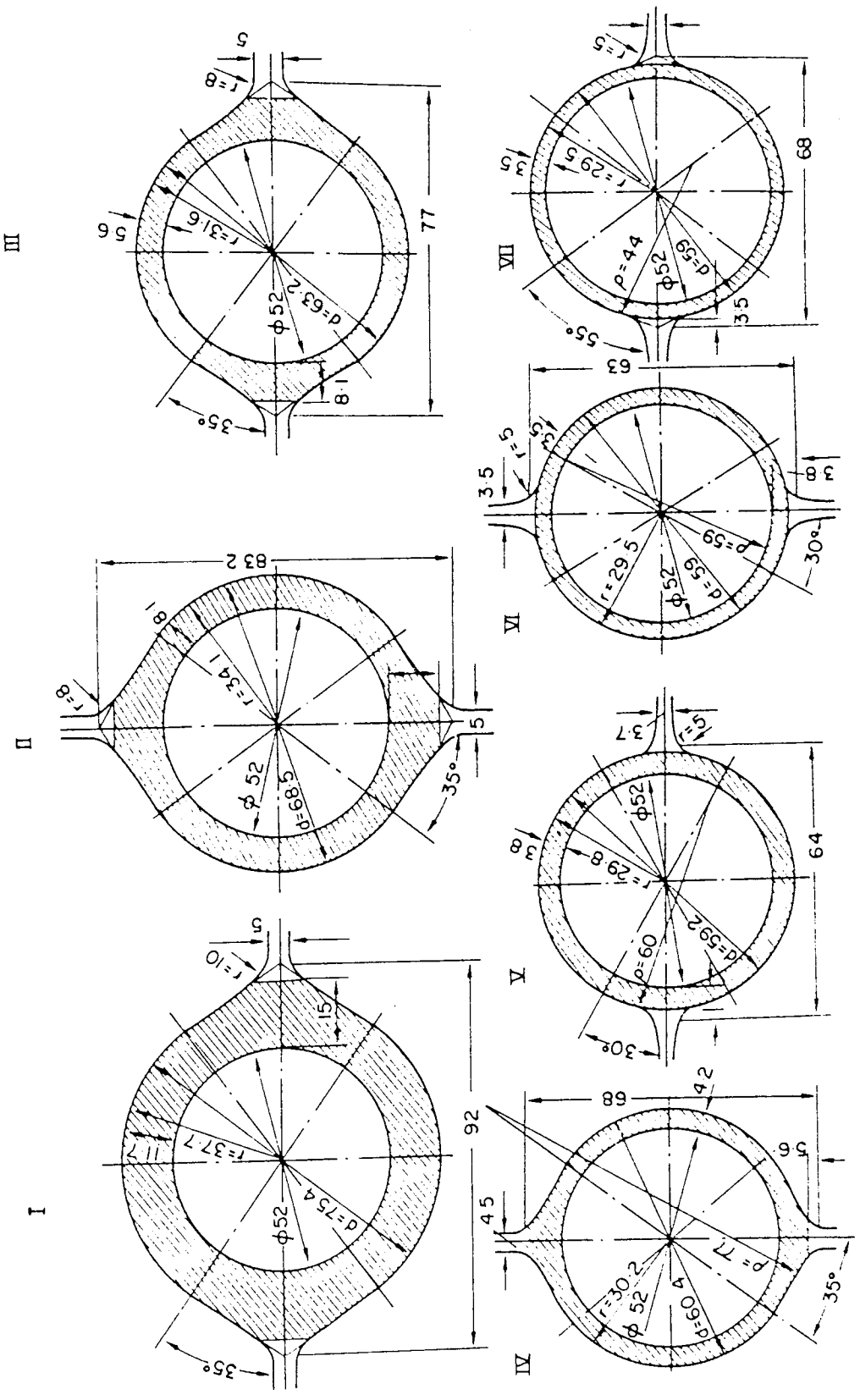

THE WAY IN WHICH THE TUBE CROSS-SECTION CHANGES IN PASSING THROUGH THE STANDS

FIGURE 2.1

Chekmarev, Onishchenko and Ol'dztsevskii (32) are also concerned with mandrel rolling, here with forward flow and inter-stand deformation.

A Russian paper, by Vatkin and Druyan (33), is one of the earliest published theories for mandrel rolling and will be considered in Chapter 3. The experimental work was carried out on lead and steel tubes on a laboratory mill with rolls of 270 mm (10.6 in.) dia.

The publication by Fazan and Blain (34) of IRSID is primarily concerned with the principles of the stretch-reducing process and the relationship between thickness change and inter-stand tension. They also acknowledge that the position of the neutral point varies with the roll groove angle as a consequence of the variation of roll radius. The roll radius being defined as the distance from the roll centre to the point of no-slip at the exit plane. In this respect it is then indicated that a knowledge of the tube exit velocity would be useful. They suggest that line (N), FIGURE 2.2. represents the locii of the points of no-slip on the surface of the tube in the deformation zone. The authors then propose that as an approximation line (N) divides the surface of contact into two equal zones, i.e. zone I = zone II.

One of the few British references to tube rolling was by Cole (35) (1969). He employed a converted milling machine as a single stand two-roll mill, with pin loadcells incorporated in the groove of the upper roll. To simulate hot

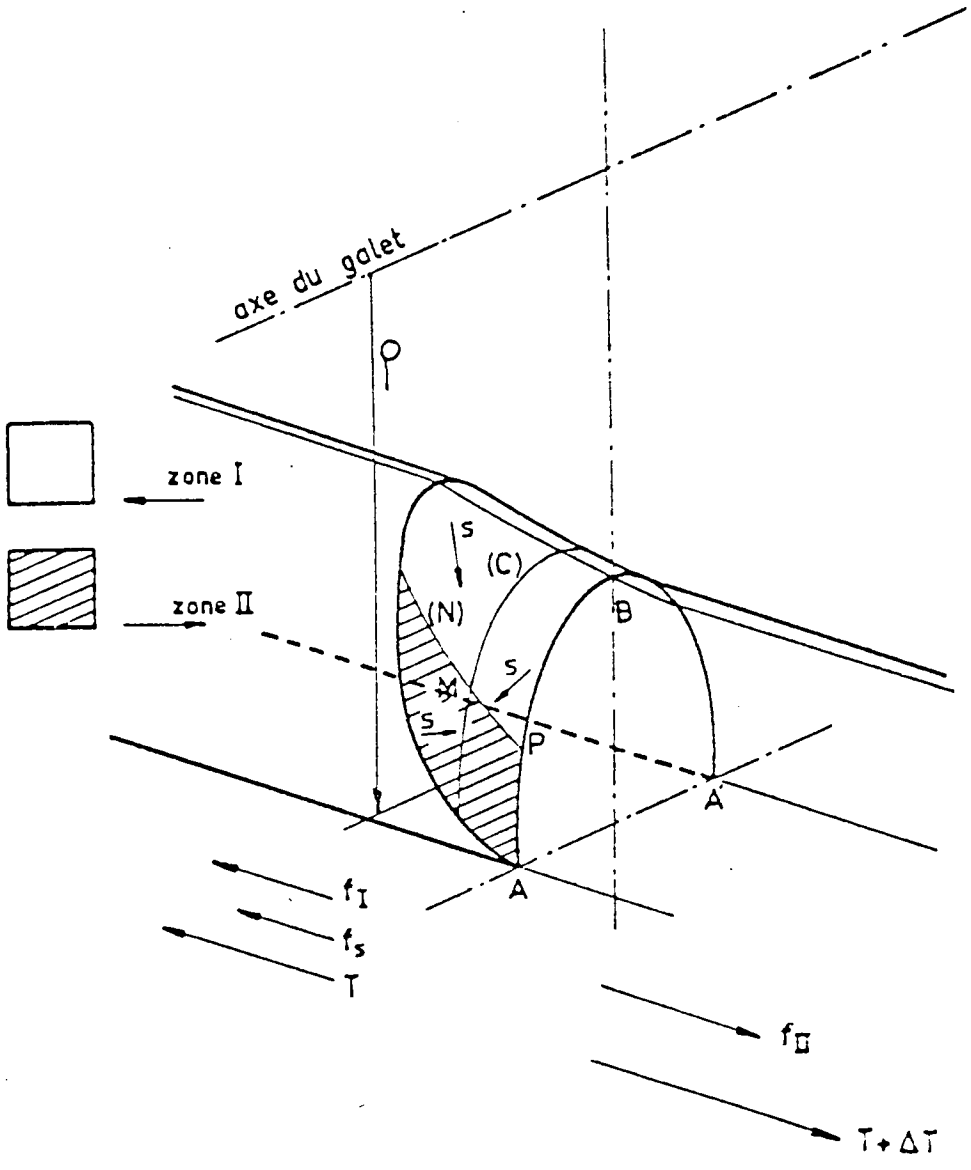

LOCII OF NO-SLIP POINTS OF TUBE SURFACE IN DEFORMATION ZONE

FIGURE 2.2

steel, lead tube was rolled in a circular groove which represented the finishing stand of a production mill. Cole conducted experiments to investigate the roll groove pressure distribution for sinking, stretch-reducing and mandrel rolling. Changes in the tube reduction being effected by varying the roll gap. Unfortunately, since the roll groove profile was circular, the tube thickened and thinned at the roll root and shroud respectively. This deformation pattern was the converse of the actual tube behaviour in the tube production mill. Furthermore, as a consequence of the circular groove profile, tube finning was a recurrent problem, to the extent that his experimental results could not be readily compared with the theoretical predictions. Cole also noted that the position of the neutral plane was quite different to that for the flat rolling situation, being similar to the mode first predicted by Fazan and Blain (34).

This work also included a very comprehensive literature survey on tube rolling and of the methods of measurement of the roll groove contact pressures.

The comparisons which were made of the mean roll pressure indicated a theoretical prediction of the order of 6.0 N/mm^2, with the measured value being in the region of 17.0 N/mm^2.

A report published in 1970 by Neuhoff and Pfeiffer (36) described a continuous tube mandrel rolling mill which comprised of seven or nine two-roll stands, each stand offset at 90^{o} to each other. Operational difficulties of the mill were discussed, in particular changes in wall thickness and tool surface life and various measures were suggested to improve these problems. Roll and mandrel forces were also considered to optimize the forces.

In a theoretical paper on tube rolling by Okamoto (37) a deformation factor ν was introduced and defined by:

$$\varepsilon_2 = - (0.5-\nu) \varepsilon_1$$

where ε_1 and ε_2 are the maximum and intermediate principal strains respectively. Since the strains were not constant over the tube section he introduced a "mean deformation factor" ν which was defined as:

$$\nu = \frac{r_a \cdot r_b}{r^2} \nu_m$$

where r_a and r_b are the outside and inside radii of the tube and r the radius corresponding to ν at any position in the tube section.

Employing the stress-strain relationships and the von-Mises yield criterion the following equations for the principal stresses were derived:

$$\sigma_1 = \frac{K_f}{\sqrt{3}} \left(\frac{1.5 + \nu}{\sqrt{\nu^2 + 0.75}} \right) + \sigma_3$$

$$\sigma_2 = \frac{K_f}{\sqrt{3}} \frac{2\nu}{\sqrt{\nu^2 + 0.75}} + \sigma_3$$

$$\sigma_3 = \frac{K_f}{\sqrt{3}} \ln \left(\nu + \sqrt{\nu^2 + 0.75} \right) + \frac{K_f}{\sqrt{3}} \ln \sqrt{0.75} - C$$

where K_f is the tensile yield stress and C is an integration constant.

Two theoretical cases were developed; tube sinking and tube plug drawing. Neither friction nor redundant deformation were considered.

Overfilling or underfilling of the roll groove in the mandrel rolling process was the main object of a theoretical study by Okamoto and Hayashi (38) in 1971. They noted that overfilling produces tube finning whilst underfilling affects tube roundness. The tube deformation zone, relative to the mandrel-tube interface, was then divided into two regions; the roll groove root and the roll groove shroud. In the groove root region tube contact with the mandrel produces axial tube compression, whilst at the shroud the "free" tube bore created axial tension.

From plasticity theory and Okamoto's previously discussed (37) deformation factor ν, fundamental equations were derived. Then the products of the axial stress and tube area in the groove root and shroud respectively were expressed in the axial compatability equation:

$$f = \sigma A + \sigma' A'$$

This equation was utilised as an assessment of over-filling or underfilling of the tube in the roll groove gap. They stated that if $f > 0$ the tube overfills, while if $f < 0$ underfilling occurs. When $f = 0$ the deforming tube just fills completely the roll groove gap.

Friction was not considered in the analysis on the assumption that the forward and backward slip regions nullify each other. This condition is rarely achieved since frictional conditions change from stand to stand in a multi-stand mandrel mill.

Although the authors presented calculations for an eight-stand two-roll mandrel mill with f = 0 no verification was possible since little information relevant to the rolling conditions was given.

Gulyaev et al (39) published a paper in 1971 which was a semi empirical study of oval groove pass design to optimize tube ovalization, i.e. the realisation of a reduction in the final transverse wall thickness variation. The authors appeared to be the first to note that the total deformation zone is greater than the geometrical zone, consisting of a free or pre-zone and a contact or true geometric zone. They quote a figure of between 0.85 and 0.90 for the ratio between the actual area of tube-roll contact and the theoretical, presumably, geometric value. Experimental work by Haleem (40) indicates that the ratio between the actual arc of contact and the geometric one is approximately 0.7.

In 1973 Lomachenko et al (41) at the Urals Tube Research Institute published test results from an experimental investigation of transverse wall thickness variations when hot reducing tube in two- and four-roll stands. They noted a significant

reduction in the transverse wall thickness variations for the four-roll stand compared with the variations produced in the two-roll stand.

Material flow irregularities in a eight stand two-roll mandrel mill was the subject of a further paper by Pfeiffer (42) in 1973. He considered the deviations of the tube dimensions from the nominal at the front and rear tube ends i.e. front and rear belly formation. Pfeiffer confirmed that the variations in tube dimensions at the rear tube end (rear belly), could be attributed to the mandrel acceleration at the exit from the mill. With regard to front belly formation he suggested that this could be reduced by increasing the tube diameter or wall thickness thereby lowering the rate of cooling from a thicker tube. This implied that the tube was less susceptible to shrinking on the mandrel consequently reducing the material flow in the forward direction.

By holding the mandrel in a fixed position at the tube entry and noting the roll and mandrel forces Pfeiffer assessed the coefficient of friction μ_2 between the tube and mandrel at any stand from the expression:

$$\mu_2 = \frac{Z}{2P_w}$$

where P_w is the roll force and Z is the mandrel force. This particular approach has the advantage that it considers all the actual rolling conditions.

Haleem (40) (1978) continued Cole's (35) work, improving the performance of the pin loadcells and assessed the roll groove

pressure for specific tube D/t ratios. Sinking and stretch-reducing conditions were investigated for the two-grooved roll arrangement. Two types of passes were considered, round to oval and oval to oval, the latter operation simulating inter-stand rolling conditions. Recordings of roll loads, torques, tube velocities and roll pressure distributions were obtained. He formulated a new theoretical approach for the mean roll pressure based on the energy principle, noting a better correlation with experiment than had previously been displayed by the equilibrium analyses. Haleem also studied the neutral zone and the pre-contact or "free" plastic deformation zone relevant to the process parameters.

Cole's (35) and Haleem's (40) single stand mill was employed by Labib (43) (1982) for an investigation into the mandrel rolling of thin lead tube through two-grooved rolls. Rolling trials assessed the behaviour of the R.S.F., roll torque and roll groove pressure distribution for specific tube $\frac{D}{t}$ ratios and various conditions of the mandrel surface. Again pin loadcells were used to measure the pressure distribution around and along the roll groove, the latter result enabling the arc of contact to be established.

His results indicated a non-uniform pressure distribution and the existence of a free deformation zone i.e. tube deformation prior to the contact zone. Labib also noted that the roll loads and torques were greatly effected by change in tube thickness and friction condition at the mandrel-tube interface. Furthermore, the application of front and back tension to the tube decreased the roll loading. Increasing the mandrel

A new theoretical approach based on the energy principle was proposed and compared with existing equilibrium approaches. The total work done was then calculated and the tube and mandrel velocities assessed for application to a multi-stand mill. In general, good agreement was obtained between the theoretical predictions and experimental results.

The works of Cole (35), Haleem (40) and Labib (43) will be examined in more detail in the appropriate chapters of this thesis.

2.(ii)DETAILED REVIEW OF PUBLISHED WORK ON THE LONGITUDINAL ROLLING OF TUBE THROUGH THREE-GROOVED ROLLS.

The first known reference to the rolling of tube by the three-roll arrangement is that of Boettcher and Pomp (44). In their work they considered the elongation and change in thickness occurring during sinking on both two- and three-roll mills and they also considered the stretch-reducing process in which the tube is subjected to inter-stand tension. The relative orientation of adjacent two- and three-roll stands with respect to the tube was discussed and emphasis was placed on the greater reductions of area per stand which could be achieved by the three-roll system. Although they presented experimental results they did not produce a theory to predict elongation or the change in the tube wall thickness.

In 1955, Neumann and Hancke (45), working in München Gladbach, published a paper on the theory of the deformation taking place in stretch-reducing mills and analysed the strain distribution for three magnitudes of longitudinal tension. They showed that: for zero tension, i.e. pure sinking, half of the material compressed circumferentially flows axially and half radially so that a corresponding increase in length and wall thickness is produced; for a longitudinal tension equal to half of the yield stress, the thickness remains constant and the material flows longitudinally purely as a consequence of the reduction in diameter; thirdly, for the limiting condition of the longitudinal tension being equal

to the yield stress, equal reductions of diameter and thickness result. Neumann and Hancke go on to derive expressions for the relative rotational speeds of stands, for the coefficient of friction and for the stress coefficient (the stress coefficient is the ratio of longitudinal stress to the yield stress and is sometimes known as the stretch coefficient). By analysing the roll force and friction coefficient in relation to the stress coefficient, roll pass design criteria for a three- roll arrangement with interstand tension were presented. Also indicated was the method of attaining maximum tube reductions consistent with tube quality for a variety of tube outside diameters. Some of this analysis was verified by experimental results and an example was given of a three-roll pass design with the determination of the relative roll speeds for a stretch-reducing mill employing sixteen stands for the reduction of tube from 75.50 mm x 3.40 mm (2.97 in x 0.134 in) to 21.25 mm x 2.05 mm (0.837 in to 0.081 in). This example also presents, for each stand; the tube wall thickness, the effective stress coefficient, the actual roll speed and the tube outside diameter. Further work indicates how the length of tube, with wall thickening taking place at the tube ends, can be assessed; it is claimed that the method is confirmed by experimental results but these are not stated. It is suggested that the maximum safe limit (practical limit) for the stress coefficient is 0.86. It is also interesting to note that they were clearly unaware of any USSR work since they state that the only available data concerning material flow is contained in the work of Blair (6) and of Boettcher and Pomp (44).

A Russian reference by Gulyaev et al (46) on the rolling of welded tubes on a three-roll stretch-reducing mill states that the advantages of the three-roll over the two-roll configuration are that up to 14% deformation can be achieved in a single pass, that eccentricity and wall thickening are decreased and that the working length of the mill can be reduced or that the same total deformation work can be done using fewer stands. Discrepancies between their theory and their results vary from 4% to 18%. The mill had eighteen stands with non-adjustable roll speeds and produced tubes having a diameter range from 13.5 mm to 66.0 mm and thickness range from 2.25 mm to 4.50 mm.

A second paper by Gulyaev and Yurgelenas (47) in 1961 was concerned with roll design and tube elongation in two-, three-and four-roll mills, all with non-adjustable group drives; the four-roll mill was then at the planning stage. The basic dimensions for oval groove passes are calculated from geometical considerations and a graph shows the relationship between the ovality of the pass and the percentage deformation per stand both for stainless steel tubes and for carbon and low alloy steel tubes, furthermore they also take account of the physical condition of the stand. This roll pass design process is extended to enable optimum groove ovality to be achieved consistent with tube quality, i.e. the reduction of non-uniform thickening and twisting of the tube. Reasonable comparison appears to be achieved with the few experimental results presented. The production of a better quality tube with shorter mill lengths is discussed for three- and four-roll arrangements, although the authors note that the resultant

roll drive systems can be very complex. Locations, outside the USSR, of these tube rolling mills are then listed. From a knowledge of the roll speeds and pass shape a method for determining the axial elongation of the tube is given for a sinking condition. If tube tension is applied then a 'slip factor' must be introduced. This factor is determinable from tables and from a graphical relationship involving the tube reduction and size per stand. This method is extended so that an iterative approach can be applied to enable the required tube quality to be produced by two-, three- and four-roll arrangements. A semi-empirical expression is then developed for determining the length of tube end thickening under given rolling conditions. Some of these predictions are compared with results from production mills.

The reference by Vater (48) is on the representation of deformation ratios by flow diagrams. The technique is applied specifically to a three-roll stretch-reducer and the deformation ratios are defined as the ratios of logarithmic strains; longitudinal to circumferential and radial to circumferential. By the introduction of a yield criterion and by also considering the tube thickness/diameter ratio, Siebel arrived at an equation governing the deformation in 1948 and it is this equation which appeared in the Neumann and Hancke (45) paper. The Vater flow diagram plots the relationship between the two strain ratios and the relative longitudinal stress (stress coefficient) for various values of the tube thickness/diameter ratio. The criterion for the application of this work is the minimising of tube defects; bore 'squaring' (or rather 'hexagonning'), for thick tubes,

and internal wrinkles and radial collapse causing folding for thin tubes. Simultaneous torque measurements were made on each drive shaft of a three-roll stand for a small deformation of 2.7%, rolling from round to triangular form, initial diameter 40 mm (1.57 in), thickness 3.6 mm (0.142 in). These measurements showed a most pronounced non-uniformity of distribution of the torque between the three rolls; a case is quoted in which one roll took over 78% of the total torque. The uniformity was improved when rolling tubes from triangular form to triangular form, but it was still possible for one roll to take 50% of the total. No explanation was forthcoming for this non-uniformity of torque distribution.

In the textbook by Danilov et al (10) roll groove design for two- and three-roll mills is discussed, the authors mentioning that, in general, oval pass grooves are employed. By considering the relative tube reduction per stand and the roll groove ovality coefficient as discussed by Gulyaev (47), the authors determine the roll groove pass design and manufacture for a three-roll arrangement. This analysis also includes the influence of roll speed and the attainment of the correct tube wall thickness. Furthermore they note that variation of the actual tube wall thickness from the calculated value can be controlled by judicious roll speed changes in adjacent stands, e.g. if the tube wall thickness between the stands is below that specified by calculation, then a compressive longitudinal stress is applied to the tube and vice versa. No mention is made

however, of possible tube buckling which could result from axial compression of the tube between the stands. An example is tabulated of the roll pass profile dimensions per stand, and also included are values of roll speeds for a three-roll mill (operating under stretch conditions) with differential group drives to each stand. In this case two sets of roll pass dimensions were indicated for eighteen and thirteen stand mills rolling 30 mm (1.18 in.) and 50 mm (1.97 in.) dia. tubes respectively.

A Japanese reference, by Mise, Takai and Matsuki (49) is a report of tests on a three-roll stretch-reducing mill of twenty-four stands, the stand spacing being 300 mm (11.8 in.). Tubes were reduced from 130 mm to 60.3 mm diameter (5.12 in - 2.37 in.) in fourteen and nineteen stands. The wall thickness change and rolling torque at each stand were measured, and the resistance to deformation and inter-stand tension were estimated. A considerable amount of experimental evidence was amassed.

A paper by Biller (50) in 1967 was concerned with the production and possible elimination of 'polygonning' in the bores of thick walled steel tubes when rolled by a three-roll stretch mill. It was pointed out that Neumann (51) had suggested that an uneven reduction in the tube cross-section at each stand was a reason for this condition, particularly when non-circular pass profiles were employed. To amplify this, Biller compared the tube cross-section

shape and position for two successive three-roll passes, and showed in diagrams how unequal reductions developed at some angular co-ordinates. From this work he noted the importance of the stress condition at two critical planes in the tube cross-section, and his subsequent analytical work involved the use of Vater's (48) flow diagrams to indicate the tube deformation ratios at these planes. The formation of bore polygonning is illustrated by noting the discepancy between the deformation ratios (radial strain/ longitudinal strain) and the stress coefficient for these two critical planes. He further discussed the reaction of the bore polygonning to changes in the rolling and tube parameters, making the following statements:

(i) an increase in the friction coefficient tends to reduce the polygonning effect,

(ii) polygonning decreases with an increase in the ratio of roll diameter/tube diameter,

(iii) there is some theoretical evidence that the polygonning is increased as the tube progresses through the mill,

(iv) the polygonning effect is also increased if thicker walled tubes are rolled,

(v) the polygonning orientation and magnitude is appreciably influenced by the stress coefficient, which can have an optimum value for zero polygonning (i.e. a truly circular bore). An optimum value of 0.32 for the stress coefficient is quoted for a tube D/t ratio of 10, this optimum value reducing with decreasing D/t ratio, (D/t ratio = o.d./wall thickness).

A theoretical analysis for the determination and subsequent manufacture of the optimum roll groove profile and opening for a three-roll stretch-reducing mill was the subject of a paper by Valenta (52). He was primarily concerned with the degree of roll groove relief, i.e. the opening of the groove towards the roll shroud, noting its influence on tube quality and inter-stand tension. By the combination of experimental and theoretical work he suggested that the process of designing and production of the roll groove profile could be optimised. Finally,he observed that small changes in the amount of roll groove relief could substantially affect the tube quality and thickness reduction. No experimental results relating to current mill experience were indicated; the author stated that this approach did produce a more accurate determination of the roll groove profile for optimum tube production.

A further Russian reference by Gulyaev, Yurgelenas and Zimin (53) appeared in 1968. They point out that the use of tube reductions per stand of 10% - 14% in modern reducing mills was not only a result of the application of inter-stand tension but also of improved roll supports and an increase in the rolling temperature to 1100^{o}C. However, since large reductions would be likely to be detrimental to the tube quality, they emphasise the necessity for the determination of the optimum reduction per stand. The work of Shevchenko (7) was stated to be the first to establish an experimental relationship between the critical reductions per stand and the tube D/t ratio

and this they presented in a graphical manner. Although this relationship was derived initially for non-stretch sinking on two- and three-roll mills, they state that these critical deformations per stand are also determinable for stretching conditions. The authors note that welded tubes can sustain higher deformation in the first stand than seamless tubes due to their better cross-sectional geometry. By a consideration of the yielding and loading conditions they apply a formula derived by Shveikin et al (54) for two- and three-roll mills to present graphs which relate the critical deformation per stand and the D/t ratio, to a coefficient (Z) of plastic deformation (53). They appear to indicate that some of the results obtained from this relationship are at variance with those found on current mills both in the USSR and elsewhere. For example, in some of the two-roll stretch-reducing mills in the USA, because of the high tension (Z_{av} = 0.6-0.7) and a rolling temperature of over 1000^{o}C, the deformations per stand attain 10 per cent and in two-roll mills for welded tubes in the USSR and the USA 12% - 14%, while according to Shveikin's (54) formula the highest critical deformation for the two-roll reducing mills with a D/t ratio of 26 and Z_{av} = 0.7 is equal to 6.4%. A similar discrepancy is quoted for a three-roll Mannesmann-Meer mill in West Germany. They conclude this section by stating the limits for the tube D/t ratio as 40-44 and 50-54 for two- and three-roll reduction mills respectively. Finally, the paper states that, without tension, deformation of up to 7% can be permitted in two-roll oval passes and up to 12% - 14% with

tension. In three- and four-roll oval passes rolling without tension, maximum deformation should not exceed 10.3% and 11.8% respectively.

Another Russian reference by Anisiforov et al (55) appeared in 1968 and discussed the distribution of the total reduction between the individual stands of a reducing mill. They note, that in general, the pass reduction in the middle stand remains constant, decreasing gradually to zero at the end. The effect, on tube stability and quality, of employing greater reductions per stand is considered, and although a shorter mill length would result, a selective decrease in the reduction at a number of intermediate stands may be more beneficial. Such a mill schedule, they claim, would improve tube quality, reduce roll wear, lower the maintenance and allow more flexibility of the finished tube size. An example of a rolling schedule with decreasing reductions per stand towards the end of the mill is given for D/t ratios of 16.7-33.4, with a maximum reduction in the first two to four stands of 7%-8% and a subsequent gradual decrease in reduction to 5% - 6% for the following stands. An improvement in tube quality was noted with a decrease in mill loading on the latter stands. The authors then point out that this type of rolling schedule is difficult to achieve because of dimensional tolerances, the machining of pass profiles and the influence of roll wear. However, they comment on the usefulness of considering the difference between the actual and calculated mean pass diameters, and its change

due to roll pass wear and rigidity and the machining tolerances. They note that changes in the actual pass diameter produced by wear, increase from the first to the last stands due to the increase in the roll speed. A semi-empirical relationship and other formulae are introduced to account for these various factors, enabling the design and manufacture of the stand to be optimised for a mill schedule having 'falling' reductions. Typical roll pass designs for three-roll reducing mills with allowances for cutter diameters and their mountings are also given.

Blazynski (56) in 1970, published a general article on the recent developments in seamless tube-making which briefly discussed the longitudinal tube rolling process. The advantages of the three-roll arrangement compared with the two-roll arrangement were discussed, e.g. current mill practice for the tube sinking process employs a tube diameter reduction per stand of up to about 14% for the three-roll arrangement, whilst only a 3% to 5% tube diameter reduction is possible for the two-roll arrangement. Since this article was a review no attempt was made by the author to discuss detail aspects of the process.

The three-roll stretch reducing mill at the Weldless Steel Tube Co., was the subject of a paper published in 1973 by Procter & Jubb (57). They indicated that for the stretch reducing process the deformation flow equations discussed by Newmann and Hanke (45) could be utilised to optimize the reducing mill schedule with respect to the roll speeds and the size of the initial tube. It was stated that the

problem of tube bore polygonization increased with thicker tubes and larger tube diameter reduction and was a function of the stress coefficient and the roll groove pass design - a condition previously developed by Biller (50). Proctor and Jubb also noted that a roll groove profile which produced a more uniform circumferential surface contact between tube and roll groove, i.e. the contact surface approaching that of a conical frustrum, reduces bore polygonization. They then assumed, for calculating the roll speeds, that the position of the neutral point occurred at the roll groove root for all stands - an incorrect assumption as previously noted by Blair (6). However, they allowed for this inaccuracy by utilizing an additional roll speed control arrangement known as the "stretch vernier" which, when judiciously applied, could minimize the problem of tube end thickening. Finally, the authors discussed the various techniques incorporated in the mill to maintain control of tube quality.

A paper published in 1974 by Gulyaev et al (58) considered the transverse variation in the tube wall thickness during stretch reduction in two-and three-roll mill arrangments. They developed a complex cyclic function based on the tube perimeter for the wall thickness variation at a transverse section of the tube and compared their analysis with test measurements for both the two-roll and three-roll mill arrangements. This function includes a harmonic component with fluctuations of the second and fourth orders predominating on the two-roll mill and third and sixth orders on the three-roll mill.

CHAPTER THREE

THEORETICAL APPROACHES

(i) THEORETICAL ANALYSES OF THE SINKING AND MANDREL ROLLING PROCESSES

(ii) THE PROPOSED THEORIES

3.(i) THEORETICAL ANALYSES OF THE SINKING AND MANDREL ROLLING PROCESSES

A comprehensive assessment of the mechanics of the longitudinal rolling of the tube through two-and three-grooved rolls was made by Cole (35) in 1969. He detailed a critical analysis of the available theoretical treatments for the sinking, stretch reducing and mandrel rolling processes. All the theories, primarily for the two-rolled configuration, were based on the classical slab equilibrium approach, the majority of them being Russian in origin. Cole commented on the limitations of these approaches and suggested the energy or apparent strain method as an alternative technique for a more realistic analysis of the processes. The energy method was applied to the sinking and stretch reducing processes by Haleem (40) in 1978 and to the mandrel rolling process by Labib (43) in 1982; in both cases the two-roll configuration was considered.

Although this present investigation deals with the three-grooved roll process, the number of rolls does not significantly influence the fundamental principles of the theoretical treatment. Consequently the subsequent sections will consider a brief description of the equilibrium analyses and a more detailed examination of the energy method available for the two-grooved roll arrangement. The two-roll arrangement is the configuration examined by most research workers, since this arrangement is the one most universally employed in tube mill practice. Until recently stretch reducing has been associated with the application of inter-

stand tension to the basic sinking process, however current industrial mandrel mills also utilize inter-stand tension. Theoretically the presence of front and back tube tensions in either sinking or mandrel rolling does not affect the fundamental analysis, only the boundary conditions are modified and therefore any theoretical treatment need only consider the sinking and mandrel rolling processes for the two-roll configuration. Consequently the following resumes of the published theoretical analysis will refer to sinking and mandrel rolling for the two-roll arrangement, commencing with the equilibrium approach and concluding with the more recent energy method.

3.(i).1. PREVIOUS SINKING THEORIES

Four studies illustrating the various approaches to the theoretical analysis of the sinking process will be discussed in this section. The first three, by Shveikin&Gun (59) 1958, Vatkin (8) 1954 and Kirichenko (23) 1964, are Russian in origin and since a comprehensive review of these theories and others was made by Cole (35) only a brief resumé will be made here. However the fourth, a more recent theory, by Haleem (40) 1978 will be summarised in more detail.

3.(i).1.1 SHVEIKIN AND GUN (59) 1958

Considering the theory of axially symmetric thin shells, Shveikin and Gun proposed a simple sinking theory for the prediction of roll pressure. Friction between the tube and roll contact surfaces was neglected and the arc of contact was replaced by a chord as shown in FIGURE 3.1.

The roll pressure equation took the form:

$$P = \sigma_y \left[\frac{t_o}{d_{om}} + \frac{t_1}{d_{1m}} \right] \qquad (3.(i).1)$$

In general this equation overestimates the roll pressure but the agreement with the test results on steel tubes of Vatkin (8) was acceptable. Cole (35) however commented that the values of the yield stress of steel utilised in equation (3.(i).1), i.e. 294 N mm^{-2} for cold rolling and 59 N mm^{-2} for hot rolling, were serious underestimates, casting doubt on the stated agreement of Shveikin and Gun.

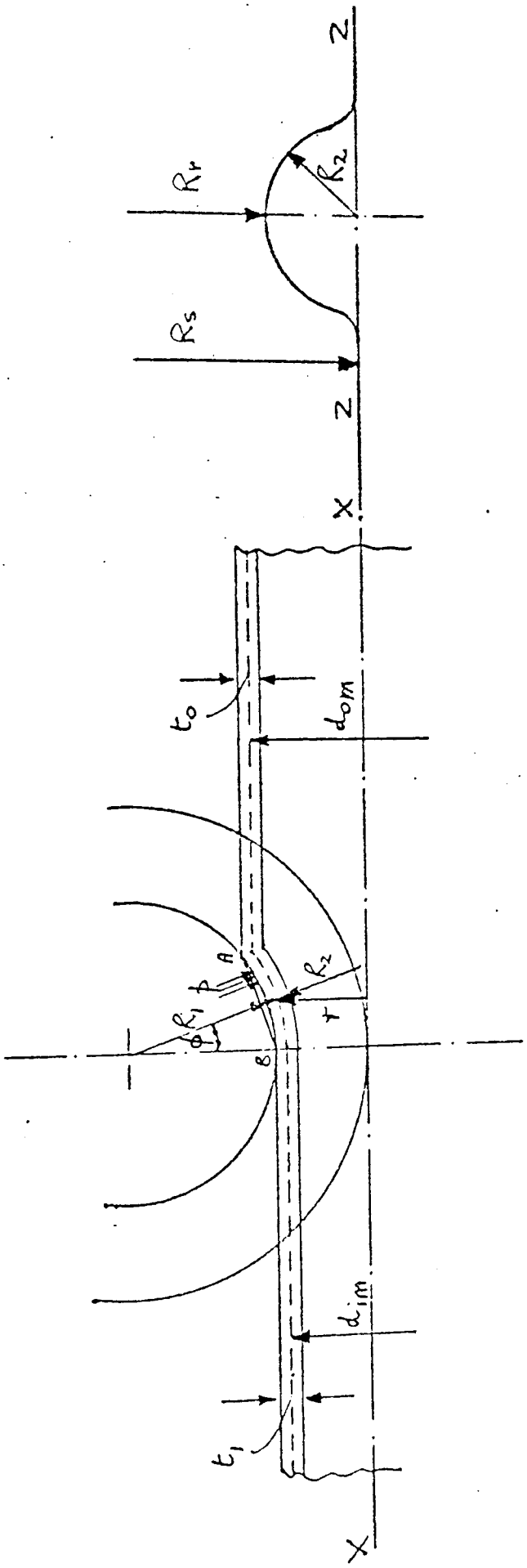

EQUILIBRIUM SINKING ANALYSIS - Shveikin and Gun (59)

FIGURE 3.1

3 (i).1.2. VATKIN (8) 1954

Vatkin developed differential equations by considering the equilibrium of forces acting on an element of tube in the deformation zone as shown in FIGURE 3.2. His main assumptions were:-

1) no change of wall thickness i.e. $t_o = t_1$
2) the principal stresses were:
   i) the longitudinal stress σ_x ,
   ii) the radial stress on the tube outer surface σ_r,
   iii) the circumferential stress σ_θ ,
3) the yield criterion was:

$$\sigma_x - \sigma_\theta = 1.15\ \sigma_y$$

4) by considering the equilibrium of a semi-circular section of the tube:

$$\sigma_\theta = \sigma_r \frac{d_g}{2t} \qquad \text{at any section,}$$

5) the arc of contact was replaced by a chord having the same length for all positions round the groove,
6) Coulomb friction existed between the tube and roll contact surface i.e. $\tau = \mu p$ at any section.

Pressure distribution equations for the entry and exit zones were derived in the form:

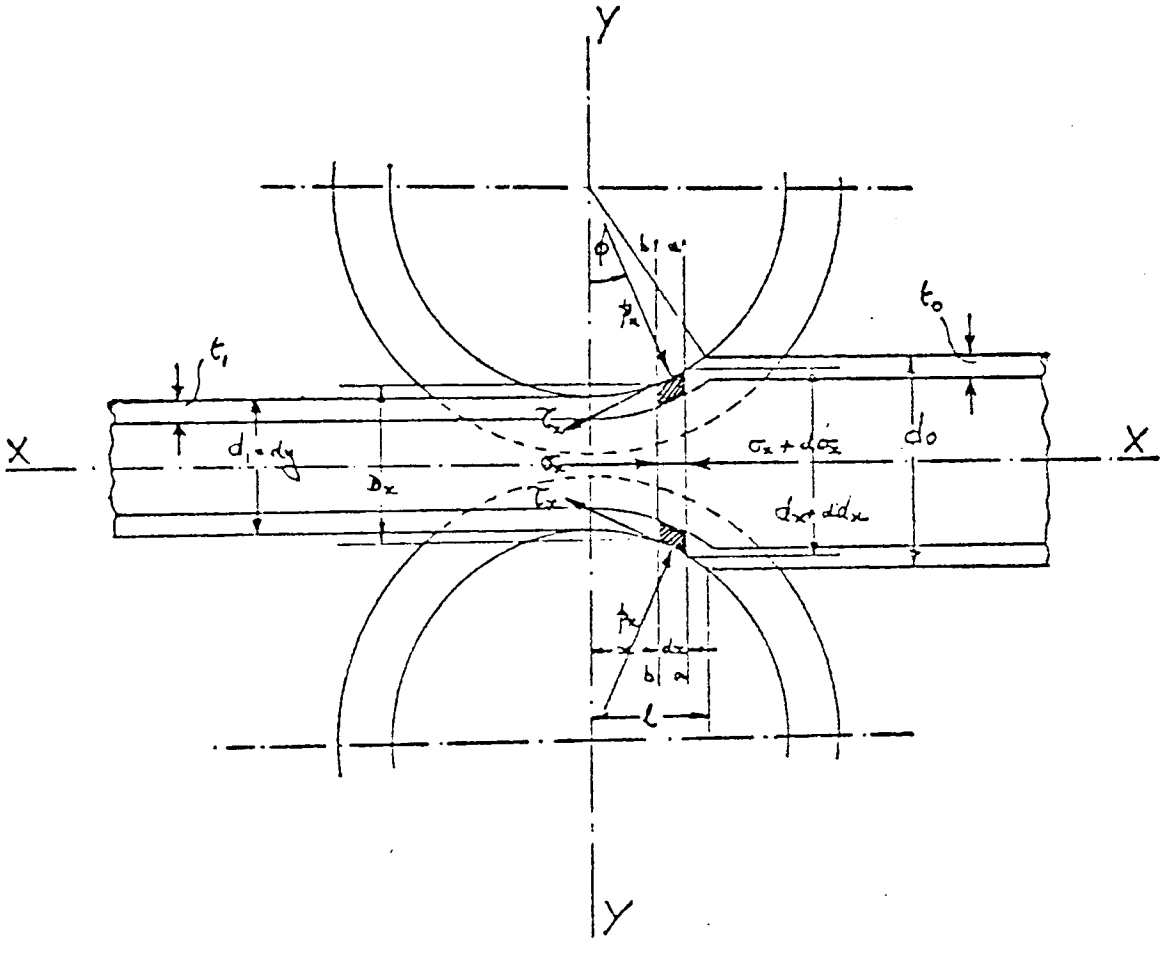

EQUILIBRIUM SINKING ANALYSIS - Vatkin (8)

FIGURE 3.2

$$p_x = -k^* Q_1 \left[\left(\frac{1}{Q} - 1 \right) \left(\frac{d_o + d_{1i}}{d_x + d_{1i}} \right)^{\frac{1}{Q}} - 1 \right] \quad (3.(i).2)$$

for the entry zone, and

$$p_x = -k^* Q_1 \left[\left(\frac{1}{Q} + 1 \right) \left(\frac{d_x + d_{1i}}{d_1 + d_{1i}} \right)^{\frac{1}{Q_1}} - 1 \right] \quad (3.(i).3)$$

for the exit zone.

From which the equation for the average roll pressure was deduced as:

$$p_{av} = \frac{k^* Q}{\delta} \left\{ \left[\left\{ d_o + d_{1i} \right\} - \frac{\left\{ d_o + d_{1i} \right\}^{\frac{1}{Q}}}{\left\{ d_1 + d_{1i} \right\}^{\frac{1}{Q}} - 1} \right] - \delta \right\} \quad (3.(i).4)$$

in which:

$$k^* = 1.15\, \sigma_y \frac{2t}{d_g}$$

$$\frac{1}{Q} = \mu \frac{4L}{\delta} - 1 \quad , \text{ and } \quad d_{1i} = d_1 - 2t,$$

He compared these theoretical predictions with his previously referred to experimental results (8). For the cold rolling of steel he assumed a value for μ of 0.25 and for σ_y 294 Nmm^{-2} which, as previously noted, was a serious underestimate. Vatkin attributed his higher theoretical roll pressure values to a large μ coefficient, although Cole, noting the assumed low yield stress, disputed this reasoning.

Records of the roll pressure showed a peak i.e. a neutral plane approximately in the middle of the deformation zone. However the results of tests carried out by Haleem (40) indicated that the position of the neutral plane is a function of the groove angle θ, which moves the position of this plane towards the exit or entry planes.

3 (i) 1.3 KIRICHENKO (23)

Kirichenko also considered the equilibrium approach employing the same basic assumptions to those of Vatkin (8), with the yield criterion being of the type:

$$\sigma_x - \sigma_\theta = k\,\sigma_y \quad \text{with k being not defined.}$$

However he considered the general case of an oval tube being rolled in an oval groove as shown in FIGURE 3.3.

By resolving the forces in the radial direction as indicated in FIGURE 3.4., he deduced the following relationship:

$$p = \frac{2\,\sigma_\theta\, t}{(\cos\phi + \mu \sin\phi \cos\theta)\, d_x}$$

This differed from Vatkin's (8) expression:

$$p = \frac{2\sigma_\theta\, t}{d_g}$$

in which the friction contribution was ignored.

From the geometrical considerations of rolling an oval tube in an oval groove as shown in FIGURES 3.3 and 3.4, Kirichenko presented equations for estimating the arc of contact (L) and the angle of contact (ϕ) of the form:

$$L = \left[\left\{ R_1 + E_1 - \sqrt{r_1^2 - Z^2} \right\}^2 - \left\{ R_1 - \sqrt{r_o^2 - E_o + Z} \right\}^2 \right]^{\frac{1}{2}}$$

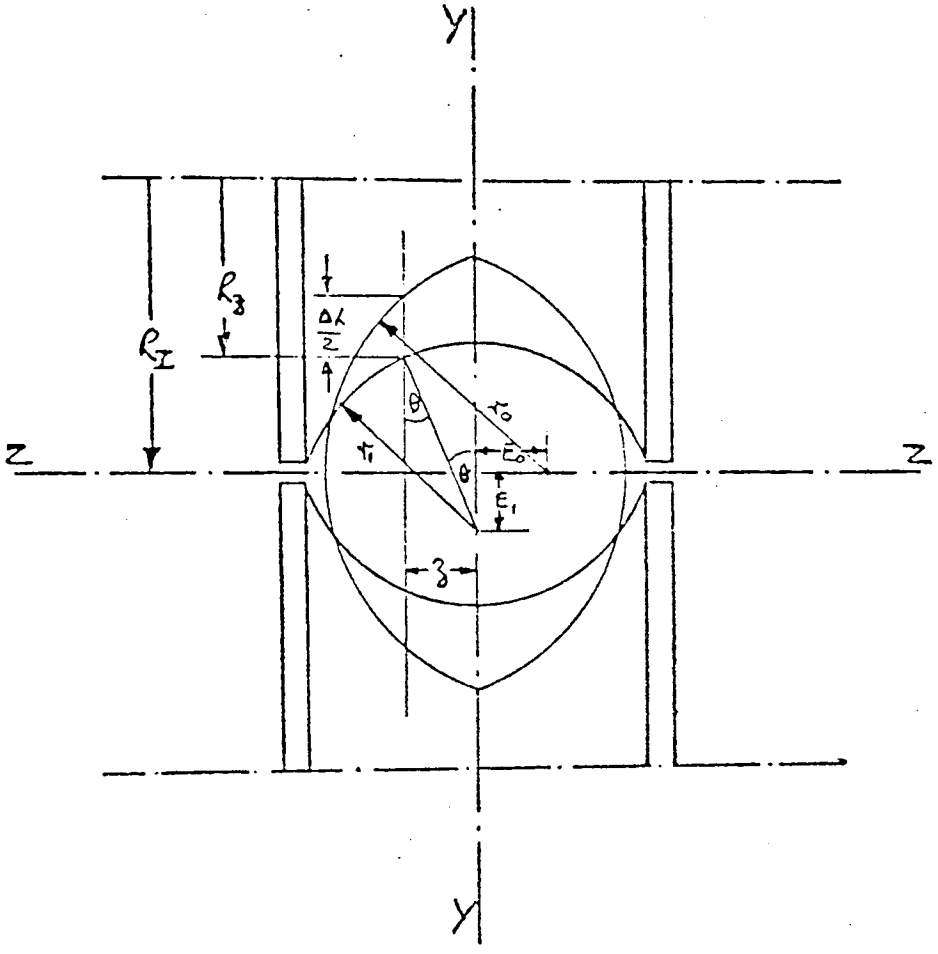

OVAL TUBE BEING ROLLED IN AN OVAL GROOVE

- Kirichenko (23)

FIGURE 3.3

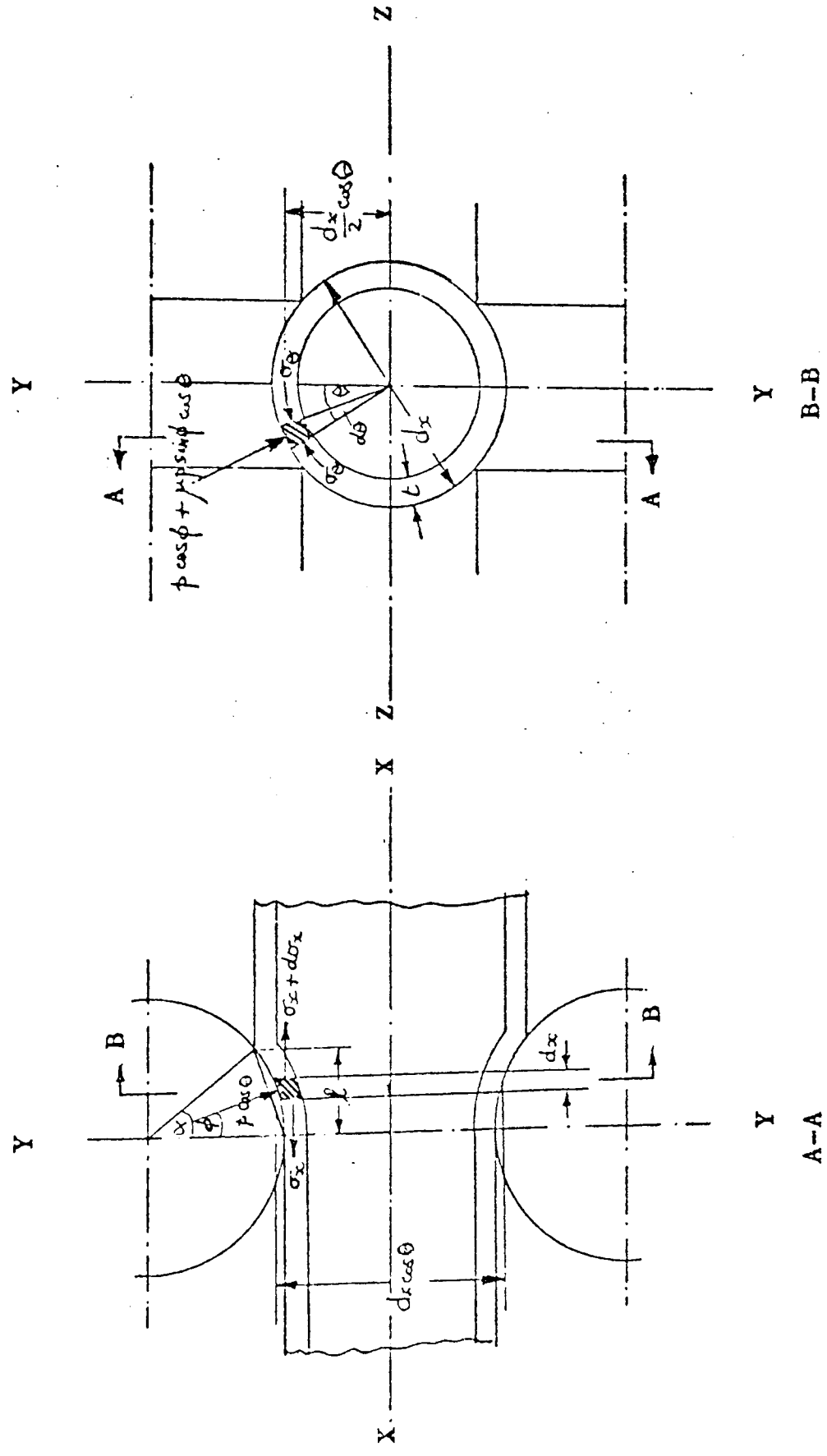

EQUILIBRIUM OF FORCES IN THE RADIAL DIRECTION

FIGURE 3.4

and $$\tan\phi = \frac{\sqrt{r_0^2 - (E_0 + z)^2} - \sqrt{r_1^2 - z^2} + E_1}{\left[\left(R_1 + E_1 - \sqrt{r_1^2 - z^2}\right)^2 - \left(R_1 - \sqrt{r_0^2 - (E_0 + z)^2}\right)^2\right]^{\frac{1}{2}}}$$

From consideration of the equilibrium of forces acting on an element in the deformation zone, Kirichenko solved the resulting differential equations for the roll pressure distribution, which were:

$$p^1 = \left[\frac{kt}{\left(r_1 + x\tan\phi\cos\theta - \frac{t}{2}\right)\left(\cos\phi + \mu\sin\phi\cos\theta\right)}\right] \left[\frac{1}{1+A} + \left(\frac{r_1 + L\tan\phi\cos\theta - \frac{t}{2}}{r_1 + x\tan\phi\cos\theta - \frac{t}{2}}\right)^{1+A}\left(\frac{A}{1+A}\right)\right] \quad (3.(i).5)$$

for the inlet zone.

and

$$p'' = \left[\frac{kt}{\left(r_1 + x\tan\phi\cos\theta - \frac{t}{2}\right)\left(\cos\phi - \mu\sin\phi\cos\theta\right)}\right] \left[-\frac{1}{B-1} + \left(\frac{r_1 + x\tan\phi\cos\theta - \frac{t}{2}}{r_1 - \frac{t}{2}}\right)^{B-1}\left(\frac{B}{B-1}\right)\right] \quad (3.(i).6)$$

for the outlet zone.

Where, $$A = \frac{\cos\theta\,(\mu - \cos\theta\tan\phi)}{\sin\phi\,(\mu\tan\phi\cos\theta - 1)}$$

and $$B = \frac{\cos\theta\,(\mu + \tan\phi\cos\theta)}{\sin\phi\,(1 - \mu\tan\phi\cos\theta)}$$

Cole (35) noted that Kirichenko's equation for calculating the angle of contact gave a considerable overestimate and that μ must be greater than $\tan \phi$ for A to be positive.

Kirichenko presented graphs FIGURE 3.5., showing the variation of roll pressure along the arc of contact, but gave no experimental results.

In another publication (22) Kirichenko developed an equation based solely on the friction forces for the roll torque in the longitudinal rolling of bars and tubes. With reference to FIGURES 3.6 and 3.7 the following equation was presented for the roll torque T :

$$T = m \int_{z_1}^{z_2} \left[\int_{\gamma}^{\alpha} \tau R_2 R_2 \, d\phi - \int_{o}^{\gamma} \tau R_2 R_2 \, d\phi \right] \frac{dz}{\cos\theta} \qquad (3.(i).7)$$

where m is the number of rolls per stand and γ the neutral angle.

By assuming Coulomb friction and a uniformly distributed normal roll pressure p, the above equation integrated to give:

$$T = m \mu p R_{AV} (A_{tot} - 2A_{out})$$

where:

R_{AV} is the mean roll radius in the deformation zone,

A_{tot} is the total contact area,

A_{out} is the area of the exit zone.

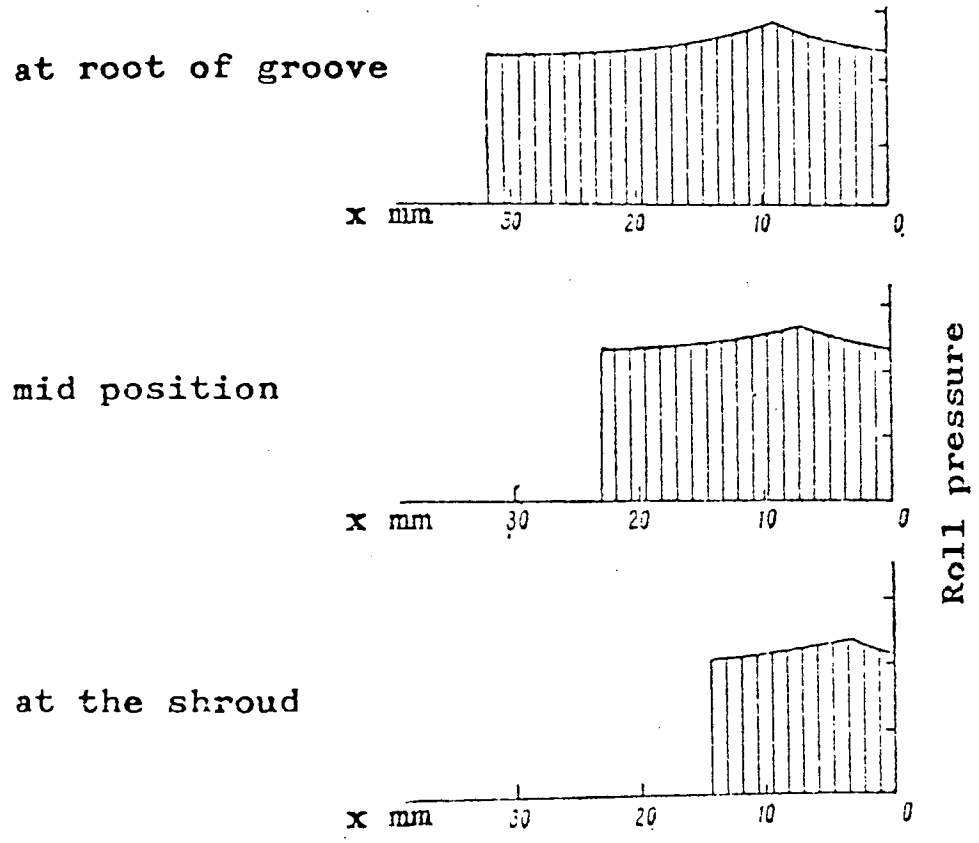

VARIATION OF ROLL PRESSURE ALONG THE ARC OF CONTACT

FIGURE 3.5

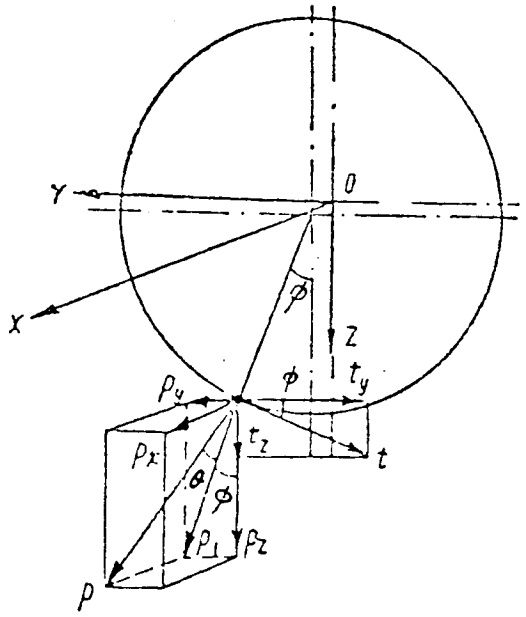

STRESSES ON AN ELEMENT IN THE DEFORMATION ZONE

FIGURE 3.6

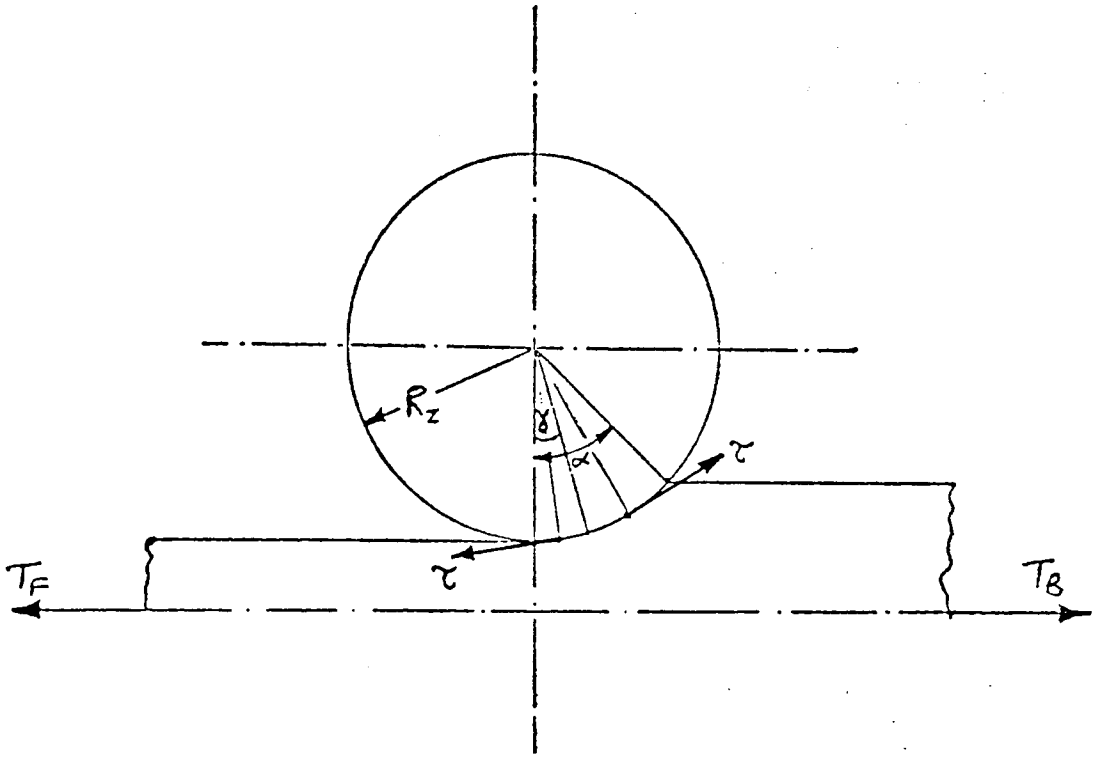

CONTACT SHEAR STRESSES IN THE DEFORMATION ZONE

FIGURE 3.7

3 (i). 1.4 HALEEM (40) 1978

Haleem noted the unsatisfactory comparison of Cole's (35) experimental rolling loads for sinking with the theoretical predictions of Shveikin and Gun (59), Vatkin (8) and Kirichenko (23). Since all of these theories were based on the equilibrium approach the shortcomings of this method were listed as follows:

1) All previous tube sinking theories require a knowledge of the principal stresses for eventual substitution into a yield criteron. While the assumed principal stress directions of longitudinal, tangential and radial are satisfactory for cold rolling, where the frictional shear stresses are low, the assumption for hot rolling with the attendent higher sticking type shear stresses is questionable.

2) The three investigations used Tresca's criterion in the modified form:

$$\sigma_1 - \sigma_3 = \beta \sigma_y \qquad \text{where} \quad 1.00 \leqslant \beta \leqslant 1.15$$

Kirichenko did not define β, Shveikin and Gun assumed 1.00, and Vatkin in using 1.15 implied plane strain deformation, which Cole (35) stated was unacceptable for tube sinking.

Sachs (60) commented that although the von Mises criterion was more accurate it involves considerable calculation and sufficient accuracy can be achieved by taking β as 1.10.

Haleem then stated that the above assumptions were inherent to any equilibrium approach and together with the imprecise friction evaluation were believed to be responsible for the lack of correlation found in Cole's work. Consequently attention was directed toward the strain energy or apparent strain method of analysis for determining the mean roll pressure.

He then described the strain energy method as follows: The work done per unit volume of rolled tube comprises three components:

1) Work of homogenous deformation W_h required to change the shape of the tube. This is the minimum possible work to achieve the desired reduction.
2) Work done against friction W_f at the tube-roll interface.
3) Redundant work W_r required to shear the tube as it passes into and out of the deformation zone.

For tube sinking the redundant work for small reductions can be neglected.

The total work of deformation per unit volume is equal to the area under the true stress-strain curve as shown in FIGURE 3.8., for the appropriate total strain.

Assuming $W_t = W_h + W_f$

and the apparent strain concept:

$$\bar{\varepsilon}_A = \bar{\varepsilon}_m + \bar{\varepsilon}_f$$

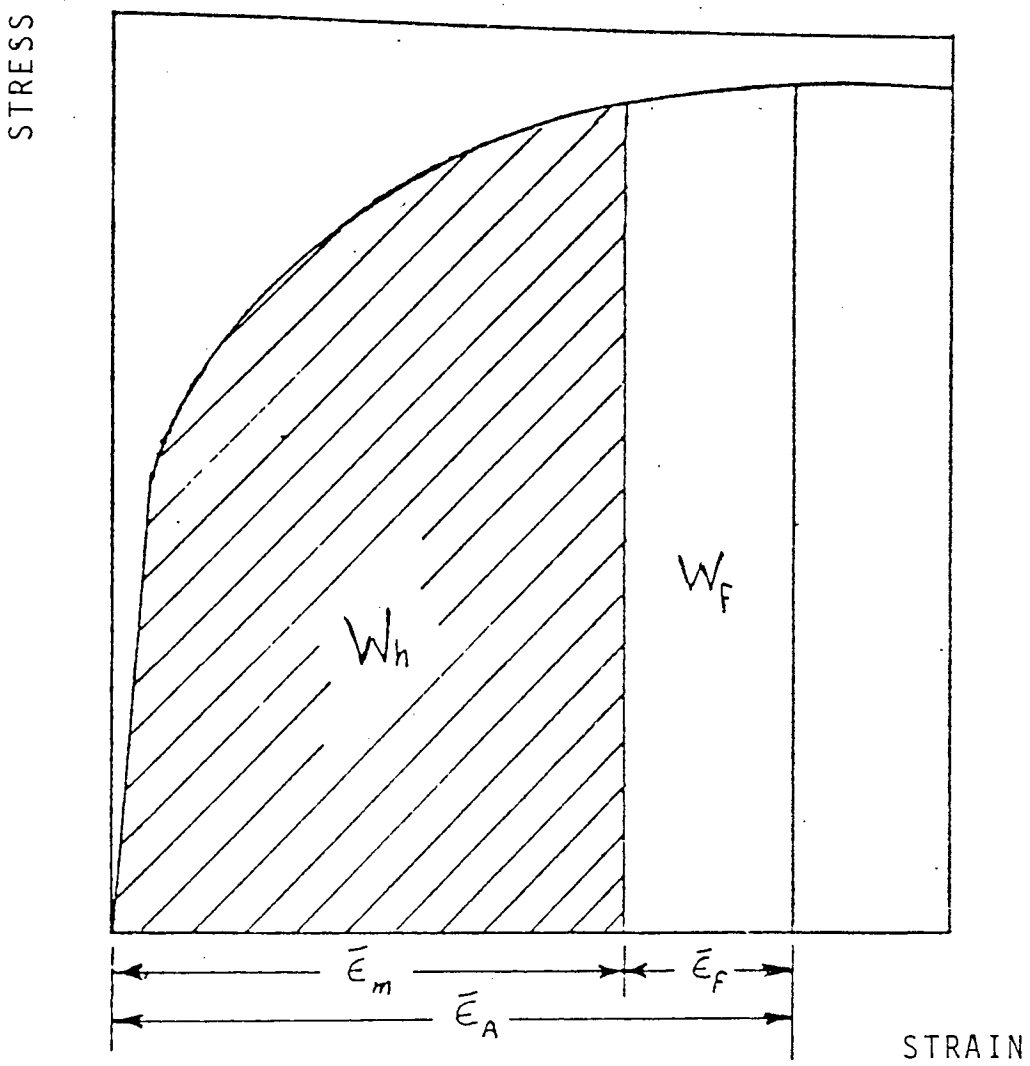

WORK OF DEFORMATION

FIGURE 3.8

Hence the total work of deformation W_t is equal to the integral of the true stress strain curve between the limits of zero strain and $\bar{\varepsilon}_A$ i.e. the total area under the curve shown in FIGURE 3.8.

The two components of the total work of deformation are then:

Work of homogeneous deformation W_h:

The internal work of homogeneous deformation W_{hi} is:

$$W_{hi} = \int_0^{\bar{\varepsilon}_m} \sigma_y \, d\varepsilon$$

$$= \bar{\sigma}_y \, \bar{\varepsilon}_m \qquad \text{assuming an average yield stress.}$$

To calculate the external work of homogeneous deformation W_{he}, for the tube rolling process, its equivalence to the deformation of a tube under external pressure can be assumed as indicated in FIGURE 3.9., such that:

$$dW_{he} = p_h \, S \, dr$$

where p_h is the uniform pressure for homogeneous deformation,

S is the surface area of application of p_h

$dW_{he} = 4L \, r_g p_h \theta_c dr$ and $L = R_r \phi_m$ for tube rolling

Substitution and integration between r_o and r_1 gives:

$$W_{he} = 2 \, p_h \, R_r \, \phi_m \, r_g \, \theta_c \, \delta$$

where $\delta = d_o - d_1 = 2(r_o - r_1)$

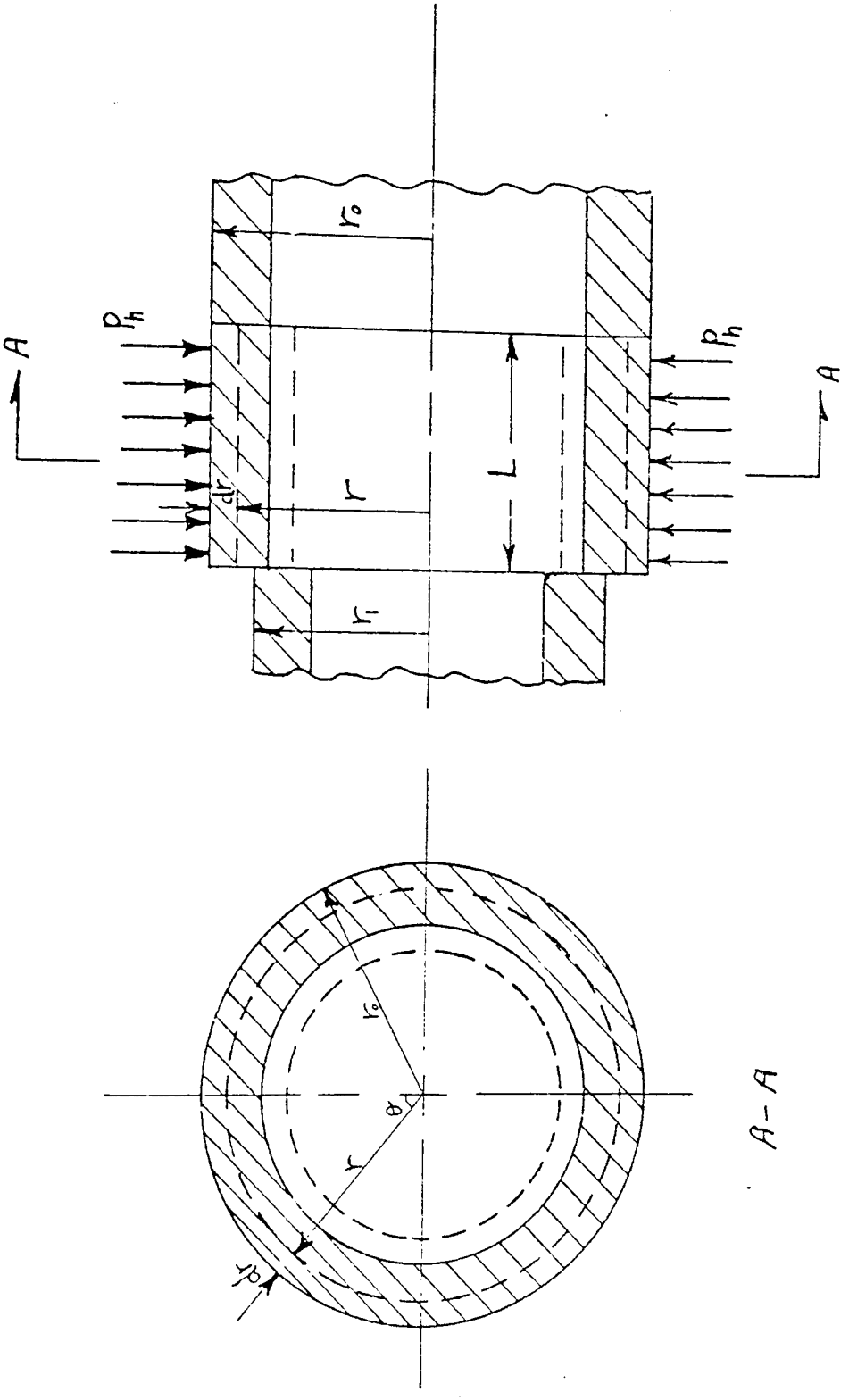

DEFORMATION OF A TUBE UNDER EXTERNAL PRESSURE

FIGURE 3.9

The work of homogeneous deformation per unit volume is:

$$W_{he}/Vol = \frac{W_{he}}{V}$$

where $V = A_o U_o \frac{\phi_m}{\omega}$ and with $U = \omega R_r$

$$V = A_o R_r \phi_m$$

$$W_{he}/Vol = \frac{2 p_h r_g \theta_c}{A_o}$$

Assuming no energy losses:

$$W_{hi} = W_{he}$$

and $$p_h = \frac{\bar{\sigma}_y \bar{\varepsilon}_m A_o}{2 r_g \theta_c \delta} \qquad (3.(i).8)$$

This equation gives the contribution of the roll pressure associated with homogeneous deformation.

Work done against friction W_f:

The mechanics of friction are complex and determination of the exact functional relationship between the frictional shear stress τ and the other variables is difficult (61). For metal forming without lubrication there are two types of friction:

$\tau = \mu p$ the Coulomb type sliding friction

and $\tau = m \frac{\sigma_y}{\sqrt{3}}$, the constant shear yield stress type of friction,

where m is a particular constant friction factor in the range: $0 \leqslant m \leqslant 1$.

For complete sticking friction $\tau = \frac{\sigma_y}{\sqrt{3}}$ and it has been shown by many workers that in hot rolling a combination of sliding and sticking friction is prevalent. Consequently the constant shear stress concept was adopted in the form:

$$\tau = m \frac{\sigma_y}{\sqrt{3}}$$

Test results suggest that the surface of contact i.e. the friction interface between tube and roll groove can be divided into two equal zones as shown in FIGURE 3.10.

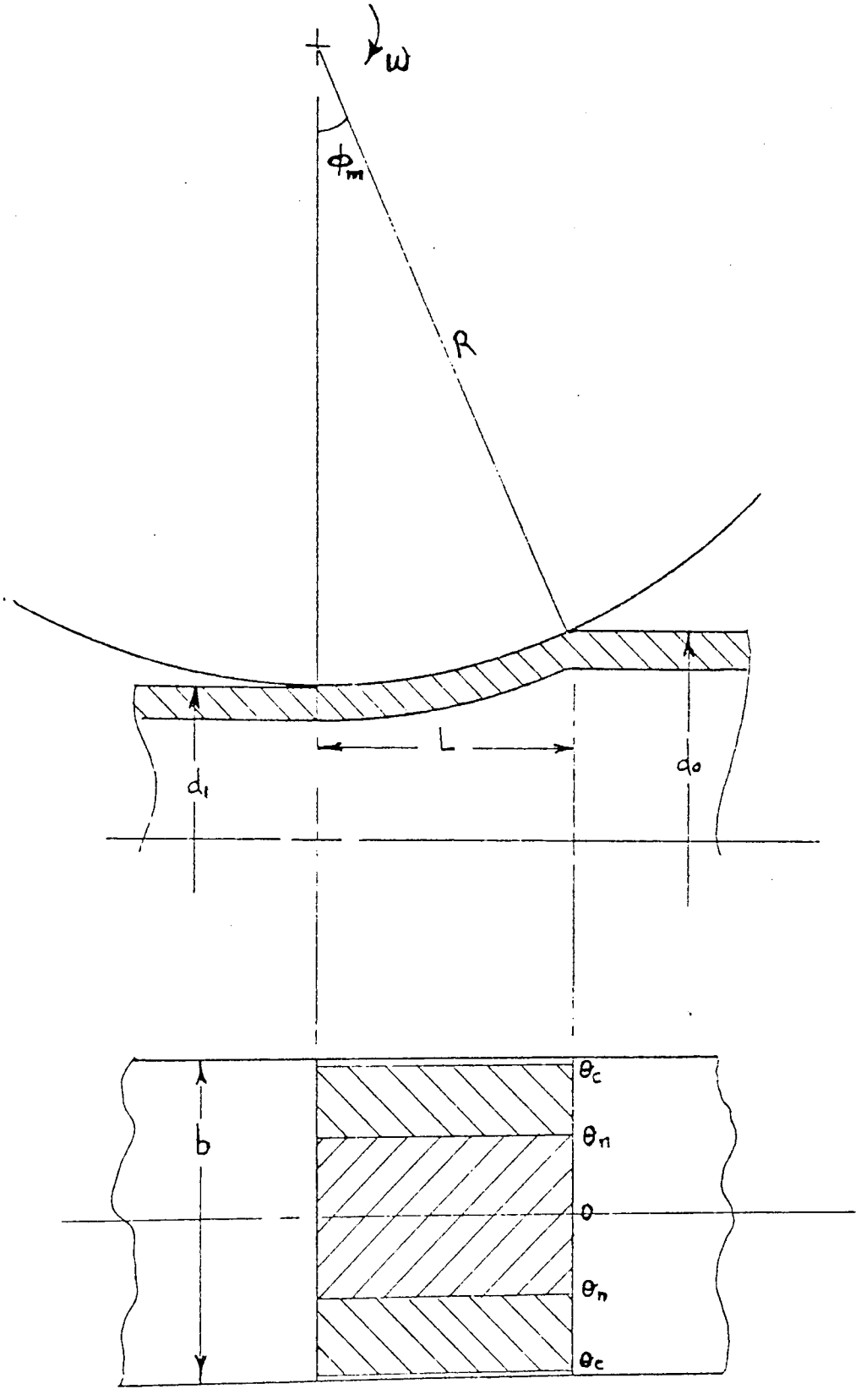

DIVISION OF TUBE-ROLL FRICTION INTERFACE
INTO TWO EQUAL ZONES

FIGURE 3.10

The first zone corresponds to the exit side of the deformation zone in flat rolling and has the limits:

$$\theta = 0 \quad \text{to} \quad \theta = \theta_n$$

where, approximately $\theta_n = \frac{\theta_c}{2}$

The second zone is bounded by θ_n and θ_c and corresponds to the entry zone in flat rolling.

As for homogeneous deformation the internal friction work W_{fi} can be stated as:

$$W_{fi} = \int_{\bar{\varepsilon}_m}^{\bar{\varepsilon}_A} \sigma_y \, d\varepsilon$$

and if the associated mean yield stress $\bar{\sigma}_{yf}$ is introduced:

$$W_{fi} = \bar{\sigma}_{yf}(\bar{\varepsilon}_A - \bar{\varepsilon}_m) = \bar{\sigma}_{yf}\bar{\varepsilon}_f$$

Assuming that the tube velocity U at a vertical plane through any point on the surface of contact is constant, and that U is proportional to ϕ, then:

$$U = U_o \left[1 + J \left(1 - \frac{\phi}{\Phi_m}\right) \right]$$

where J is the tube reduction ratio.

The tangential roll velocity can be written as $R_\theta . \omega$, noting

that from the groove geometry FIGURE 3.11:

$$R_\theta = R_r + r_g (1 - \cos \theta)$$

The relative velocity between the tube and the rolls V_r is:

$$V_r = V - U$$

The rate of external friction work in the first zone (1) is:

$$\dot{W}_{fe1} = 4 \int_s \tau \, V_r \, ds$$

Appropriate substitution and a double integration between 0 and ϕ_{m1} and 0 and θ_n gives:

$$\dot{W} = \frac{2}{\sqrt{3}} m_1 \bar{\sigma}_{yf} R_r r_g \phi_m \theta_c \left\{ \omega \left[R_r + r_g \left(1 - \frac{2 \sin \frac{\theta_c}{2}}{\theta_c}\right)\right] - U_o \left[1 + \frac{J}{2} \right] \right\}$$

where, for zone (1), $\tau = m_1 \dfrac{\bar{\sigma}_{yf}}{\sqrt{3}}$

Similarly for the second zone (2), with $\tau = m_2 \dfrac{\bar{\sigma}_{yf}}{\sqrt{3}}$

$$\dot{W} = \frac{2}{\sqrt{3}} m_2 \bar{\sigma}_{yf} R_r r_g \phi_m \theta_c \left\{ \omega \left(R_r + r_g \left[1 - \frac{2}{\theta_c} (\sin \theta_c - \sin \frac{\theta_c}{2}) \right] \right) - U_o \left[1 + \frac{J}{2} \right] \right\}$$

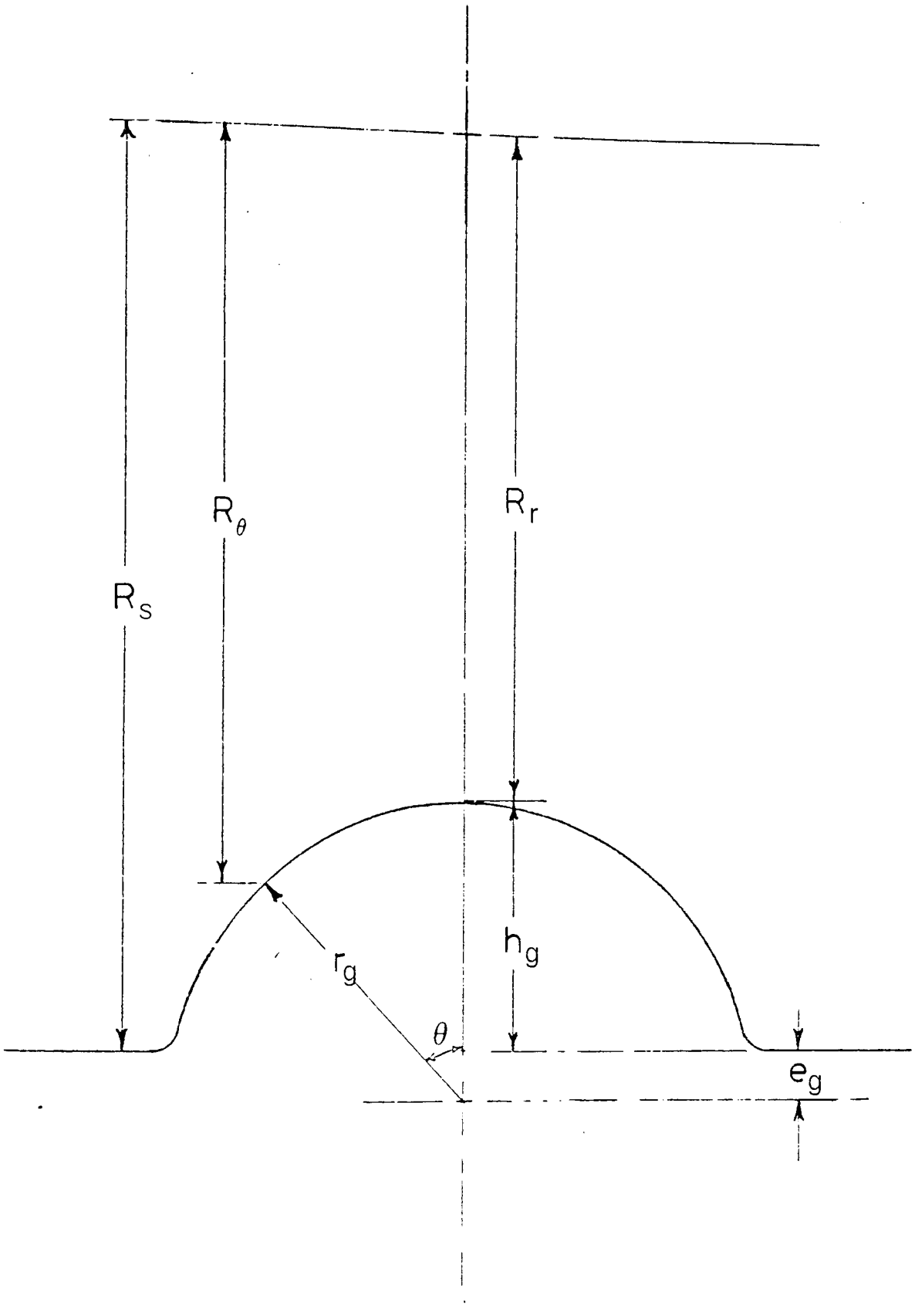

GEOMETRY OF GROOVE

FIGURE 3.11

Now the volume rolled per unit time $\dot{V}$ is $A_o U_o$ and

$U_o = \omega R_r$

$$\dot{V} = A_o R_r \omega$$

But

$$W_{fe} = \frac{\dot{W}_{fe}}{\dot{V}} = \frac{\dot{W}_{fe}}{A_o R_r \omega}$$

Since the total work of the external friction forces W_{fe} per unit volume is:

$$W_{fe} = W_{fe1} + W_{fe2}$$

appropriate substitution and noting that $U_o = \omega R_r$ gives:

$$W_{fe} = \frac{2}{\sqrt{3}} \frac{\bar{\sigma}_{yf} r_g^2 \phi_m \theta_c m_2}{A_o} \left\{ \left[1 + \frac{m_1}{m_2} \right] \left[1 - \frac{J R_r}{2 r_g} \right] - \frac{2}{\theta_c} \left[\sin \theta_c - \sin \frac{\theta_c}{2} \left(1 - \frac{m_1}{m_2} \right) \right] \right\} \qquad (3\ (i)\ 11)$$

Assuming no energy losses:

$$W_{fe} = W_{fi}$$

From the definition of the frictional strain $\bar{\varepsilon}_f$:

$$\bar{\varepsilon}_f = \frac{2}{\sqrt{3}} \frac{r_g^2 \phi_m \theta_c m_2}{A_o} \left\{ \left[1 + \frac{m_1}{m_2} \right] \left[1 - \frac{J R_r}{2 r_g} \right] - \frac{2}{\theta_c} \left[\sin \theta_c - \sin \frac{\theta_c}{2} \left(1 - \frac{m_1}{m_2} \right) \right] \right\} \qquad (3(i)\ 12)$$

The frictional stress ratio $\frac{m_1}{m_2}$ can accommodate any sticking/sliding friction combination enabling either lower or upper bound solutions to be considered.

TOTAL MEAN ROLL PRESSURE (p_m):

By definition the apparent strain $\bar{\varepsilon}_A$ is:

$$\bar{\varepsilon}_A = \bar{\varepsilon}_m + \bar{\varepsilon}_f$$

and

$$p_m = p_h \left[\frac{\bar{\varepsilon}_A}{\bar{\varepsilon}_m} \right]$$

$$p_m = p_h \left[1 + \frac{\bar{\varepsilon}_f}{\bar{\varepsilon}_m} \right]$$

ROLL SEPARATING FORCE (R.S.F.):

The product of the total mean roll pressure and the horizontal projection of the area of contact on each roll gives the roll separating force.

ROLLING TORQUE (T):

To evaluate the rolling torque Haleem introduced the concept of the lever arm as used in flat rolling. Here the roll separating force is assumed to act at some distance from the roll axis. This distance, the lever arm, is generally expressed as a ratio of the length of the arc of contact. For hot flat rolling the ratio is usually assumed to be 0.5. Haleem then considered various definitions of the arc of contact length and for round to oval passes employed a mean value for the ratio of 0.66.

His new theoretical approach for estimating the mean roll pressure based on the strain energy of deformation compared favourably with his test results, and showed an improvement on the equilibrium approach used by Russian workers. Furthermore the appropriate choice of the shear factor m, generally in the range $0.55 \leqslant m \leqslant 1.0$, enabled his theory

to be satisfactorily applied to tube sinking under various frictional conditions. However his determination of the rolling torque using the lever arm concept was shown to be only of limited value and somewhat unreliable in application.

Haleem concluded his theoretical studies by discussing various approaches for the prediction of the change in wall thickness for tube sinking, stating that the predictions of all the theories did not differ greatly for $\frac{D}{t}$ ratios above 5.

3 (i).2. PREVIOUS MANDREL ROLLING THEORIES

Four mandrel rolling theories will be examined in this section. Two of these theories, by Vatkin and Druyan (33) 1966, and Fomichev and Kirichenko (62) 1968 are Russian in origin and were discussed in detail by Cole (35). Only a brief discussion of these two theories will therefore be presented here,whilst the other two theories by Okamoto and Hayashi (38) and by Labib (43) are of more recent origin and will be examined in more detail.

3 (i).2.1. VATKIN AND DRUYAN (33) 1966

Vatkin and Druyan analysed the general case of rolling a tube on a circular mandrel through a non-circular groove. They considered the equilibrium of longitudinal forces acting on a transverse element of tube in the deformation zone FIGURE 3.12 and the following differential equation was derived:

$$\frac{\partial \sigma}{\partial x} + \left(\sigma_x - p\right)\frac{1}{t}\frac{\partial t}{\partial x} + \frac{1}{t}\left(\tau + \tau_m\right) = 0 \qquad (3(i)13)$$

In the above equation the tube thickness (t) was assumed to be small compared with 2 r_m, where r_m is the mandrel radius. Cole (35) pointed out that this assumption was not justified since the mandrel rolling process is generally employed as a "breaking-down" sequence, the ingoing "tube" being a relatively thick pierced bloom.

The whole of the region of deformation was assumed to be homogeneous and the authors used a yield criterion in the form:

$$p - \sigma_x = \beta \sigma_y$$

The frictional conditions were:

$$\tau = \pm \mu \beta \sigma_y$$

$$\tau_m = \pm \mu_m \beta \sigma_y$$

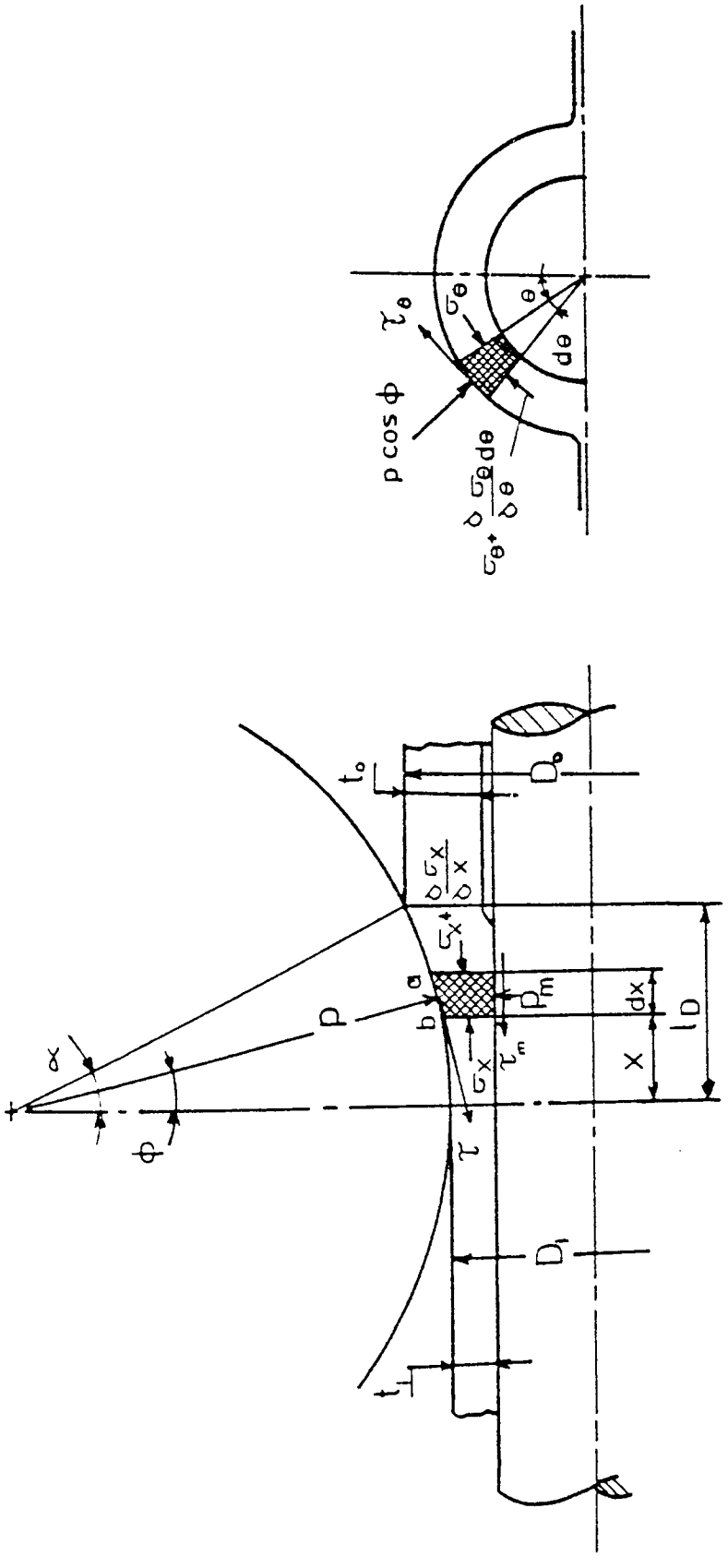

Forces acting on an element in the deformation zone (From Vatkin and Druyan (33))

FIGURE 3.12

Assuming that the tube velocity is equal to the mandrel velocity at the neutral section, the positive sign in the above expressions applies to the entry zone and the negative sign to the exit zone.

Appropriate substitutions from these equations into equation (3.12) gives:

$$\frac{\partial p}{\partial x} = \frac{\beta\ \sigma_y}{t}\ \frac{\partial t}{\partial x}\ \mp \left(\mu + \mu_m\right)\frac{\beta\ \sigma_y}{t} \qquad (3(i)14)$$

This differential equation was solved by deducing expressions for the tube thickness variation through the pass and around the groove, replacing the arc of contact with a chord and the assumption of a parabolic distribution of normal pressure across the width of the roll groove. Thus the following relationships were obtained:

For the entry zone:

$$p' = \beta\ \sigma_y \left\{ \left[1 - \left(\frac{2\theta}{\pi}\right)^2\right] - \left(1 - \frac{\mu + \mu_m}{\Delta t}\, l_x\right) \ln \frac{to,\ \theta}{t_{x,\ \theta}} \right\} \qquad (3\ (i)15)$$

For the outlet zone:

$$p'' = \beta\ \sigma_y \left\{ \left[1 - \left(\frac{2\theta}{\pi}\right)^2\right] + \left(1 + \frac{\mu + \mu_m}{\Delta t}\, l_x\right) \ln \frac{t_{x,\ \theta}}{t_{1,\ \theta}} \right\} \qquad (3(i)16)$$

For a given set of conditions μ and μ_m were assumed to be constant. The mean specific roll pressure was then presented as:

$$p_{av} = \frac{\beta \sigma_y}{b_{av}} \left\{ \frac{\pi}{3} (t_o + W) - (1 - \frac{\mu + \mu_m}{t} l_D) \left[W(\ln t_o - \frac{t_o}{\Delta t} \ln t_o + \frac{t_1}{\Delta t} \ln t_1) + t_{av} + d_m \right] \right\} \qquad (3(i)17)$$

where b = average projected width of the region of contact,

W = tube thickness at the exit plane + mandrel dia.,

$t_{av} = \frac{1}{2}(t_o + t_1)$,

l_D = length of the region of deformation.

Similar equations were then presented for conditions in which the velocity of the mandrel was either always greater or always less than the velocity of the tube.

Vatkin and Druyan assumed that the peripheral angle of contact between tube end rolls was constant at $\pm\frac{\pi}{2}$ throughout the deformation zone i.e. full contact at any position along pass. This is not the case, since the peripheral angle of contact changes from a minimum at the entry plane to a maximum at the exit plane. Furthermore, the assumption of

a parabolic pressure distribution round the groove was at variance with the stated constant frictional conditions.

The authors stated that good agreement existed between theory and experiment, although Cole (35) noted that the yield stress values quoted appeared to be in error by a factor of ten.

Throughout the paper no definition was provided for the factor β and no values assigned to μ and μ_m. Moreover the non-dimensional equation for the specific pressure (p_{av}) is in error since it includes the terms ln t_o and lnt_1.

3(i).2.2 FOMICHEV AND KIRICHENKO (62) 1968

Fomichev and Kirichenko also considered the equilibrium of forces in the longitudinal direction acting on an element in the deformation zone for the mandrel pass shown in FIGURE 3.13. The following assumptions were made:

1. The groove shape was considered to be circular,
2. The arc of contact was replaced by a chord,
3. The elemental areas associated with the axial stresses, σ_x and $(\sigma_x + d\sigma_x)$ were approximated to a rectangle of area $\frac{1}{2}(D_x - d_m)$ by $\frac{1}{2}(\frac{1}{2}Dd\theta + \frac{1}{2}d_m d\theta)$,
4. The radial stress, σ_r, and the longitudinal stress, σ_x, were again considered to be principal stresses with the yield criterion as:

$$\sigma_r - \sigma_x = k^1$$

where k^1 is a function of the yield stress σ_y where:

$$k^1 = \beta\,\sigma_y \quad \text{and} \quad \frac{2}{\sqrt{3}} \geqslant \beta \geqslant 1$$

The resulting differential equation is of the form:

$$\frac{d\sigma_x}{dD_x} + \frac{2\sigma_x D_x}{(D_x^2 - d_m^2)} - \frac{2D_x}{(D_x^2 - d_m^2)}(p\cos\theta\tan\phi \mp \tau)\frac{\cos\theta}{\tan\phi}$$

$$\pm \frac{2\tau_m d_m}{(D_x^2 - d_m^2)}\frac{\cos\theta}{\tan\phi} = 0 \qquad (3.(i)18)$$

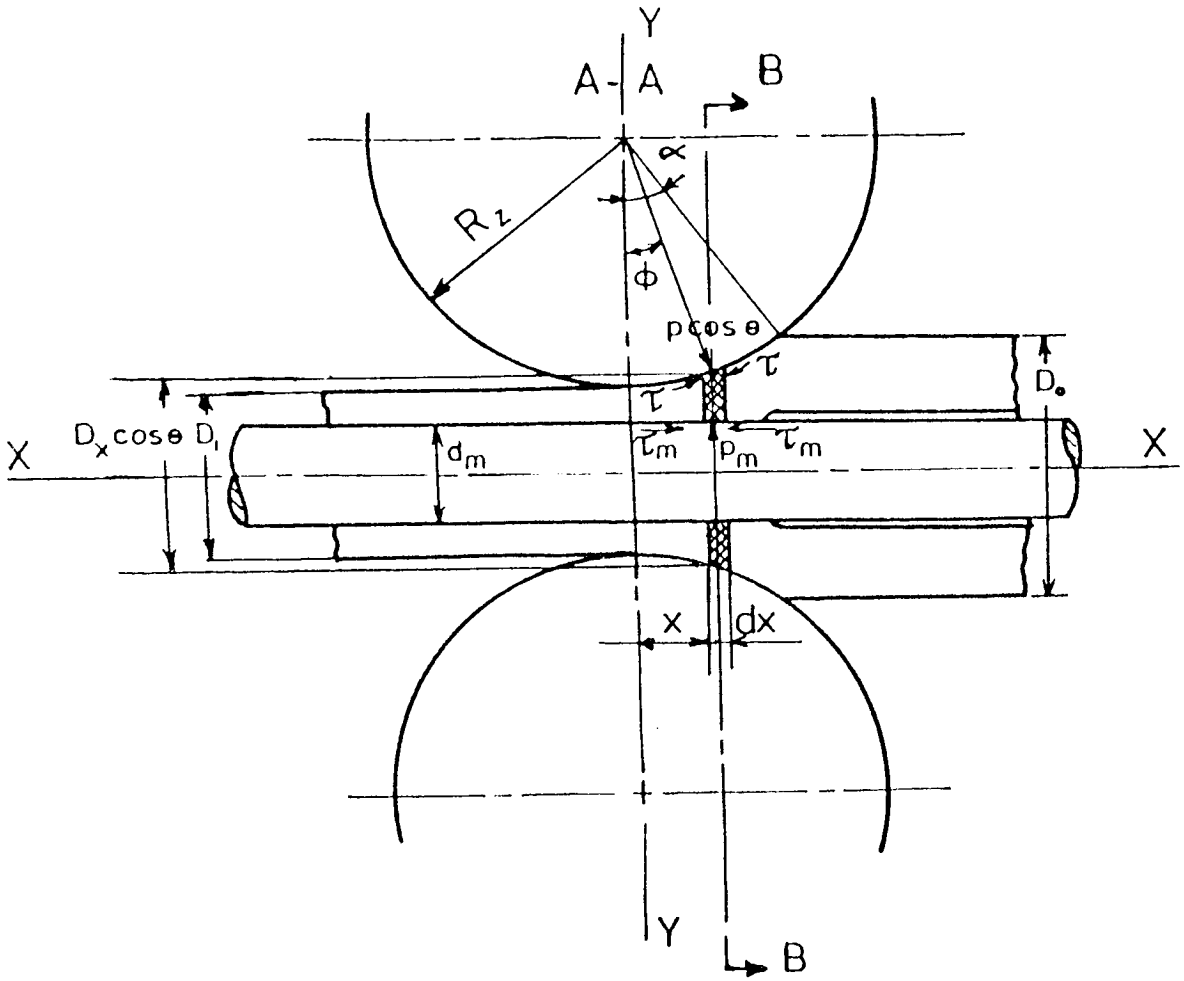

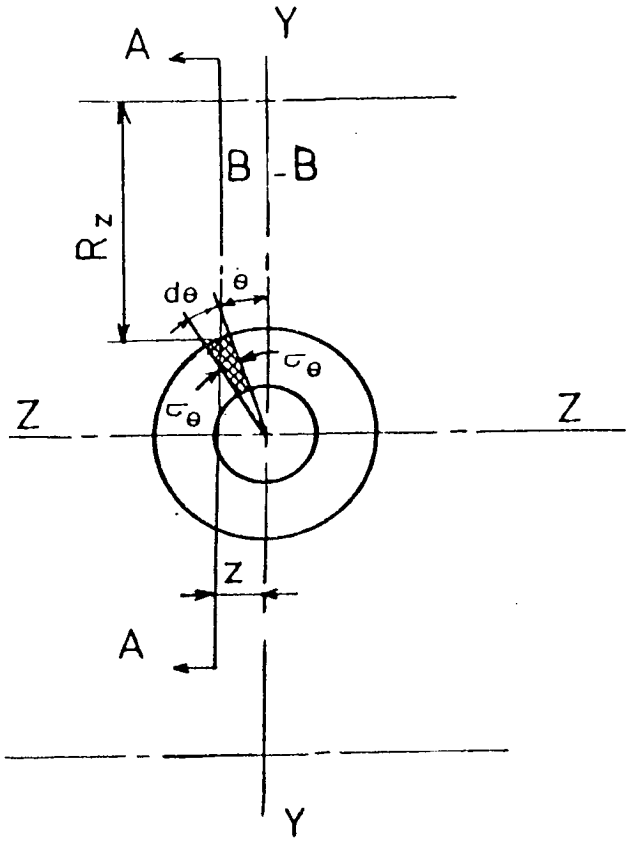

Forces acting on an element in the deformation zone.
(From Fomichev and Kirichenko (62))

Assuming a Coulomb type of friction, constant over the whole of the deformation region, the solution of the above equation substituted in the yield criterion gave the following relationships for the distrubution of normal roll pressure in the entry zone (p^1) and the exit zone (p^{11}):

$$p^1 = \frac{k^1 \cos\phi}{\cos^2\theta\cos\phi + \sin^2\theta + \mu\cos\theta\sin\phi}\left[\frac{A}{1-A} + \left(\frac{q_o}{k^1} - \frac{A}{1-A}\right)\left(\frac{D_o^2 - d_m^2}{D_x^2 - d_m^2}\right)^{1-A}\right] \qquad (3(i)19)$$

$$p^{11} = \frac{k^1 \cos\phi}{\cos^2\theta\cos\phi + \sin^2\theta - \mu\cos\theta\sin\phi}\left[\frac{A}{1-A} + \left(\frac{q_1}{k^1} - \frac{A}{1-A}\right)\left(\frac{D_1^2 - d_m^2}{D_x^2 - d_m^2}\right)^{1-A}\right] \qquad (3(i)20)$$

where $A = \frac{\cos\theta}{\tan\phi}\left[\frac{\cos\theta\sin\phi \mp \mu\cos\phi}{\cos^2\theta\cos\phi \pm \sin^2\theta \pm \mu\cos\theta\sin\phi} \mp \mu_m\right]$

q_o is the axial stress at entry,

q_1 is the axial stress at exit.

If the differential equation is solved on the basis of a constant shear stress type of friction of the form τ = constant, the pressure distribution becomes:

$$p^1 = \frac{\cos\phi}{\cos^2\theta\cos\phi + \sin^2\theta}\left[k^1 - \tau\cos\theta\tan\phi + \frac{N}{M} - \left(\frac{q_o}{k^1} - \frac{N}{M}\right)\cdot\left(\frac{D_o^2 - d_m^2}{D_x^2 - d_m^2}\right)^M\right] \qquad (3(i)21)$$

$$p^{11} = \frac{\cos\phi}{\cos^2\theta\cos\phi + \sin^2\theta}\left[k^1 + \tau\cos\theta\tan\phi + \frac{N}{M} - \left(\frac{q_1}{k^1} - \frac{N}{M}\right)\cdot\left(\frac{D_1^2 - d_m^2}{D_x^2 - d_m^2}\right)^M\right] \qquad (3\ (i)22)$$

where $M = 1 - \dfrac{\cos^2\theta\ \cos\phi}{\cos^2\theta\cos\phi + \sin^2\theta}$

$$N = \frac{\cos\theta}{\tan\phi}\left(\frac{k^1\cos\theta\sin\phi \mp \tau\cos^2\theta\sin\phi\tan\phi \mp \tau \mp \tau_m\frac{d_m}{D_{av}}}{\cos^2\theta\cos\phi + \sin^2\theta}\right)$$

D_{av} is the mean diameter of the tube in the region of deformation.

These theoretical predictions compared well with the experimental results of Vatkin (63), although Cole (35) expressed some doubt on Fomichev and Kirichenko's deductions of the normal roll pressure distribution based on Coulomb friction generally indicating higher values than those based on a constant shear stress criteria. Furthermore, no definition was provided for the shear stress constant.

The simplified geometry of the pass meant that the variation of tube wall thickness around the roll groove was ignored, an unsatisfactory assumption in the mandrel rolling process where the thickness varies considerably around the groove.

Finally no consideration was given to the peripheral angle of contact between the tube and roll or to the contact area.

3(i).2.3. OKAMOTO AND HAYASHI (38) 1970

In this case Okamoto and Hayashi were concerned with the theoretical prediction of overfilling or underfilling of a given groove shape in the mandrel rolling process.

As shown in FIGURE 3.14 they divided the deformation zone into two areas, the groove side where the tube inner surface is in contact with the mandrel, and the flange side, toward the shrouds, where the tube inner surface is free. In the groove side the tube is deformed under outside pressure, inside pressure and axial compression,whilst in the flange side the tube is deformed under outside pressure and axial tension. All stresses were assumed uniform and mean values of thicknesses taken.

Okamoto's shape or deformation factor ν was utilised in their theoretical treatment, which when combined with the volume constancy condition i.e. $\Phi_1 + \Phi_r + \Phi_\theta = 0$ was defined as:

$$\nu = 0.5 + \frac{\Phi_\theta}{\Phi_1}$$

where $\Phi_1, \Phi_r, \Phi_\theta$ are the longitudinal , radial and circumferential natural strains respectively.

The constant in the above definition was chosen so that in simple tension, or compression, where $\nu = 0$,

$$\Phi_\theta = -0.5\Phi_1.$$

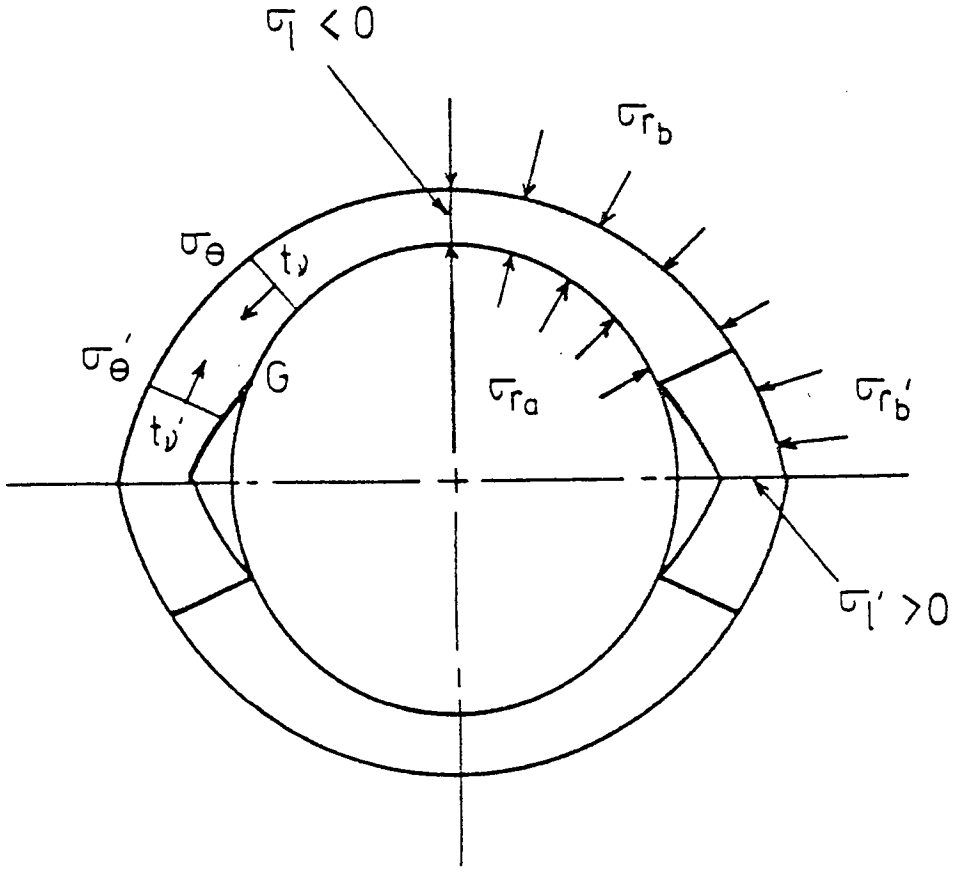

Stress distribution in the deformation zone (From Okamoto and Hayashi (38))

FIGURE 3.14

The deformation factor ν is determined from the deformation strains and is purely for simplying the calculation of the stresses.

Okamoto and Hayashi then derived fundamental equations for the deformed tube in the groove and flange areas as follows:

For the groove side:

- the deformation factor ν is defined as:

$$\nu = 0.5 + \frac{\Phi_\theta}{\Phi_1}$$

- the volume constancy condition is:

$$\Phi_1 + \Phi_\theta + \Phi_r = 0$$

where Φ_1, Φ_θ and Φ_r are the longitudinal, tangential and radial strains respectively.

- stress-strain relationships:

$$\frac{\sigma_1 - \sigma_\theta}{\Phi_1 - \Phi_\theta} = \frac{\sigma_\theta - \sigma_r}{\Phi_\theta - \Phi_r} = \frac{\sigma_r - \sigma_1}{\Phi_r - \Phi_1}$$

- von-Mises flow condition:

$$(\sigma_1 - \sigma_\theta)^2 + (\sigma_\theta - \sigma_r)^2 + (\sigma_r - \sigma_1)^2 = 2k_f^2$$

i.e. $(k_f)^2 \equiv (\sigma_y)^2$

From the above basic relationships, the following equations can be obtained:

- Equilibrium equation in the radial direction:

$$\sigma_{r_b} - \sigma_{r_a} = \int_{r_a}^{r_b} (\sigma_\theta - \sigma_r) \frac{dr}{r}$$

$$= \frac{k_f}{\sqrt{3}} \frac{2\nu}{\sqrt{\nu^2 + 0.75}} \ln \frac{r_b}{r_a}$$

- Equation of the tangential stress:

$$\sigma_\theta = \frac{k_f}{\sqrt{3}} \frac{2\nu}{\sqrt{\nu^2 + 0.75}} + \sigma_r$$

- Equation of the axial stress:

$$\sigma_1 = \frac{k_f}{\sqrt{3}} \frac{1.5 + \nu}{\sqrt{\nu^2 + 0.75}} + \sigma_r$$

- Approximate equation for the mean radial stress:

$$\sigma_r = \tfrac{1}{2}(\sigma_{r_b} + \sigma_{r_a})$$

Similarly for the flange side:

$$\nu' = 0.5 + \frac{\Phi_\theta'}{\Phi_1'}$$

$$\Phi_1' + \Phi_\theta' + \Phi_r' = 0$$

$$\sigma_{r_b}' = \frac{k_f}{\sqrt{3}} \frac{2\nu'}{\sqrt{\nu'^2 + 0.75}} \cdot \ln \frac{r_b'}{r_a'}$$

$$\sigma_\theta' = \frac{k_f}{\sqrt{3}} \frac{2\nu'}{\sqrt{\nu'^2 + 0.75}} + \sigma_r'$$

$$\sigma_1' = \frac{k_f}{\sqrt{3}} \frac{1.5 + \nu'}{\sqrt{\nu'^2 + 0.75}} + \sigma_r'$$

$$\sigma_r' = \tfrac{1}{2}\sigma_{r_b}'$$

The compatibility equations between the groove side and the flange side are:

For the axial elongation:

$$\Phi_1 = \Phi_1'$$

For the tangential stress:

$$\sigma_\theta = \xi \, \sigma'_\theta \qquad \xi = (t'_\nu / t_\nu)$$

The authors then stated that the above fifteen equations in seventeen unknowns could be solved by trial and error by assuming any two unknowns and solving the fifteen simultaneous equations.

Overfilling or underfilling of the material in the groove could be assessed by assuming Φ'_θ and that $\Phi'_r = 0$, from which Φ'_1 and Φ_1 are obtained. The value of Φ'_θ is readjusted until $\Phi'_1 = \Phi_1$, completion of the remaining calculations enabling the balance of the longitudinal tension, σ^1_1, and longitudinal compression, σ_1, to be examined from the equation:

$$f = \sigma_1 A + \sigma^1_1 A^1$$

If $f < 0$, the tube overfills the groove, while if $f > 0$ the tube underfills. When $f = 0$ the tube just fills the groove shape.

Friction was ignored in their analysis; a fundamentally serious omission in the mandrel rolling process.

3(i).2.4 LABIB (43) 1982

In his preamble Labib commented on the limitations of the equilibrium method where the influence of the frictional shear stresses is ignored in assigning the principal stresses to the tangential, radial and longitudinal directions. The analysis was completed by substitution in an appropriate yield criterion. He noted that although this approach is quite satisfactory for cold forming with the associated low frictional stresses, hot forming, where sticking friction generally prevails produces a less successful conclusion.

Labib continues by proposing the energy method as a more realistic analysis for assessing the average roll pressure for the sticking friction condition. A brief summary of his theoretical analysis now follows:

The work done per unit volume of the rolled tube is considered to be the sum of the following components:

1. Work of homogeneous deformation, W_h, which represents the minimum possible work required to change the tube shape.

2. Redundant work, which is the work lost due to unnecessary internal shearing of the tube material produced by the constraints imposed on the material flow. Two forms of redundant deformation can be recognized in the mandrel rolling process:

a) Redundant deformation due to the material shearing as it enters the deformation zone,

b) Redundant deformation due to longitudinal shearing of the material as a result of longitudinal velocity differences at the inner and outer tube surfaces.

Only the former type of redundant deformation is significant and need be accounted for.

3. Frictional work, which is the work done to overcome friction between tube and rolls and between tube and mandrel.

4. External work supplied by the applied front and back tensions.

The total work done by the rolls per unit volume, W_t, can be written as:

$$W_t = W_h + W_r + W_f$$

where W_h is the homogeneous work per unit volume,

W_r is the redundant work per unit volume,

W_f is the work done against friction per unit volume.

In the case of rolling with applied front and back tensions, the total work done per unit volume, W_T is:

$$W_T = W_t + W_{a,b}$$

where $W_{a,b}$ is the work done by the applied front and back tensions.

The peripheral angle of contact, Ψ_c, at any angle of angle ϕ ,and the associated contact area between tube and rolls is then assessed for the three groove shapes shown in FIGURES 3.15 and 3.16.

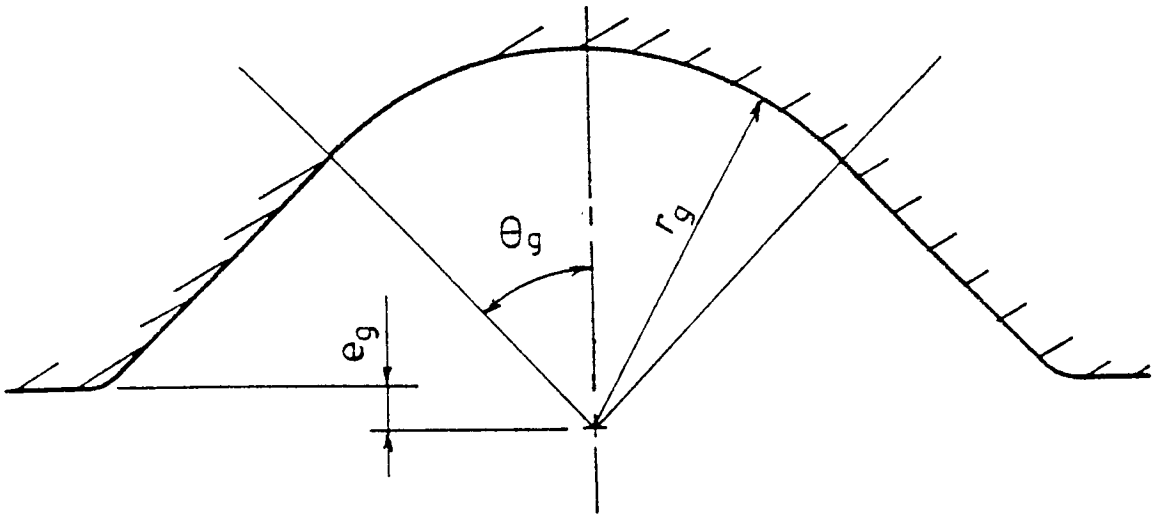

Groove(B)

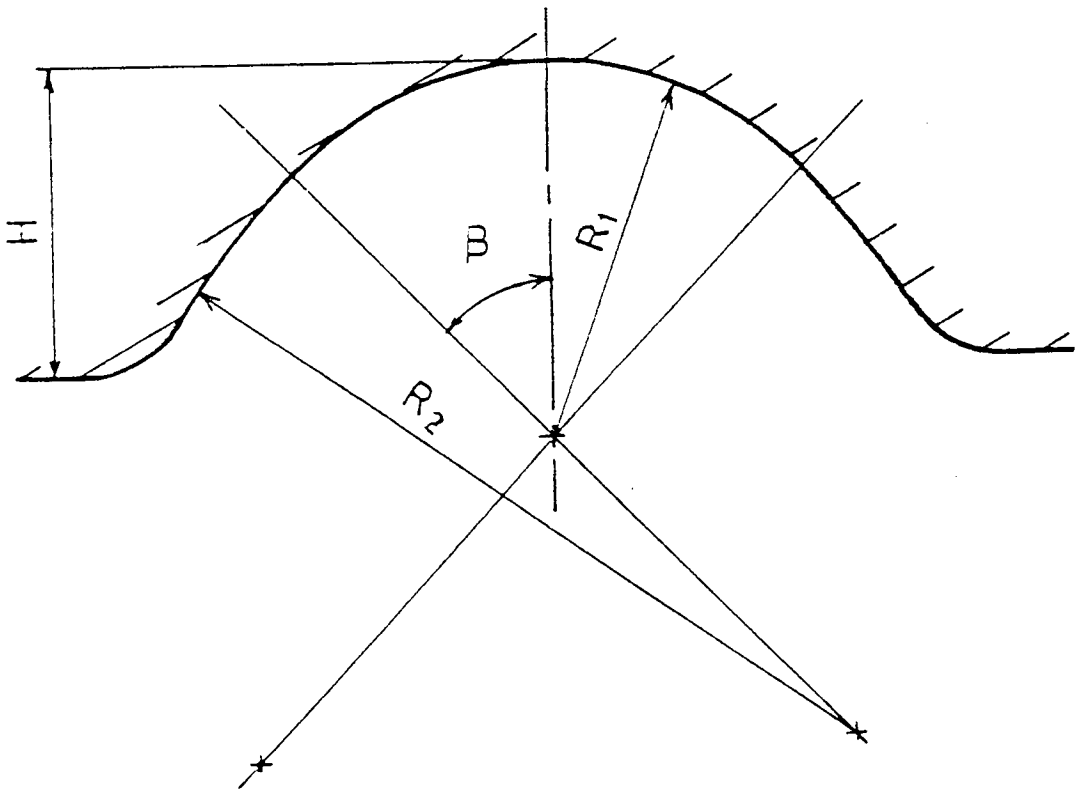

Groove(C)

SOME TYPES OF PASS CONFIGURATIONS

FIGURE 3.15

FIGURE 3.16

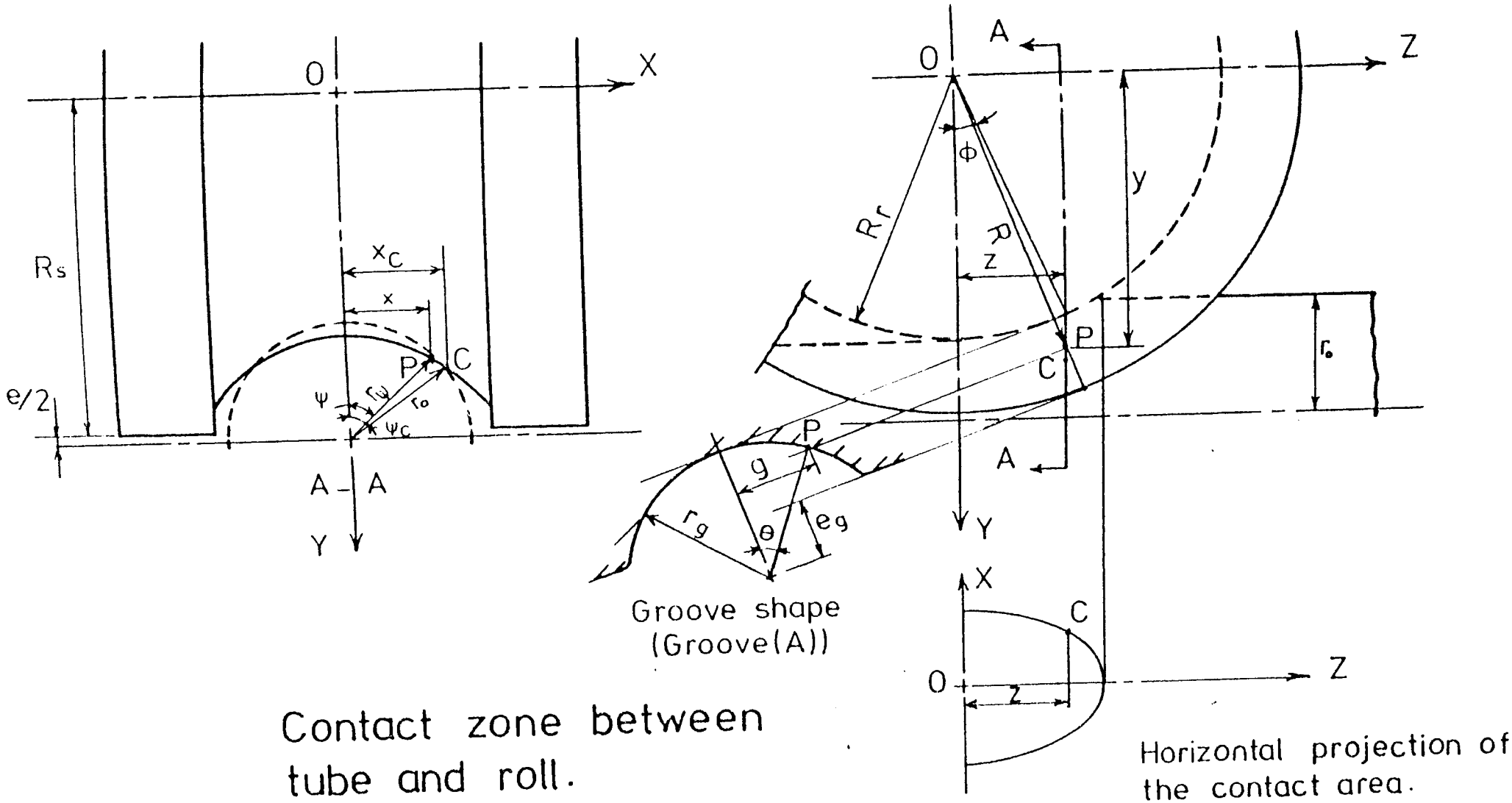

Groove shape
(Groove(A))

Contact zone between tube and roll.

Horizontal projection of the contact area.

Peripheral angle of contact, Ψ_c , at any angle of contact ϕ :

Ignoring lateral spread of the tube material, contact between tube and groove commences when the instantaneous groove radius, r_ψ , at any angle of contact ϕ, equals the tube radius r_o, as shown in FIGURE 3.16.

The following equation can be written for the contact point C :

$$\cos \theta_c = \frac{1}{r_g} (R_s - R_c + e_g)$$

where R_c is the distance of point C from the roll centre O.

From the shown geometry:

$$g = r_g \sin \theta_c = r_o \sin \Psi_c$$

$$y_c = (R_s + \frac{e}{2}) - r_o \cos \Psi_c$$

$$R_c^2 = z_c^2 + y_c^2$$

Since $z = R_r \sin\phi$

then $R_c^2 = R_r^2 \sin^2\phi + y_c^2$

Rearranging and substituting gives:

$$(C^2 - r_o{}^2 F) \cos{}^2\Psi_c - 2D.C. \cos\Psi_c +$$

$$(D^2 - r_g{}^2.F + r_o{}^2.F) = 0 \qquad (3(i)23)$$

where $A = R_r{}^2 \sin{}^2\phi$

$$B = \left[(R_s + e_g)^2 - (R_s + \frac{e}{2})^2 + r_g{}^2 - r_o{}^2\right]$$

$$C = 2r_o\,(R_s + \frac{e}{2})$$

$$F = 4\,(R_s + e_g)^2$$

$$D = A - B$$

The equation (3(i)23) is a second degree equation in $\cos\Psi_c$, which can be solved to give the peripheral contact angle Ψ_c at the corresponding contact angle ϕ.

Contact area between tube and rolls:

With reference to FIGURE 3.16., for any arbitrary point P (x,y,z) on the roll groove surface:

$$y^2 + z^2 = R^2 \text{ or } R = (y^2 + x^2)^{\frac{1}{2}}$$

$$\cos\theta = \frac{1}{r_g}\,(R_s - R + e_g)$$

$$x = g = r_g \sin\theta$$

$$x^2 = r_g{}^2 \sin^2\theta$$

Appropriate substitution gives:

$$x^2 + \left[b - (y^2 + z^2)^{\frac{1}{2}} \right]^2 = r_g^{\,2} \qquad (3(i)24)$$

where $R_s + e_g = b$

Noting that the elemental length, dL, of the contact curve between tube and rolls is:

$$dL = (dx^2 + dy^2)^{\frac{1}{2}}$$

Further substitution, etc., gives:

$$dL = \left\{ \frac{x^2 \left[1 + \frac{z^2}{\left[b-(r_g^{\,2}-x^2)^{\frac{1}{2}} \right]^2 - z^2} \right]}{(r_g^{\,2} - x^2} + 1 \right\}^{\frac{1}{2}} dx \qquad (3(i)25)$$

To obtain the contact area between tube and roll, equation (3.24) is integrated twice, first with respect to x between limits $x = 0$ and $x_c = r_o \sin \Psi_c$, and secondly with respect to z between limits $z = 0$ and $z = R_r \sin\phi_m$, where ϕ_m is the maximum angle of contact which can be found from the geometry of tube and groove as:

$$\cos \phi_m = 1 - \frac{r_o - (r_g - e_g) - e/2}{R_r} \qquad (3(i)26)$$

Due to the complex nature of the derived equations numerical methods had to be employed to produce a solution.

Horizontal projection of the contact area:

By noting the co-ordinates of any point in the XOZ plane FIGURE 3.16 and appropriate substitution in the equation of the contact curve, the horizontal projection of the contact area can be determined. Again, because of the complexity of the solution numerical methods had to be employed.

Work of homogeneous deformation W_h:

Considering the true stress curve shown in FIGURE 3.17., the increment of plastic work per unit volume required to deform the material is:

$$dW = \sigma_y \, d\varepsilon$$

The total work per unit volume is equal to the area under the true stress strain curve for the appropriate strain ε ,

$$W = \int_0^{\varepsilon} \sigma_y \, d\varepsilon$$

Neglecting the rotation of the axes of strain increments in mandrel tube rolling, the work of homogeneous deformation can be written as:

$$W_h = \bar{\sigma}_y \quad \bar{\varepsilon}_h$$

where $\bar{\sigma}_y$ is the mean yield stress of the material corresponding to strain $\bar{\varepsilon}_h$.

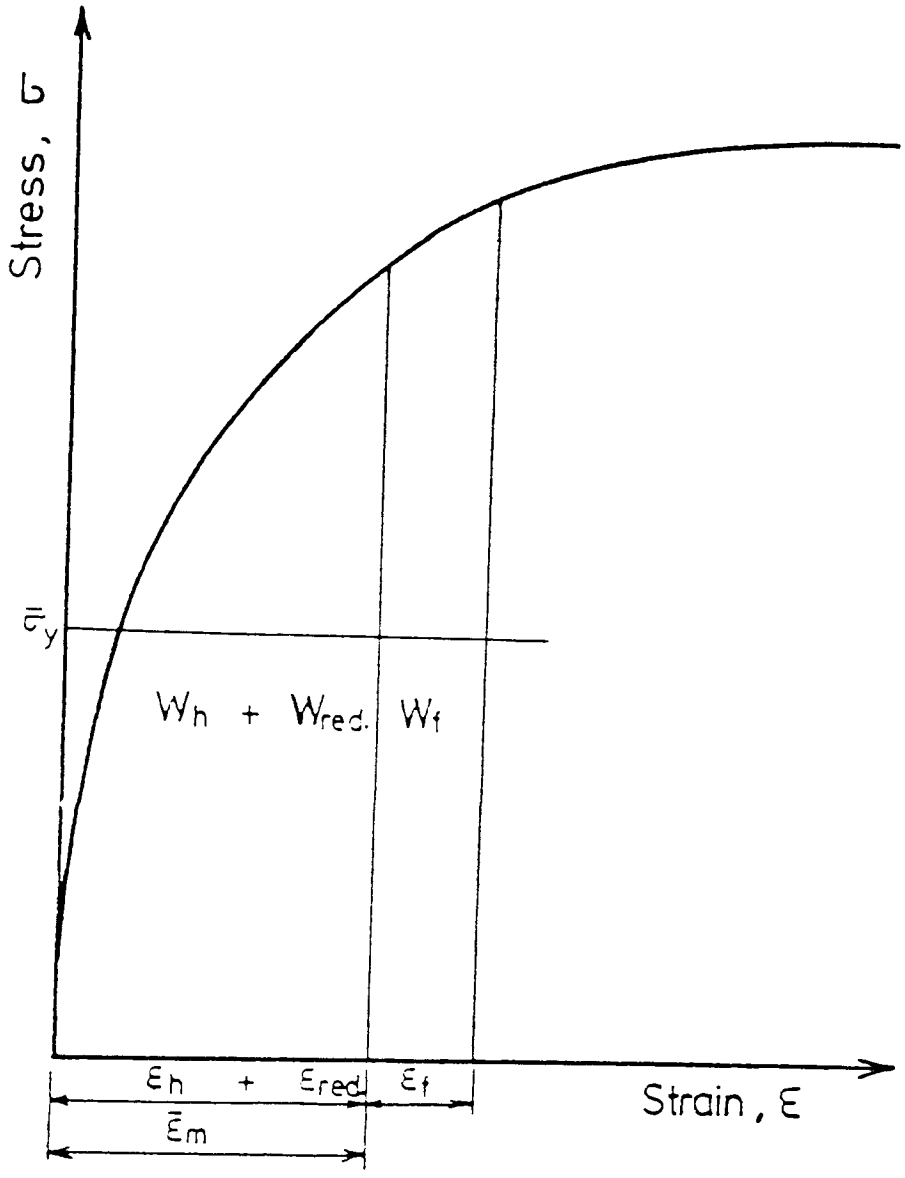

Total work of deformation.

FIGURE 3.17

Redundant work:

Only the redundant work caused by the shearing of the material as it enters the deformation zone will be considered. Making similar assumptions to that of Haleem and with reference to FIGURE 3.18, the mean tube linear velocity can be expressed as:

$$U_o = U_1 - a\,\phi$$

where "a" is a constant determined from the conditions at the entry plane.

From the volume constancy condition with appropriate substitutions:

$$U = \frac{U_o}{1-J}\left[1 - \frac{J\phi}{\phi_m}\right] \qquad (3(i)27)$$

where J is the tube reduction ratio

By assuming that the transverse section through AR is a line of velocity discontinuity, then, for any point on that line, the velocity discontinuity Δv is:

$$\Delta v = v \cos\alpha\,, \qquad \text{where } v = \frac{U}{\sin\alpha}$$

The velocity discontinuity Δv gives rise to shear of maximum resistance τ within the deformed material, where, from the von Mises' yield criterion:

$$\tau = \frac{\sigma_y}{\sqrt{3}}$$

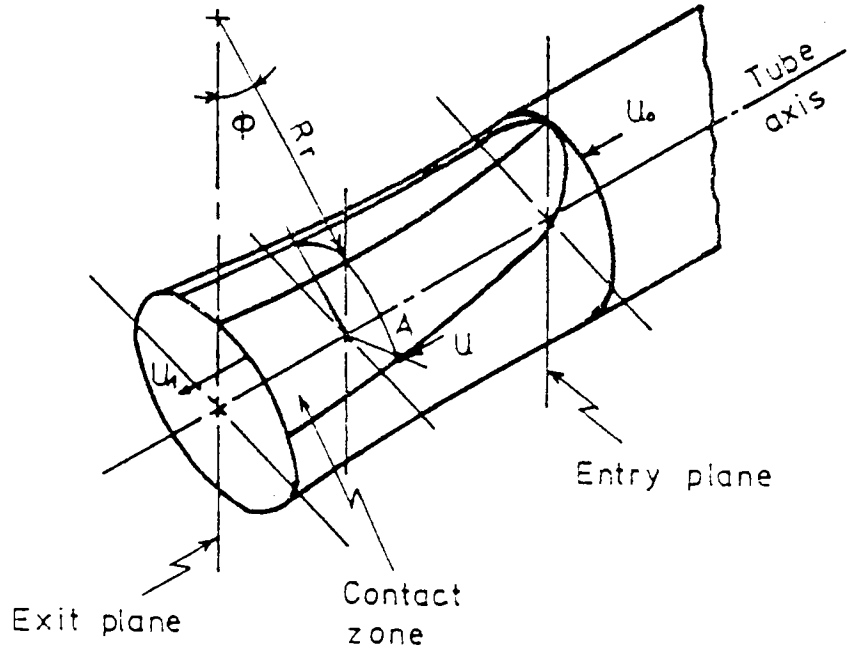

(a) Contact zone between tube and roll.

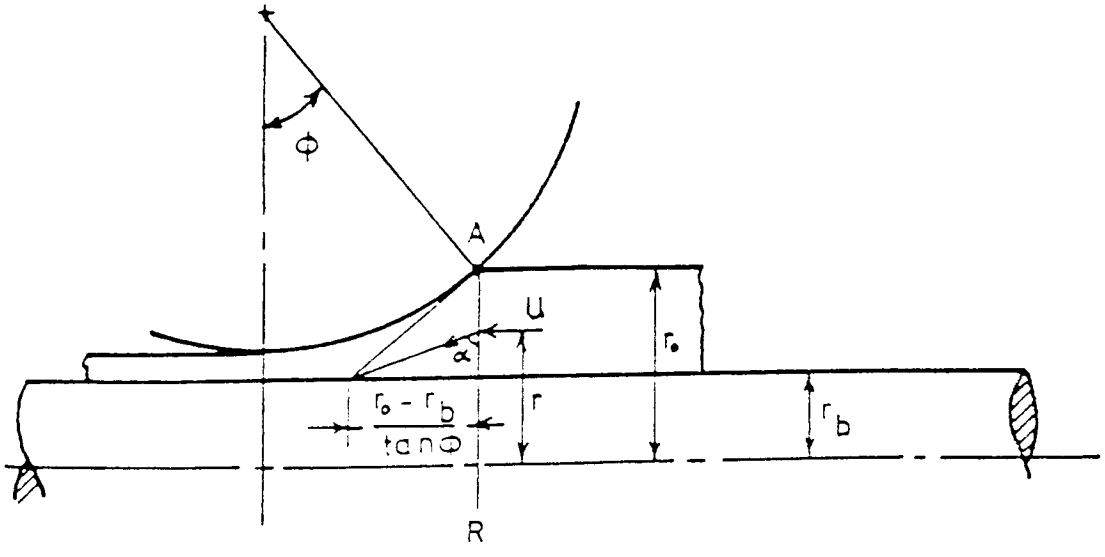

(b) Section passing through point A and tube axis.

Determination of redundant work.

FIGURE 3.18

The total redundant work per unit time is found by first integrating the shear stress times the velocity discontinuity over the line R i.e. r_b to r_o and subsequently integrating from ϕ_o to ϕ_m:

$$\dot{W}_{\substack{r/unit\\length}} = \int_R \tau . \Delta v . dr$$

$$\dot{W}_{\substack{r/unit\\length}} = \frac{\bar{\sigma}_y}{\sqrt{3}} \frac{U_o}{1-J} \left[1 - \frac{J\phi}{\phi_m}\right] \frac{\tan\phi}{2} (r_o - r_b)$$

Now $$\dot{W}_r = \int_o^{\phi_m} \frac{\dot{W}}{\text{unit length}}$$

$$= \frac{\bar{\sigma}_y}{2\sqrt{3}} \frac{U_o}{1-J} (r_o - r_b) R_f \frac{\phi_m^2}{6} \left[3 - 2J\right]$$

$$W_r = \frac{\dot{W}_r}{A_o U_o} = \frac{\bar{\sigma}_y}{12\sqrt{3}} \frac{(r_o - r_b)}{A_o (1-J)} . R_r . \phi_m^2 \quad (3-2J)$$

But W_r also equals $\bar{\varepsilon}_{red} . \bar{\sigma}_y$:

$$\bar{\varepsilon}_{red} = \frac{(r_o - r_b)}{12\sqrt{3}\ A_o (1-J)} R_r . \phi_m^2 (3-2J)$$

Work done against friction:

Here the complexity of the calculation of the friction losses is noted and two types of frictional shear stresses are discussed, namely:

1) Coulomb friction, where $\tau = \mu p$

2) constant friction, where $\tau = \frac{m}{\sqrt{3}} \sigma_y$ with m

for a given set of conditions is in the range $0 \leqslant m \leqslant 1$ i.e. from frictionless to full sticking conditions.

Although sticking friction does not prevail over the whole arc of contact, even for rolling lead tube (40), the concept of a constant surface shear stress is utilised since only average roll pressures are required and friction loss calculations are considerably simplified.

The work done against friction per unit time, $\dot{W}_f$, is given by:

$$\dot{W}_f = \int_S \tau \, v_r \, ds = A_o U_o W_f$$

where v_r is the relative velocity between the two surfaces in contact and ds is the elemental surface of contact.

The work done against friction between tube and rolls W_{fa} is given, with reference to FIGURE 3.19 by:

$$\dot{W}_{fa} = \int_S \tau \, v_r \, ds \qquad (3.(i)29)$$

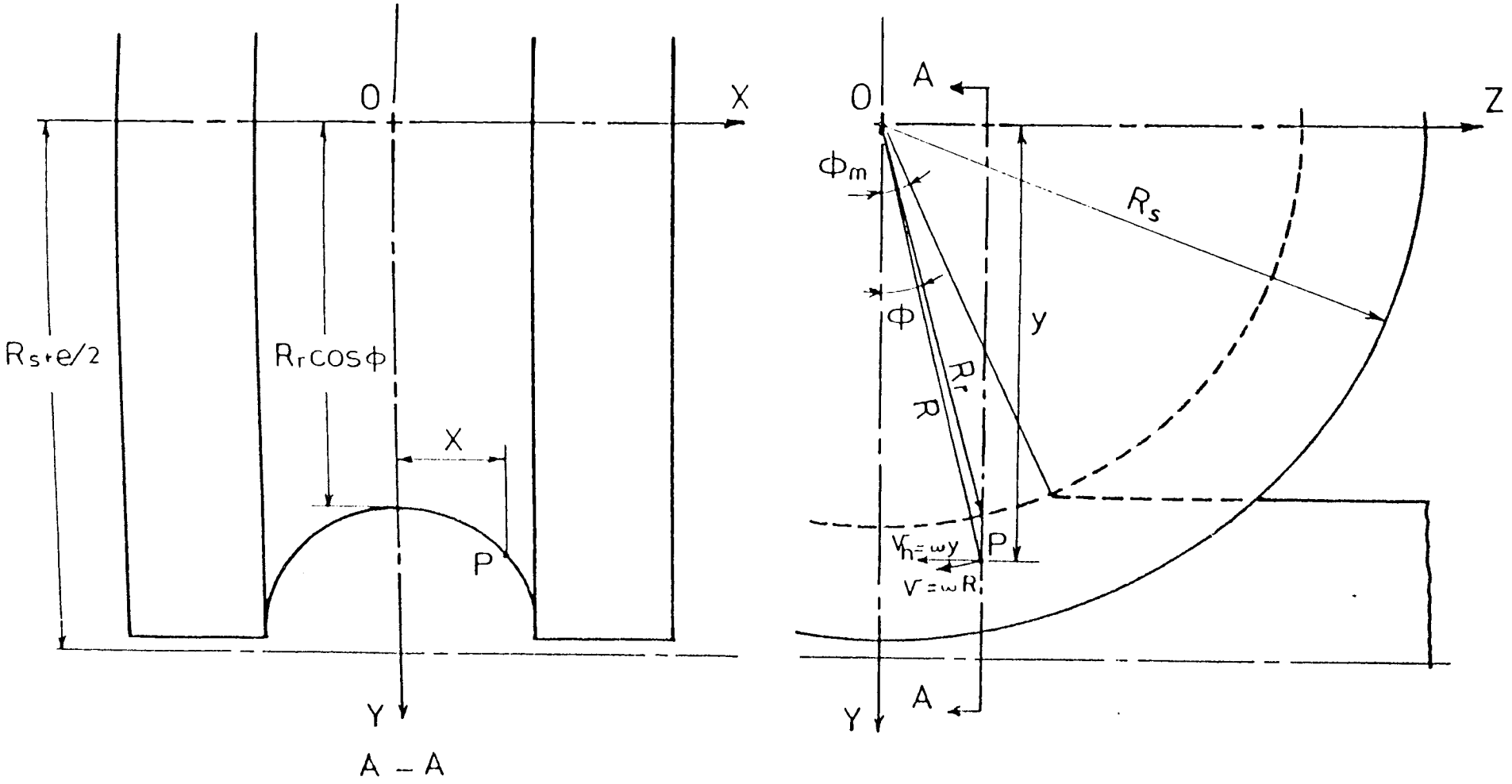

FIGURE 3.19

Roll speed at any point on the groove surface

The previously derived equations for the equation of the contact surface at any angle ϕ, the tube velocity U, the elemental tube length dL are appropriately substituted to give:

$$\dot{W}_{f_a} = \int_0^{\phi_m} \int_0^{xc} \left[\omega \sqrt{\left[b - (r_g^2 - x^2)^{\frac{1}{2}} \right]^2 - z^2} \right.$$

$$\left. - \frac{U_o}{1-J} \left(1 - \frac{J\phi}{\phi_m} \right) \right]$$

$$\left\{ \frac{x^2 \left[1 + \frac{z^2}{\left[b-(r_g^2-x^2)^{\frac{1}{2}} \right]^2 - z^2} \right]}{r_g^2 - x^2} + 1 \right\}^{\frac{1}{2}} dx \, R_r d\phi$$

(3(i)30)

where x_c is the distance in the x-direction which corresponds to the above equation is again solved by numerical methods.

The work done against friction between tube and mandrel W_{fb} is given, with reference to FIGURE 3.16, by:

$\dot{W}_{fb} = \int_s \tau \, v_r \, ds$, where it is assumed that the same peripheral contact angles ϕ_c subtended between tube and

forms will apply also between tube and mandrel.

A similar procedure to the above analysis gives:

$$\dot{W}_{f_b} = \int_0^{\phi_m} \int_0^{\psi c} \tau \left[v_b - \frac{U_o}{1-J} \left(1 - \frac{J\phi}{\phi_m}\right) \right] r_b . d\psi . R_r d\phi$$

(3(i)31)

which is again solved by numerical methods.

Work done by the applied front and back tensions:

The work done by the front tension per unit volume, W_a, is:

$$W_a = \sigma_a$$

and the work done by the back tension per unit volume, W_b, is:

$$W_b = \sigma_b$$

TOTAL MEAN ROLL PRESSURE (p_m):

By assuming that the pressure distribution round the groove and along the arc of contact is uniform, the total mean roll pressure can be calculated by equating W_t to the work done by the externally applied roll pressure, noting that the inside (mandrel) pressure does not contribute to any work.

The total work done by the external roll pressure per unit volume is:

$$W_e = \int_{t_1}^{t_o} p_m \, S \, \frac{dt}{V}$$

where p_m = total mean roll uniform pressure,

S = surface area of contact,

V = rolled material volume = $A_o V_o$,

dt = change in tube wall thickness.

Substituting and solving gives:

$$W_e = p_m \frac{S\,(t_o - t_1)}{V}$$

and $$W_e = W_h + W_r + W_f$$

ROLL SEPARATING FORCE (R.S.F.):

The product of the total mean roll pressure and the horizontal projection of the area of contact on each roll gives the roll separating force.

ROLLING TORQUE (T):

The total rolling torque T_t can be estimated by considering the moment of the resultant vertical force, i.e. the R.S.F., about the roll axis and if "a" is the lever arm:

$$T_t = 2\ (R.S.F.)\ a$$

To complete his theoretical analysis Labib considered a further two groove shapes as shown in FIGURE 3.15.

Good agreement was shown to exist between Labib's theoretical predictions based on the energy approach and his experimental results. Furthermore,by the use of the developed computer programmes it was possible to achieve the correct combination of rolling parameters to yield the minimum total work done per unit volume. Labib then concluded by stating that only the theory by Vatkin and Druyan (33) led to results which compared favourably with experiment.

3 (ii). THE PROPOSED THEORIES

Despite the acknowledged shortcomings of the equilibrium approach, as commented upon in the introduction (Chapter 1.) and the earlier part of this chapter, this type of analysis, together with the more recent apparent strain or energy method, will be developed and compared with each other for the three-roll sinking and mandrel rolling processes.

The main criticism of the equilibrium approach is the distortion of the assumed principal planes by the inevitable shear stresses. A friction stress will naturally produce a rotation of the principal planes from the longitudinal and circumferential directions. The thinner the tube wall thickness the greater this effect will have on the assumed principal planes in the main tube deformation zone away from the roll-tube interface.

The apparent strain or energy method does not provide information on the distribution of the pressure round the roll groove, or along the arc of contact, only the mean roll pressure is evaluated; however this is quite sufficient for most practical applications.

The work done per unit volume of rolled tube can be assumed to comprise the following components:

1. Work of homogeneous deformation (W_h),

2. Work against friction (W_f),

3. Redundant work (W_r),

It can be stated that the three individual work components are additive:

$$W_t = W_h + W_f + W_r$$

This is the basic assumption in the strain energy approach and can be compared to the assumed principal stress directions and yield criterion in the equilibrium analysis.

The apparent strain concept yields:

$$\bar{\epsilon}_A = \bar{\epsilon}_h + \bar{\epsilon}_f + \bar{\epsilon}_r \qquad (3(ii).1)$$

and the total work of deformation (W_t) is the integral of the true stress/strain curve between the limits of zero strain and $\bar{\epsilon}_A$.

3. (ii). 1. POSITIONS OF NEUTRAL POINTS AND CONTACT ZONES OF DEFORMATION

For both the sinking and mandrel rolling processes the simplified equation for the relative velocity (v_r) between the roll and the tube can be applied to the three-roll configuration to approximately obtain the neutral points and the roll contact deformation zones as follows:

Since the horizontal component of the roll velocity in the contact zone is of the same order as the actual roll velocity, then:

$$v_r = \omega \left[R_r + r_g (1 - \cos \theta) \right] - U_o \left[1 + J \left(1 - \frac{\phi}{\phi_m} \theta \right) \right] \qquad (3.(ii).2)$$

The neutral points (ϕ_n, θ_n) are described by equating v_r to zero, giving expression:

$$\theta_n = \cos^{-1} \left\{ 1 + \frac{Rr}{r_g} - \frac{Uo}{\omega r_g} \left[1 + J \left(1 - \frac{\phi_n}{\phi_m} \right) \right] \right\}$$

From a knowledge of the roll angular velocity (ω), the tube inlet velocity (U_o), the tube reduction (J) and the maximum roll root contact angle (ϕ_m), the co-ordinates of the neutral points (ϕ_n) and (θ_n) on the roll-tube contact surface zone can be deduced. This information also indicates the direction of v_r i.e. the friction direction for the relevant deformation zone.

3.(ii).2. SINKING PROCESS

3.(ii)2.1. Equilibrium Analysis

Since Kirichenko's theory (23) gave an acceptable lower estimation (m=o) prediction of the roll root groove pressure, this equilibrium model, as shown in FIGURE 3. 20. will be used for formulating the basic load equilibrium equations. These equilibrium equations are now adjusted to accommodate the modified constant shear yield stress type of friction, which has been accepted by many workers as being more relevant to hot rolling, and, with suitable modification for the rolling of lead tube as discussed by Haleem (40) and Labib (43).

It was shown earlier that this constant shear type of friction τ is of the form:

$$\tau = m \frac{\sigma_y}{\sqrt{3}}$$ where m is termed the friction factor.

FIGURE 3.20

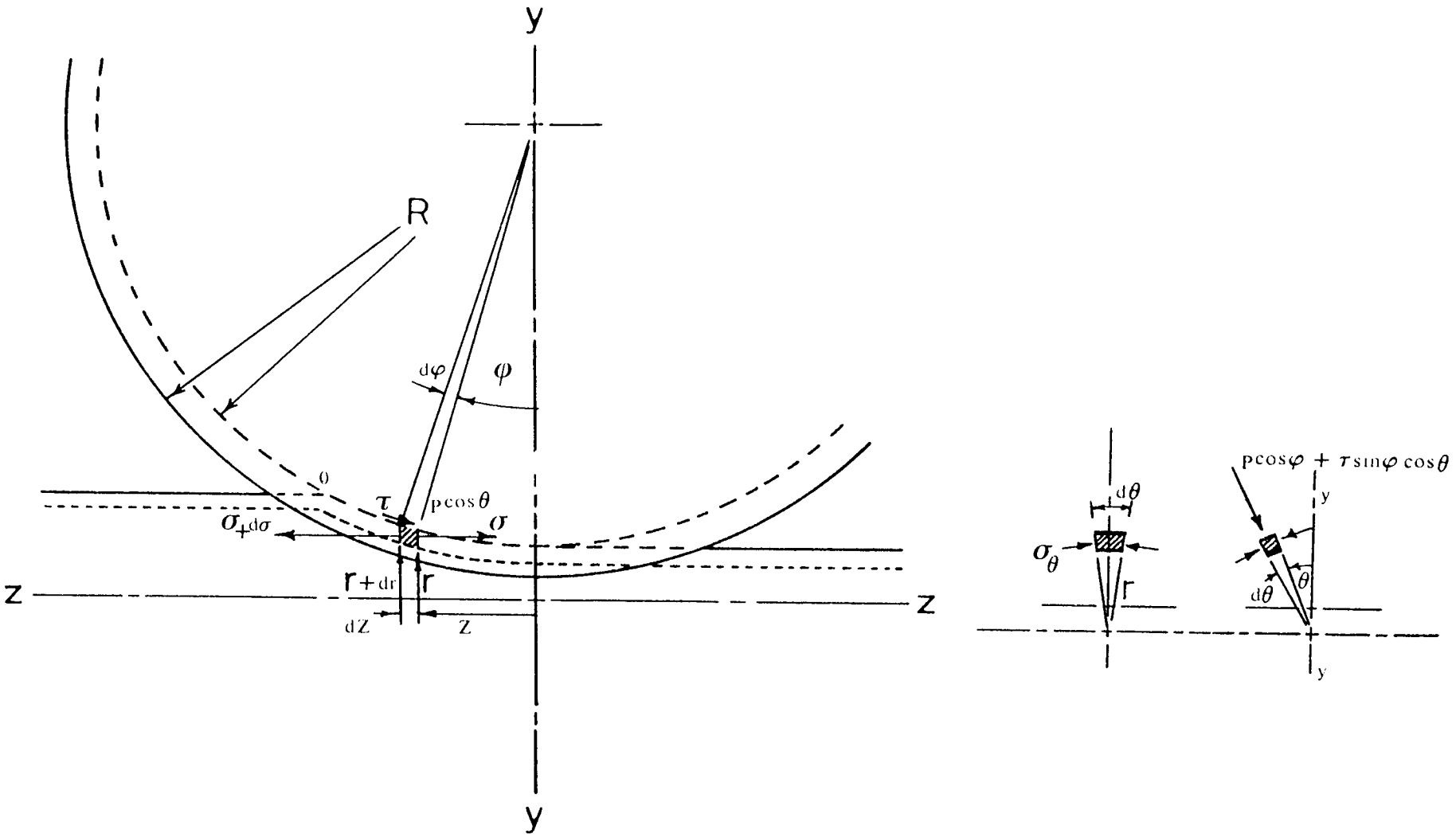

EQUILIBRIUM SINKING MODEL - Kirichenko's (23)

These adjusted equilibrium equations in the y and x directions are respectively as follows:

$$(p\cos\phi \pm \tau \sin\phi \cos\theta)\, r\,d\theta - 2\sigma_\theta t \sin\frac{d\theta}{2} = 0 \qquad (3.(ii).4)$$

and

$$(r - \frac{t}{2})d\sigma_z + \sigma_z dr + (p\sin\phi\cos\theta \mp \tau\cos\phi)\frac{dx}{t\cos\phi}$$

$$(r + \frac{dr}{2}) = 0 \qquad (3.(ii).5)$$

Making the usual assumptions: $\sin\frac{d\theta}{2} \simeq \frac{d\theta}{2}$, $r > t$, negligible change in the tube wall thickness and allowing the arc of contact to approximate to a chord, equations (3.(ii).4) and (3.(ii).5) become:

$$\sigma_\theta = \frac{r}{t}(p\cos\bar{\phi} \pm \tau \sin\bar{\phi}\cos\theta) \qquad (3.(ii).6)$$

and

$$r\,d\sigma_z + \sigma_z dr + (p\sin\bar{\phi}\cos\theta \mp \tau\cos\bar{\phi})\frac{r\,dr}{t\sin\bar{\phi}} = 0 \qquad (3.(ii).7)$$

where $\tan\bar{\phi} = \frac{dr}{dx}$ and $\bar{\phi} \simeq \frac{\hat{\phi}}{2}$

with $\bar{\phi}$ and $\hat{\phi}$ the mean and maximum roll contact angles respectively. A modification of the von Mises yield

criterion is now employed:

$$\sigma_z - (-\sigma_\theta) = \beta \sigma y \qquad (3.(ii).8)$$

where $\beta = 1.10$

Substitution between equations (3.(ii).6), (3.(ii) 7.&8.)to eliminate σ_z and σ_θ gives:

$$\frac{dp}{dr} + \frac{p}{r}\left[2 - \frac{\cos\theta}{\cos\bar{\phi}}\right] \pm \frac{1}{r}\left[\tau\left(2\tan\bar{\phi}\cos\theta + \frac{1}{\sin\bar{\phi}}\right)\right]$$

$$- \frac{1}{r^2}\left[\beta\frac{\sigma_y\ t}{\cos\bar{\phi}}\right] = 0 \qquad (3.(ii).9)$$

which is of the form:

$$\frac{dp}{dr} + A\frac{p}{r} \pm \frac{B}{r} - \frac{C}{r^2} = 0 \qquad (3.(ii).10)$$

where $A = \left[2 - \frac{\cos\theta}{\cos\bar{\phi}}\right]$

$B = \left[\tau\left(2\tan\bar{\phi}\cos\theta + \frac{1}{\sin\bar{\phi}}\right)\right]$

$C = \left[\beta\frac{\sigma_y\ t}{\cos\bar{\phi}}\right]$

This resulting differential equation, where the roll pressure

p is a function of r, is presented in this manner since at the tube outlet, the roll pressure, in the abscence of tube tension, can be readily equated to the required homogeneous tube deformation pressure for the plane stress condition.

The analysis of a fully plastic tube in plane stress subjected to external pressure is given in Appendix A . It will be noted that for convenience a graphical solution relating the homogeneous roll pressure p_1 to the relevant tube $\left(\frac{D}{t}\right)_1$ ratio at the outlet section is presented. Sufficient at this stage to state that:

$$p_1 = c\,\sigma_y$$

where c is obtained from the aforementioned graphical solution.

The solution of this differential equation (3.(ii).10) for the roll pressure p is of the form:

$$p = \left(\frac{C}{A-1}\right)\frac{1}{r} + E\,\frac{1}{r^A} \mp \frac{B}{A}$$

where E is the constant of integration and is determined from the boundary conditions as follows:

At the tube outlet, $r = r_1$ and the homogenous tube deformation pressure p_1 is given by $c\,\sigma_y$

$$p_h = \left[\frac{C}{A-1}\right] r_1^{\frac{1}{}} + E\,\frac{1}{r_1^A} \mp \frac{B}{A}$$

$$E = r_1^A \left[(c\ \sigma_y) + \left(\frac{C}{1-A}\right) \frac{1}{r_1} \pm \frac{B}{A} \right]$$

The complete solution is:

$$p_h = \left(\frac{C}{1-A}\right)\left[\frac{r_1^{(A-1)}}{r^A} - \frac{1}{r} \right] + \left(\frac{r_1}{r}\right)^A \left[c\ \sigma_y \pm \frac{B}{A} \right] \mp \frac{B}{A} \qquad (3.(ii).11)$$

For the range of the tube $\frac{D}{t}$ ratios and reductions considered, it can be shown that:

$$\left(\frac{C}{1-A}\right)\left[\frac{r_1^{(A-1)}}{r^A} - \frac{1}{r} \right] \simeq 0$$

The simplified complete solution then becomes:

$$p_h = \left(\frac{r_1}{r}\right)^A \left[c\ \sigma_y \pm \frac{B}{A} \right] \mp \frac{B}{A}$$

or

$$p_h = \left(\frac{d_1}{d}\right)^A \left[c\ \sigma_y \pm \frac{B}{A} \right] \mp \frac{B}{A} \qquad (3.(ii).12)$$

3.(ii).2.2. Apparent Strain/Energy Analysis

Developing the form of analysis used by Haleem (40) for sinking through two-grooved rolls the three components of the total work of deformation will now be evaluated for the three-grooved roll configuration.

Work of homogeneous deformation (W_h):

Haleem's equation (3.(i).8) gives the following expression for p_h the roll pressure associated with homogeneous deformation:

$$p_h = \frac{A_o \ \bar{\sigma}_y \ \bar{\varepsilon}_h}{2 \ r_g \ \delta \ \theta_c}$$

where $\bar{\varepsilon}_h = \sqrt{\frac{2}{3} \ (\varepsilon^2_z + \varepsilon^2_t + \varepsilon^2_\theta)}$

This expression for p_h can readily be applied to the three-roll configuration FIGURE 4.4. by appropriate substitution for θ_c and rewriting the p_h equation as:

$$p_h = \frac{A_o \ \bar{\sigma}_y \ \bar{\varepsilon}_h}{3 \ r_g \ \delta \ \theta_c} \qquad (3.(ii).13)$$

Work against friction (W_f):

From Haleem's previously discussed analysis on the complex determination of the frictional work, the apparent frictional strain ($\bar{\varepsilon}_f$) for the three-roll configuration will now be developed.

Haleem's assumed model for the relative roll-tube velocity direction over the contact surface area as shown in FIGURE 3. 21. (a) is only valid for small tube reductions. For it is implicit in his model that only a small change of roll radius along the neutral line (zero relative roll - tube velocity) is being considered. Thus, for constancy of volume, this percentage change in roll radius must approximate to the percentage change in tube cross-sectional area. Therefore, it is proposed that better models for the behaviour of the neutral line for increasing tube reductions are those illustrated in FIGURE 3. 21. (b) and 3. 21. (c)

This modification to the original Haleem model is especially relevant to the three-roll process with the shallower arcuate groove profile producing a comparatively smaller change between the roll root and the roll shroud velocities. This suggests that for the models shown in FIGURE 3. 21 the two-roll process can accommodate a larger overall tube reduction within the radial depth of the roll groove than that available in the three-roll arrangement.

Tentative evidence to support these relative velocity models is given in Chapter 6 and the relevant pin load cell results of Haleem.

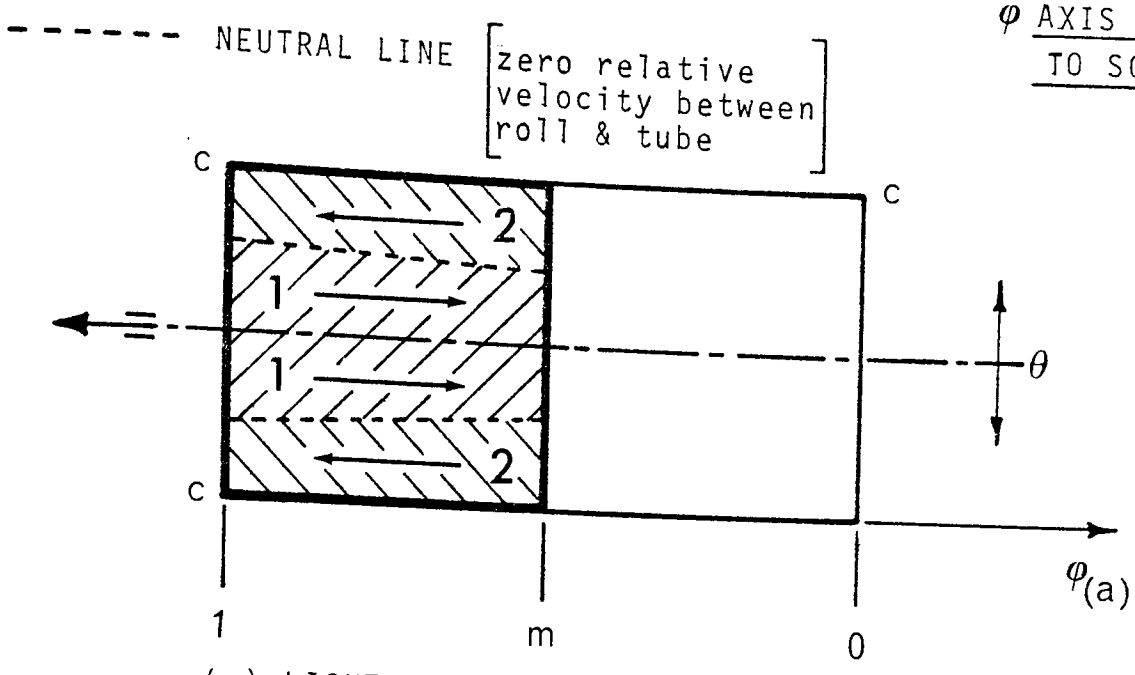

(a) LIGHT REDUCTION

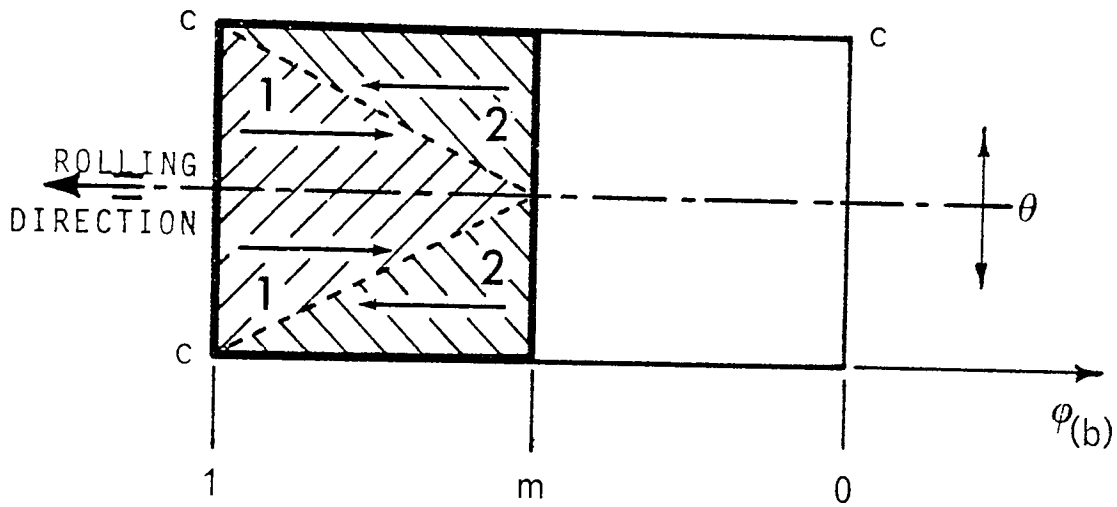

(b) MEDIUM REDUCTION

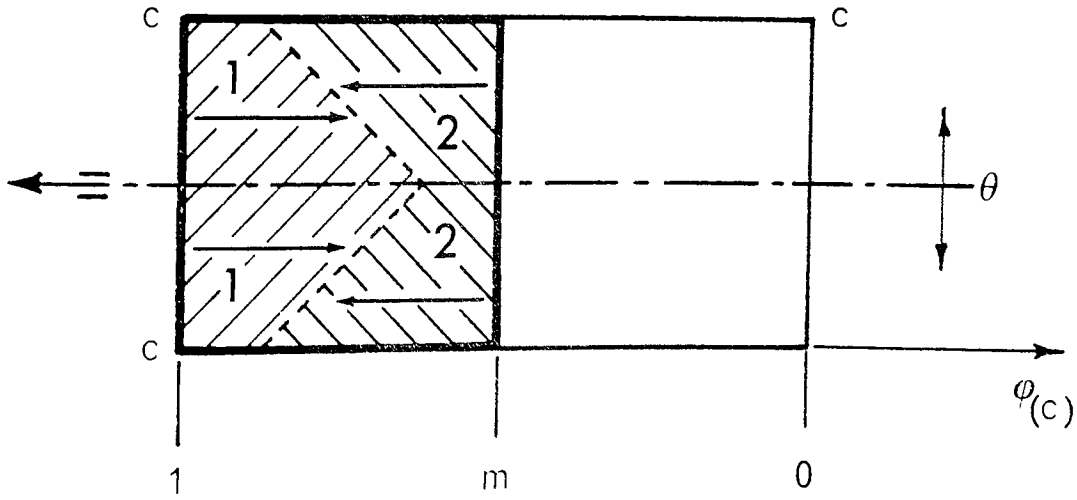

(c) HEAVY REDUCTION

PROPOSED DEFORMATION ZONES & RELATIVE VELOCITY MODES (SINKING)

For the smaller tube reductions Haleem's analysis relevant to FIGURE 21. (a) can be re-structured:

$$\dot{W}_{Fe1} = 6\int_0^{\phi_m}\int_0^{\theta_n} \tau\, v_r\, R_r\, r_g\, d\phi\, d\theta \qquad \text{for zone 1}$$

$$= 6\int_0^{\phi_m}\int_0^{\theta_n} \frac{m_1\, \sigma_{yf} R_r\, r_g}{\sqrt{3}} \left\{ U_m \left[1 + \frac{J}{2}\left(1 - \frac{\phi}{\phi_m}\right)\right] - \omega\left[R + r_g\,(1 - \cos\theta)\right]\right\} d\phi d\theta$$

and $$\dot{W}_{fe2} = 6\int_0^{\phi_m}\int_{\theta_n}^{\theta_c} \tau\, v_r R_r r_g d\phi\, d\theta \qquad \text{for zone 2}$$

$$= 6\int_0^{\phi_m}\int_{\theta_n}^{\theta_c} \frac{m_2\, \sigma_{yf}\, R_r\, r_g}{\sqrt{3}} \left\{ \omega\left[R + r_g(1 - \cos\theta)\right] - U_m\left[1 + \frac{J}{2}\left(1 - \frac{\phi}{\phi_m}\right)\right]\right\} d\phi\, d\theta$$

Assuming that when $\phi = \frac{\phi_m}{2}$, $U = \omega\bar{R}$ giving $U_m = \frac{\omega\bar{R}}{1 + \frac{J}{4}}$

from equation (3.(i).9), where $\bar{R}$ is the corresponding mean

roll radius.

By definition $W_{fe} = \dfrac{\dot{W}_{fe1} + \dot{W}_{fe2}}{\dot{v}_m} = \bar{\varepsilon}_f \; \bar{\sigma}_{yf}$ then:

$$\bar{\varepsilon}_f = \frac{2\sqrt{3}\, r_g^{\,2}\, \phi_m (1+\frac{J}{4}) R_r}{A_m \quad \bar{R}} \left\{ \left[\left(\frac{4\bar{R}}{r_g(4+J)} + \frac{\bar{R}J}{r_g(4+J)} \right) - (1 - \frac{\sin\theta_n}{\theta_n}) m_1 \theta_n \right] + \left[\left(\frac{Rr}{r_g} - \frac{4\bar{R}}{r_g(4+J)} \right) - \frac{\bar{R}J}{r_g(4+J)} + \left(1 - \frac{(\sin\theta_c - \sin\theta_n)}{(\theta_c - \theta_n)} \right) \right] m_2 (\theta_c - \theta_n) \right\} \qquad (3.(ii).14)$$

Following Haleem's analysis by assuming that $\theta_n \simeq \frac{\theta_c}{2}$ and considering similar frictional shear conditions in zones 1 and 2.

i.e. $m_1 = m_2 = m$, then:

$$\bar{\varepsilon}_f = \frac{\sqrt{3}\, r_g^2 \phi_m \; (1+\frac{J}{4}) \quad R_r \; m}{A_m \qquad \bar{R}} \left[2 \sin \frac{\theta_c}{2} - \sin \theta_c \right] \qquad (3.(ii).15)$$

For the larger tube reductions the model associated with FIGURE 3. 21. (b) approximately verified in section 7. 1. 2 is now developed for the assessment of $\bar{\varepsilon}_f$:

$$\dot{W}_{fe1} = 6 \int_0^{\theta_c} \int_0^{\left(\phi_m - \theta \frac{(\phi_m)}{\theta_c}\right)} \tau\, v_r R_r r_g \, d\phi d\theta \qquad \text{for zone 1}$$

$$= 6 \int_0^{\theta_c} \int_0^{\left(\phi_m - \theta \frac{(\phi_m)}{\theta_c}\right)} \frac{m_1 \sigma_{yf} R_r\, r_g}{\sqrt{3}} \left\{ U_m \left[1 + \frac{J}{2} \left(1 - \frac{\phi}{\phi_m} \right) \right] \right.$$

$$\left. - \omega \left[R + r_g (1 - \cos\, \theta) \right] \right\} d\phi d\theta$$

$$\text{and } \dot{W}_{fe2} = 6 \int_0^{\theta_c} \int_{\left(\phi_m - \frac{(\phi m)}{\theta_c}\right)}^{\phi_m} \tau\, v_r R_r r_g \, d\phi d\theta \qquad \text{for zone 2}$$

$$= 6 \int_0^{\theta_c \phi_m} \int_{\left(\phi_m - \frac{(\phi_m)}{\theta_c}\right)} \frac{m_2\, \sigma_{yf} Rr\, r_g}{\sqrt{3}} \left\{ \omega \left[R + r_g\, (1 - \cos\theta) \right] \right.$$

$$\left. - U_m \left[1 + \frac{J}{2} \left(1 - \frac{\phi}{\phi_m} \right) \right] \right\} d\phi d\theta$$

Noting that: $\phi = \left(\phi_m - \theta \left(\frac{\phi_m}{\theta_c}\right)\right)$ and assuming that when $\phi = \phi_m$, $U_m = \omega R_r$ from equation (3.(i).9).

As before, $W_{fe} = \frac{\dot{W}_{fe1} + \dot{W}_{fe2}}{\dot{V}_m} = \bar{\varepsilon}_f \, \bar{\sigma}_{yf}$,

$$\bar{\varepsilon}_f = \frac{6 \, r_g^2 \theta_c \, \phi_m}{\sqrt{3} \quad A_m} \; m_1 \left[\frac{R_r J}{6 \, r_g} + \frac{1}{\theta_c^2} - \frac{1}{2} - \frac{\cos \theta_c}{\theta_c^2} \right] + m_2 \left[\right.$$

$$\left. \frac{1}{2} + \frac{1}{\theta_c^2} - \frac{R_r J}{12 r_g} - \frac{\sin\theta_c}{\theta_c} - \frac{\cos \theta_c}{\theta_c^2} \right]$$

Assuming $m_1 = m_2 = m$ then:

$$\bar{\varepsilon}_f = \frac{2\sqrt{3} \; m \; r_g^{\,2} \; \theta_c \, \phi_m}{A_m} \left[\frac{RJ}{12 r_g} + \frac{2}{\theta_c^2} - \frac{\sin\theta_c}{\theta_c} - 2 \, \frac{\cos\theta_c}{\theta_c^2} \right]$$

(3.(ii).16)

Redundant work (W_r)

Haleem stated that the redundant work due to surface shear could be neglected, but he drew attention to the presence of a free zone, acknowledging the existence of circumferential bending and unbending of the tube as it passed through the free zone. This region of deformation continued until complete control by the roll groove was established. This contribution to the redundant work is significant for thicker walled tubes and requires consideration.

Although observations of the shadowgraph profiles (see PLATE 7. 1) from current tube sinking tests on the three-roll configuration indicate the occurrence of circumferential bending in the roll groove root region, with some discernable at the shrouds, for the purpose of the following rudimentary analysis complete circumferential bending and unbending will be assumed. With reference to FIGURE 3. 22 it is suggested that full plastic bending and unbending of the tube to the reverse curvature $\frac{1}{\bar{R}_f}$ in the free deformation zone is followed by full plastic bending and unbending of the tube to the mean roll profile curvature $\frac{1}{\bar{R}_c}$ in the controlled zone.

Furthermore, with:

$\bar{D}$ = tube mean diameter

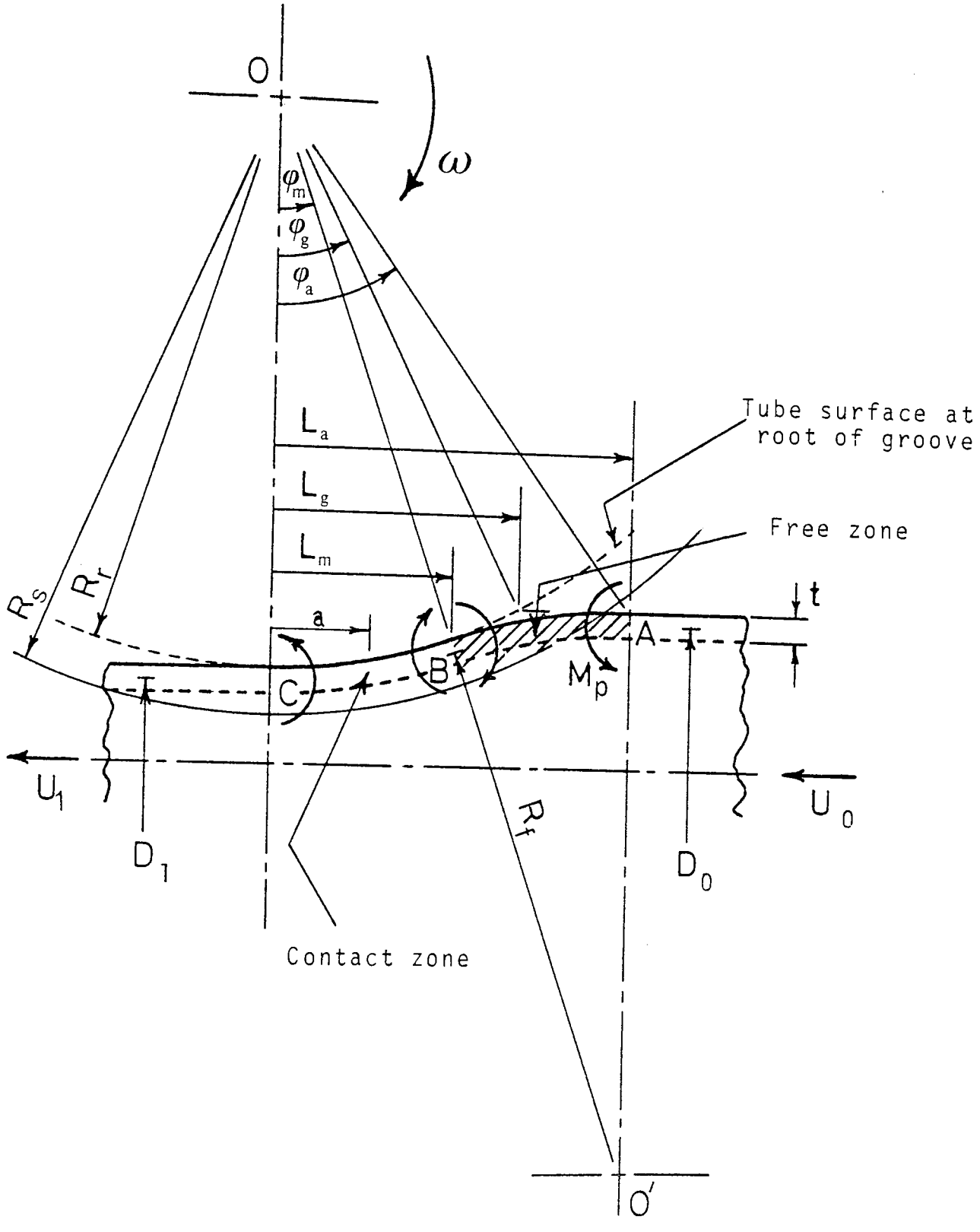

EFFECT OF THE FREE DEFORMATION ZONE ON THE TUBE-ROLL ARC OF CONTACT

$\bar{t}$ = mean tube wall thickness,

$\bar{R}_f$ = mean radius of curvature of tube bending and unbending in the free deformation zone,

$\bar{R}_c$ = mean radius of curvature of tube bending and unbending in the controlled deformation zone,

ω = angular velocity of rolls,

M_p = full plastic bending moment under plane strain per unit circumferential length,

and the suffices o, m, 1, refer to the planes shown in FIGURE 3. 22.

For the purpose of this analysis the following assumptions will be made:

1. uniform bending stress across the tube wall thickness,
2. complete single and double plastic circumferential moments at A/C and B respectively.

The redundant work done per unit volume (W_r) at the four plastic hinges is:

$$W_r = \frac{\pi M_p}{A_m U_m} \left[D_o \omega_o + 2D_m \omega_m + D_1 \omega_1 \right] \qquad (3.(ii).17)$$

where, A_m = tube cross sectional area at plane m,

v_m = tube velocity at plane m,

ω , ω_m, ω_o = rate of rotation of the respective plastic hinges.

Haleem showed that for the range of $\frac{D}{t}$ tube ratios considered in this present series of sinking tests:

$$R_f \simeq R_c$$

Furthermore the roll angular velocity $\omega \simeq \omega_m$ and if $\bar{R}$ is the mean roll radius:

$$v_m = \omega_m \bar{R}$$

For the range of tube reductions considered, D_m and ω_m can be considered to represent the mean diameter and mean rate of rotation of the plastic hinges respectively, thus giving:

$$W_r = \frac{4 \pi M_p D_m \omega_m}{A_m v_m} = \frac{4 \pi M_p D_m}{A_m \bar{R}} \qquad (3.(ii).18)$$

but $A_m = \pi D_m \bar{t}$

and for plastic bending in plane strain $M_p = \frac{2}{\sqrt{3}} \sigma_y \frac{\bar{t}^2}{4}$

$$\therefore W_r = \frac{2}{\sqrt{3}} \frac{\sigma_y \bar{t}}{\bar{R}}$$ which, from equation (3.(i).8)

can be written as: $W_r = \frac{3 p_r r_g \theta_c \delta}{A_o}$

$$\therefore \quad p_r = \frac{2\,\sigma_y\,\bar{t}\,A_o}{3\sqrt{3}\,\bar{R}\,r_g\theta_c\delta} \qquad (3.(ii).19)$$

Utilising the apparent strain concept, this expression for the work done per unit volume (W_r) can also be written as

$$W_r = \sigma_y\,\bar{\varepsilon}_r$$

giving for the apparent redundant strain $\bar{\varepsilon}_r$:

$$\bar{\varepsilon}_r = \frac{2\,\bar{t}}{\sqrt{3}\,\bar{R}} \qquad (3.(ii).20)$$

As previously noted the implicit overestimation of the redundant work by reason of the partial nature of the circumferential bending and unbending of the tube, suggests that the analysis should be treated with caution.

3.(ii).3. MANDREL ROLLING

3.(ii).3.1. Equilibrium Analysis.

As noted by Labib (43) and other workers only partial circumferential contact occurs at the roll groove-tube interface and the tube-mandrel interface during the rolling process. This geometry compels a two part equilibrium analysis which is developed as follows; see FIGURE 3. 23.

The mandrel-tube-roll interface

This deformation region for $-\gamma_c < \theta < \gamma_c$ experiences the full mandrel rolling process. The simplified mandrel equilibrium equations as formulated by Vatkin and Druyan (33), relevant to thin walled tubes, will form the basis for this part of the analysis. The resulting equation is as follows:

$$\sigma_z dt + t d\sigma_z + p dt \pm F dt = 0 \qquad (3.(ii).21)$$

where $F = \pm \dfrac{(\tau_r + \tau)}{\tan \bar{\phi}}$

and as before a constant shear stress type friction τ of the form:

$$\tau_r = m_r \frac{\sigma_y}{\sqrt{3}} \qquad \text{for the roll-tube interface}$$

and $$\tau_b = m_b \frac{\sigma_y}{\sqrt{3}} \qquad \text{for the tube-mandrel interface}$$

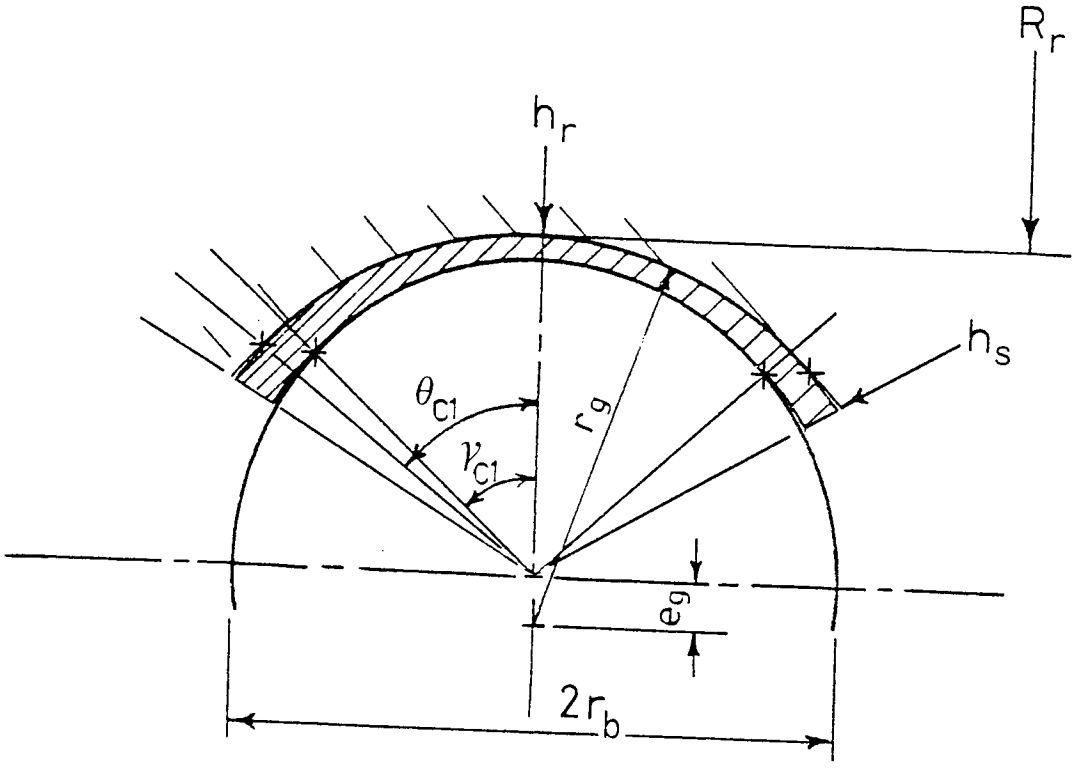

+ EXIT CONTACT POINTS

Geometry of tube and groove at the exit plane

FIGURE 3.23

The tube-roll interface

This deformation region for $\gamma_{cl} < \theta < \theta_{cl}$ experiences a sinking process, with a comparatively small change in tube wall thickness as confirmed by the experimental results shown in TABLE 6. 4. To simplify the sinking analysis the associated circumferential deformation zone is assumed to extend to the roll shrouds. This assumption is reasonable for three-roll tube rolling and is supported in general by the aforementioned experimental results (note column $t_{(\theta-\gamma)}$ TABLE 6. 4.

Consequently the derived sinking roll pressure equation can be applied as an approximation for calculating the mean roll pressure for this deformation region.

Furthermore the radial pressure p at the mandrel-tube-roll surfaces is assumed equal and constant since the tube is thin walled and there is a small mean roll contact angle $\bar{\phi}$; σ_z is the longitudinal stress and t is the current tube wall thickness.

Applying the yield criterion in plane strain for the region $-\gamma_c < \theta < \gamma_c$:

$$\sigma_z - (-p) = \frac{2}{\sqrt{3}} \sigma_y$$

Noting that for thin walled tubes $\tan\bar{\phi} \simeq \bar{\phi}$, these two equations combine to give:

$$dp = \frac{dt}{t} \left(\frac{2}{\sqrt{3}} \sigma_y \pm F \right)$$

The solution of which is:

$$p = \left(\frac{2}{\sqrt{3}} \sigma_y \pm F \right) \ln t + G \qquad (3.(ii).22)$$

Assuming that the change of direction, i.e. the sign, of the frictional shear stresses τ and τ_r occurs at the same roll angle, namely, the neutral angle ϕ_n, (Labib's work suggested this experimentally and theoretically) then a two part solution to equation (3.(ii).22) is implied, as in flat rolling.

Hence:

for the tube in the inlet "mandrel" deformation zone $\phi_n < \phi < \phi_m$ (approx.):

$$p = \left(\frac{2}{\sqrt{3}}\sigma_y - F\right) \ln t + G_1 \ldots$$

and to evaluate G_1:

put $p_o \approx \frac{2}{\sqrt{3}}\sigma_y$ for plane strain compression when $t = t_o$,

$$\therefore p_{(n-o)} = \frac{2}{\sqrt{3}}\sigma_y + \left(\frac{2}{\sqrt{3}}\sigma_y - F\right) \ln \frac{t}{t_1} \qquad (3.(ii).23)$$

for the tube in the outlet "mandrel" deformation zone $0 < \phi < \phi_n$ (approx.):

$$p = \left(\frac{2}{\sqrt{3}}\sigma_y + F\right) \ln t + G_2$$

as before:

$$p_1 \approx \frac{2}{\sqrt{3}}\sigma_y \quad \text{when } t = t_1$$

$$\therefore p_{(1-n)} = \frac{2}{\sqrt{3}}\sigma_y + F\right) \ln \frac{t}{t_1} + \frac{2}{\sqrt{3}}\sigma_y \qquad (3.(ii).24)$$

3.(ii).3.2. Apparent Strain/Energy Analysis.

The extensive analysis of the mandrel rolling process through two-grooved rolls by Labib (43) discussed earlier in this chapter can be simplified and applied to the three-roll configuration. This can be achieved by taking account of the flatter roll groove and the arcuate triangular nature of the three-roll gap profile.

As shown by Haleem (40) and Labib (43) the individual apparent strain components and their contributions to the total work done can be derived and summed, thereby determining the total mean roll pressure.

Work of homogeneous deformation (W_h)

The determination of the homogeneous work is identical to that described for the sinking process and irrespective of the roll configuration the measurement of the principal strains yields:

$$W_h = \sigma_y \bar{\varepsilon}_h$$

$$= \sigma_y \sqrt{\frac{2}{3} (\varepsilon_z^2 + \varepsilon_t^2 + \varepsilon_\theta^2)}$$

where ε_z , ε_t and ε_θ are assessed from experimental measurements.

Redundant Work (W_r)

As a consequence of the mandrel controlling the bore of the deforming tube, the shear redundant work is minimal and can be neglected. This is also confirmed by Labib's theoretical analysis.

Work done against friction (W_f):

To assess the friction work the assumptions adopted by Labib are used i.e. the constant shear stress concept $\tau = m \frac{\sigma_y}{\sqrt{3}}$, and that sticking friction does not necessarily prevail over the complete roll contact surface. The rate of work done against friction per unit volume over the contact surface defined by the deformation zones can be written in the same format i.e.

$$\dot{W}_f = \int_S \tau \, v_r \, ds$$

Work done against friction between tube and rolls (W_{fr}):

Equation (3. (i). 29) as given by Labib enables the work done per unit volume against friction between the tube and the rolls to be evaluated for the two-roll configuration. However, for the more uniform rolling process produced by the three-roll configuration, the expression for W_{fr} becomes essentially that given by Haleem in equation (3. (i). 10), with the appropriate limits as presented in FIGURE.3.19.

As suggested experimentally by Labid, see FIGURE. 3.24. and considering the larger tube reductions relevant to the mandrel rolling process, a simplified model for the roll-tube velocity zones is displayed in FIGURE. 3.25.

For zone 1:

$$\dot{W}_{fr1} = 6 \int_0^{\phi_n} \int_0^{\theta_c} \frac{m_1 \sigma_y R_r r_g}{\sqrt{3}} \left\{ U_o \left[1 + J \left(1 - \frac{\phi}{\phi_m} \right) \right] - \omega \left[R_r + r_g (1-\cos\theta) \right] \right\} d\phi d\theta$$

For zone 2:

$$\dot{W}_{fr2} = 6 \int_{\phi_n}^{\phi_m} \int_0^{\theta_c} \frac{m_2 \sigma_y R_r r_g}{\sqrt{3}} \left\{ \omega \left[R_r + r(1-\cos\theta) \right] - U_o \left[1 + J \left(1 - \frac{\phi}{\phi_m} \right) \right] \right\} d\phi d\theta$$

Approximately writing $\phi_n = k\,\phi_m$, assuming that when $\phi = \phi_m$,

$$U_o = \frac{\omega R r}{1 + J(1-k)} = \omega R_o$$

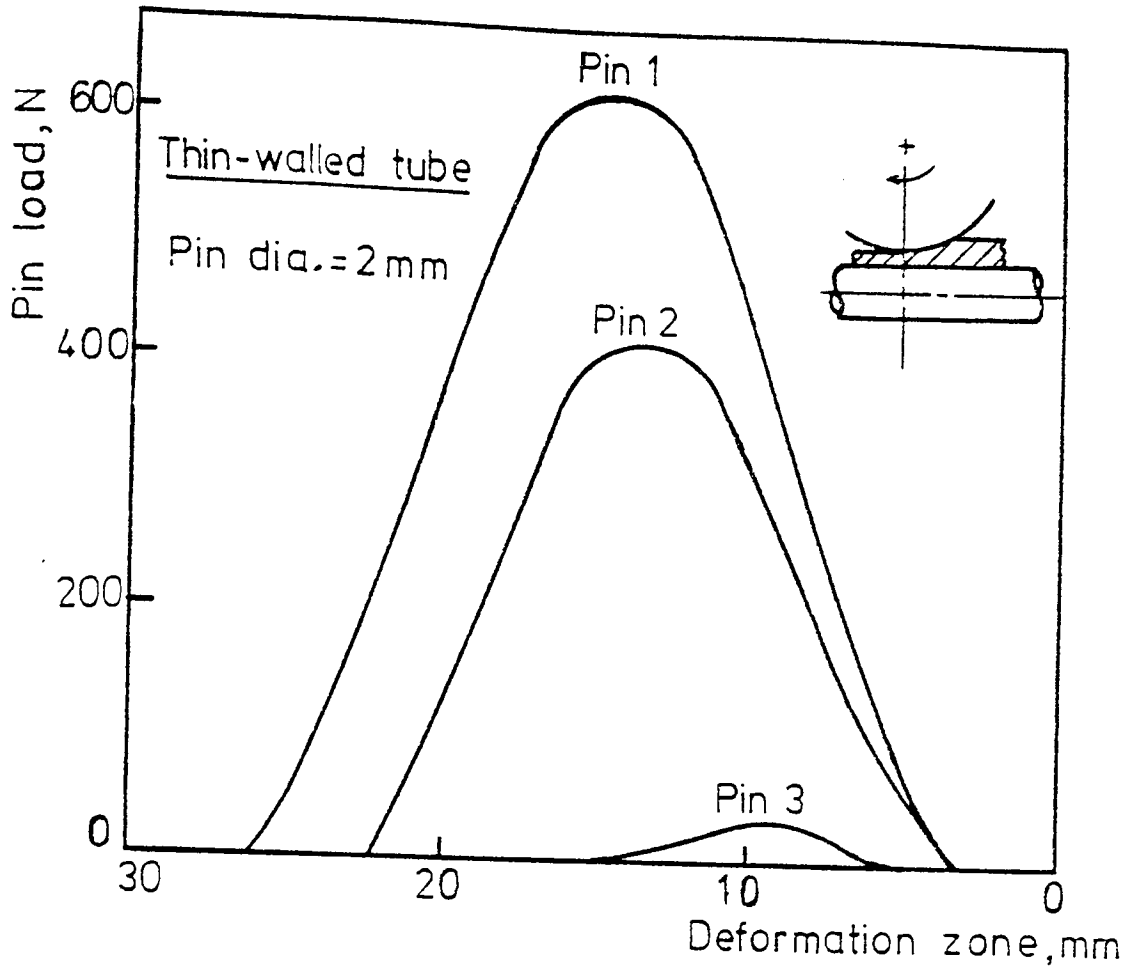

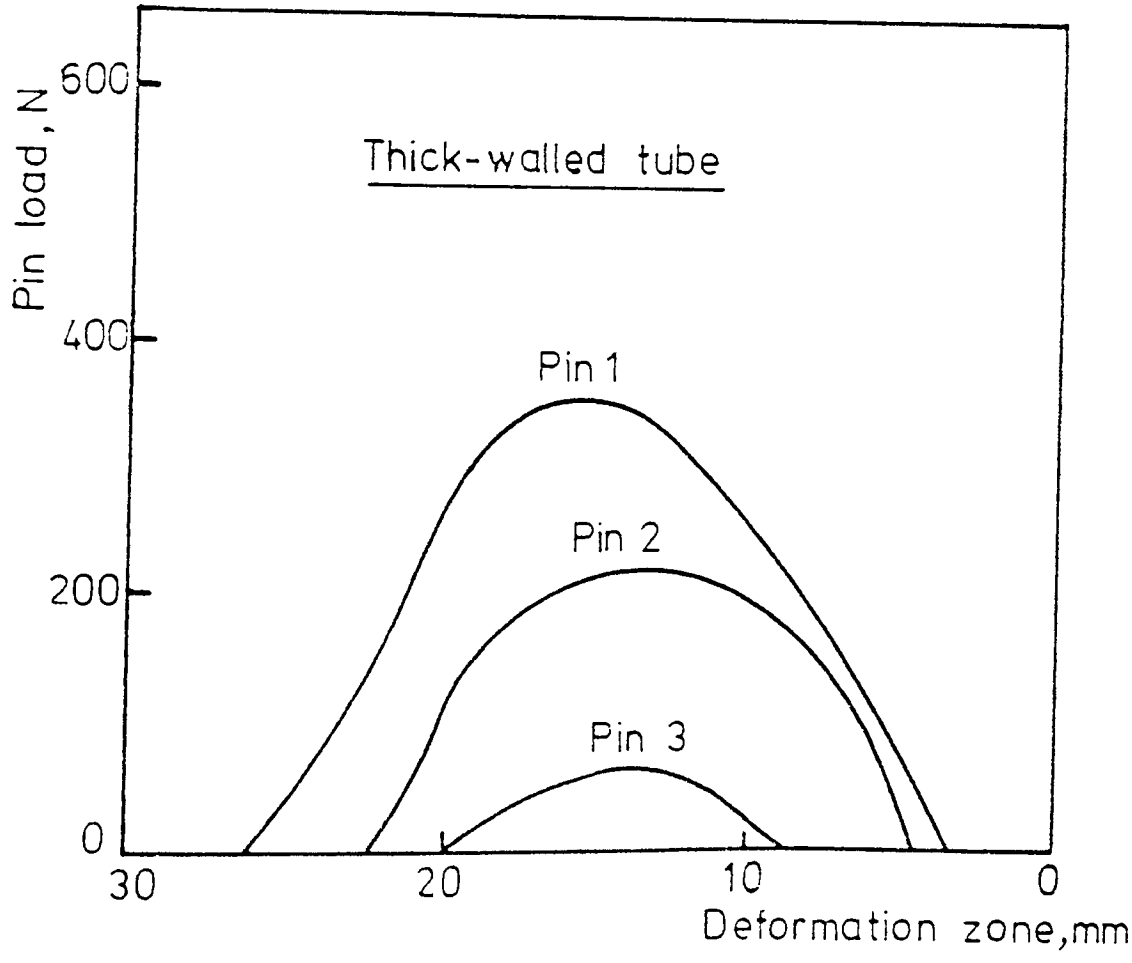

Typical pressure curves

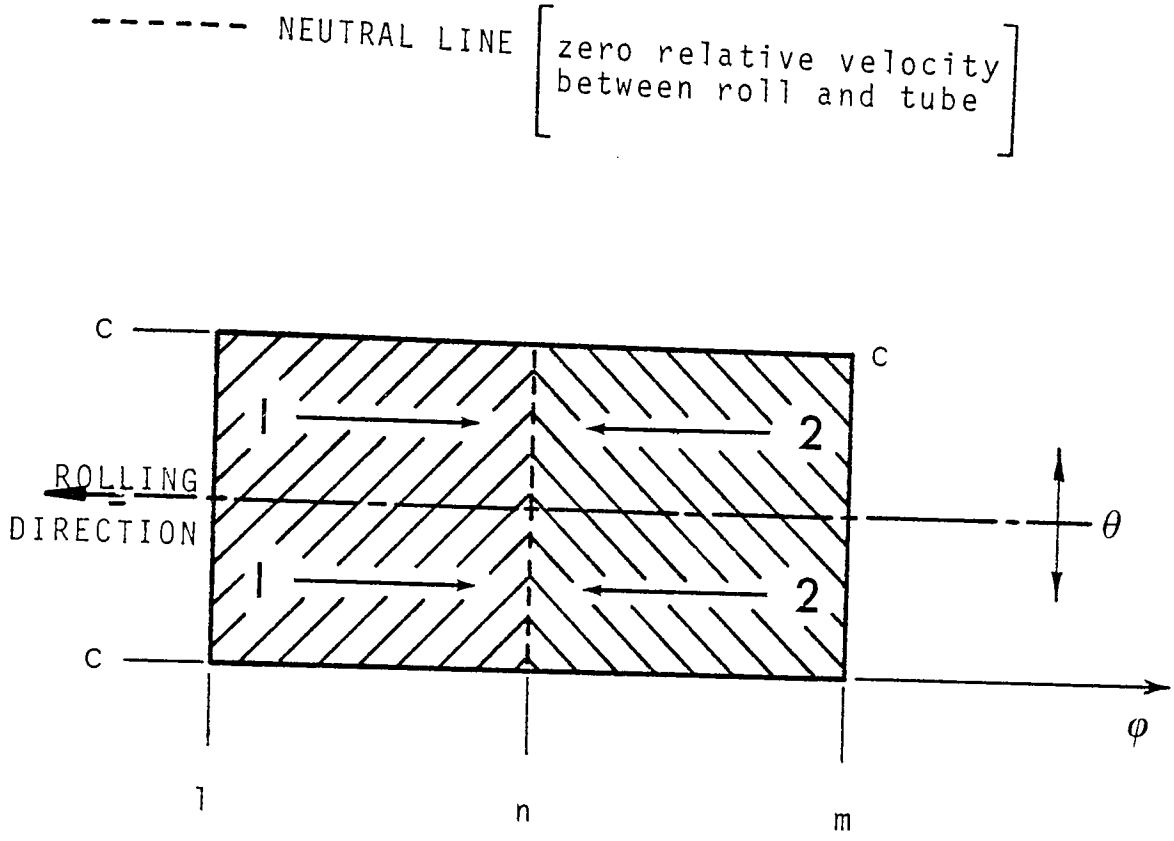

DEFORMATION ZONES AND

RELATIVE VELOCITY MODES (MANDREL ROLLING)

FIGURE 3.25

and noting that:

$$W = \frac{\dot{W}_{fr1} + \dot{W}_{fr2}}{\dot{V}_n} = \bar{\varepsilon}_{fr}\ \bar{\sigma}_y \quad \text{then:}$$

$$\bar{\varepsilon}_{fr} = \frac{2\sqrt{3}\ r_g^2\ \theta_c\ \phi_m}{A_n} \left\{ m_1 k \left[\frac{\frac{R_r Jk}{2r_g}}{1 + J(1-k)} - \frac{(1-\sin\theta_c)}{\theta_c} \right] + m_2(1-k) \left[\frac{(1-\sin\theta_c)}{\theta_c} - \frac{\frac{R_r Jk}{2r_g}(k-1)}{1+ J\ (1-k)} \right] \right\}$$

Finally, assuming $m_1 = m_2 = m$:

$$\bar{\varepsilon}_{fr} = \frac{2\sqrt{3}\ r_g^2\ \theta_c\ \phi_m m}{A_n} \left\{ k \left[\frac{\frac{R_r Jk}{2r_g}}{1 + J(1-k)} - \frac{(1-\sin\ \theta_c)}{\theta_c} \right] + (1-k) \left[\frac{(1-\sin\ \theta_c)}{\theta_c} - \frac{\frac{R_r Jk}{2r_g}(k-1)}{1 +J(1-k)} \right] \right\}$$

(3.(ii).25)

Work done against friction between tube and mandrel (W_{fb}):

The rate of work done against friction between tube and mandrel per unit volume as presented by Labib can again be simplified and then integrated for application to the three-roll configuration to give:

For zone 1:

$$\dot{W}_{fb1} = \frac{6}{\sqrt{3}} m_1 \bar{\sigma}_y R_r r_b \gamma_c \int_o^{\phi_n} \left[\left\{ U_o + U_o J \left(1 - \frac{\phi}{\phi_m}\right) \right\} - v_b \right] d\phi$$

For zone 2:

$$\dot{W}_{fb2} = \frac{6}{\sqrt{3}} m_2 \bar{\sigma}_y R_r r_b \gamma_c \int_{\phi_n}^{\phi_m} \left[v_b - \left\{ U_o + U_o J \left(1 - \frac{\phi}{\phi_m}\right) \right\} \right] d\phi$$

Equal peripheral contact angles (θ_c) between tube and rolls and between tube and mandrel is assumed.

Noting that $v_b = U_r$ when $\phi = \phi_n$

i.e. $v_b = \omega R_r = U_o + U_o J \left(1 - \frac{\phi_n}{\phi_m}\right)$

By definition $W_{fb} = \dfrac{\dot{W}_{fm1} + \dot{W}_{fm2}}{\dot{V}_o}$

and again approximately writing $\phi_n = k\,\phi_m$ with $m_1 = m_2 = m$, then:

$$\bar{\varepsilon}_{fb} = \frac{2\sqrt{3}\, m\, r_b\, R_r \gamma_c \phi_m\, J}{A_o} \left[k^2 - k + \frac{1}{2} \right] \qquad (3.(ii).26)$$

3.(ii).4 TUBE DEFORMATION MODELS

3.(ii).4.1. SINKING

From the relevant experimental evidence supplied by Haleem (40) and the photographs from the present work displayed in PLATE 7.1 the arc radius of the free zone (R_f) can be taken to be similar to the roll radius at the root of the groove (R_r). This suggests that in the current work the measured arc contact length (L_m) is approximately equal to half the arc length over the complete deformation region (L_a). Therefore one is lead to the somewhat rudimentary assumption that the total tube reduction can be divided approximately equally between the respective reductions in the free and contact deformation regions.

These assumptions together with the roll contact deformation zone modes FIGURE 3.21., will form the basis of the assumed theoretical model for the sinking process. Appendix H.1.1/2 presents a worked example.

3. (ii).4.2. MANDREL ROLLING

Mandrel rolling exhibits partial peripheral contact between the working surfaces and,for the three-roll stand,higher tube reductions. Consequently the process approaches that of flat rolling at the root of the roll groove.

Labib (43) utilised his pin load cell readings to establish a typical roll groove pressure/roll angular contact graph as shown in FIGURE. 3.24 . This graph indicates the peak roll pressure values which define the boundary of the tube deformation zones. These zones,approximately equal, represent the friction vector directions at the roll-tube surface. Therefore in the absence of further evidence,equal deformation zones will form the basis for the mandrel rolling model as presented in FIGURE. 3.25.

Labib also assessed the pre- or free deformation zone , observing a piling up of the tube material prior to actual roll contact causing the contact area between the roll and tube to increase. This piling up of the tube material was observed in the current three-roll investigation. However, its presence appeared to be not so pronounced (see shadowgraph profiles PLATE 7.3) and due to lack of further experimental evidence will be neglected in the theoretical deformation model.

Appendix H.2.1/2 presents a worked example.

3.(ii).5. ROLL SEPARATING FORCE AND TORQUE FOR SINKING AND MANDREL ROLLING BY THE EQUILIBRIUM AND ENERGY METHODS

To evaluate for each roll, the roll separating force and the roll torque, the mean roll pressure acting over the relevant surfaces area of contact between the roll and tube is required and is obtained as follows:

3.(ii).5.1. Surface area of contact (S)

To a first approximation since it is suggested by photographic evidence see PLATE 7.2 , the real surface and the horizontal projected areas of contact are assumed to be rectangles and semi-ellipses for sinking and mandrel rolling respectively. With reference to FIGURE 3.11 and FIGURE 3.23 , the following expressions are presented for the real surface area of contact (S_s) and the projected area of contact (S_p) per roll, respectively:

$$\left.\begin{aligned} S_{rs} &= L_m\, 2r_g\, \theta_{cl} \\ S_{ps} &= L_m\, 2r_g \sin\theta_{cl} \quad \text{for sinking,} \end{aligned}\right\} \qquad (3.(ii).27)$$

and

$$S_{rm} = \frac{\pi}{2} L_m r_g\, \theta_{cl} \qquad (3.(ii).28)$$

$$S_{pm} = \frac{\pi}{2} L_m r_g \sin\theta_{cl} \quad \text{for mandrel rolling.}$$

(3.(ii).28)

3.(ii).5.2. Mean total roll pressure (p_m)

Haleem's and Labib's derivation of the basic equation for the mean roll pressure (p_m) equation and, with no contribution to the total work per unit volume (W_e) by the normal mandrel pressure, is:

$$p_m = \frac{\bar{\sigma}_y \bar{\varepsilon}_A A_o}{3 r_g \delta \theta_{cl}} \quad \text{for sinking,} \quad (3.(ii).29)$$

$$p_m = \frac{\bar{\sigma}_y \bar{\varepsilon}_A A_o}{3 r_g \theta_{cl} (t_o - \bar{t}_1)} \quad \text{for mandrel rolling.}$$

(3.(ii).30)

3.(ii).5.3. Roll separating force (R.S.F.)

The product of the mean roll pressure (p_m) and the horizontal projection of the area of contact on each roll (S_p) gives the individual roll separating force.

3.(ii).5.4. Roll Torque

The total roll torque (T_t) can be estimated by considering the moment of the individual resultant radial roll force i.e. approximately the R.S.F., about the roll axis, and introducing the concept of the lever arm (a), shown in FIGURE 3.22:

$$T_t = 3\ (R.S.F.)a \qquad (3.(ii).31)$$

Alternatively, to display graphically the experimental R.S.F. against roll torque relationship and provided linearity is present, to deduce the relevant linear equation.

CHAPTER FOUR

THE COMPLETE EXPERIMENTAL THREE-ROLL MILL

4. THE COMPLETE EXPERIMENTAL THREE-ROLL MILL

4.1. DESIGN CONSIDERATIONS

The premise of this thesis is to consider the mechanics of the three-roll longitudinal tube rolling process for the sinking, mandrel rolling and stretch reducing of hot steel tube, or, as in this case lead tube at room temperature as an analogue for hot steel.

In the laboratory it is common to simulate 'actual' metal working conditions by the use of a stable, low strength model work material such as lead or wax. At room temperature these materials behave in a manner similar to hot steel, but because with model materials temperature effects are absent and the yield stress is low, test procedures are more reproducibly and easily carried out; pure lead has been selected for the proposed test programme. Nevertheless, because it may be desirable to compare the hot rolling of steel with the rolling of lead, the basic mill has been designed to roll hot steel.

For an investigation into the three-roll longitudinal tube rolling process which is to supply information relating to roll forces, roll torques and tube tensions the following characteristics must be possessed by any experimental mill:

1. Minimum speed variation between the three rolls,
2. Easy adjustment of the roll gap, easy removal of

the rolls, or the exchange of the roll diameter and profile.

3. The ability to apply easily a known and controllable axial tension in the tube.
4. A cost effective design for the basic units compatible with accurate and reproducible results.

Since a single stand three-roll model mill was envisaged, the design of the main item i.e. the power unit with drive to the three rolls, was complicated by the necessity to change roll diameters and speeds and to apply front and back tension to the workpiece; these difficulties become greatest when the system is entirely mechanical. This necessity tends to direct thought, therefore, to the consideration of a more 'flexible' system, where each roll is driven independently by direct electric or hydraulic means. These latter systems, although possessing flexibility, have the disadvantage of probable speed variation between the rolls. It is particularly important in an experimental investigation to minimise this speed variation, but complicated roll speed control arrangements would be required for its minimisation. This disadvantage however is eliminated in a mechanical system where constant speed of the three rolls is ensured by gearing and this arrangement is generally used in existing production mills.

From experimental evidence available of the two-roll longitudinal tube rolling process in which a mechanical roll drive system was employed and in which pure lead was used as the model metal, the following preliminary data were collected:

Tube dimensions: 44.45mm o.d. x 31.75mm i.d. (1.750in x 1.250in)
Power (max) per roll: 400 w ($\frac{1}{2}$ hp)
Roll speed range: 0.3 rev min^{-1} - 2.7 rev min^{-1}
Roll dia. range: 170mm-340mm (7in-13in)
Power (max) for front or back tension: 400 w ($\frac{1}{2}$ hp)

The power requirements quoted exclude transmission losses and other inefficiencies but are relevant to the rolling of lead tube. Therefore, the projected power requirements, detailed later, were increased to include losses and to allow for the possibility of hot steel tube being rolled in future tests.

With this information it is possible to present arguments for various proposed systems for driving an experimental three-roll longitudinal tube-rolling mill.

4.2. MECHANICAL SYSTEM

A schematic diagram of a mechanical system for the three-roll longitudinal tube rolling mill is shown in FIGURE 4.1.

4.2.1. Main Power Unit

Power input to the system is provided by a flange mounted electric motor and Kopp Variator coupled to a standard reduction gear giving a variable output speed range.

4.2.2. Power Division Unit

The power from the main unit is transmitted to the three drive shafts by helical gears which reduces spurious teeth 'noises' i.e. torque variation, to a minimum.
Considerations in the design of this multi-drive system were:

Scheme (i)

As shown in FIGURE 4.1., by transmitting the output power from the main unit to a large annular sun gear, which then divides the power to the three drive shafts via the three small planet gears. The large

SCHEMATIC DIAGRAM

OF MECHANICAL SYSTEM

FIGURE 4.1

sun gear is annular for passage of the tube and to assist in the application of tube tension.

Scheme (ii)

To employ a standard multi-spindle unit (as for drilling machines) with helical instead of spur gears. This unit having one input and three output shafts, off-set from the tube axis for reasons given above.

Scheme (i) although perhaps ideal, would require a substantial fabricated supporting structure and when complete with bearings would be an expensive arrangement.

Scheme (ii) employing a standard power division unit would certainly be the cheaper. However, with the need to off-set this unit in relation to the tube axis, an initial angular displacement would be imposed on each of the three drive shafts at the universal joints, possibly restricting adjustment of the roll diameter over the specified range and also decreasing the transmission efficiency.

It may be noted that the recommended maximum angular displacement of universal joints is 15^{o}. A condition likely to limit the adjustment of the drive shafts in scheme (i) rather than scheme (ii).

4.2.3. Drive Shafts and Roll Drive Units

The three drive shafts which transmit power to the rolls, each contain two universal joints and an axial sliding arrangement to accommodate changes in roll diameter and for this purpose it was decided to employ standard automobile propellor shafts.

Each of the three drive shafts was coupled to a standard worm gear unit mounted on a sliding cross head (as used on shaping machines) to facilitate changes in the roll diameter and profile.

4.2.4. Tube Tension Units

The front tension unit has been designed to apply a constant axial tension (or 'pull') to the tube irrespective of changes in the tube speed. Consequently, a d.c. shunt motor with feed-back control is required. A bull-block drum on the output shaft will produce the front tension via a steel cable attached to the rolled tube and wound round the drum.

A similar unit was planned to provide a controlled back tension with an eddy current dynamometer replacing the d.c. shunt motor.

4.3. HYDRAULIC SYSTEM

4.3.1. Without Feedback Speed Control

A hydraulic system for the three-roll longitudinal tube rolling mill is shown schematically in FIGURE 4.2. The system comprises a hydraulic pump-electric motor unit, 'driving', via associated piping and valves, etc., three hydraulic motors, i.e. one hydraulic motor per roll.

A feature of the system is a facility for the pump unit to be connected to the hydraulic motors either in a series or a parallel arrangement, thereby enabling their respective performances on test to be assessed.

A problem associated with this form of drive system is speed variation between the rolls, particularly at low roll speeds. Although this factor may not be of great importance on multi-roll production mills applying tube tension between the stands, speed variation between the rolls is certainly not desirable in a controlled experimental investigation, particularly where performance comparisons are required with previous two-roll experimental work where the rolls are mechanically coupled.

For this hydraulic system a 2% speed variation between the three rolls at 10 rev min^{-1} and a 5% speed variation between the three rolls at 2 rev min^{-1} have been quoted.

The above quoted percentage speed variations between the rolls, particularly at a roll speed of 2 rev min^{-1}, are unsatisfactory for an experimental investigation. A feedback arrangement is therefore required to control directly the roll speeds to ensure that the speed variation between the rolls does not exceed 1% over the specified roll speed range of from 2 rev min^{-1} to 10 rev min^{-1}.

4.3.2. With Feedback Speed Control

A hydraulic system with associated feedback roll speed controls for the three-roll longitudinal tube rolling mill is shown schematically in FIGURE 4.3.

This system employs a hydraulic motor with reduction gear synchro for each roll and these are 'driven' through parallel connections by the hydraulic pump-electric motor unit. The addition of a tachometer to one of the rolls and servo valves to each of the three rolls, with relevant hydraulic equipment, enables the 'loop' to be closed. This design involves both a velocity and positional feedback for one roll and for the remaining two rolls a

NOTATION FOR FIGURES 4.2. & 4.3.

A - accumulator
Cv - check valve
CV - control valve
Em - electric motor
FC - flow control
Hm - hydraulic motor
Hp - hydraulic pump
Oc - oil cooler
Rv - relief valve
Sv - servo valve
S - synchro
T - tachometer

SCHEMATIC DIAGRAM OF HYDRAULIC SYSTEM

(WITHOUT FEEDBACK SPEED CONTROL)

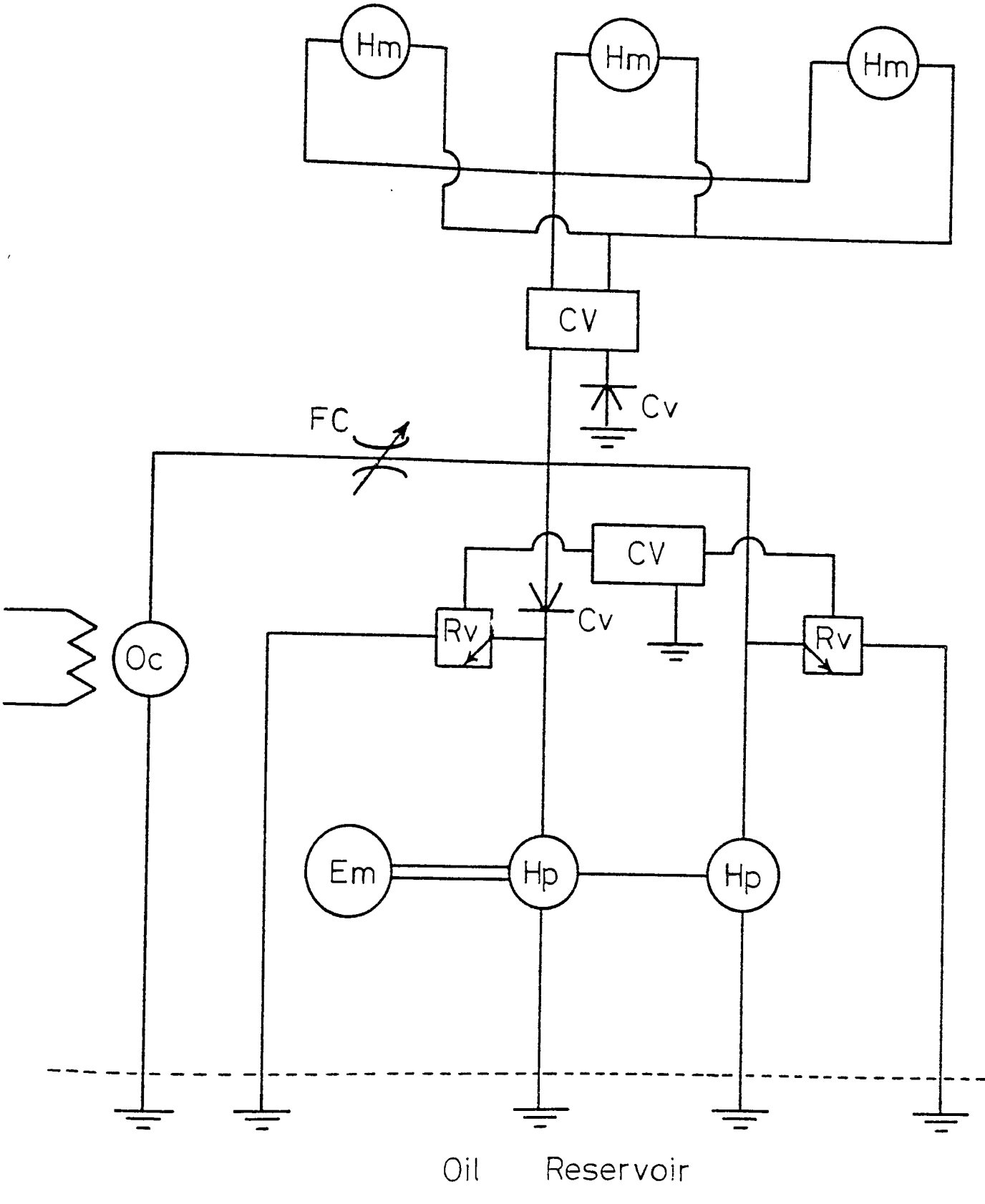

FIGURE 4.2

SCHEMATIC DIAGRAM OF HYDRAULIC SYSTEM

(WITH FEEDBACK SPEED CONTROL)

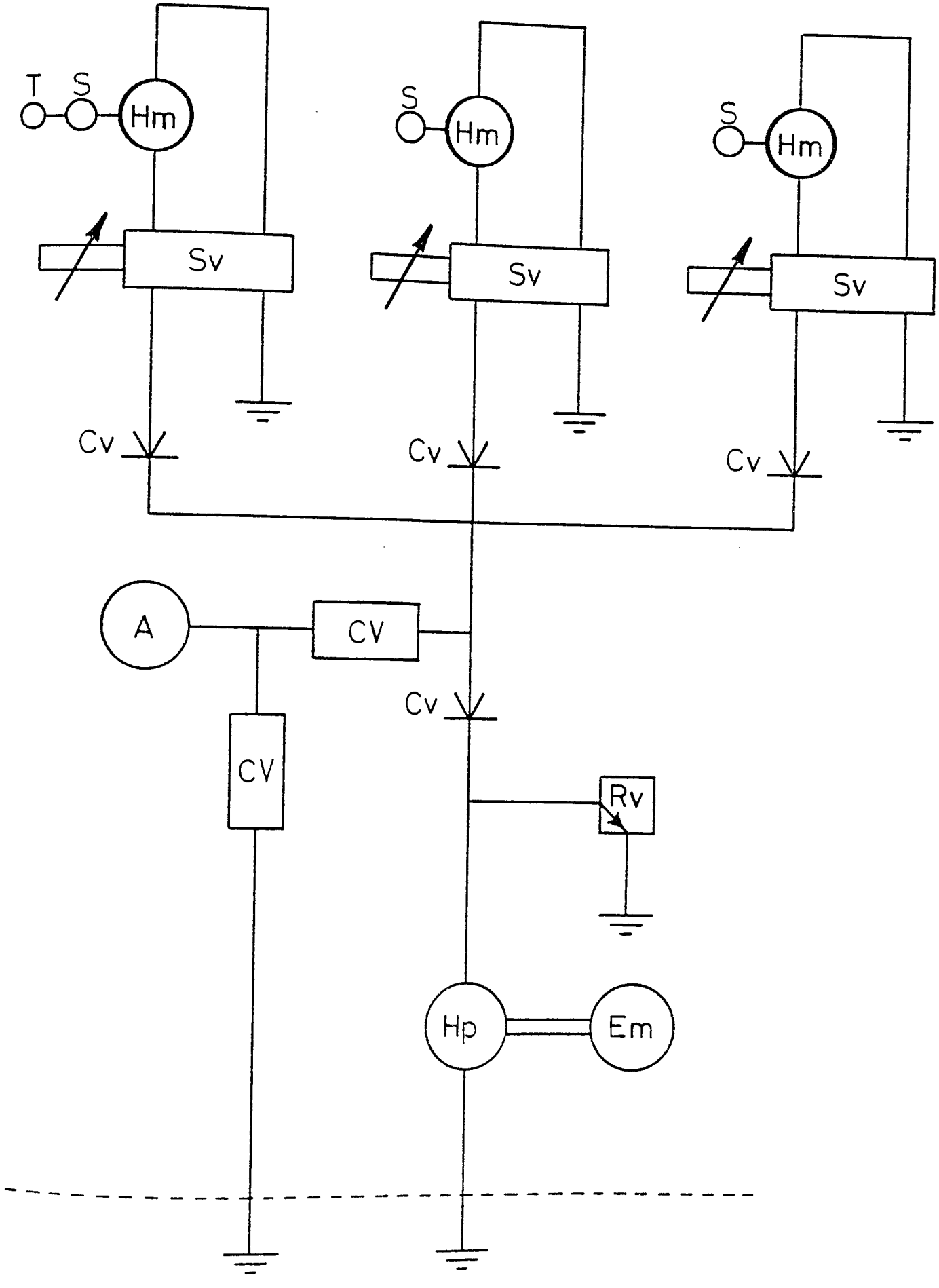

positional feedback from the relevant synchro. A point to note is that planetary spur gearing is employed in the reduction unit which is incorporated in the hydraulic motor and as previously mentioned this type of gear form could introduce spurious 'noise' into the system with a disturbance of measurement.

It was anticipated that the system would meet the requirements of a 1% speed variation between the rolls adequately for any set roll speed in the specified range of from 2 to 10 rev min^{-1}.

4.3.3. Tube Tension Units

Although hydraulic pumps could be coupled to cylinders and pistons which could be utilised to apply the front and back tension to the rolled tube, a mechanical arrangement was adopted since it was cheaper and more practicable.

4.4. ELECTRIC SYSTEM

Although a 'flexible' drive system for the three rolls could be accomplished by employing independent electric motors for each roll, such an arrangement would require gearing to obtain the very low roll speeds and servomechanisms to control the speed variation between the rolls to within the specified limit of 1%.

Thus an electric system would be of a complex and costly nature by comparison with the mechanical and hydraulic proposals and therefore its study was not pursued.

4.5. ESTIMATED COST COMPARISON OF THE VARIOUS SYSTEMS

The following is an estimated cost comparison of the various proposed systems considered based on prices, etc., relevant to the early 1970's.

Proposed Mechanical System

		Total Cost (£)
(i)	Roll wormgear speed reducer (Ratio 35/1) x 3	100
(ii)	Main power unit x 1 Electric motor (3½ hp x 960 rev min^{-1}) + Kopp Variator + Reduction gear (Ratio 8/1)	1,060
(iii)	Front tension arrangement x1 As above + additional reduction gear (Ratio 30/1)	720
(iv)	Power division unit x 1 Standard multi-spindle unit (spur gearing only)	250
	OR	
	Helical sun gear (x1) + Helical planet gear (x4)	220

		Total Cost (£)
(v)	Drive shaft x 3 By Hardy Spicer - 13/10 series (Land Rover) with companion flanges	100
(vi)	Supporting structure for power division and main power units	400
(vii)	Framework for complete mill including facility for roll adjustment	1,000
	Estimated total cost of mechanical system	3,600

Proposed Hydraulic System Without Feedback Roll Speed Control	Total Cost (£)
(i) Electric motor (10 hp x 960 rev min^{-1}) Hydraulic pump unit x 1	320
(ii) Hydraulic motor x 3 (one per roll)	820
(iii) Flow control unit x 1	120
(iv) Ancillary equipment (i.e. Control and relief valves, cooler, filter, manifold and general pipework, etc.)	780
Estimated cost of hydraulic system without control devices	2,040

With Feedback Roll Speed Control	Total Cost (£)
(i) Electric motor (15 hp x 1440 rev min^{-1})	Cost of individual units not available
Hydraulic pump unit x 1	
(ii) Hydraulic motor/reduction unit x 3 (one per roll)	
(iii) Synchro x 3 (one per roll)	
(iv) Tachometer x 1 (on <u>one</u> roll)	
(v) Servo valve x 3 (one per roll)	
(vi) Ancillary equipment	
Estimated cost of hydraulic system with control devices	4,900

4.6. DESIGN CONCLUSIONS

Since these design requirements are not simply reconciled when roll axes are inclined at 120^{o} to each other and when the system is entirely mechanical, as is the case in the two-roll mill, the designer is tempted to adopt a more 'flexible' design i.e. a hydraulic or electric system. However, in a 'flexible' system, which might incorporate independently driven rolls, it may be difficult to ensure that the components perform as precisely as they would if the components were mechanically connected. For example, it is not easy to design a 'flexible' roll drive system to ensure that the rolls rotate at precisely the same speed as one another and at the same time satisfy the requirement that tube of different diameters is to be rolled or that one set of rolls is to be replaced by a set of a greater diameter. Nevertheless it is particularly important in a fundamentally reliable investigation to eliminate any difference in speed between the rolls.

It is apparent that the mechanical system and the hydraulic system with feedback roll speed control are the only design proposals capable of fulfilling the requirements for an experimental three-roll longitudinal tube rolling mill. A critical appraisal of these two systems was therefore required.

In capital expenditure and probably in running costs also, the mechanical system is the cheaper. However, it should be appreciated that economy can be an unsatisfactory yardstick to apply to a fundamental investigation where the conclusions have important implications. Basically, the mechanical system is the simpler and the more flexible if adjustments are required, however the hydraulic system is more compact; but compactness could well create maintenance difficulties - of great importance in an experimental investigation. Finally, the important question of speed variation between the rolls must be emphasised. Here the mechanical system where the rolls are geared to each other is superior and although the hydraulic system may well have achieved a minimum speed variation between the rolls, its use would probably entail considerable adjustment and time.

Therefore on the basis of the foregoing consideration the mechanical system with the helical sun and planet gearing for the power division unit was the better proposition, not only as regards meeting the required specification but for maintenance and relative cheapness. Consequently the temptation to adopt a 'flexible' system was resisted and a mechanical system albeit with its attendant problems was adopted.

4.7. DESIGN IMPLEMENTATION

The final design details of the units comprising the mechanical three-roll mill, are as follows:

To deform the tube as required and to accommodate transmission losses, a 3½hp electric motor for the main power unit was considered initially, however, to allow for the possible future rolling of hot steel a 7½hp motor was chosen. The complete main power unit is shown in PLATE 4.1; this photograph illustrates the original roll support units, which were later superseded by the present units shown in PLATE 4.2. With reference to PLATE 4.1., the main motor unit (A) comprises a 7½hp electric motor, a Kopp Variator, and a reduction gear (32:1). This unit has an output speed range of from 10 rev min^{-1} to 90 rev min^{-1}. Following the motor unit, an electro-magnetic clutch (B) was introduced to separate the main drive when necessary. In series with this clutch a further reduction unit (C) 4 1/3: 1 ratio was added to enable the power divider unit (D) to produce the appropriate output speed range to the wormgear reduction units and rolls; these latter items are also shown in PLATE 4.3.

To accommodate insertion of the three roll separating load cells, three roll support mounting brackets were

COMPLETE EXPERIMENTAL THREE-ROLL
TUBE ROLLING MILL (ORIGINAL)

PLATE 4.1

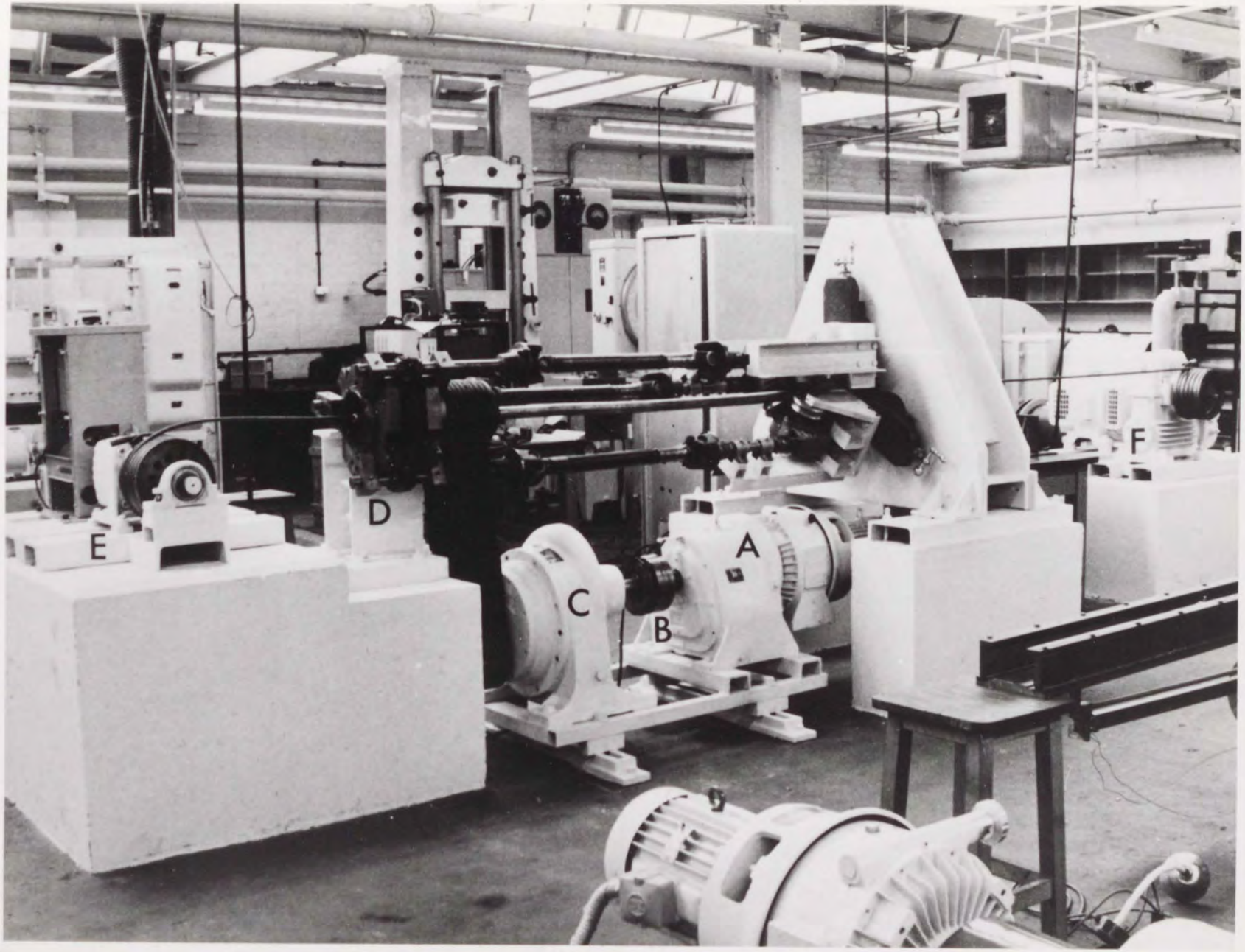
E
D
C
B
A
F

COMPLETE EXPERIMENTAL THREE-ROLL

TUBE ROLLING MILL (PRESENT)

PLATE 4.2

THE THREE-ROLL STAND
WITH INSTRUMENTATION

PLATE 4.3

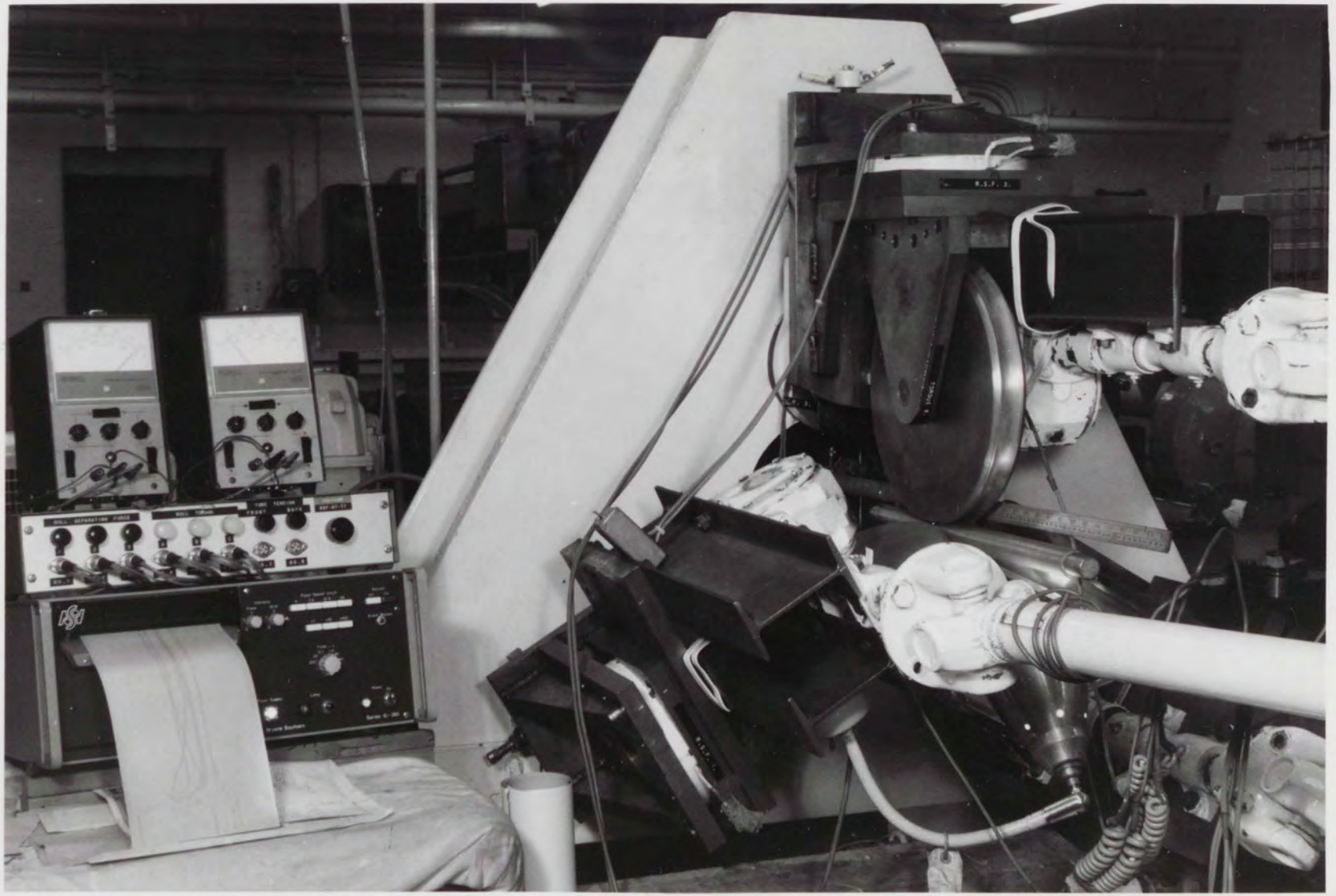

constructed, PLATE 4.4. These located the worm-gear and roll units on the adjustable radial crossheads mounted in the vertical plane. This provided diametral adjustment for each set of three-grooved rolls, which were additionally supported by bearing yokes at each roll shaft end as shown in PLATE 4.3. The radial sliding cross-heads are attached to the apices of an equilateral triangular structure comprising of 10 in x 10 in universal column stiffened by 1 in thick steel plate at each apex to form the three-roll vertical support framework, PLATE 4.4.

Following discussions with British Leyland (Longbridge) the Department was fortunate to receive a selection of double helical gears which, with modifications, proved ideal for providing the required division of the main drive, PLATE 4.1. and 2. Plain phosphor bronze bushes are used to support and locate the hollow main drive shaft and the three equi-angularly positioned drive shafts. Flexible V-belt drives transmit the drive from the main power unit to the hollow drive shaft. A 5hp dc shunt motor coupled to a double wormgear reduction unit (ratio 250:1) was selected for the front tension unit since a constant torque is required. This motor produces the required constant torque when a suitably adjusted voltage is supplied to the armature. A

R.S.F. 3.
TORQUE 8.
S.F. 3.
TORQUE 5.

drum which pulls the steel cable and so through grips applies tension to the tube, is keyed to the output shaft of the double wormgear reduction unit.

A constant torque system was also selected for the back tension unit and additionally, since the in-going tube speed is so low, an eddy current dynamometer coupled to a speed increaser unit was included. The degree of back tension available is controlled by manual adjustment of the d.c. current to the dynamometer. Again, as for the front tension unit, a drum with its associated steel cable and tube grips is employed except that in this case the drum is keyed to the "input" shaft of the dynamometer; i.e. the ingoing tube 'drives' the dynamometer. The speed increaser unit is required to multiply the relatively low speed of the drum so that the increased input speed presented to the dynamometer is in its constant torque speed range. A harmonic drive system possessing a high torque capacity and good efficiency was chosen for the speed increaser unit.

The front and back tube tension assemblies are shown respectively in PLATES 4.6., and 5,and in PLATE 4.1. at (F) and (E) respectively.

COMPLETE BACK TUBE TENSION UNIT

PLATE 4.5

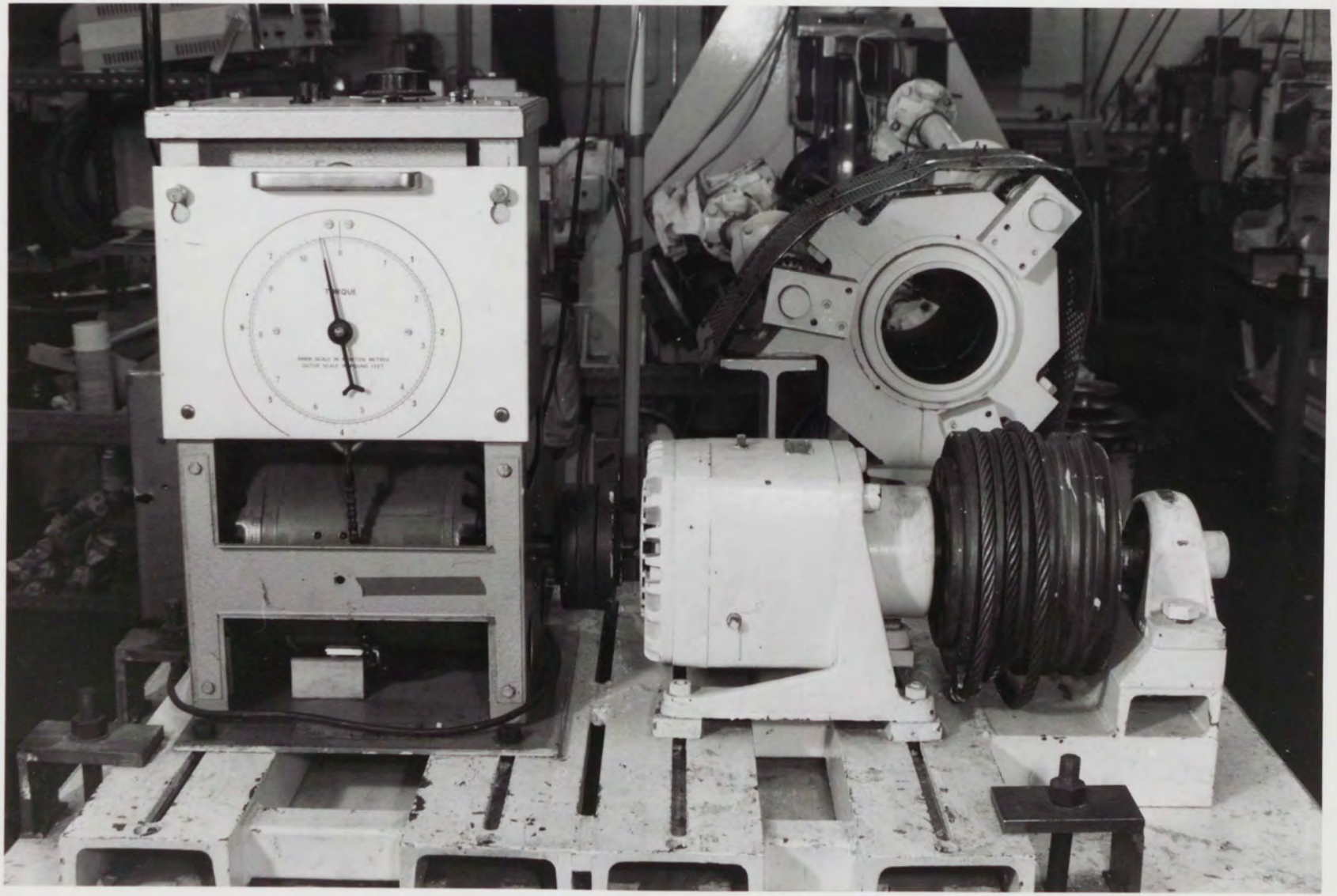

COMPLETE FRONT TUBE TENSION UNIT

PLATE 4.6

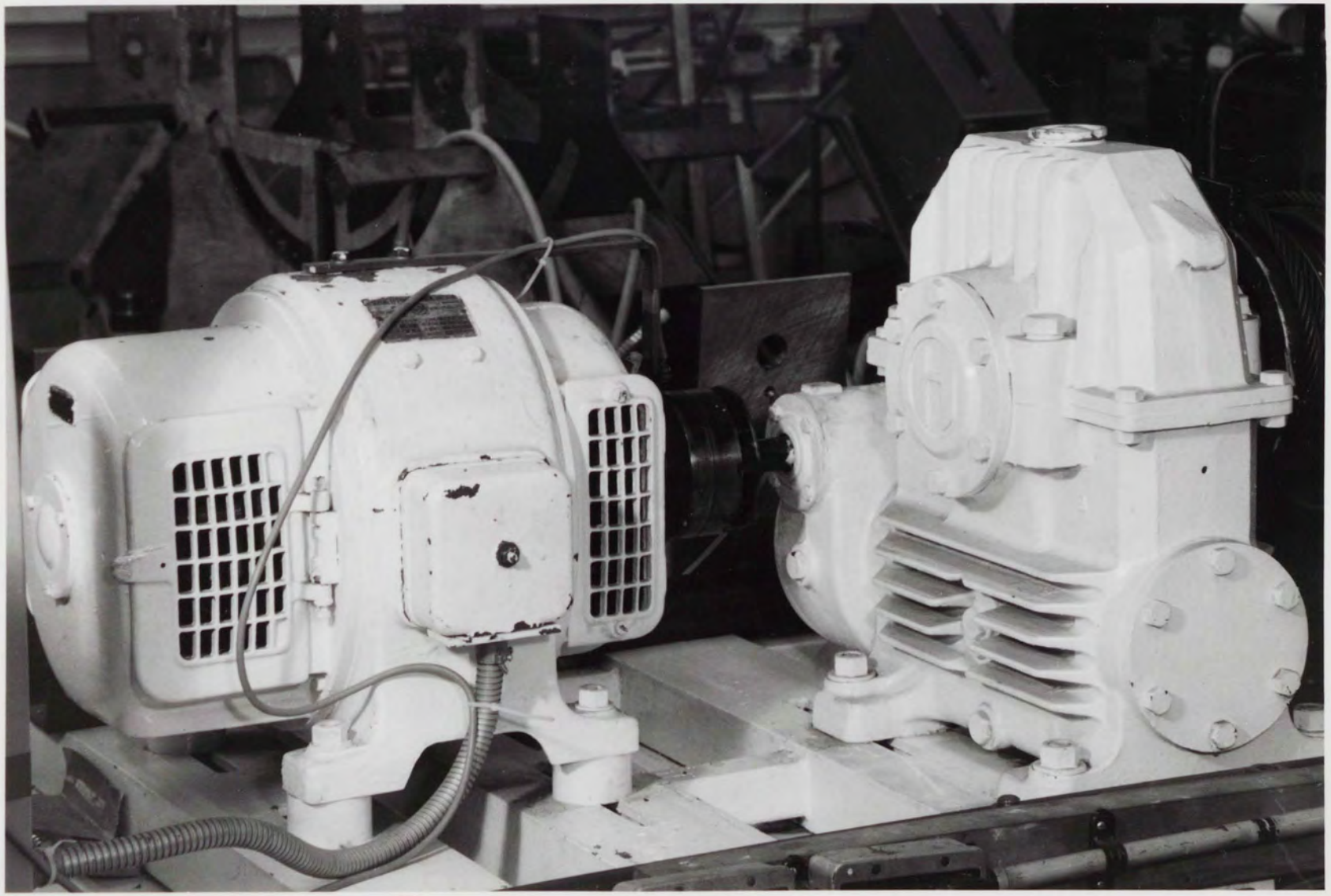

The main power drive unit was securely attached to the laboratory floor whilst the three-roll support framework, the power division unit and the front and back tube tension assemblies were mounted on reinforced concrete blocks of appropriate cross-section and height. To allow for longitudinal adjustment the front and back tension assemblies were located on slotted channel sections. The complete experimental three-roll mill is shown in PLATES 4.1. and 2., and relevant detailed drawings contained in Appendix B .

The philosophy of utilising where ever possible standard "bolt-on" components, allowed the final design of the three-roll tube mill to provide a flexible system which could form the basis for possible future research work employing similar mechanical configurations e.g. the three-roll piercing process, the Assel mill elongator etc. Furthermore, if the three-roll mill is eventually dismantled many of the standard components should find ready acceptance in other laboratory equipment.

4.8. ROLL SIZES

Since one of the variables to be considered was ratio: $\frac{\text{roll diameter}}{\text{tube diameter}}$ three different sets of roll diameters (measured to the roll shroud or flange) of 170mm (6.693in), 255mm (10.039in) and 340mm (13.386in) were chosen with the 255mm (10.039in) roll corresponding approximately to current three-roll mill practice.

The roll material was commercial mild steel since no heat treatment was necessary as the roll stresses were relatively low and the number of trials limited.

4.9. ROLL GROOVE PROFILE

In production mills, the roll groove profiles have various degrees of ovality for two reasons:

(1) to accommodate the inherent 'out of roundness' of the ingoing tube,

(2) to achieve a reduction in the outer diameter with a minimum distortion of the circularity of the bore.

(In the diametral reduction of tube by semi-circularly grooved rolls, deformation is produced by the sides of the groove before being produced by the root of the groove. This feature of the process results in the production of elliptically shaped tube. Thus the groove is designed to be semi-oval in shape and this maintains the essentially circular section of the tube). As it is intended to simulate mill rolling conditions, the groove profile is based on current designs.

The following is a brief analysis for the determination of the basic profile of the groove in a three-roll mill. Tube mill practice for the two-grooved roll configuration utilizes a relationship:

$$\alpha = 0.758 \beta + 0.989$$

where

$$\beta = \frac{D_{ingoing} - D_{outgoing}}{D_{ingoing}}$$, i.e. the tube reduction

and

D = tube o.d.

where

$$\alpha = \frac{A_1}{B_1}$$ i.e. the degree of ovality

and

A_1 = roll major dia.(in.)

B_1 = roll minor dia.(in.)

The mean outgoing tube diameter is given by:

$$\frac{A_1 + B_1}{2}$$

To cover the envisaged experimental programme, it is assumed that the maximum reduction in area will be 25% (this includes tube rolling on a mandrel), consequently, if

$\beta = 0.25$

and $\alpha = 1.179$

with $A_1 + B_1 = 2.70$

the degree of ovality is approximately 1.18.

At this stage the transfer from a two-roll to a three-roll profile is undertaken. The degree of ovality required is 1.18; therefore with reference to FIGURE 4.4., the ratio r_g/h_s is equated to 1.18.

Since $(h_f + h_s)$ must equal 1.30 in., the geometry of the configuration gives:

$$h_s = 0.691 \text{ in.,(17.55mm)}$$
$$r_g = 0.815 \text{ in., (20.70mm)}$$

and the eccentricity,

$$e_g = 0.206 \text{ in. (5.23mm)}$$

The resultant groove profile is indicated in FIGURE 4.4. and although somewhat less sophisticated than profiles operating in some mills, it is none-the-less a good approximation possessing the characteristics of reproducibility and ease of manufacture.

THREE-ROLL GROOVE PROFILE

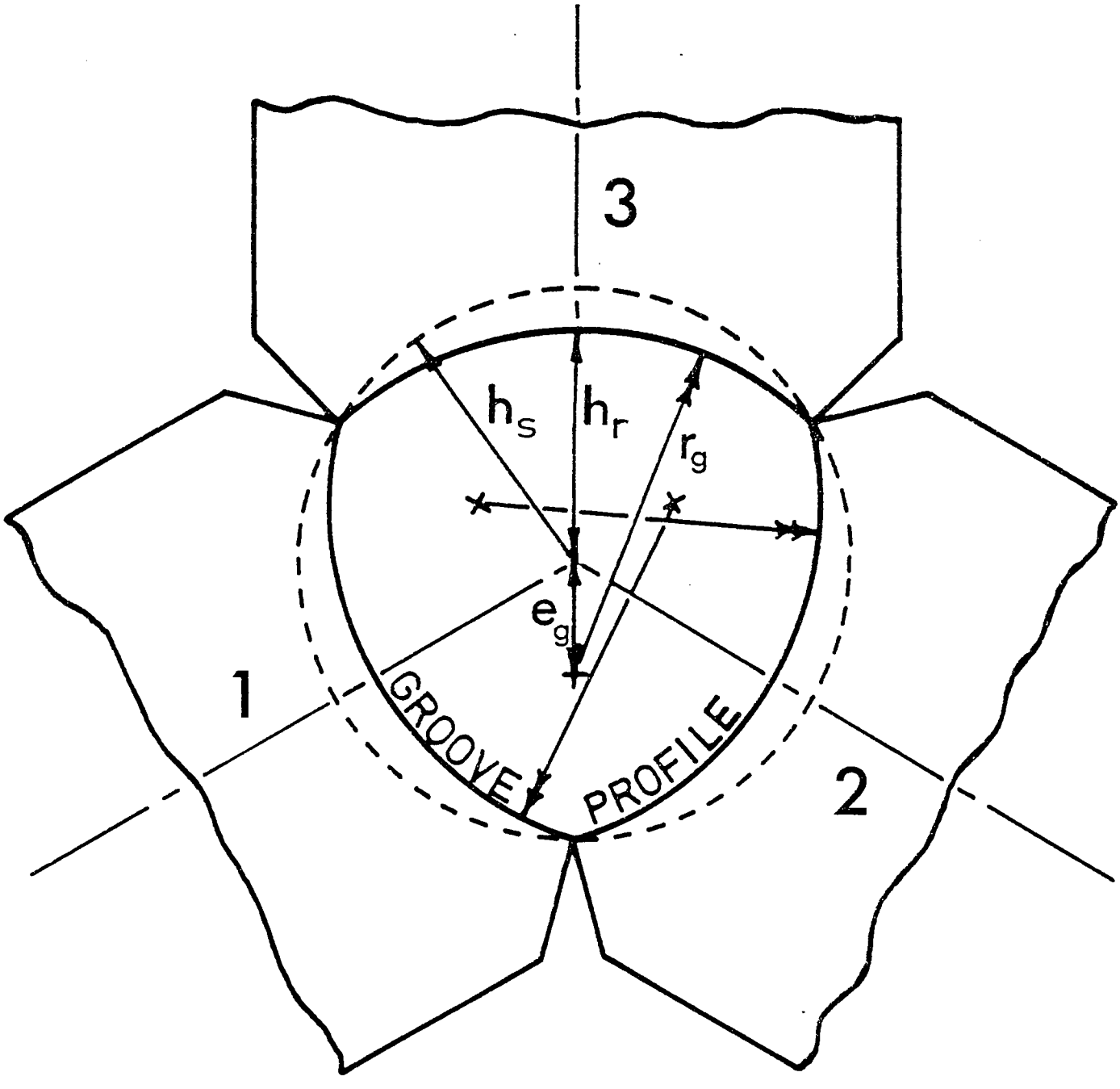

FIGURE 4.4

4.10. MEASURING EQUIPMENT

4.10.1. Roll Separating Force (R.S.F.) Loadcells.

The inherent design of the three-roll tube mill placed restrictions on the axial height and allowable compression of the R.S.F. loadcells. After numerous loadcell designs and trials had been considered and rejected, a relatively new design of loadcell was utilised which satisfied, load, sensitivity and minimal deflection specifications while at the same time being axially compact.

The design analysis of the axially compact load-cell employed is presented in Appendix C, and the finalised version shown in PLATE 4.7. It can be seen that the loadcell consists of a continuous ring of rectangular section. On one face are eight equally spaced integral sectoral support pads and on the other face there is a similar number of equally spaced support pads at the mid-positions of the aforementioned pad spacing. Consequently the ring is formed from a continuous series of circumferentially shaped beams which strain in bending and torsion. When a compression force is applied to the loadcell, the active strain gauges, which are bonded to the ring on the face opposite

to the sectoral support pads, respond to a tensile bending strain. The "inactive" strain gauges are bonded to the inner and outer peripheral surfaces in the circumferential direction in line with the neutral surface. This strain gauge arrangement, shown in FIGURE 4.5., employing a total of thirty two strain gauges was adopted to compensate for temperature variations around the ring and any distortion other than that caused by axial compression.

The three loadcells, one per roll, were manufactured by turning and milling a bar of softened En 23 steel. After heat treatment (hardening at 850^{o}C for ½hr. and oil quenched, and tempered at 200^{o}C for 1½hr and air-cooled to give 52 Rockwell C) the inner and outer peripheries were fine-turned concentric and all the faces of the mounting support pads normal to the loadcell axis were ground flat and parallel.

Thirty two standard linear electrical strain gauges were then bonded to the loadcell in positions previously indicated and shown in PLATE 4.7.

As a protection against a possible hostile environment each loadcell was encapsulated in SILCOSET 105, a room temperature vulcanising resilient silicone rubber, PLATES 4.7., 8, and 9 show a loadcell before and after encapsulation and *in situ* respectively.

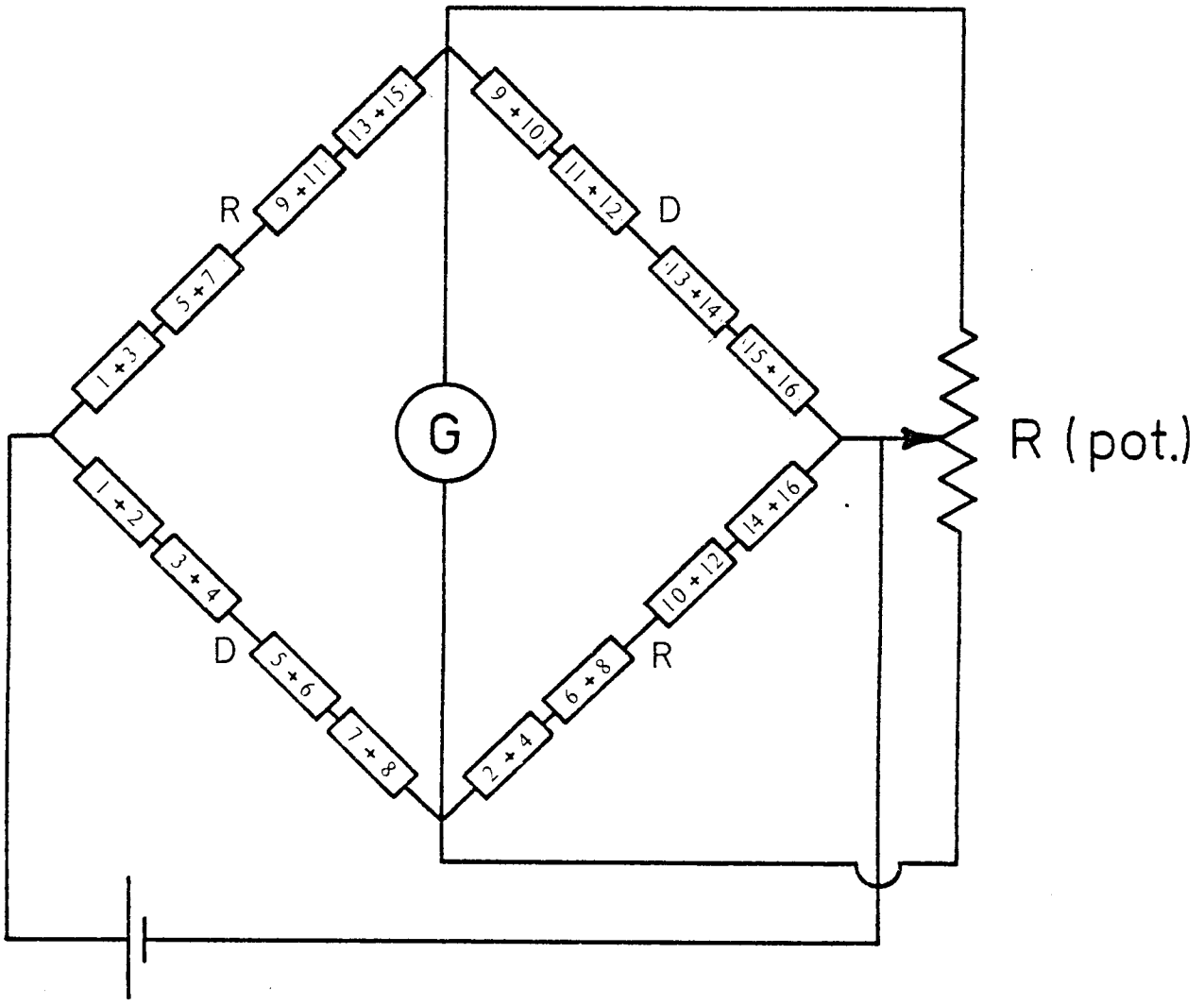

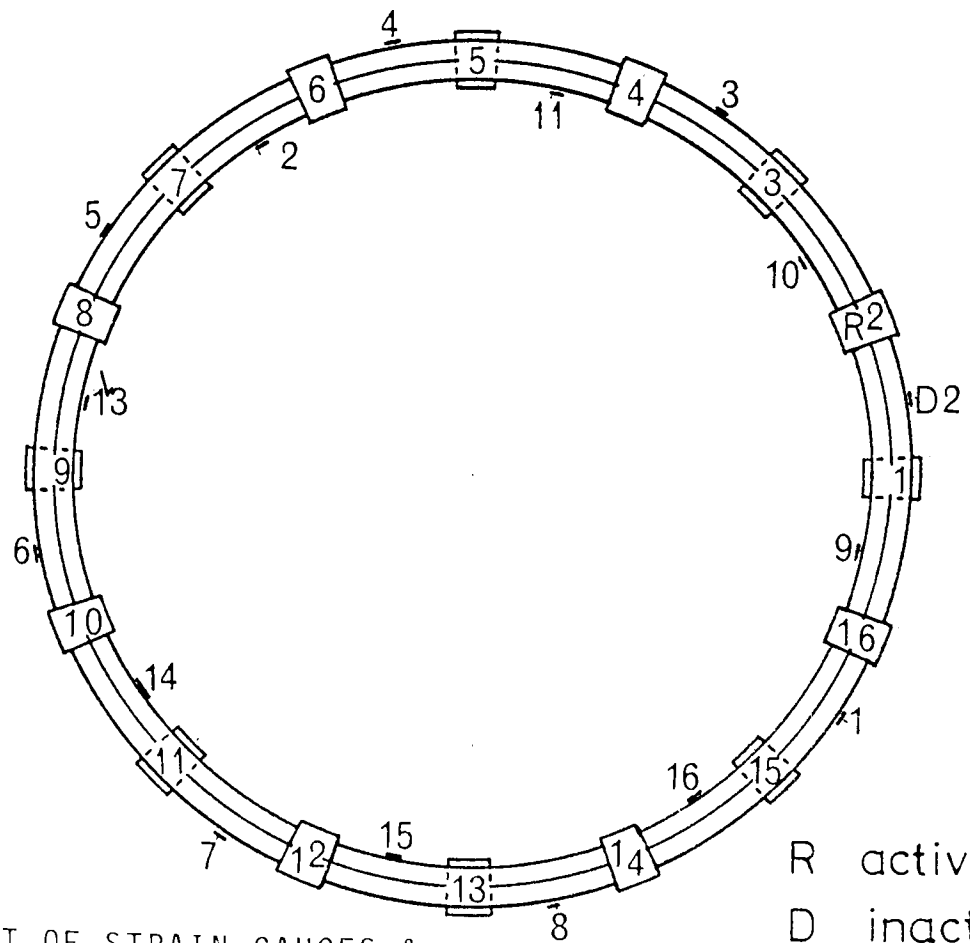

R active gauges R

D inactive gauges D

ENT OF STRAIN GAUGES &

T DIAGRAM OF AXIALLY COMPACT RING LOAD-CELL

AN AXIALLY COMPACT ROLL LOAD-CELL

(AFTER ENCAPSULATION)

PLATE 4.8

"IN SITU" CALIBRATION

OF A ROLL LOAD-CELL

PLATE 4.9

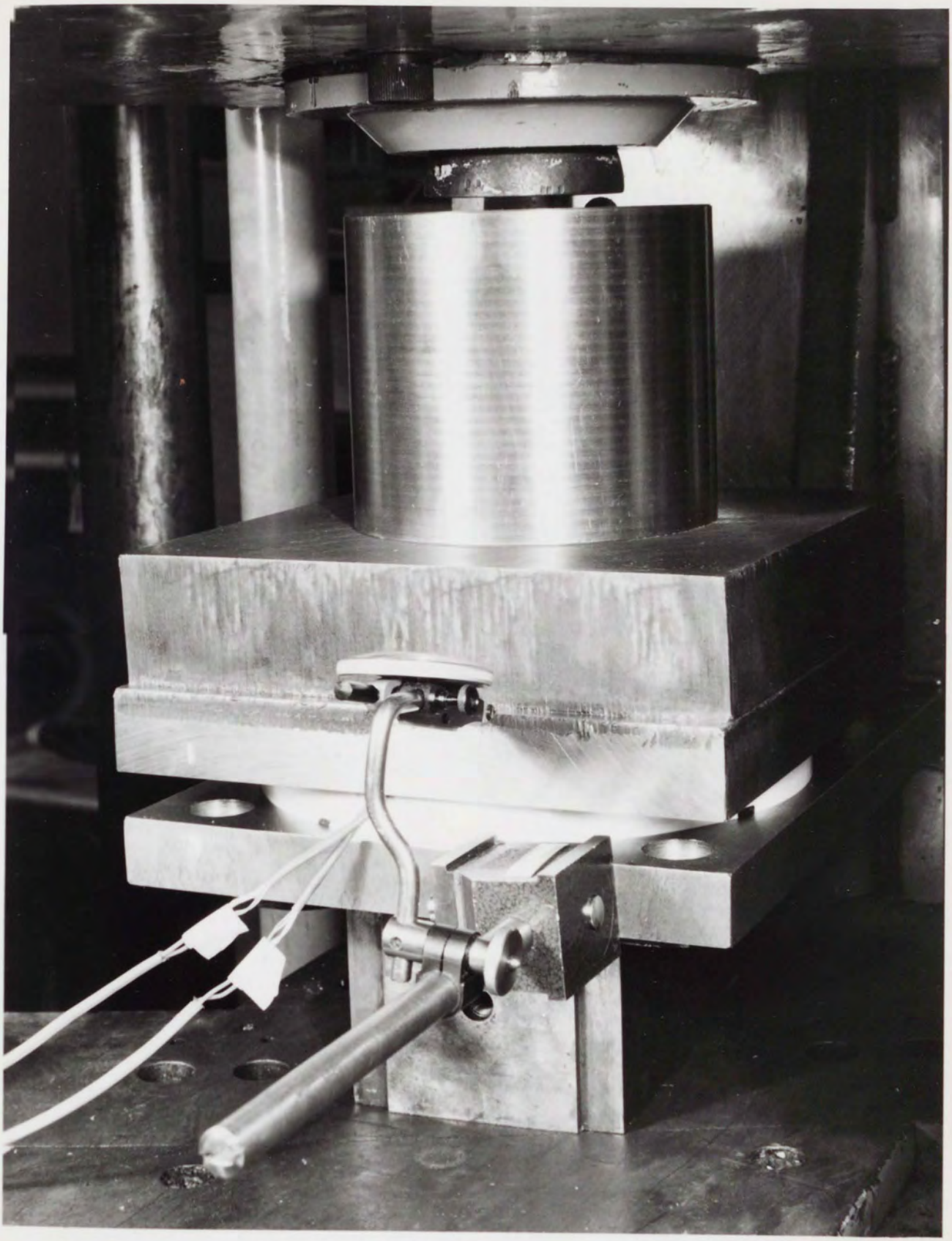

To facilitate positive location of the loadcells each outer face of the sectoral support pads were partially drilled and tapped and attached with socket screws to the recessed upper and lower mounting platens as shown in PLATE 4.4. As previously discussed these mounting platens transmitted the full R.S.F. from the roll through to the roll support mounting bracket and adjustable sliding cross head.

Because of the novel nature of the R.S.F. load-cells, exhaustive "calibration" trials were conducted. Initially, to confirm the insensitivity of the loadcell to mounting conditions at the sectoral pads, compressive load "calibration" tests were carried out under the following conditions:

1. loadcell loaded between plane platens,
2. " " within recessed mounting platens,
3. " " " " " "
   and socket screws attached finger tight,
4. ditto and spanner tight.

The resulting "calibration" graphs are shown in FIGURE 4.6.

Further compressive load "calibration" tests were conducted with the applied load at various

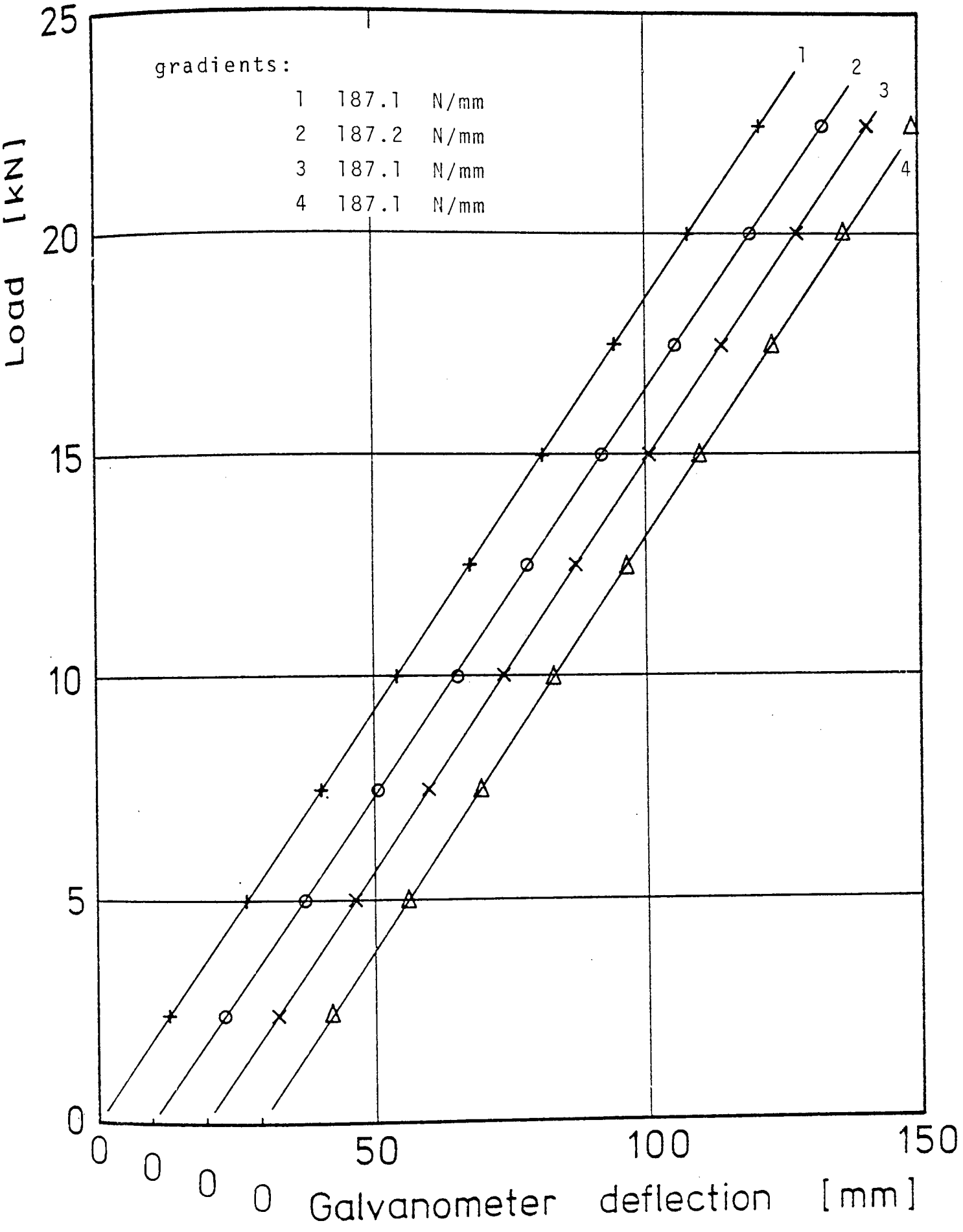

"CALIBRATION" TRIALS OF THE AXIALLY COMPACT LOAD-CELL

FOR VARIOUS MOUNTING CONDITIONS (12.0v)

FIGURE 4.6

eccentricities with respect to the loadcell axis, and with the applied load acting as a shear load i.e. parallel to the plane of the loadcell, simulating any longitudinal tube forces that may be transmitted to the loadcell. These"calibration" graphs are shown respectively in FIGURE 4. 7 and FIGURE 4.8.

All these "calibration" tests show straight lines, through the relevant displaced origin, with minimal scatter and negligible response to loadings other than the desired uniaxial compressive load.

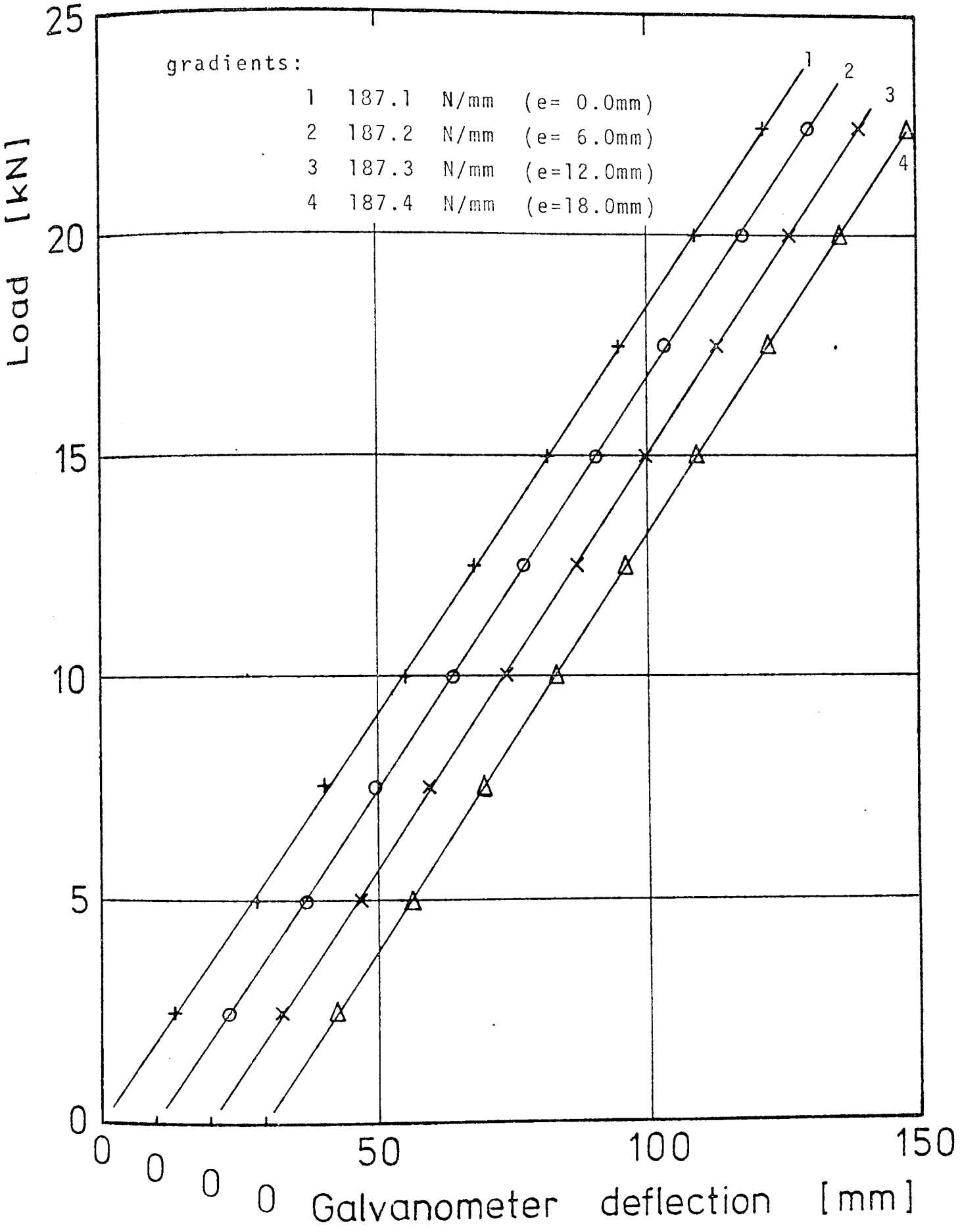

"CALIBRATION" TRIALS OF THE AXIALLY COMPACT LOAD-CELL FOR VARIOUS LOAD ECCENTRICITIES (e) - (12.0v)

FIGURE 4.7

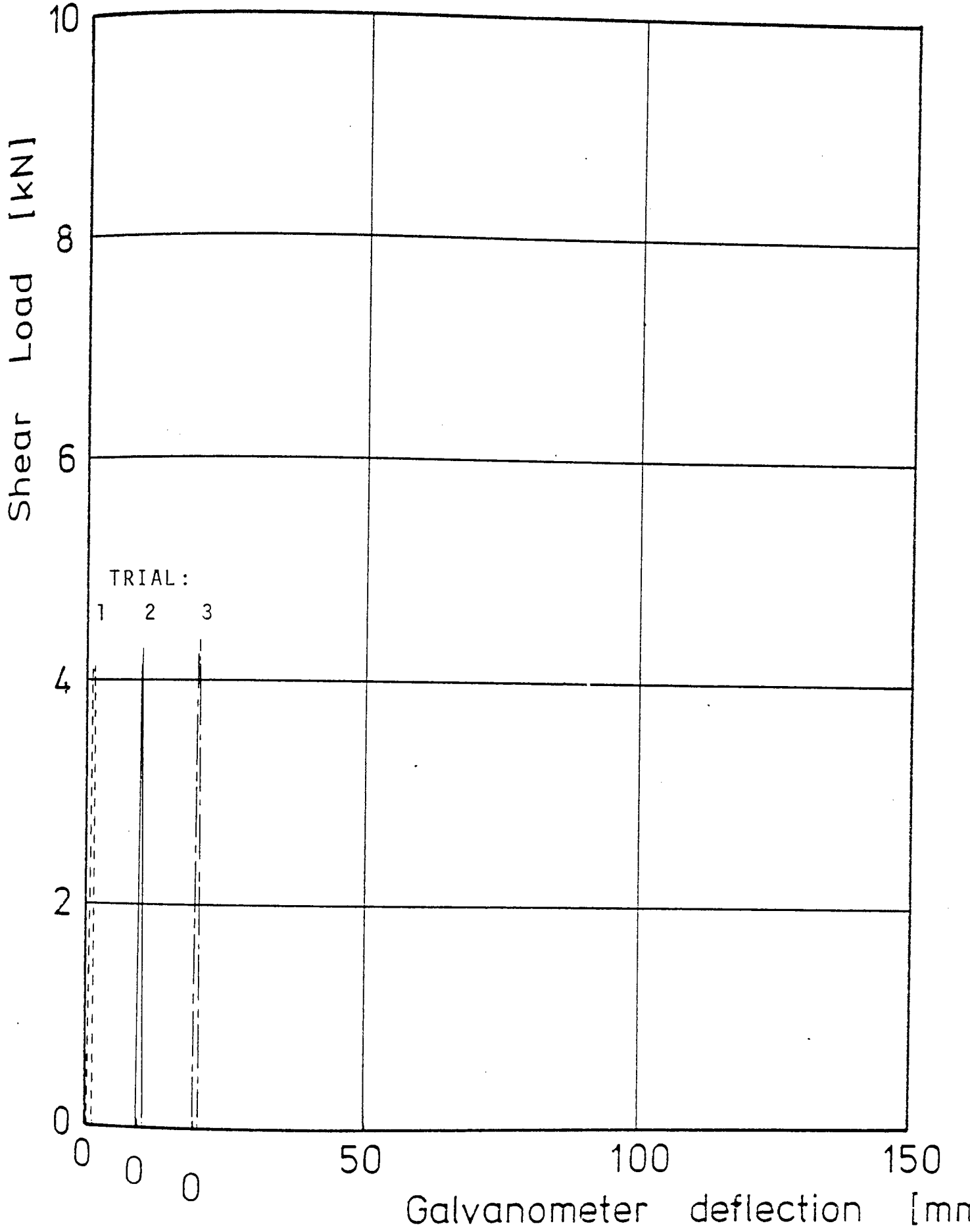

"CALIBRATION" TRIALS OF THE AXIALLY COMPACT LOAD-CELL FOR SHEAR LOAD

FIGURE 4.8

4.10.2. Roll Torque Cells

The roll torques on each of the three roll shafts were measured by means of eight 45^{o} electrical resistance torque strain gauges bonded directly on the entire peripheral length of the shafts as shown in PLATE 4.4. and connected in the bridge circuit shown in FIGURE 4.9. This standard bridge arrangement maximised the torque output signal, compensated for temperature variation, and eliminated any unwanted bending and thrust responses.

4.10.3. Tube Velocity

A knowledge of the inlet and outlet tube velocity during the rolling process was a necessary pre-requisite for the assessment of the deformation zones. As this requirement manifested itself during the early part of the experimental programme an elementary arrangement was set up to measure this velocity.

The arrangement shown in PLATE 4.4., comprised of a metre rule horizontally fixed by a tripod at the roll stand and placed adjacent to the tube specimen. By using the blimp facility on the u.v. recorder known lengths of the tube could be appropriately

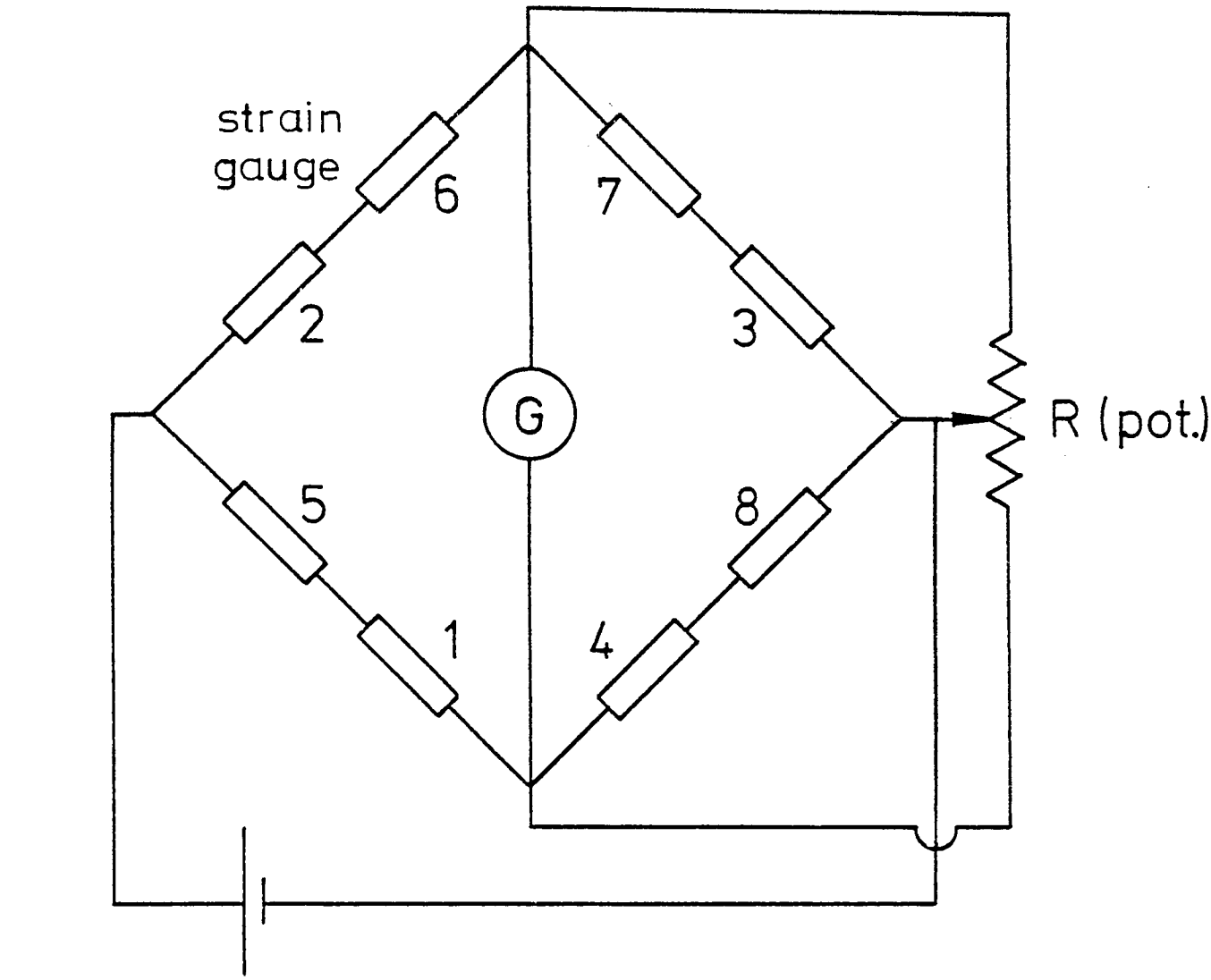

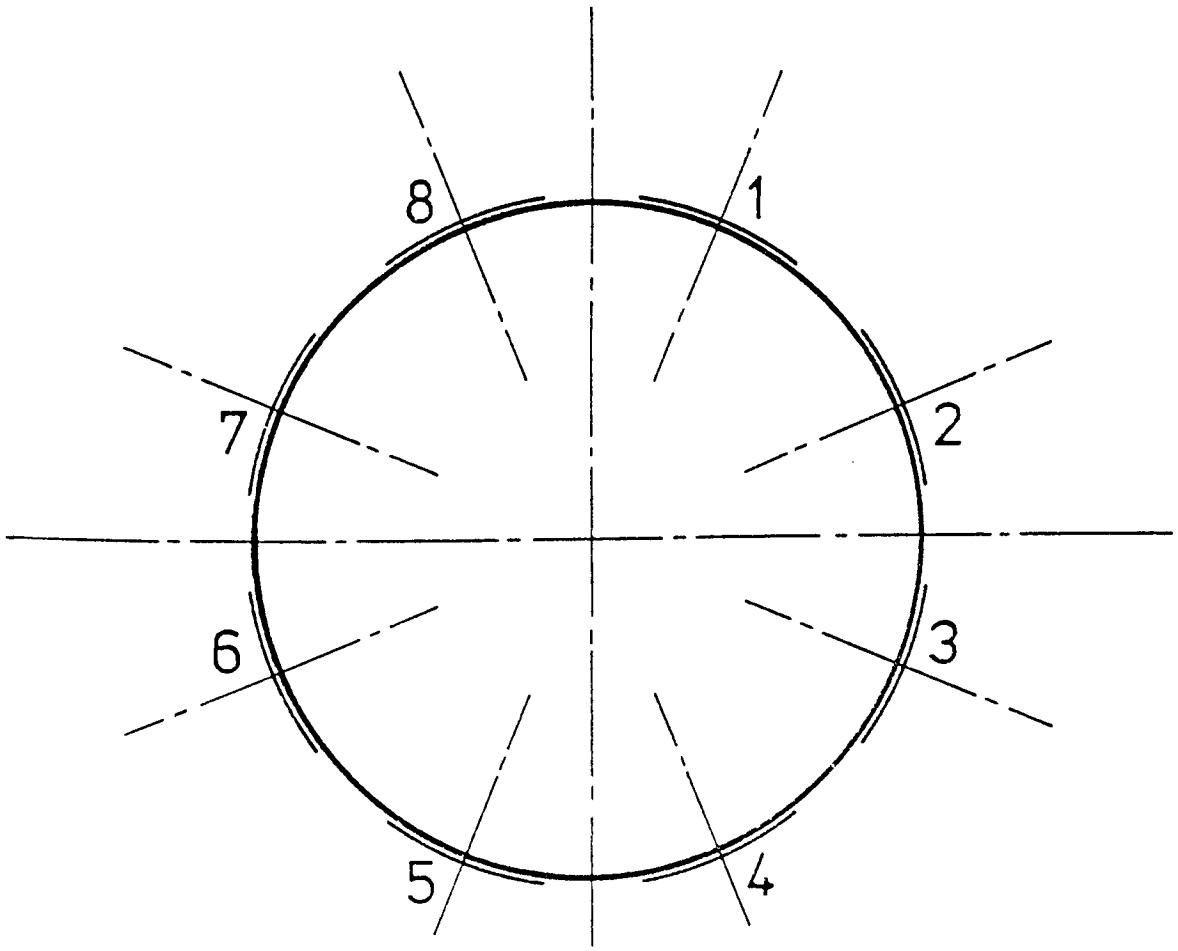

ALIGNMENT OF STRAIN GAUGES & CIRCUIT DIAGRAM OF TORQUE CELL

timed as the specimen entered and exited from the roll gap.

4.11. INSTRUMENTATION

Recordings of signals from the three R.S.F. load-cells and the three torque cells were made using a u.v. (ultra-violet) recorder. The recorder was a ten channel Bryan Southern type.

The basic requirements for any load or torque cell electrical circuit were, a stabilised d.c. supply voltage, a bridge balancing circuit and a galvanometer all interconnected in the fundamental Wheatstone bridge circuit shown in FIGURE 4.10.

The galvanometers, placed in parallel inside the u.v. recorder were of the mirror type, suspended coil, torsion filement. Ultra-violet light from a print source within the recorder was reflected by the galvanometer mirror onto a photosensitive paper which provided the tracing of the applied signal from the galvanometer

The balancing potentiometers for all the bridge circuits were assembled together in one balancing box unit. The screened leadwires from the three

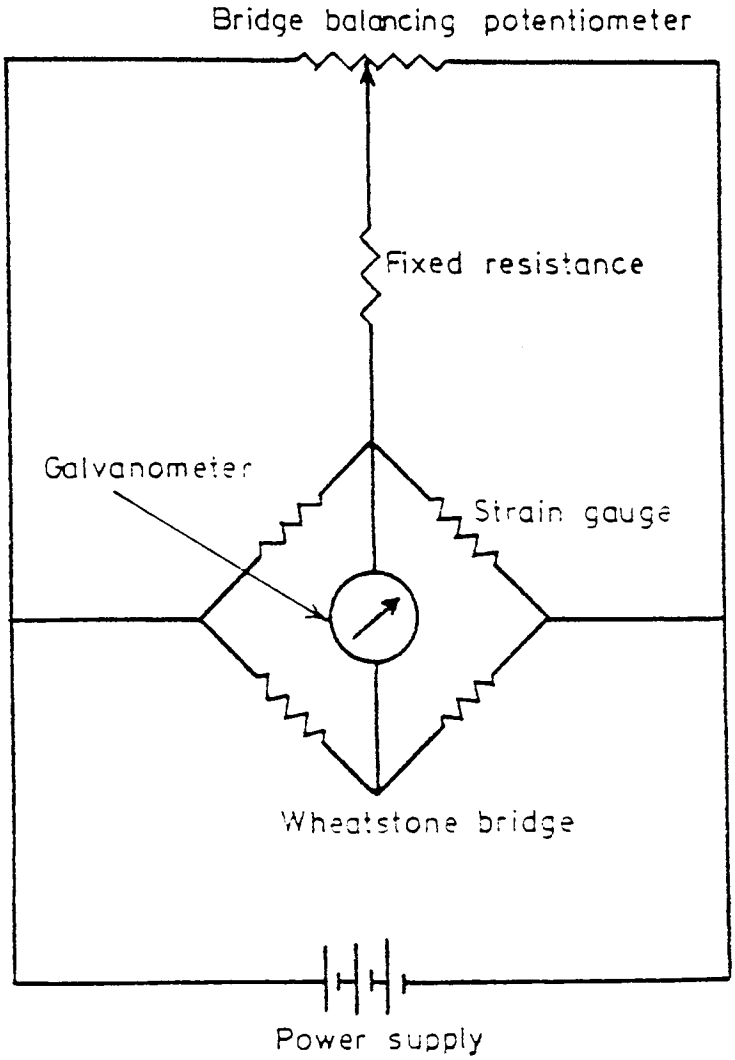

Electrical connections to each loadcell

FIGURE 4.10

loadcells and the three torque cells were connected directly to the balancing box and then coupled to the appropriate stabilised d.c. power supplies and u.v. recorder as shown in PLATE 4.3.

The measuring circuit sensitivity depends on the magnitude of the applied d.c. voltage to the Wheatstone bridge circuit and the natural frequency characteristic of the galvanometer. Working with such highly sensitive galvanometers meant that precise initial balancing of all bridge circuits was imperative, otherwise interference between un-balanced circuits rendered measurements spurious. This balancing was carried out by means of the variable potentiometer connected in parallel with one arm of each bridge circuit.

Preliminary measurement and tests were carried out to optimize the voltage level, the potentiometer resistance and the galvanometer characteristic for each individual circuit; these tabulated values are presented in Appendix D .

Because of the space restrictions present in the three-roll configuration the employment of a slip-ring per shaft to collect the torque cell signals was rejected and the lead wires to each torque cell were allowed to wrap themselves around the roll shaft.

This arrangement was quite feasible since the roll speeds were low (<3 rev min^{-1}) and a maximum of only five rotations of the roll shafts was envisaged.

The screened leadwires from the three torque cells incorporated a helically wound portion to allow controlled untensioned winding of the "flexible" leadwires around the rotating roll shaft.

4.12. CALIBRATION

Working calibrations were required for;

i) the compressive R.S.F. loadcell,
ii) the torque cells integral with the roll shaft.

The problem of calibrating for the subsequent measurement of the R.S.F. could be approached in two different ways: direct and indirect. The direct method would be to apply a known force, actually in the three-roll gap, to each roll groove in turn. This suggests that a a hydraulic cylinder/piston in series with a proving ring would have had to be employed, however, the space limitations imposed by the three-roll configuration would have made such a calibration technique extremely difficult.

The indirect method was therefore to be preferred for the individual calibration of each R.S.F. load-cell. Similar reasoning confirmed the indirect method for the individual calibration of each roll torque cell.

Preliminary tube rolling trials were conducted under sinking and mandrel conditions to evaluate the R.S.F. and roll torque ranges. These indicated that for

sinking the maximum R.S.F. and maximum roll torque were of the order of 10 kN and 320 Nm respectively and for mandrel rolling 25 kN and 700 Nm respectively.

4.12.1. Calibration of the R.S.F. Loadcells

Simulation of the actual loading conditions on the testing machine was readily achieved since the R.S.F. loadcells complete with their recessed locating platens and roll support mounting brackets were always subjected to the full compressive load. To complete the simulation of the actual rolling conditions the same leadwires and associated instrumentation were used for the calibration tests as were to be utilised in the tube rolling trials. The working calibration for both increasing and decreasing values of load were performed on a Denison Universal Testing Machine which had recently been checked and certificated.

The working calibrations for the three R.S.F. load-cells are reproduced in FIGURES 4.11 and 12 for both sinking and mandrel rolling conditions with the respective d.c. bridge supply voltage and all show straight lines through the origin with negligible scatter of points i.e. a linear, reproducible relationship between the R.S.F. load and the galvanometer deflection.

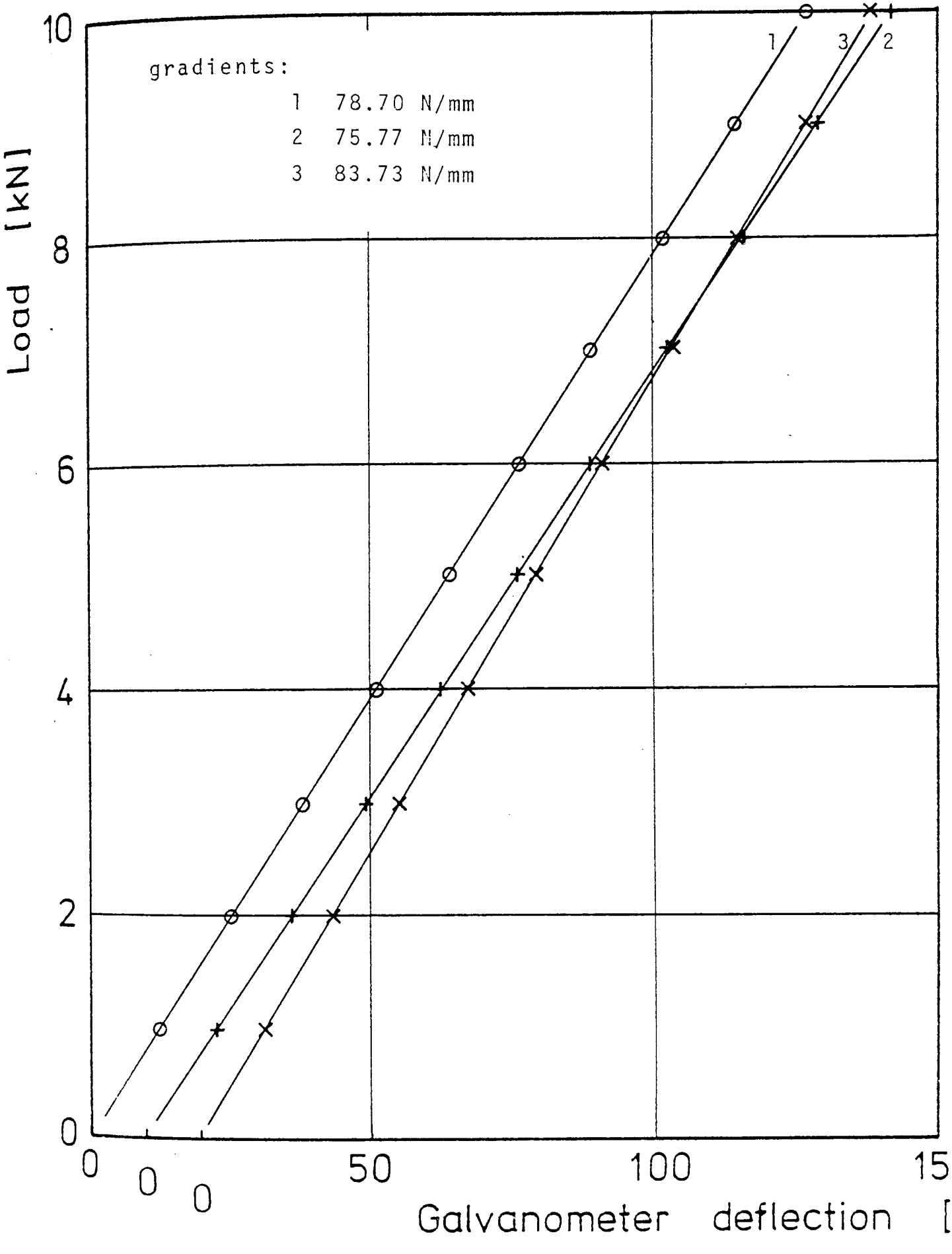

"WORKING" CALIBRATIONS FOR 1, 2 and 3 R.S.F. LOAD-CELLS

30 v d.c. bridge supply voltage.

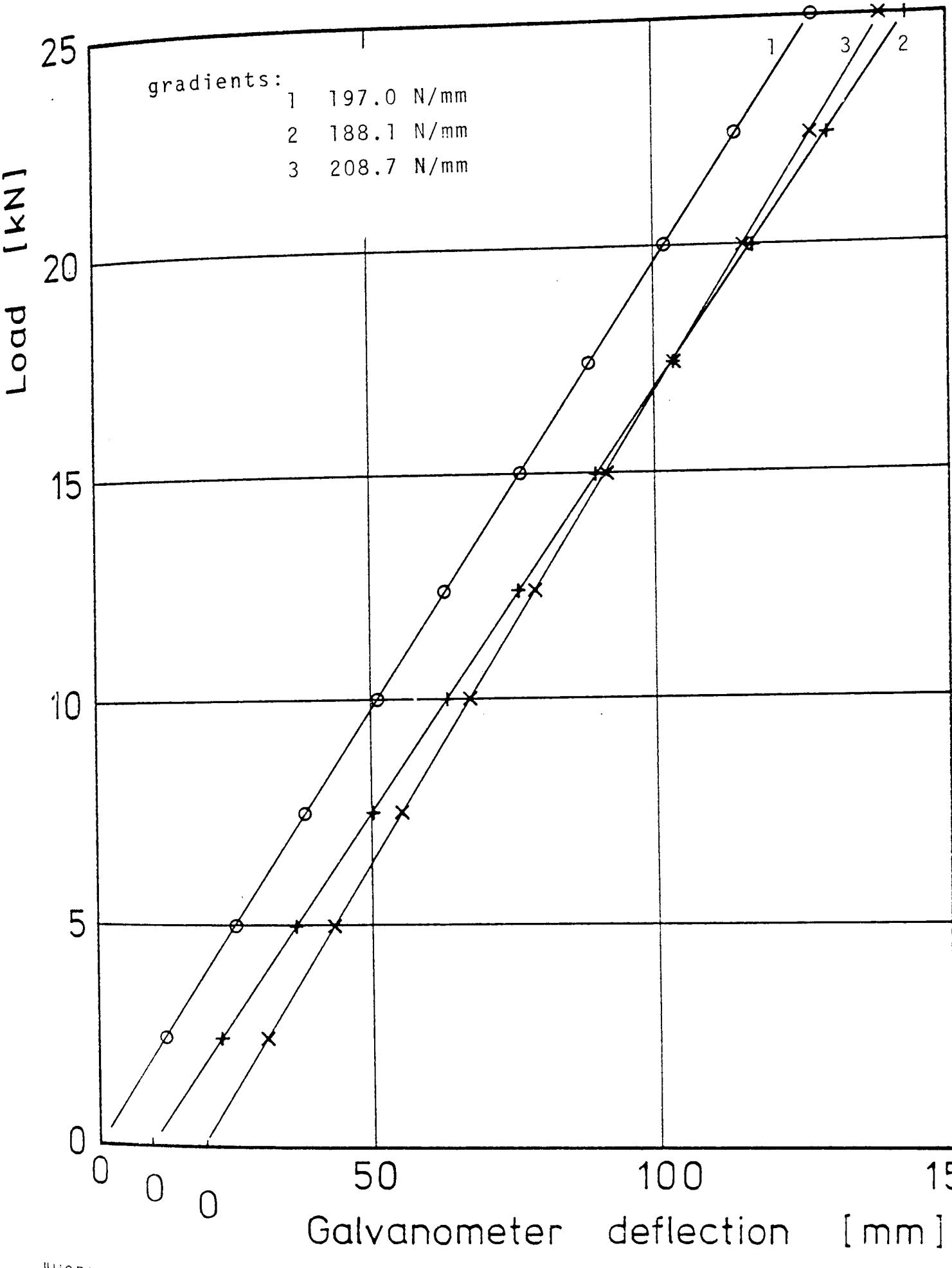

"WORKING" CALIBRATIONS FOR 1, 2 and 3 R.S.F. LOAD-CELLS
12 v d.c. bridge supply voltage

4.12.2. Calibration of the torque cells

As previously stated the indirect method of calibrating the torque cells was preferred with the wormgear units containing the roll shafts removed from the mill and firmly clamped to a bedplate. The torque cells were calibrated by the application of static moments to each roll shaft at the roll position. These moments were provided by the use of a lever arm and weights and is shown in position in PLATE 4.10. The lever arm, of 1m length, had a keyed boss end fixing which transmitted the moment from the lever to the roll shaft. The other end of the lever arm located a weight hanger to which known weights were applied.

Working calibrations of the torque cells were taken for both increasing and decreasing values of torque. Since the ends of roll shafts were supported by bearing yokes (PLATE 4.10) and to simulate actual roll torque conditions the torque cell calibrations were conducted under the following calibrations.

1. With (1) and without (2) the bearing yoke in position.

2. With the moment arm in various positions

"IN SITU" CALIBRATION

OF A ROLL TORQUE-CELL

PLATE 4.10

along the roll shaft,

3. with the roll shaft inclined at 120^{o}.

These additional calibration checks were carried out to confirm the insensitivity of the torque cells to bending and axial load conditions.

All the calibration graphs shown in FIGURE 4.13, 14, 15 and 16 show straight lines through the origin with negligible scatter of the points and insensitivity to unwanted signals.

Throughout all the calibration tests of the R.S.F. loadcells and roll torque cells the associated instrumentation was allowed sufficient time "to warm up" and stabilise, preliminary load and torque cycling carried out and the required d.c. supply voltage constantly monitored and adjusted if necessary.

As a further check for linearity of the variation of load and torque cell outputs with bridge voltage, comparisons of ratios of gradients and voltages for a particular load or torque cell were precise and therefore the calculation of roll load or torque for a situation in which the bridge voltage was other than that specified in the calibration could be carried out with confidence.

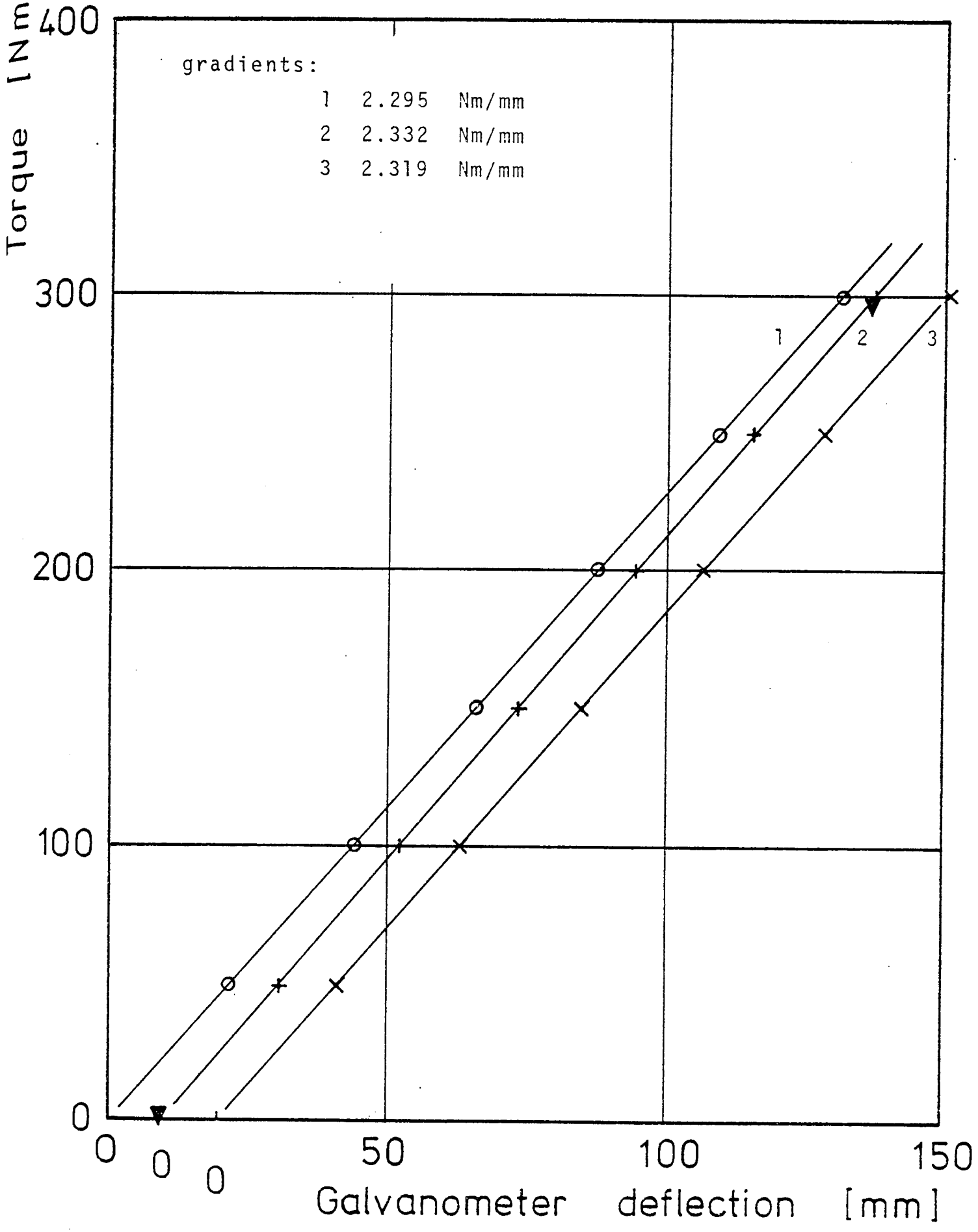

"CALIBRATION" TRIALS OF 1,2 and 3 TORQUE CELLS
WITHOUT BEARING YOKE (3.6 v)-(▼) bending arm extended by 30mm

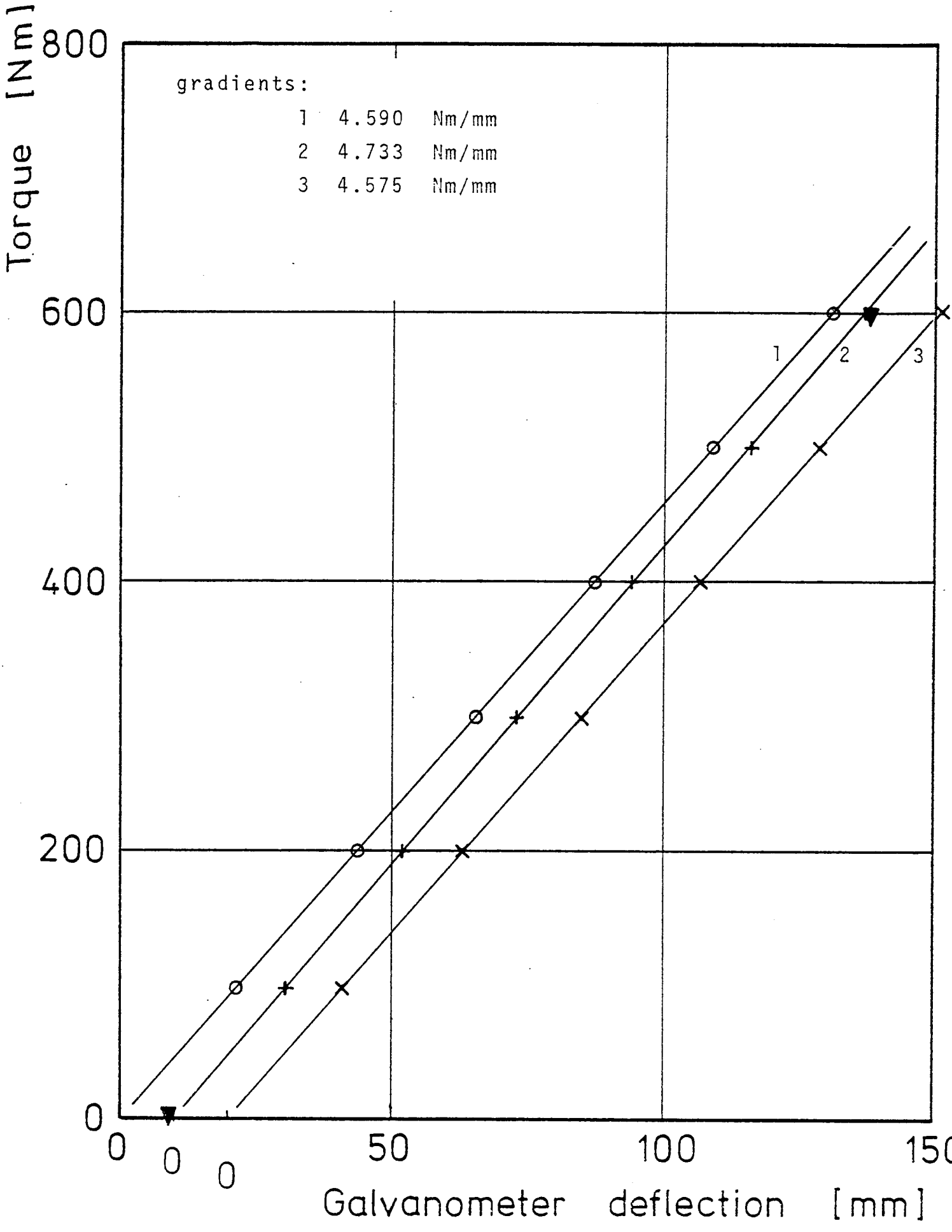

"CALIBRATION" TRIALS OF 1, 2 and 3 TORQUE CELLS
WITHOUT BEARING YOKE (1.8 v)-(▼) bending arm extended by 30mm

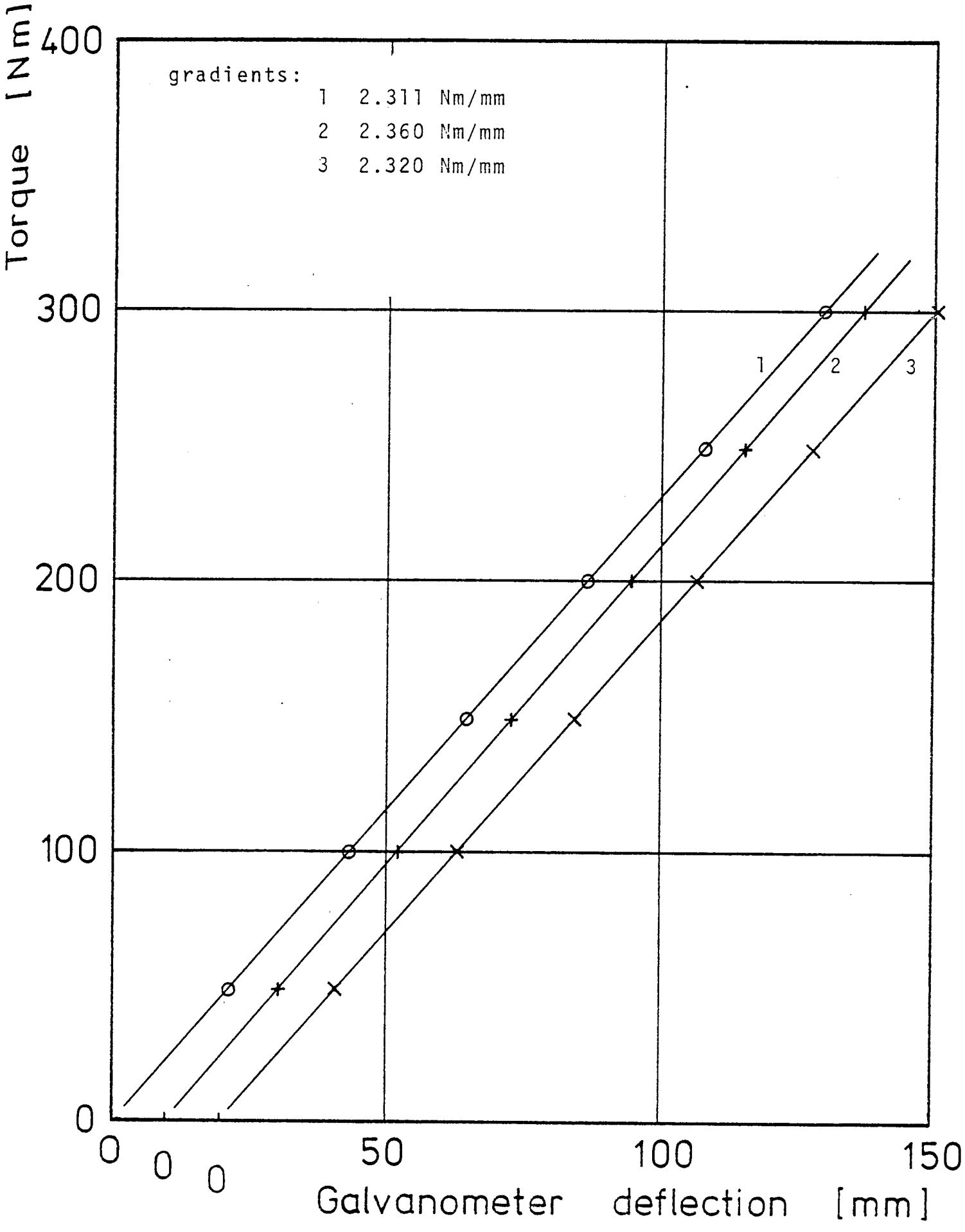

"WORKING" CALIBRATIONS FOR 1, 2 and 3 TORQUE CELLS
3.6 v d.c. bridge supply voltage.

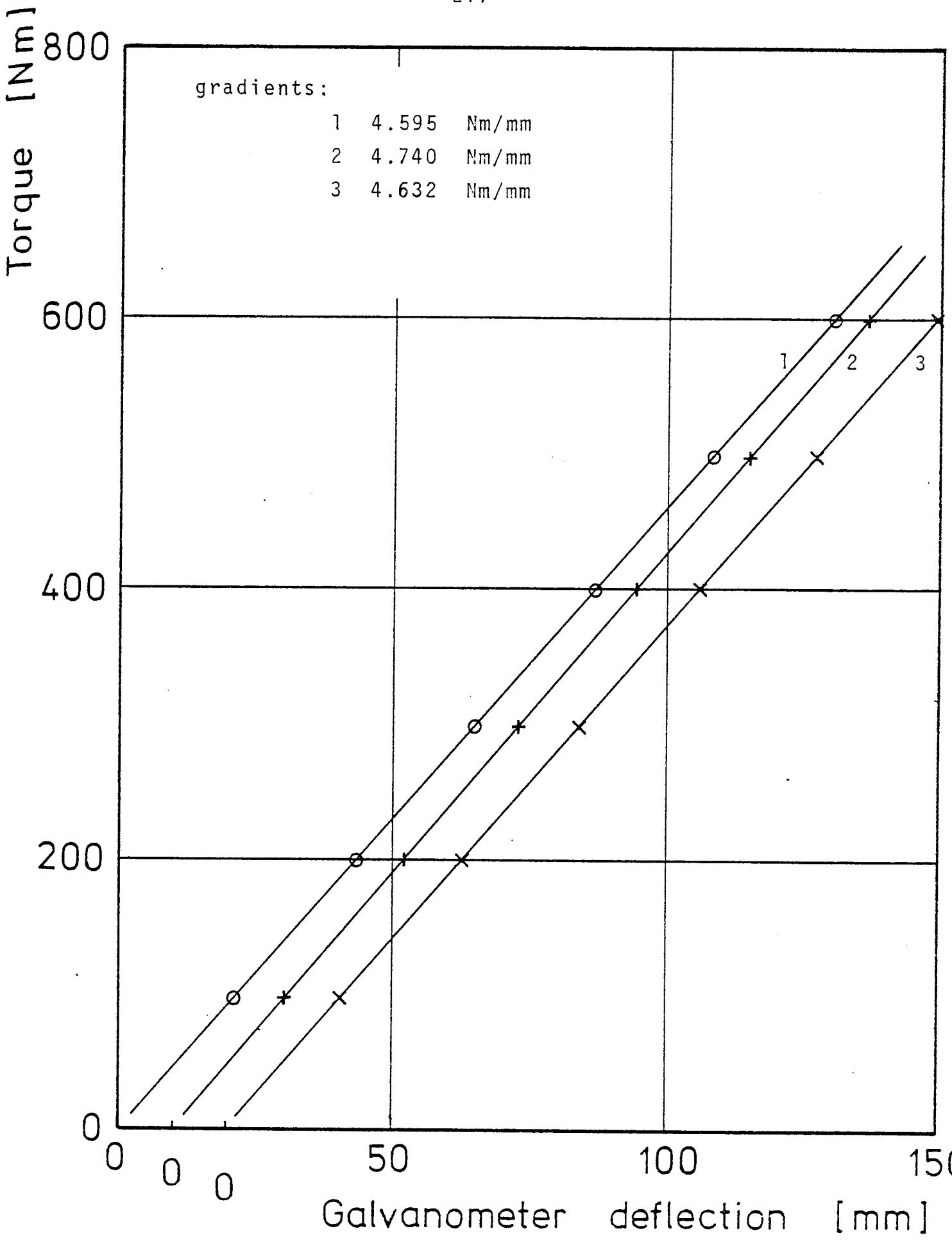

"WORKING" CALIBRATIONS FOR 1, 2 and 3 TORQUE CELLS
1.8 v d.c. bridge supply voltage.

It is important to note that calibrations were not carried out until every bridge circuit was in balance, since it was apparent that any out of balance circuit affected the response of the others. This was most probably due to the close proximity of all balancing potentiometers in the one balancing box, any interference present was constant and reproducible and did not affect the working calibrations.

4.13. MANDREL SIZES

The experimental programme required three tube reductions for each of five tube $\frac{D}{t}$ ratios, that is fifteen mandrel diameters. Appropriate calculations for these mandrel diameters is given in Appendix E. A table of these mandrel diameters is also included.

The mandrels, of approximate length 700 mm, were machined from commercial mild steel bars and the majority were ground finished parallel to the required size. Because of cost and convenience the remaining mandrels were made from bright drawn steel bar smooth finished with emery cloth in the lathe.

4.14. INITIAL TUBE PREPARATION

As previously stated, lead, which is "hot worked" at room temperature, was selected as an analogue material for hot steel in the tube rolling tests. Chapter 5 discusses in more detail the use of lead as a model material.

For much of the present investigation it was difficult to obtain lead tubes of sufficient quality for the tube rolling tests. Tube quality is defined in terms of tube straightness, dimensional accuracy and concentricity. Since another research worker also required lead tubes the decision was taken to manufacture the tubes in the laboratory. Scrap lead tubes from previous tests were melted down to form billets which were extruded over a long mandrel to produce thick walled tubes of one metre length. The extrusion unit, designed and manufactured in the Department is shown in FIGURE 4.17 and was appropriately inserted in an Avery testing machine which provided the required extrusion pressure. PLATE 4.11 shows a lead tube billet and two extruded tubes. Two tube sizes were extruded 44.45 mm outer diameter by 31.75 mm inner diameter and 44.45 mm outer diameter by 38.10 mm inner diameter.

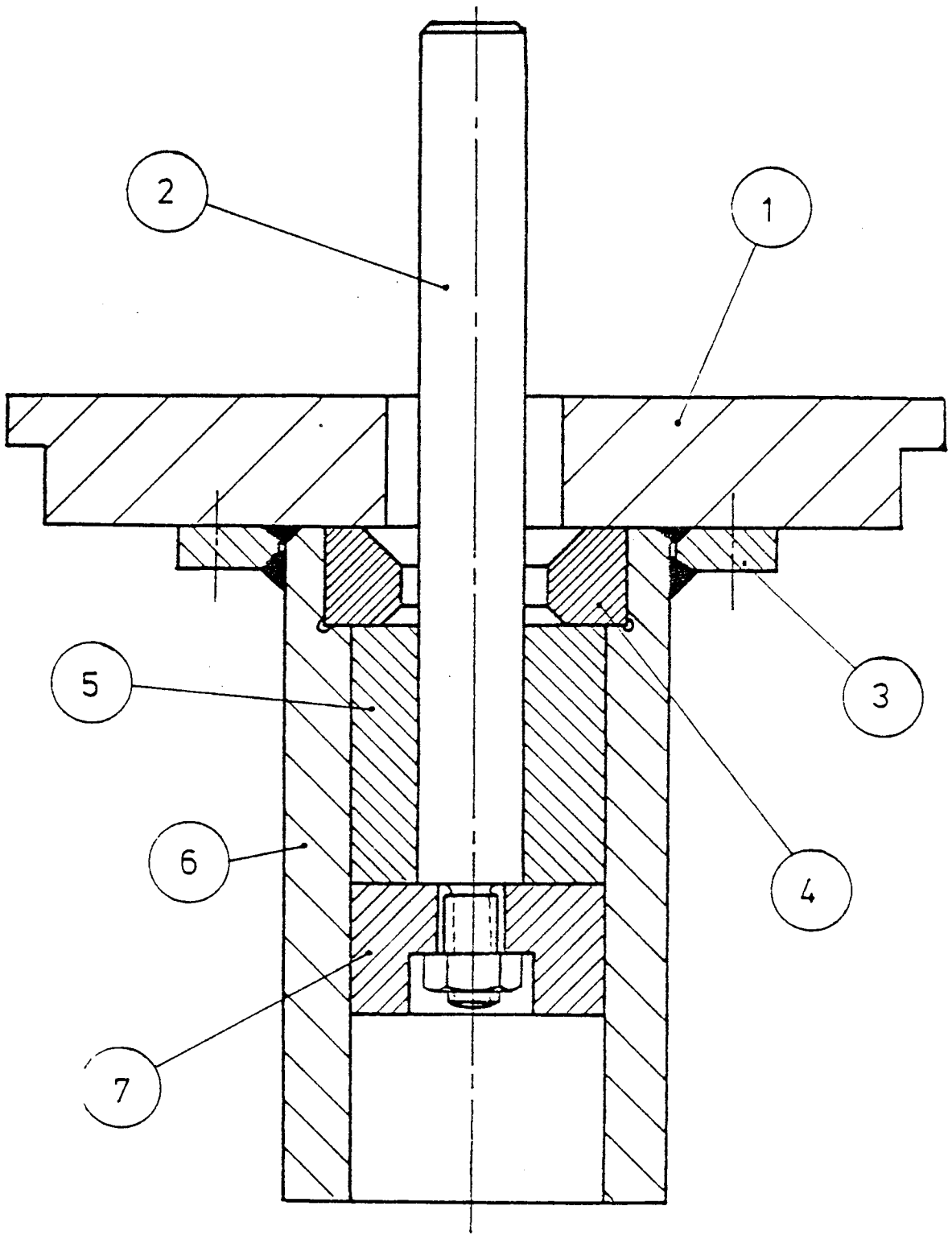

Tube extrusion attachment

No.	Description
7	Ram
6	Container
5	Lead billet
4	Die
3	Flange
2	Mandrel
1	Press plate

CAST LEAD TUBE BILLET

AND TWO EXTRUDED TUBES

PLATE 4.11

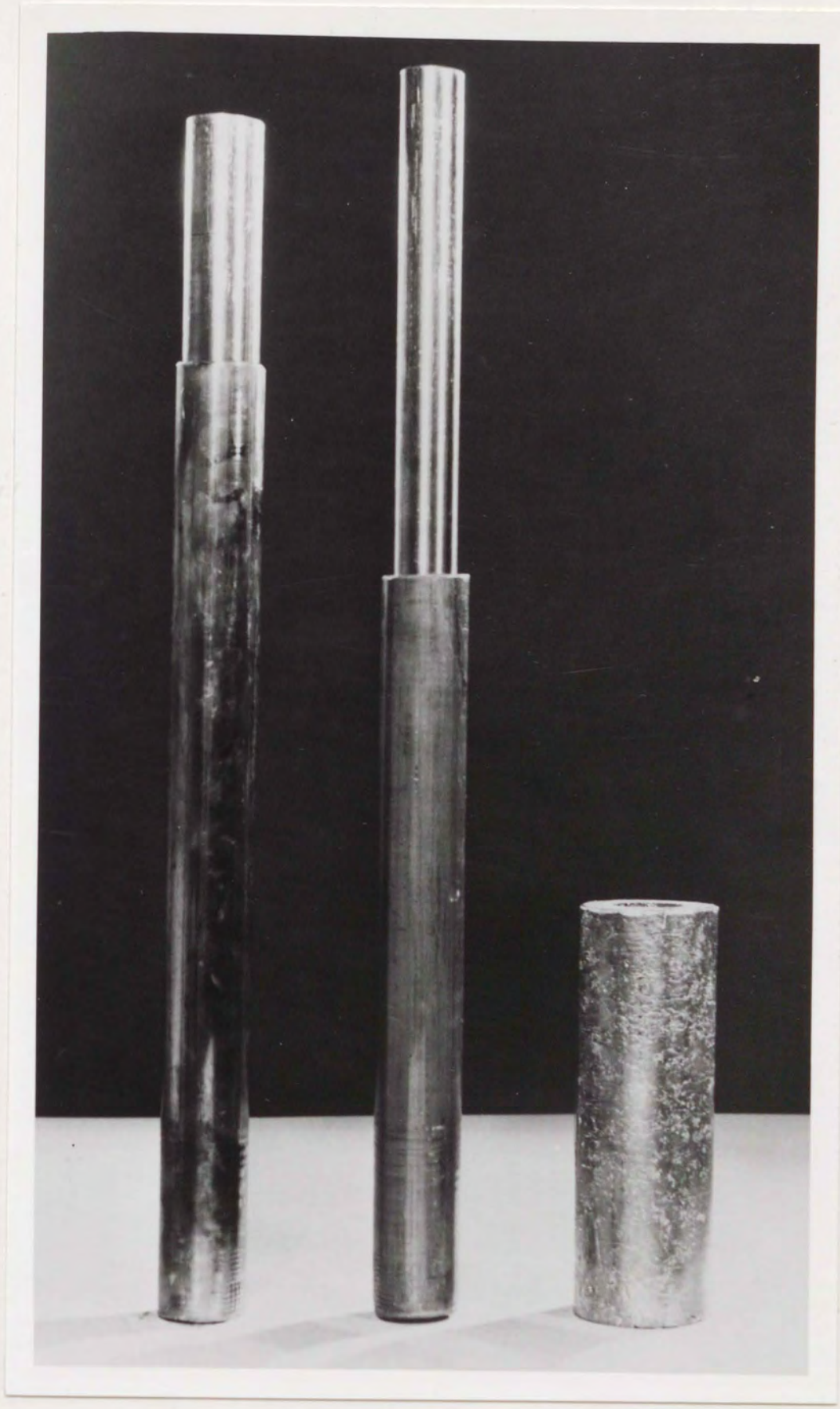

As a consequence of the extruded tubes inherently possessing some degree of eccentricity, convenient lengths of the extruded tube were push drawn by hand on an appropriate mandrel through a series of ring dies and then turned in the lathe to the required diameter. This somewhat protracted process ensured homogenity of the finished lead tube, uniform surface finish, eliminated tube eccentricity and for mandrel rolling ensured a close pass tube rolling process.

CHAPTER FIVE

EXPERIMENTAL PROCEDURE

5. EXPERIMENTAL PROCEDURE

The objective of the experiments were to examine how the various rolling parameters e.g. reduction of tube cross-sectional area, ratio tube diameter to tube thickness, ratio roll diameter to tube diameter, influenced the roll separating force and roll torque for the sinking and mandrel rolling processes.

The experimental procedure will be described in the following sections, commencing with the estimation of roll-tube contact area, measurement of tube longitudinal strain, specification of mandrel diameters, preparations for the tests and rolling conditions, examination of the process parameters, assessment of the reduction of tube cross-sectional area and concluding with the measurement of the yield stress of lead.

5.1. MEASUREMENT OF TUBE VELOCITY

The tube velocity measurements were conducted for the larger roll diameters of 255 mm and 340 mm for both sinking and mandrel rolling.

As discussed in Chapter 4 marked sections on the tube were timed over specified distances thereby enabling the tube inlet and outlet velocities to be deduced.

Some tube velocity results are shown in TABLE 6.I.11.

5.2. ESTIMATION OF ROLL-TUBE CONTACT AREA

Since the radial and longitudinal roll groove pressure distribution was not being determined, a knowledge of the root arc of contact and the contact area of the tube during the rolling process had to be assessed by an alternative method. Ideally this could be achieved by part rolling an appropriate length of tube, immediately retracting the three rolls leaving a partially rolled tube from which the required information of the roll-tube contact surface could be measured. Unfortunately, initial trials indicated that the slow manual retraction of each of the three-rolls by the vertical sliding cross heads allowed radial static compression of the tube by the three-rolls

at the roll contact surfaces. This indenting action of the rolls produced an exaggerated impression of the required tube contact surface during rolling. The only realistic solution was to part forward roll the tube, stop and immediately reverse the three-rolls, and reverse roll the tube over the previously rolled surface until the partially rolled tube was retracted from the roll gap.

Preliminary trials showed that a part rolled length corresponding to approximately two-thirds of the overall test tube length was sufficient to obtain satisfactory measurements of the roll load, torque and roll-tube contact area.

5.3. MEASUREMENT OF TUBE LONGITUDINAL STRAIN

To directly measure the longitudinal strain in the surface of the rolled tube, circumferential grid lines were scribed on the external surface of all the tubes and the final axial grid co-ordinates of the rolled tube were measured precisely with a travelling microscope. In the vicinity of the anticipated instantaneous stoppage of the three rolls on the tube, the grid line spacing of the pre-rolled tube was

concentrated at 0.150 in whilst for the remainder of the tube the spacing varied from 1 in to 4 in depending on the nature of the rolling test.

The production of the circumferentially scribed grid lines around the outer tube surface required the careful insertion of the appropriately oil lubricated mandrel (for ease of retraction) in the specimen tube. The tube and mandrel were positioned in the lathe between centres and with a suitable scribing tool in the tool post the required grid lines were engraved. To cut the 0.150 in grid the compound slide screw was utilised,whilst for the larger grid spacings the tool post carriage was set from the reading of the lathes screwcutting dial. This procedure was carried out for all the test tubes intended for partial rolling for both the sinking and mandrel rolling processes. However, to save labour the 0.150 in grid lines were not engraved on the specimen tubes which were to be completely rolled end to end in the normal manner.

To accommodate the increase in length of the arc of contact produced when rolling tube with the larger roll diameters, the overall length of the 0.150 in grid was appropriately increased; thus for the 170mm, 255mm and 340mm diameter rolls the

overall grid lengths were approximately 1.5 in, 2.0 in and 2.5 in respectively.

The instantaneous cessation of rolling of the specimen tube in the 0.150 in grid region, with the subsequent reverse rolling, was carried out in an attempt to obtain a knowledge of the distribution of the longitudinal strain imparted to the tube surface as it passed through the roll gap. It was, however, appreciated that the secondary reduction imparted to the reverse rolled tube would probably distort a true and readily interpreted distribution of the surface longitudinal strain.

Since the mean reduction in tube cross-sectional area is also numerically equal to the mean longitudinal strain,a knowledge of this strain is useful for comparison with the more direct methods of assessing the tube reduction discussed elsewhere in this chapter.

5.4. MEASUREMENT OF TUBE WALL THICKNESS AND PERIPHERAL ANGLES OF CONTACT

The majority of the sinking and mandrel tube specimens were sectioned before and after rolling and suitably prepared for display on the shadowgraph. These profiles of the sectioned specimens allowed the initial tube thickness and the final tube thickness at the critical sections to be measured. Furthermore, the shadowgraph technique enabled the roll-tube and the roll-tube-mandrel peripheral contact angles to be determined for the sunk and mandrel rolled specimens respectively.

A more detailed example of this work is given in Appendix F.

The tube specimen sections were also employed for the assessment of the tube cross-sectional area as described later in paragraph 5.10.

5.5. SPECIFICATION OF MANDREL DIAMETERS

Mandrels were used for the production of the specimen tubes for the sinking and mandrel rolling processes. The relevant mandrels used in the manufacture of the tubes were also employed for mandrel rolling.

For the trials in which a "fixed" roll gap was required changes in tube reduction were produced by controlling the outer and inner diameters of the pre-rolled specimen tube. Since four tube $\frac{D}{t}$ ratios were considered, each at three reductions of area a minimum of twelve mandrels was required for the manufacture of all the tubes.

Calculations for all the mandrel diameters and the associated tube outer diameters for each assumed tube reduction are given and listed in Appendix E.

5.6. PREPARATION OF SPECIMEN TUBES

To provide homogeneity of tube wall thickness and concentricity of the inner and outer surfaces, great care was taken in preparing the specimen tubes for rolling, especially those tubes produced in the laboratory from the cast billets. The previous chapter described the prolonged process in the initial preparation of the tubes and consequently every effort was made to minimise waste during the rolling tests. This was achieved primarily by making the tube of lengths sufficient to achieve uniform levels of roll separating force and roll torque for each roll i.e. the attainment of steady state rolling conditions

during the tests. Earlier work by Haleem (40) and Labib (43) and preliminary tests showed that, depending on the rolling condition, a required tube length of from 300mm to 400mm was sufficient to reach steady state conditions.

To ensure that all the test tubes had the same external surface finish, care was taken in the final turning of the tubes to the required outside diameter. All the tubes were machined in the lathe on the appropriate mandrel under similar cutting conditions.

As mentioned in the previous chapter some of the preliminary specimen tubes were extruded in the laboratory from cast billets, however the majority of the tubes utilised in the tests were supplied as drawn by an external manufacturer.

5.7. FINAL PREPARATIONS BEFORE EACH TEST

Before the commencement of each test session the mechanical and electrical balance of all the load and torque cell Wheatstone bridge circuits was checked and any imbalance appropriately rectified. Furthermore the precise voltage setting for each bridge circuit was monitored and verified by a digital voltmeter.

To ensure the electrical stability of all the strain gauge bridge circuits a "warming-up" period of about two hours was allowed before the commencement of each test session. All three-roll grooves were then checked for alignment, carefully "cleaned" with emery cloth and degreased with tissues and Inhibisol before each test.

To achieve minimum strain rates during the rolling process, particularly important in mandrel rolling with the attendant higher roll loads, the rotational speed of the rolls was set at the lowest value i.e. 0.33 rev min^{-1} and this setting was maintained for all the test sessions. For both the sinking and mandrel rolling processes all the circumferentially grid marked tube specimens were cleaned and degreased internally and externally with tissues and Inhibisol.

5.8. SINKING CONDITIONS

For the sinking tests, commencing with the 170mm diameter rolls in position, three tubes with diameter dimensions producing light, medium and heavy reductions were utilised for each of the following three tube outside diameter to tube wall thickness ratios 6.5, 10.7 and 17.6; which made a total requirement of nine specimen tubes. Each specimen possessed both the 0.150 in and the larger circumferential grids and were partially forward rolled to the 0.150 in grid area and then instantaneously reversed rolled out of the roll gap. A number of similar specimen tubes, but without the 0.150 in grid, were then completely forward rolled as a single pass for comparison purposes. This test procedure was repeated for the 255mm and 340mm diameter rolls.

All sinking tests were conducted with the test tubes rolled free from external restraint apart from some initial tube guidance to ensure longitudinal rolling of the tubes in a direction perpendicular to the plane of the three rolls.

5.9. MANDREL ROLLING CONDITIONS

A similar test procedure to the sinking trials was employed for each mandrel rolling condition i.e., for each of three roll diameters, three reduction and three tube $\frac{D}{t}$ ratios test tubes were partially rolled to and from the 0.150 grided area. However, for mandrel mill conditions thinner walled tubes of $\frac{D}{t}$ ratios 10.7, 17.6 and 22.6/28.9 were partially rolled at appropriately higher tube reductions. Again,a number of test tubes were completely mandrel rolled in a single pass.

These mandrel rolling tests were carried out for each of two mandrel/tube bore surface conditions:

1. Dry conditions - the mandrel/tube bore surface was clean, smooth and dry.

2. Lubricated conditions - the mandrel and tube bore surfaces were initially clean, smooth and dry but they were lubricated with Castrol graphited grease. Any excess lubricant was removed and great care taken during the rolling tests to prevent any lubricant from being squeezed out on to the roll groove surfaces. This was done by protecting the specimen tube ends with paper towels during the rolling process.

Each mandrel was carefully inserted in the appropriate circumferentially grided specimen tube and rolled exactly longitudinally, the mandrel giving full support to the tube during the rolling process.

Since the same mandrels were utilised in the production of the specimen tubes all the mandrel tests were effectively of a "close-pass" nature i.e. zero clearance between the tube inner diameter and the mandrel. All external test tube surfaces were clean, smooth and dry.

Since the actual longitudinal tube rolling process is effectively carried out under "dry" conditions, similar roll-tube contact surface conditions were present in the simulated rolling of the lead specimen tubes. This condition was achieved by thoroughly cleaning, degreasing and the drying of all external surfaces of the rolls and the tube before each test.

5.10. PROCESS PARAMETERS

The following parameters were examined in the present investigation:

5.10.1. Reduction of Tube Cross-sectional area

Since the three-grooved roll gap was ostensibly fixed, changes in tube reduction had to be effected by controlling the cross-section of the pre-rolled tube. The maximum reduction of area was restricted by the load carrying capacity of the three-roll mill stand, especially in the mandrel rolling process. Heavy tube reductions were also limited by the maximum angle of bite and the prevention of appreciable fin formation of the tube at the roll shrouds.

In mandrel rolling, with the tube bore constrained, an acceptable assessment of tube "root" reduction is readily achieved. However the sinking process, with the tube bore free, presented a more intractable problem since it was difficult to predict the behaviour of the tube wall thickness. Consequently preliminary sinking trials were carried out which indicated a small increase in the tube wall thickness, hence the rudimentary assumption of

a constant tube wall thickness during sinking enabled an initial estimate of the tube reduction to be obtained.

In both sinking and mandrel rolling some mill springback of the rolls was observed, particularly at high roll loads and further preliminary trials were conducted to assess the contribution of this factor on the anticipated tube reductions.

All these preliminary trials enabled a better prediction of the actual tube reduction to be made.

To stimulate actual mill practice, tube reductions for sinking were of the order of 5%, 10% and 15% whilst for mandrel rolling, tube reductions of 8%, 16% and 24% were considered.

By the very nature of the three-grooved roll profile all the external peripheries of the final rolled specimen tube cross sections were of an arcuate triangular shape, possessing, particularly at high sinking roll loads an appreciable lateral finning at the roll shrouds.

The rolled tube cross sections in the sinking process resulted in the inner peripheries

displaying the same basic arcuate triangular shape as the outer peripheral profile, with a slight increase in wall thickness toward the roll shrouds.

In the mandrel rolling process the mandrels utilised were also those over which the specimen tubes had been manually push drawn during the initial preparation. This initial condition gave in tube drawing terminology , a close pass, that is the bore of the test tubes were in contact with the mandrel throughout the rolling deformation process, consequently giving the maximum reduction of wall thickness. The process resulted in specimen tubes of uniform bore, but with varying thickness on account of the three-groove roll configuration.

Examples of rolled cross sections for both sinking and mandrel rolling processes are shown in PLATE 7.4

The slow rotational speed of 0.33 rev min^{-1} employed in all the tests enabled the experimental procedures to be conducted in an unhurried manner.

5.10.2. Tube ($\frac{D}{t}$) ratio

To maintain a fixed tube $\frac{D}{t}$ ratio for a particular series of tube reductions both the outer and inner pre-rolled tube diameters had to be adjusted. For both sinking and mandrel rolling the required tube diameters and therefore the $\frac{D}{t}$ ratio can readily be determined for each specified tube reduction.

To relate to current mill practice and the previous work of Haleem (40) and Labib (43) tube $\frac{D}{t}$ ratios of 10.7, 17.6, 22.6/28/9., were employed for the sinking and mandrel rolling processes respectively.

5.11. ASSESSMENT OF REDUCTION IN TUBE CROSS-SECTIONAL AREA

The determination of the tube reduction requires an assessment of the initial and final tube cross-sectional area. Inherently the cross-sections of the rolled tubes are not circular, primarily as a result of the three-roll groove profile and, to a lesser extent the presence in many cases of developing or actual fins. Because of this cross-section irregularity the assessment of the tube reduction can not be made from direct measurements of the final outer diameter and wall thickness. Alternative techniques had therefore to be employed. The initial tube cross-sectional area can be readily obtained from direct measurements of the concentric outer and inner tube diameters. However the measurement of the final tube cross-sectional area does not present such an amenable solution. The following methods are available for the assessment of the tube cross-sectional area.

Weighing is the first method, i.e. a specimen is cut from an appropriate central section of the rolled tube and the ends faced parallel in a lathe. The length and weight of the specimen are then obtained and the cross-sectional area of the tube

determined from a knowledge of the density of lead, the tube material.

There are various approaches to the second method, all of which involve a direct measurement of the tube specimen cross section by obtaining an image of the cross-section either by photographic means or employing a shadowgraph. The required area is assessed by using a planimeter or by analysis.

As discussed in Chapter 4 since the mean area reduction is equal to the mean longitudinal strain imparted to the tube, a knowledge of this strain should also give the required tube reduction.

A number of research workers have utilised the weighing method for the determination of the tube reduction. The principal disadvantage of the weighing method is that it does not provide any indication of the variation of tube wall thickness across the cross-section, although techniques are available to alleviate this difficulty. Assessment of the longitudinal strain of the tube, or to be more precise the outer tube surface, is likely to be less accurate since the inner surface of the tube may not experience the same strain, and if finning of the tube is present there is distortion of the outer surface at the roll shrouds.

In the present investigation both the weighing and the longitudinal strain methods are utilised and compared, since both are more accurate, quicker and less expensive than the image method. Furthermore,any optical system can produce distortion of the projected image.

Great care had to be taken in machining the ends of the cut specimen in the lathe, otherwise distortion of the specimen could occur. This problem was particularly apparent for the very thin-walled, mandrel rolled specimens. Minor twisting of the specimen could be tolerated since this did not affect the mean length or significantly effect the cross-sectional area.

The density of the same pure lead as used in this investigation was obtained by Labib (43) from appropriate measurements of specimens taken from rolled and unrolled tube. From experiments he established the density of this lead as 11.36 x 10^{-3} gm/mm^3. A value very close to that given in various references.

5.12. LEAD AS A MODEL MATERIAL

Although the possible rolling of hot steel tube was taken into account in the initial design stages of the three-roll mill stand, the problems associated with the handling, heating and maintaining the temperature of the hot steel tube at a constant level militated against its usage for these experiments. Furthermore, the attendant increased load carrying capacities required of the front and back tube tension units and cable in rolling hot steel confirmed its substitution by a model material such as lead.

Any model material must satisfy the following conditions:-

1. simulate the stress-strain characteristics of the hot steel rolled in the production mill at temperatures in the region of 1,100^{o}C, that is, a material which has a stress strain curve similar in shape to that of hot steel.

2. deform at lower stresses than hot steel, thereby reducing the rolling loads and torques.

Such a model material is pure lead.This material has been used by many workers to simulate hot steel since it recystallises at room temperature, is non-

strain hardening, shows a close similarity in the shape of the stress-strain curve to hot steel and deforms at low stresses.

Lead however has a lower coefficient of friction compared with that of hot steel, but the different frictional conditions can be taken into account when comparing the experimental results using lead with those given by hot steel. This can be readily achieved by substituting the appropriate known coefficient of friction or friction factor values into the theoretical equations for either rolling lead or hot steel tubes.

One of the first full experimental investigations into the properties of pure lead as a model material was carried out by Loizou and Sims (64). They determined the yield stress of pure lead in uniaxial compression at different strain rates and temperatures, and concluded that the yield stress depends on the temperature, strain rate and the current strain magnitude - particularly at high strain rates. The influence of strain rate on the yield stress of pure lead is shown in FIGURE 5.1., and is a good representation of the behaviour of hot steel.

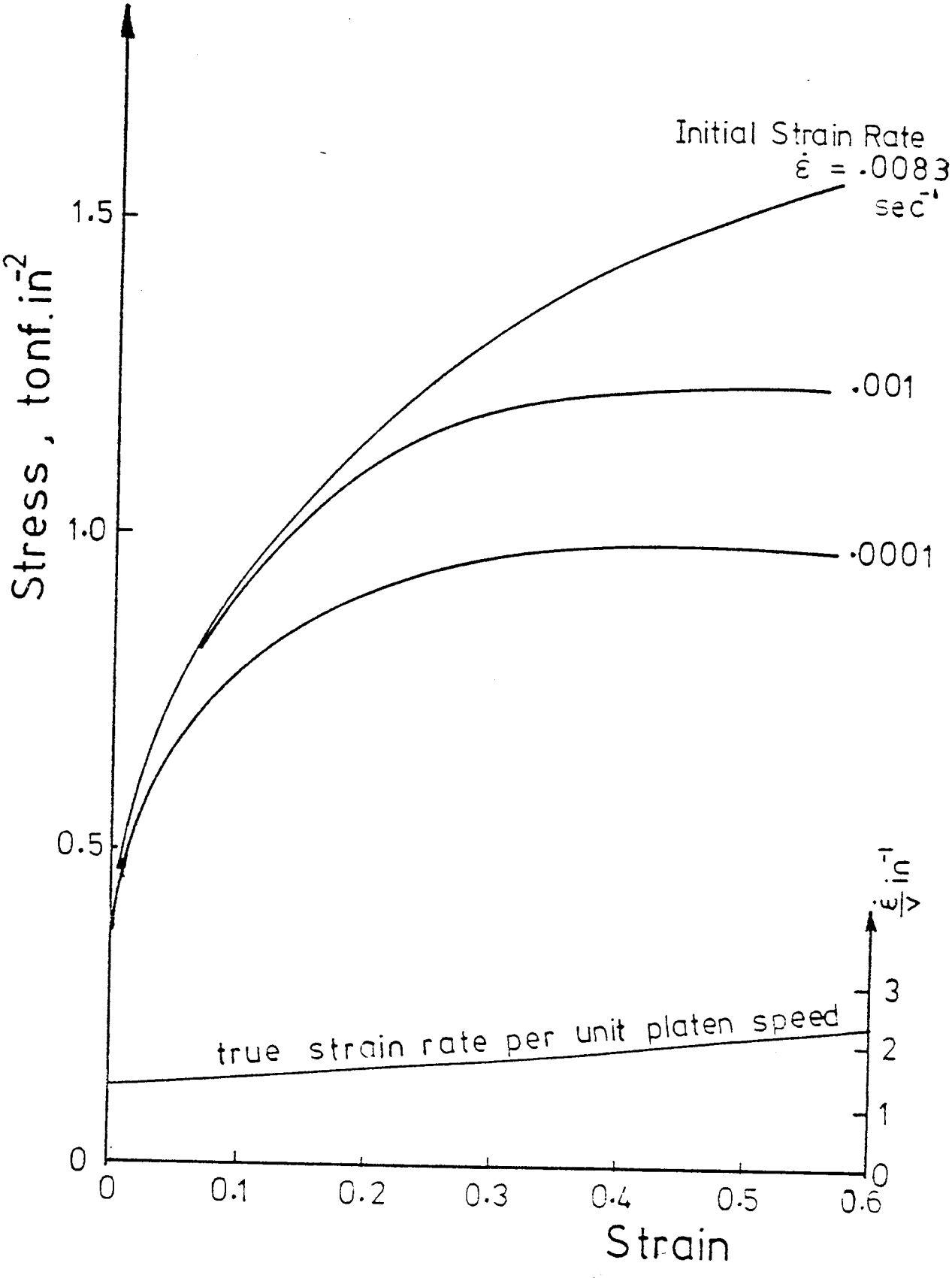

True Stress v Strain for pure Lead in Uniaxial Compression

(From Ingham 65)

FIGURE 5.1

The stress-strain characteristics of the same pure lead as that used in the present series of tests was determined by Ingham (65) at comparable low strain rates and these results were appropriately employed in this investigation. Ingham performed uniaxial compression tests at constant machine platen speeds on pure lead cylindrical specimens 20 mm diameter by 20 mm height. The specimens had three concentric lubrication grooves on each end face to reduce friction at the platen/specimen interface during the compression tests. The curves shown in FIGURE 5.1., illustrate the relationship between the true stress and true strain at different platen speeds, the lower line in the figure showing the inherent increase in the strain rate of the specimen during the compression test. However it was shown that the values of the yield stress resulting from the compression tests conducted at constant platen speeds could be assumed to apply for constant specimen strain rate compression tests without incurring significant error. Utilising the lower line of FIGURE 5.1. Ingham showed that even at a high reduction of 50% the strain rate was only twice the initial value and did not have any significant effect on the yield stress value. Consequently, the true stress-true strain curves for 99.99% pure lead at constant platen speed shown in FIGURE 5.1., were considered to represent

the yield stress at the indicated constant strain rates.

The strain rate in the actual tube rolling process is required to obtain the mean yield stress from the true stress-strain curve shown in FIGURE 5.1. In both rolling processes the strain rate varies from entry to exit and from point to point on the contact surface between the tube and roll. The arc of contact also varies from entry to exit. Consequently an accurate evaluation of the mean strain is impractical. By assuming that the maximum mean strain rate $\bar{\lambda}_r$ occurs at the root of the groove and the strain rate is zero just outside the contact zone, the mean value can be taken to be the total mean strain rate $\frac{\bar{\lambda}}{2}r$.

From FIGURE 5.2 the strain rate at any point of instantaneous tube radius r on the arc of contact at the root of the groove is:

$$\lambda_r = \frac{1}{r}\frac{dr}{dt}$$

where. $r = (R_s + \frac{e}{2}) - R_r \cos\phi$

and $e = h_s$

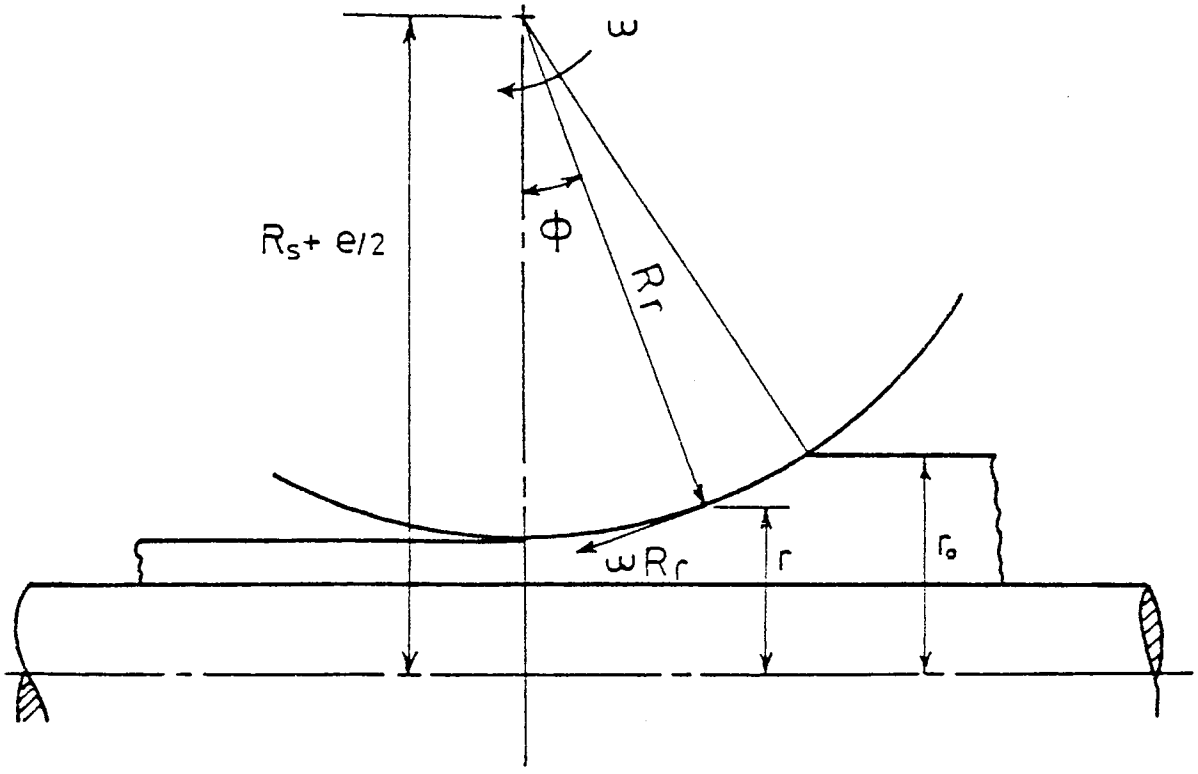

$$r = (R_s + e/2) - R_r \cos \Phi$$

where $e = h_s$

Section at the root of the groove

FIGURE 5.2

and $\frac{dr}{dt} = \omega R_r \sin\phi$

The mean strain rate $\bar{\lambda}_r$ at the root of the groove is:

$$\bar{\lambda}_r = \frac{\int_0^{\phi_m} \lambda_r \, d\phi}{\phi_m}$$

by substituting for λ_r and integrating:

$$\bar{\lambda}_r = \frac{\omega}{\phi_m} \ln \left[\frac{R_s + \frac{e}{2} - R_r \cos \phi_m}{R_s + \frac{e}{2} - R_r} \right]$$

The total mean strain rate $\bar{\lambda} = \frac{\bar{\lambda}_r}{2}$

$$= \frac{\omega}{2\phi_m} \ln \left[\frac{R_s + \frac{e}{2} - R_r \cos \phi_m}{R_s + \frac{e}{2} - R_r} \right]$$

With an estimate of the total mean strain rate, the corresponding true stress-strain curve can be selected from FIGURE 5.1.

The mean yield stress $\bar{\sigma}_y$ is determined from this curve as the stress corresponding to the total generalised strain $\bar{\varepsilon}_m$ as follows:

Preliminary trials and calculations indicated that the mean strain rate was of the order of .008 and that the maximum total generalised strain approached 0.50. It can be seen from FIGURE 5.1., that at these values the change in shape of the stress-strain curve with strain rate is small and can be neglected. At this strain rate of .008 and between zero and 0.50 generalised strains, the corresponding stress-strain curve is utilised to estimate the mean yield stress. This can be described by the equation:

$$\bar{\sigma}_y = 22.04\ (\bar{\varepsilon}_m)^{0.298}\ N.mm^{-2} \qquad (5.1)$$

From the above equation the mean yield stress is calculated.

It can be stated that:

$$\bar{\varepsilon}_m = \varepsilon_h + \varepsilon_{red} \qquad (5.2)$$

where ε_h is the generalised homogeneous strain,

ε_{red} is the redundant strain corresponding to the redundant work W_r,

furthermore $$\varepsilon_h = \sqrt{\frac{2}{3}}\sqrt{\varepsilon_z^{\,2} + \varepsilon_t^{\,2} + \varepsilon_\theta^{\,2}} \qquad (5.3)$$

where ε_z is the longitudinal strain,

ε_t is the thickness strain,

ε_θ is the circumferential strain,

$$\varepsilon_z = \ln \frac{A_o}{A_1} = \ln \frac{z_1}{z_o},$$

$$\varepsilon_t = \ln \frac{t_1}{t_o}, \qquad (5.4)$$

$$\varepsilon_\theta = -(\varepsilon_z + \varepsilon_t)$$

where A_o and A_1 are the tube cross sectional areas before and after rolling respectively,

z_o and z_1 are the outer tube surface gauge lengths before and after rolling respectively,

t_o and t_1 are the tube wall thickness's before and after rolling respectively.

CHAPTER SIX

TEST RESULTS

ADDENDUM I

6. TEST RESULTS

The test results are presented chronologically in the following tables, which contain all the recorded data relevant to each test. Each set of results are classified according to the test phase and all relate to rolling with the 170 mm shroud diameter rolls.

TABLE 6.1/2 (Sinking/Mandrel Rolling) - Tube entry and exit dimensions; tube-roll contact angles, and tube reductions of area.

TABLE 6.3/4 (Sinking/Mandrel Rolling) - Tube final thickness, measured and calculated; "principal" and homogeneous strains, total generalised strain, and mean yield stress.

TABLE 6.5/6 (Sinking/Mandrel Rolling) - Peripheral and axial longitudinal tube strains; measured and calculated

TABLE 6.7/8 : (Sinking/Mandrel Rolling) - Tube specimen condition; individual and total roll force for forward and reverse rolling, mean roll separating force.

TABLE 6.9/10 (Sinking/Mandrel Rolling) - Tube specimen condition; individual and total roll torque for forward and reverse rolling; mean roll torque.

Tube Specimen Condition

1/1	to	18	Sunk specimens - various tube $\frac{D}{t}$ ratios and reductions
20	to	28	Mandrel (lubricated) rolled specimens - various tube $\frac{D}{t}$ ratios and reductions
30	to	38	Mandrel (dry) rolled specimens - various tube $\frac{D}{t}$ ratios and reductions

Supplementary Notation:

* Tube specimen (marked with an asterisk) produced from cast lead tube; other specimens produced from lead tube supplied by an outside manufacture.

- Tube specimen (underlined) completely rolled as a single pass.

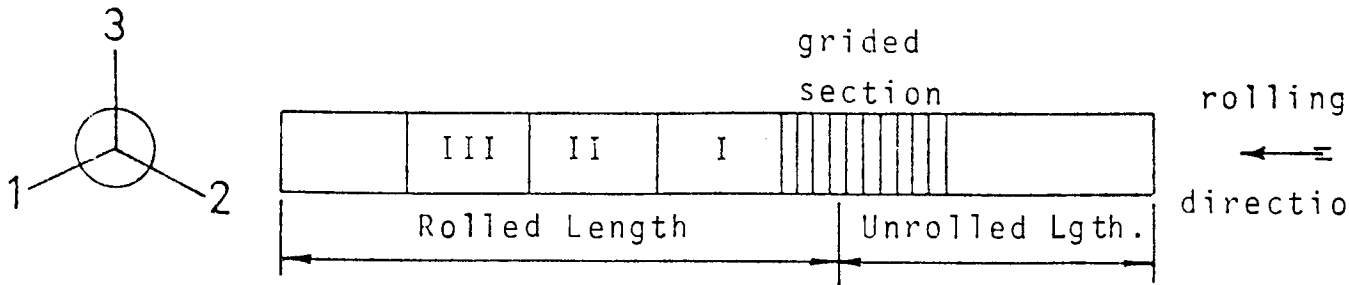

The following symbols are used in the table of results:

D	Tube outside diameter
d	Tube inner diameter
t_o	Original tube thickness
t_r	Final tube thickness at roll root
t_s	Final tube thickness at roll shroud
$\bar{t}_1$	Mean final tube thickness
$\frac{\delta r}{2}$	Semi-draft of tube at roll root
$t_{(\theta-\gamma)}$	Final thickness of tube beyond mandrel contact region
ϕ	Tube -roll contact angle (measured/calculated)
θ	Semi-peripheral contact angle between tube and roll
γ	Semi-peripheral contact angle between tube and mandrel
J	Tube reduction of area
A	Tube cross-sectional area
ε_z	Homogeneous longitudinal strain
ε_{zs}	Surface " "
ε_t	Homogeneous thickness strain
ε_θ	" circumferential strain
$\bar{\varepsilon}_h$	Generalised homogeneous strain
$\bar{\varepsilon}_r$	Redundant strain
$\bar{\varepsilon}_m$	Total generalised strain
$\bar{\sigma}_y$	Mean yield stress
P	Roll separating force (R.S.F)
T	Roll torque

Sub./Super Scripts:

o	Tube entry / inlet condition

r	Roll root
s	Roll shroud
1, 2, 3	Individual roll number

Further information relevant to the rolls is given below:

R_r (roll radius at groove root) = 85.00mm; 127.5 mm; 170 mm.

R_s (roll radius at groove shroud) = 78.31 mm; 120.81 mm 163.31 mm.

r_g (radius of groove) = 20.70 mm

h_r ("radius" at root) = 15.47 mm

h_s ("radius" at shroud) = 17.55 mm

e_g (groove eccentricity) = 5.23 mm

ω (roll angular velocity) = 36.47×10^{-3} rad/s (zero R.S.F.)

= 35.84×10^{-3} rad/s (28.5 kN R.S.F.)

(Forward Rolling)

= 34.35×10^{-3} rad/s (zero R.S.F.)

= 34.45×10^{-3} rad/s (13.4 kN R.S.F.)

(Reverse Rolling)

TABLE 6.1 SINKING (170 mm ROLLS)

E	ENTRY		$\left[\frac{D}{t}\right]_o$	EXIT				$\left[\frac{D}{t}\right]_1$	ROLL-TUBE CONTACT ANGLE			RED.OF AREA(%)	TUBE C.S.A. (mm^2)	
	D_o	t_o		D_1	t_r	t_s	t_1		φ_m	φ_m	$2\theta_{CI}$	J	A_o	A_1
	34.47	4.05	8.51	33.17	4.14	4.50	4.03	8.231	–	8.46	81	4.63	387.0	369.1
	35.05	4.36	8.04	33.31	4.42	4.81	4.42	7.536	–	9.01	86	4.57	420.4	401.2
	35.89	4.80	7.48	33.71	4.79	5.48	4.82	6.994	–	9.54	91	6.74	468.8	437.2
	36.31	5.31	6.84	33.42	5.22	6.27	5.31	6.294	9.8	10.29	95	9.28	517.1	469.1
	35.11	5.56	6.31	33.35	5.32	6.24	5.39	6.187	9.9	9.04	95	8.31	516.2	473.3
	35.82	5.45	6.57	33.56	5.43	6.46	5.58	6.014	9.7	9.62	95	5.64	519.9	490.6
	35.91	5.56	6.46	33.33	5.30	6.35	5.42	6.149	9.0	9.96	95	10.32	530.2	475.5
*	37.62	5.73	6.57	33.54	5.54	6.84	5.66	5.926	11.5	11.47	95	13.66	574.0	495.6
*	35.78	5.55	6.45	33.63	5.36	6.32	5.42	6.205	9.7	9.51	95	8.94	527.1	480.0
	39.93	6.24	6.40	33.42	6.04	7.69	6.63	5.041	14.2	13.57	95	15.55	660.4	556.5
	39.96	6.15	6.50	33.35	6.01	7.41	6.51	5.123	13.8	13.64	95	15.93	653.3	549.2
	37.55	5.82	6.45	33.25	5.78	6.83	6.01	5.532	12.0	11.66	95	11.38	580.2	514.2
1	38.02	3.44	11.1	33.42	3.52	4.35	3.66	9.131	–	11.94	95	8.56	374.0	342.0
2	37.77	3.49	10.8	33.08	3.61	4.46	3.74	8.845	12.4	12.01	95	8.30	375.9	344.7
	34.51	1.92	18.0	33.03	1.92	2.22	1.93	17.11	8.6	8.68	95	4.02	196.6	188.7
	36.72	2.09	17.6	33.12	2.10	2.65	2.17	15.26	12.2	10.99	95	7.26	227.4	210.9
	38.52	2.33	16.5	32.97	2.29	2.92	2.44	13.51	14.0	12.75	95	11.74	264.9	233.8
	35.22	3.34	10.5	33.14	3.36	3.94	3.38	9.805	9.0	9.39	94	5.62	334.5	315.7
	39.36	3.42	11.5	33.06	3.47	4.37	3.68	8.984	14.0	13.38	95	12.12	386.1	339.3

Dimensions: mm

TABLE 6.2 MANDREL ROLLING (170 mm ROLLS)

TUBE NO.	ENTRY		$\left[\frac{D}{t}\right]_o$	EXIT				ROLL - TUBE - MANDREL CONTACT ANGLE PER ROLL				RED. OF AREA(%)	TUBE C.S.A. (mm^2)	
	D_o	t_o		D_1	t_r	t_s	$\delta_r/2$	φ_m	φ_m	$2\gamma_{C1}$	$2\theta_{C1}$	J	A_o	A_1
20*	33.47	1.18	28.4	34.57	.76	1.13	.42	6.1	5.94	67	82	13.6	119.7	103.4
21	32.46	1.19	27.3	33.98	.80	1.12	.39	5.0	5.73	62	72	10.9	116.9	104.2
22	32.58	1.12	29.1	33.73	.91	1.16	.21	5.0	4.20	59	78	4.43	110.7	105.8
23	33.78	1.86	18.2	34.15	1.08	1.78	.78	7.8	8.11	81	90	18.9	186.5	151.2
24	33.81	1.84	18.4	33.98	1.26	1.85	.58	6.7	7.00	75	85	11.9	184.8	162.9
25	33.98	1.80	18.9	33.39	1.33	1.80	.47	6.7	6.29	68	77	11.0	182.0	161.9
26*	33.99	3.23	10.5	33.88	2.28	3.11	.95	7.6	8.96	84	87	16.8	312.1	259.8
27	34.29	3.21	10.7	33.88	1.91	3.12	1.30	9.0	10.50	93	88	24.6	313.4	236.3
28*	36.09	3.36	10.7	34.34	1.73	3.26	1.63	10.0	11.77	102	92	35.1	345.5	224.4
30*	32.36	1.49	21.7	33.76	1.22	1.48	.27	4.8	4.76	51	65	4.15	144.5	138.5
31	32.08	1.58	20.3	34.13	.97	1.49	.61	5.6	7.17	68	82	13.2	151.4	131.4
32	33.33	1.54	21.6	34.34	.91	1.51	.63	6.3	7.29	73	74	16.4	153.8	128.6
33/1*	33.85	3.18	10.6	34.23	2.9	3.16	.69	6.6	7.63	80	84	8.68	306.4	279.8
33/2	33.52	3.19	10.5	33.99	2.35	3.08	.84	7.4	8.42	83	82	12.2	304.0	266.8
34*	34.59	3.30	10.5	34.38	2.22	3.22	1.08	7.9	9.56	91	87	18.5	324.4	264.5
35*	34.75	3.44	10.1	34.43	1.91	3.09	1.53	8.8	11.40	96	91	28.8	338.4	241.0
36	32.93	1.96	16.8	34.00	1.37	1.88	.59	6.0	7.05	70	80	10.1	190.7	171.5
37*	34.39	1.91	18.0	34.23	1.23	1.81	.68	6.3	7.57	76	82	17.8	194.9	160.2
38	34.49	1.85	18.6	34.51	1.27	1.78	.58	6.4	6.99	75	76	14.4	189.7	162.3

TABLE 6.3 SINKING (170 mm ROLLS)

TUBE NO.	$\left[\frac{D}{t}\right]_o$	J%	t_1 (mm^2)	ε_z	ε_{zs}	ε_t	ε_θ	$\bar{\varepsilon}_h$	$\bar{\varepsilon}_r$	$\bar{\varepsilon}_m$	$\bar{\sigma}_y$
1/1	8.51	4.63	4.03	.0474	.0280	-.0050	.0424	.0521	.0583	.1104	11.43
1/2	8.04	4.57	4.42	.0467	.0400	.0137	.0604	.0633	.0633	.1266	11.91
1/3	7.48	6.74	4.82	.0698	.0670	.0042	.0740	.0831	.0694	.1525	12.58
2	6.84	9.28	5.31	.0974	.1940	.0000	-.0974	.1125	.0766	.1891	13.42
3	6.31	8.31	5.39	.0868	.1720	-.0311	-.0557	.0880	.0790	.1670	12.93
5*	6.57	5.64	5.58	.0580	.0803	.0236	-.0816	.0840	.0796	.1636	12.85
6*	6.46	10.32	5.42	.1089	.0925	-.0255	-.0834	.1139	.0792	.1931	13.50
7/1*	6.57	13.66	5.66	.1469		-.0123	-.1346	.1630	.0821	.2451	14.50
7/2*	6.45	8.94	5.42	.0936	.0791	-.0237	.0699	.0973	.0791	.1764	13.14
10*	6.40	15.55	6.63	.1712	.1747	.0606	-.2296	.2380	.0928	.3308	15.85
11*	6.50	15.93	6.51	.1736	.1749	.0569	-.2305	.2401	.0913	.3314	15.86
12*	6.45	11.38	6.01	.1208	.1270	.0321	-.1529	.1612	.0853	.2465	14.52
13/1	11.1	8.56	3.66	.0894	.0853	.0620	-.1514	.1522	.0512	.2304	13.71
13/2	10.8	8.30	3.74	.0866	.0995	.0692	-.1558	.1561	.0521	.2082	13.81
14*	18.0	4.02	1.93	.0410	.0377	.0052	-.0462	.0506	.0278	.0784	10.32
15	17.6	7.26	2.17	.0753	.0728	.0376	-.1129	.1150	.0307	.1457	12.41
16	16.5	11.74	2.44	.1249	.1180	.0461	-.1710	.1756	.0344	.2100	13.84
17*	10.5	5.62	3.38	.0578	.0618	.0119	-.0697	.0746	.0485	.1231	11.81
18*	11.5	12.12	3.68	.1292	.1220	.0733	-.2025	.2051	.0512	.2563	14.69

TABLE 6.4 MANDREL ROLLING (170 mm ROLLS)

m - measured s - "smoothed"

TUBE NO.	$\left[\frac{D}{t}\right]_o$	J%	t_{1} m / s	$t_{(\theta-\gamma)}$	ε_z	ε_{zs}	ε_t m / s	ε_θ	$\bar{\varepsilon}_h$	$\bar{\sigma}_y$
20*	28.4	13.6	1.01 1.00	1.13	.1464	.1508	-.1556 -.1631	.0167	.1795	13.21
21	27.3	10.9	1.03 1.04	1.15	.1150	.1276	-.1444 -.1335	.0185	.1447	12.39
22	29.1	4.43	1.05 1.05	1.19	.0453	.0850	-.0645 -.0679	.0226	.0692	9.94
23	18.2	18.9	1.50 1.50	1.80	.2098	.2588	-.2151 -.2159	.0061	.2459	14.51
24	18.4	11.9	1.64 1.65	1.84	.1261	.1889	-.1151 -.1066	-.0195	.1358	12.16
25	18.9	11.0	1.65 1.64	1.82	.1170	.1397	-.0870 -.0947	-.0223	.1242	11.84
26*	10.5	16.8	2.70 2.68	3.07	.1834	.1833	-.1792 -.1851	.0017	.2128	13.90
27	10.7	24.6	2.42 2.44	3.02	.2824	.3022	-.2825 -.2727	-.0097	.3206	15.70
28*	10.7	35.1	2.25 2.24	3.26	.4316	.4103	-.4010 -.4049	-.0267	.4837	17.75
30*	21.7	4.15	1.39 1.38	1.50	.0424	.0439	-.0695 -.0743	.0319	.0745	10.17
31	20.3	13.2	1.31 1.33	1.45	.1417	.1445	-.1874 -.1698	.0281	.1820	13.27
32	21.6	16.4	1.27 1.25	1.47	.1790	.1854	-.1928 -.2056	.0266	.2236	14.10
33/1*	10.6	8.68	2.89 2.89	3.18	.0908	.0968	-.0956 -.0944	.0036	.1070	11.32
33/2	10.5	12.2	2.77 2.79	3.08	.1305	.1390	-.1412 -.1355	.0050	.1537	12.61
34*	10.5	18.5	2.70 2.67	3.18	.2041	.2195	-.2007 -.2117	.0076	.2402	14.41
35*	10.1	28.8	2.41 2.42	2.99	.3394	.2976	-.3558 -.3517	.0123	.3992	16.76
36	16.8	10.1	1.72 1.72	1.91	.1061	.1238	-.1306 -.1281	.0220	.1370	12.19
37*	18.0	17.8	1.59 1.59	1.85	.1961	.1826	-.1834 -.1803	-.0158	.2179	14.00
38	18.6	14.4	1.59 1.58	1.83	.1560	.1722	-.1515 -.1571	.0011	.1808	13.24

TABLE 6.5. SINKING (170 mm ROLLS)

Tube No.	LONGITUDINAL STRAIN					$\bar{\varepsilon}_{zs}$		$\bar{\varepsilon}_h$
	Periph. Station	Rolled Tube Length Station III	II	I	Axial Mean	Surface $\bar{\varepsilon}_{zs}$	Mean $\bar{\varepsilon}_z$	
1/1	1 1-2 2 2-3 3 3-1		.028 .028			.028(III)	.0474	.0521
1/2	1 1-2 2 2-3 3 3-1		.040 .040			.040(II)	.0467	.0633
1/3	1 1-2 2 2-3 3 3-1		.067 .067			.067(I)	.0698	.0831
3	1 1-2 2 2-3 3 3-1		.172 .172			.172(II)	.0868	.0880
13/1	1 1-2 2 2-3 3 3-1	.0816 .0818 .0808 .0855 .0828 .0878 .0834	.0880 .0846 .0833 .0816 .0836 .0871 .0847	.0870 .0904 .0877 .0884 .0834 .0843 .0869	.0855 .0856 .0839 .0852 .0833 .0864	.0847(II)	.0894	.1522

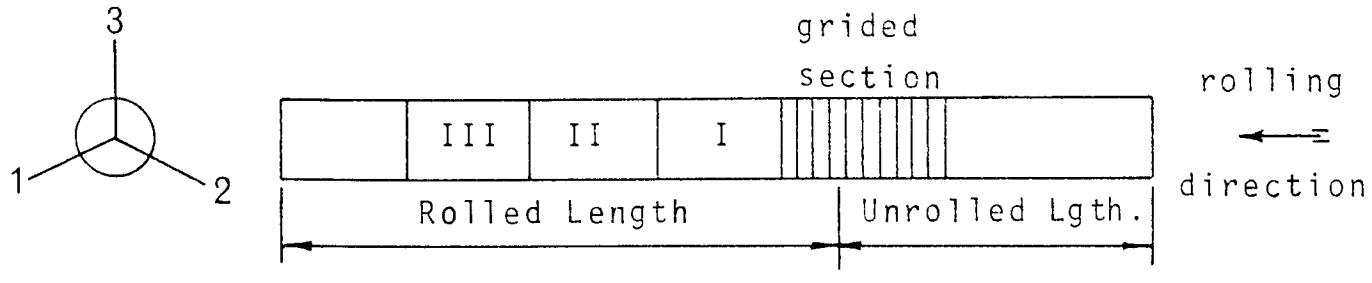

TABLE 6.5 (cont'd) SINKING (170 mm ROLLS)

Tube No.	LONGITUDINAL STRAIN ε_{zs}							$\bar{\varepsilon}_h$
	Per. Stat.	R.T.L. Station			Axial Mean	Surface	Mean	
		III	II	I		$\bar{\varepsilon}_{zs}$	$\bar{\varepsilon}_z$	
2	1 1-2 2 2-3 3 3-1			.194	.194	.194(I)	.0974	.1125
3	1 1-2 2 2-3 3 3-1		.172 .172		.172	.172(II)	.0868	.0880
5*	1 1-2 2 2-3 3 3-1		.085 .079 .080 .0813	.084 .075 .082 .080	.0845 .0770 .0810	.080(I)	.0580	.0840
6*	1 1-2 2 2-3 3 3-1			.092 .093 .094 .091 .093 .092 .093		.093(I)	.1089	.1139
7/2*	1 1-2 2 2-3 3 3-1			.0812 .0807 .0793 .0776 .0771 .0788 .0791		.0791(I)	.0936	.0973
10*	1 1-2 2 2-3 3 3-1			.1728 .1799 .1823 .1766 .1707 .1661 .1747		.1747(I)	.1712	.2380

TABLE 6.5 (cont'd) SINKING (170 mm ROLLS)

Tube No.	LONGITUDINAL STRAIN ε_{zs}							$\bar{\varepsilon}_h$
	Per. Stat.	R.T.L. Station			Axial Mean	Surface $\bar{\varepsilon}_{zs}$	Mean $\bar{\varepsilon}_z$	
		III	II	I				
11*	1			.1786				
	1-2			.1813				
	2			.1739				
	2-3			.1686				
	3			.1710				
	3-1			.1761				
				.1749		.1749(I)	.1736	.2401
12*	1			.1317				
	1-2			.1292				
	2			.1238				
	2-3			.1233				
	3			.1245				
	3-1			.1293				
				.1270		.1270(I)	.1208	.1612
13/2	1			.0999				
	1-2			.1069				
	2			.1053				
	2-3			.0983				
	3			.0924				
	3-1			.0940				
				.0995		.0995(I)	.0866	.1561

TABLE 6.5 (cont'd) SINKING (170 mm ROLLS)

Tube No.	LONGITUDINAL STRAIN ε_{zs}							$\bar{\varepsilon}_h$
	Per. Stat.	R.T.L. Station III	R.T.L. Station II	R.T.L. Station I	Axial Mean	Surface $\bar{\varepsilon}_{zs}$	Mean $\bar{\varepsilon}_z$	
14*	1	.0339	.0366	.0370	.0358			
	1-2	.0362	.0372	.0411	.0382			
	2	.0369	.0365	.0392	.0375			
	2-3	.0360	.0333	.0370	.0354			
	3	.0355	.0337	.0360	.0351			
	3-1	.0312	.0353	.0360	.0342			
		.0350	.0354	.0377		.0377(I)	.0410	.0506
15	1	.0700	.0727	.0729	.0719			
	1-2	.0735	.0754	.0787	.0759			
	2	.0778	.0741	.0790	.0770			
	2-3	.0785	.0705	.0730	.0740			
	3	.0708	.0693	.0663	.0688			
	3-1	.0670	.0697	.0666	.0678			
		.0729	.0720	.0728		.0728(I)	.0753	.1150
16	1	.1064	.1112	.1110	.1095			
	1-2	.1101	.1204	.1176	.1160			
	2	.1186	.1214	.1221	.1207			
	2-3	.1231	.1155	.1208	.1198			
	3	.1187	.1072	.1151	.1137			
	3-1	.1104	.1030	.1214	.1116			
		.1146	.1131	.1180		.1180(I)	.1249	.1756
17*	1		.0574	.0643	.0609			
	1-2		.0593	.0662	.0628			
	2		.0634	.0630	.0632			
	2-3		.0625	.0595	.0610			
	3		.0599	.0577	.0588			
	3-1		.0570	.0602	.0586			
			.0599	.0618		.0618(I)	.0578	.0746
18*	1		.1222	.1190	.1206			
	1-2		.1260	.1229	.1245			
	2		.1281	.1211	.1246			
	2-3							
	3							
	3-1		.1218	.1220		.1220(I)	.1292	.2051

TABLE 6.6 MANDREL ROLLING (170 mm ROLLS)

(lubricated)

Tube No.	LONGITUDINAL STRAIN ε_{zs}							$\bar{\varepsilon}_h$
	Per. Stat.	R.T.L. Station			Axial	Surface	Mean	
		III	II	I	Mean	$\bar{\varepsilon}_{zs}$	$\bar{\varepsilon}_z$	
20*	1							
	1-2		.1512	.1512				
	2							
	2-3							
	3							
	3-1		.1503	.1503				
			.1508			.1508(I)	.1464	.1795
21	1	.1187	.1200	.1431	.1273			
	1-2	.1249	.1219	.1312	.1260			
	2	.1187	.1328	.1260	.1258			
	2-3	.1234	.1201	.1202	.1212			
	3	.1265	.1196	.1188	.1216			
	3-1	.1225	.1201	.1264	.1230			
		.1225	.1224	.1276		.1276(I)	.1150	.1447
22	1	.0962	.0905	.0878	.0915			
	1-2	.0914	.0884	.0834	.0877			
	2	.0845	.0963	.0868	.0892			
	2-3	.0908	.0880	.0836	.0875			
	3	.0887	.0887	.0847	.0874			
	3-1	.0907	.0881	.0837	.0875			
		.0904	.0900	.0850		.0850(I)	.0453	.0692
23	1	.2765	.2671	.2561	.2666			
	1-2	.2744	.2687	.2599	.2677			
	2	.2693	.2756	.2609	.2686			
	2-3	.2674	.2681	.3072	.2809			
	3	.2702	.2675	.2595	.2657			
	3-1	.2711	.2683	.2577	.2657			
		.2715	.2692	.2588		.2588(I)	.2098	.2459
24	1	.1915	.1857	.1913	.1895			
	1-2	.1903	.1862	.1898	.1888			
	2	.1868	.1855	.1895	.1873			
	2-3	.1821	.1863	.1868	.1851			
	3	.1847	.1856	.1876	.1860			
	3-1	.1880	.1868	.1883	.1877			
		.1872	.1860	.1889		.1889(I)	.1261	.1358
25	1	.1332	.1418	.1375	.1375			
	1-2	.1360	.1395	.1333	.1363			
	2	.1334	.1408	.1363	.1368			
	2-3	.1367	.1386	.1337	.1363			
	3	.1358	.1386	.1421	.1388			
	3-1	.1363	.1386	.1360	.1370			
		.1352	.1397	.1365	.1371	.1397(II)	.1170	.1242

TABLE 6.6 (cont'd) MANDREL ROLLING (170 mm ROLLS)

(lubricated)

Tube No.	LONGITUDINAL STRAIN ε_{zs}						$\bar{\varepsilon}_h$
	Per. Stat.	R.T.L. Station			Axial Mean	Surface $\bar{\varepsilon}_{zs}$	Mean $\bar{\varepsilon}_z$	
		III	II	I				
26*	1	.1881	.1942	.1844	.1889			
	1-2	.2009	.1902	.1824	.1912			
	2	.2050	.1907	.1829	.1929			
	2-3	.1989	.1905	.1821	.1905			
	3	.1890	.1882	.1856	.1876			
	3-1	.1947	.1905	.1826	.1893			
		.1961	.1907	.1833		.1833(I)	.1834	.2128
27	1	.3066	.3072	.3024	.3054			
	1-2	.3085	.3095	.3010	.3063			
	2	.3050	.3101	.3042	.3064			
	2-3	.3071	.3078	.2996	.3048			
	3	.3071	.3036	.3040	.3049			
	3-1	.3059	.3070	.3021	.3050			
		.3067	.3075	.3022		.3022(I)	.2824	.3206
28*	1	.4142	.4125		.4134			
	1-2	.4151	.4112		.4132			
	2	.4078	.4092		.4085			
	2-3	.4065	.4098		.4082			
	3	.4097	.4106		.4102			
	3-1	.4148	.4086		.4117			
		.4114	.4103			.4103(II)	.4316	.4837

TABLE 6.6 (cont'd) MANDREL ROLLING (170 mm ROLLS)

(dry)

Tube No.	LONGITUDINAL STRAIN ε_{zs}						$\bar{\varepsilon}_h$
	Per. Stat.	R.T.L. Station III	II	I	Axial Mean	Surface $\bar{\varepsilon}_{zs}$	Mean $\bar{\varepsilon}_z$	
30*	1	.0458	.0476	.0427	.0454			
	1-2	.0503	.0473	.0435	.0470			
	2	.0483	.0468	.0472	.0474			
	2-3	.0460	.0477	.0439	.0459			
	3	.0426	.0474	.0427	.0442			
	3-1	.0479	.0472	.0432	.0461			
		.0468	.0473	.0439		.0439(I)	.0424	.0745
31	1	.1539	.1441	.1431	.1470			
	1-2	.1528	.1465	.1418	.1470			
	2	.1533	.1435	.1587	.1518			
	2-3	.1470	.1470	.1410	.1450			
	3	.1493	.1459	.1411	.1454			
	3-1	.1493	.1459	.1415	.1456			
		.1509	.1455	.1445		.1445(I)	.1417	.1820
32	1		.1868	.1863	.1866			
	1-2	.1868	.1855	.1862	.1862			
	2	.1858	.1875	.1847	.1860			
	2-3	.1848	.1862	.1849	.1853			
	3	.1833	.1856	.1855	.1848			
	3-1	.1851	.1854	.1849	.1851			
		.1852	.1862	.1854		.1854(I)	.1790	.2236
33/1*	1	.0938		.0991	.0965			
	1-2	.0998		.0957	.0978			
	2	.0957		.0976	.0967			
	2-3	.0965		.0959	.0962			
	3	.0936		.0970	.0953			
	3-1	.0965		.0957	.0961			
		.0960		.0968		.0968(I)	.0908	.1070
33/2	1							
	1-2			.138				
	2							
	2-3			.139				
	3							
	3-1			.139				
				.139		.1390(I)	.1305	.1537
34*	1	.2226	.2187	.2211	.2208			
	1-2	.2238	.2192	.2186	.2205			
	2	.2197	.2187	.2215	.2200			
	2-3	.2230	.2182	.2181	.2198			
	3	.2268	.2181	.2189	.2213			
	3-1	.2252	.2178	.2187	.2206			
		.2235	.2185	.2195		.2195(I)	.2041	.2402
35*	1		.2908	.2972	.2940			
	1-2		.2896	.3056	.2976			
	2		.2855	.3010	.2933			
	2-3		.2916	.2945	.2931			
	3		.2872	.2911	.2892			
	3-1		.2904	.2962	.2933			

TABLE 6.6 (cont'd) MANDREL ROLLING (170 mm ROLLS)
(dry)

Tube No.	LONGITUDINAL STRAIN ε_{zs}							$\bar{\varepsilon}_h$
	Per. Stat.	R.T.L. Station III	R.T.L. Station II	R.T.L. Station I	Axial Mean	Surface $\bar{\varepsilon}_{zs}$	Mean $\bar{\varepsilon}_z$	
36	1		.1270	.1243	.1257			
	1-2		.1269	.1240	.1255			
	2		.1272	.1242	.1257			
	2-3		.1267	.1236	.1252			
	3		.1270	.1232	.1251			
	3-1		.1277	.1237	.1257			
			.1271	.1238		.1239(I)	.1061	.1370
37*	1		.1824	.1854	.1839			
	1-2		.1831	.1833	.1832			
	2		.1826	.1856	.1841			
	2-3		.1825	.1817	.1821			
	3		.1821	.1853	.1837			
	3-1		.1827	.1817	.1822			
			.1826	.1838		.1826(II)	.1961	.2179
38	1	.1802	.1730	.1730	.1754			
	1-2	.1717	.1726	.1736	.1726			
	2	.1829	.1699	.1755	.1761			
	2-3	.1680	.1725	.1725	.1710			
	3	.1804	.1727	.1724	.1752			
	3-1	.1693	.1726	.1728	.1716			
		.1754	.1722	.1733		.1722(II)	.1560	.1808

For. - Forward Rev. - Reverse

TUBE NO.	$\left[\frac{D}{t}\right]_o$	RED. OF AREA	LONG. STRAIN	ROLL FORCE (kN)									R.S.F.
				ROLL 1		ROLL 2		ROLL 3		TOTAL (1+2+3)			
				For. Rev.	For. + Rev.					For. Rev.	% Ratio of Total	For. + Rev.	
1/1	8.51	4.63	.0474									5.73	1.91
1/2	8.04	4.57	.0467									7.17	2.39
1/3	7.48	6.74	.0698									9.75	3.25
2	6.84	9.28	.0974	4.20 1,35	5.55	4.25 1.37	5.62	4.47 1.52	5.99	12.92 4.24	75.3 24.7	17.16	5.72
3	6.31	8.31	.0868	4.72	4.72	4.73	4.73	5.04	5.04			14.49	4.83
5*	6.57	5.64	.0580	4.34 2.11	6.45	4.30 2.07	6.37	4.51 2.15	6.66	13.15 6.33	67.5 32.5	19.48	6.49
6*	6.46	10.32	.1089	4.031 1.449	5.480	3.949 1.387	5.336	4.364 1.658	6.022	12.344 4.494	73.3 26.7	16.84	5.61
7/1*	6.57	13.66	.1469	5.95 2.12	8.07	6.10 1.97	8.07	6.29 1.62	7.91	18.34 5.71	76.3 23.7	24.04	8.02
7/2*	6.45	8.94	.0936	3.620 1.519	5.139	3.652 1.644	5.296	3.667 1.273	4.940	10.939 4.436	71.1 28.9	15.38	5.13
10*	6.40	15.73	.1712	9.867 3.736	13.60	8.695 3.369	12.064	9.415 2.993	12.408	27.977 10.098	73.5 26.5	38.08	12.69
11*	6.50	15.93	.1736	9.122 3.077	12.20	8.539 3.288	11.83	9.143 2.721	11.86	26.804 9.086	74.7 25.3	35.89	11.96
12*	6.45	11.38	.1208	5.714 2.101	7.815	5.418 2.099	7.517	6.112 1.758	7.870	17.244 5.958	74.3 25.7	23.20	7.73

TABLE 6.7 SINKING (170 mm ROLLS)

TABLE 6.7 (cont'd) SINKING (170 mm ROLLS)

For. - Forward Rev. - Reverse

TUBE NO.	$\left[\frac{D}{t}\right]_o$	RED. OF AREA	LONG. STRAIN	ROLL FORCE (kN)									
				ROLL 1		ROLL 2		ROLL 3		TOTAL (1+2+3)			R.S.F.
				For. Rev.	For. + Rev.					For. Rev.	% Rat of Tot.	For. + Rev.	
13/1	11.1	8.56	.0894	3.703	3.703	3.288	3.288	3.759	3.759	10.75		10.75	3.583
13/2	10.8	8.30	.0866	3.683 .921	4.604	3.561 .682	4.423	4.044 1.088	5.132	11.288 2.691	80.7 19.3	13.98	4.660
14*	18.0	4.02	.0410	.637 .236	.873	.652 .227	.879	.452 .251	.703	1.741 .714	70.9 29.1	2.455	.818
15	17.6	7.26	.0753	1.629 .394	2.023	1.584 .576	2.160	1.231 .260	1.491	4.444 1.230	78.3 21.7	5.674	1.891
16	16.5	11.74	.1249	3.077 .740	3.817	3.016 1.084	4.100	2.478 .402	2.880	8.571 2.226	79.4 20.6	10.80	3.599
17*	10.5	5.62	.0578	1.645 .685	2.330	1.417 1.061	2.478	1.792 .486	2.278	4.854 2.232	68.5 31.5	7.086	2.362
18*	11.5	12.12	.1292	4.423 1.259	5.682	4.251 1.341	5.592	3.960 .804	4.764	12.634 3.404	78.8 21.2	16.04	5.346

For. - Forward Rev. - Reverse

TUBE NO.	$\left[\frac{D}{t}\right]_o$	RED. OF AREA	LONG. STRAIN	ROLL FORCE (kN)									
				ROLL 1		ROLL 2		ROLL 3		TOTAL (1+2+3)			R.S.F.
				For. Rev.	For. + Rev.					For Rev.	% Rat. of Total	For. + Rev.	
20*	28.4	13.6	.1464	10.26 8.92	19.18	10.07 8.66	18.73	11.05 9.53	20.58	31.38 27.11	53.7 46.3	58.49	19.50
21	27.3	10.9	.1150	8.59 7.47	16.06	8.58 7.37	15.95	9.45 8.16	17.61	26.62 23.00	53.6 46.4	49.62	16.54
22	29.1	4.43	.0453	6.44 5.89	12.33	6.40 5.84	12.24	7.26 6.57	13.83	20.10 18.30	52.3 47.7	38.40	12.80
23	18.2	18.9	.2098	11.28 8.99	20.27	11.11 8.83	19.94	12.24 9.69	21.93	34.63 27.51	55.7 44.3	62.14	20.71
24	18.4	11.9	.1261	9.88 8.00	17.88	9.76 7.91	17.67	10.76 8.75	19.51	30.40 24.66	55.2 44.8	55.06	18.36
25	18.9	11.0	.1170	7.15 5.35	12.50	7.15 5.26	12.41	7.81 5.88	13.69	22.11 16.49	57.3 42.7	38.60	12.87
26*	10.5	16.8	.1834	9.82 7.16	16.98	9.68 6.91	16.59	10.76 7.79	18.55	30.26 21.86	58.1 41.9	52.12	17.37
27	10.7	24.6	.2824	9.31 6.03	15.34	9.21 6.00	15.21	10.41 6.87	17.28	28.93 18.90	60.5 39.5	47.83	15.94
28*	10.7	35.1	.4316	12.99 7.95	20.94	12.61 7.70	20.31	13.84 8.79	22.63	39.44 24.44	61.7 38.3	63.88	21.29

TABLE 6.8 MANDREL ROLLING (170 mm ROLLS)

For. - Forward Rev. - Reverse

TUBE NO.	$\left[\frac{D}{t}\right]_o$	RED. OF AREA	LONG. STRAIN	ROLL FORCE (kN)									
				ROLL 1		ROLL 2		ROLL 3		TOTAL (1+2+3)			R.S.F.
				For. Rev.	For. + Rev.					For. Rev.	% Rat. of Total	For. + Rev.	
30*	21.7	4.15	.0424	6.388 5.481	11.869	6.815 5.761	12.576	7.582 6.433	14.015	20.79 17.68	54.1 45.9	38.46	12.82
31	20.3	13.2	.1417	8.656 6.842	15.498	8.415 6.702	15.117	9.170 7.436	16.606	26.24 20.98	55.6 44.4	47.22	15.74
32	21.6	16.4	.1790	11.93 10.23	22.16	11.39 9.60	20.99	12.49 10.44	22.93	35.81 30.28	54.2 45.8	66.09	22.03
33/1*	10.6	8.68	.0908	10.39 8.66	19.05	10.13 8.42	18.55	11.05 9.40	20.45	31.57 26.47	54.4 45.6	58.04	19.35
33/2	10.5	12.2	.1305	9.814 7.123	16.94	9.820 7.191	17.01	10.63 7.912	18.54	30.26 22.23	57.6 42.4	52.49	17.50
34*	10.5	18.5	.2041	11.59 8.04	19.63	11.33 7.72	19.05	12.22 8.44	20.66	35.15 24.20	59.2 40.8	59.35	19.78
35*	10.1	28.8	.3394	13.49 8.90	22.39	13.05 8.44	21.49	14.04 8.30	22.34	40.59 25.63	61.3 38.7	66.22	22.07
36	16.8	10.1	.1061	9.303 7.513	16.82	9.070 7.286	16.36	10.15 8.209	18.36	28.52 23.01	55.3 44.7	51.53	17.18
37*	18.0	17.8	.1961	11.05 8.614	19.66	10.80 8.488	19.29	11.69 9.397	21.09	33.54 26.50	55.9 44.1	60.04	20.01
38	18.6	14.4	.1560	13.12 11.37	24.49	12.90 11.02	23.92	13.61 11.77	25.38	39.62 34.16	53.7 46.3	73.79	24.60

TABLE 6.8 (Cont'd) MANDREL ROLLING (170 mm ROLLS)

TABLE 6.9 SINKING (170 mm ROLLS)

TUBE NO.	$\left[\frac{D}{t}\right]_o$	RED. OF AREA	LONG STR'N	ROLL TORQUE (N m)									
				ROLL 1		ROLL 2		ROLL 3		TOTAL (1+2+3)			MEAN ROLL TORQUE
				For. Rev.	For. + Rev.					For. Rev.	%Rat of Tot.	For. + Rev.	
1/1	8.51	4.63	.0474									49.94	16.65
1/2	8.04	4.57	.0467									66.77	22.26
1/3	7.48	6.74	.0698									95.31	31.77
2	6.84	9.28	.0974	41.00 4.38	45.38	56.20 7.30	63.50	51.50 7.40	58.90	148.7 19.08	88.6 11.4	167.8	55.93
3	6.31	8.31	.0868	37.62	37.62	53.56	53.56	52.85	52.85	144.0		144.0	48.01
5*	6.57	5.64	.0580	43.09 2.99	46.08	54.82 12.47	67.29	53.43 2.31	55.74	151.34 17.77	89.5 10.5	169.1	56.37
6*	6.46	10.32	.1089	44.95 6.50	51.45	53.00 11.39	64.39	57.21 6.53	63.74	155.16 24.42	86.4 13.6	179.6	59.86
7/1*	6.57	13.66	.1469	69.54 8.41	77.95	86.35 4.00	90.35	81.92 5.55	87.47	237.81 17.96	93.0 7.0	255.8	85.26
7/2*	6.45	8.94	.0936	34.66 4.85	39.51	42.71 4.48	47.19	57.06 15.08	72.14	134.43 24.41	84.7 15.3	158.8	52.95
10*	6.40	15.73	.1712	160.6 32.81	193.41	126.5 22.88	149.4	115.1 21.57	136.7	402.2 77.26	83.9 16.1	479.5	159.8
11*	6.50	15.93	.1736	100.3 23.33	123.6	135.2 22.65	157.9	146.1 22.29	168.4	381.6 68.27	84.8 15.2	449.9	150.0
12*	6.45	11.38	.1208	70.93 7.62	78.55	77.16 17.70	94.86	75.62 15.77	91.39	223.71 41.09	84.5 15.5	264.8	88.27

TABLE 6.9 (Cont'd) SINKING (170 mm ROLLS)

For. - Forward Rev. - Reverse

TUBE NO.	$\left[\frac{D}{t}\right]_o$	RED. OF AREA	LONG. STR'N	ROLL TORQUE (N m)									
				ROLL 1		ROLL 2		ROLL 3		TOTAL (1+2+3)			MEAN ROLL TORQUE
				For. Rev.	For. + Rev.					For Rev.	% Rat. of Total	For. + Rev.	
13/1	11.1	8.56	.0894	53.60	53.60	60.17	60.17	41.17	41.17	41.17		154.9	51.65
13/2	10.8	8.30	.0866	51.76 8.32	60.08	41.53 6.13	47.66	65.18 11.83	77.01	158.47 26.28	85.8 14.2	184.8	61.58
14*	18.0	4.02	.0410	10.91 1.40	12.31		11.95	11.12 .50	11.62			35.88	11.96
15	17.6	7.26	.0753	21.95 6.47	28.42	26.90 -.24	26.66	26.44 6.03	32.47	75.29 12.26	86.0 14.0	87.55	29.18
16	16.5	11.74	.1249	53.37 8.085	61.46	46.72 5.90	52.62	44.53 3.72	48.25	144.62 17.71	89.1 10.9	162.3	54.11
17*	10.5	5.62	.0578	20.56 6.23	26.79	31.15 3.30	34.45	22.27 9.27	31.54	73.98 18.80	79.7 20.3	92.78	30.93
18*	11.5	12.12	.1292	70.93 14.10	85.03	66.07 5.66	71.73	61.47 8.81	70.28	198.47 28.57	87.4 12.6	227.0	75.68

For. - Forward Rev. - Reverse

TUBE NO.	$\left[\frac{D}{t}\right]_o$	RED. OF AREA	LONG. STR'N	ROLL TORQUE (N m)									MEAN ROLL TORQUE
				ROLL 1		ROLL 2		ROLL 3		TOTAL (1+2+3)			
				For. Rev.	For. + Rev.					For Rev.	% Ratio of Total	For. + Rev.	
20*	28.4	13.6	.1464	43.19 31.25	74.44	56.41 36.50	92.91	52.34 43.08	95.42	151.94 110.83	57.8 42.2	262.8	87.59
21	27.3	10.9	.1150	39.28 26.34	65.62	44.81 30.98	75.79	44.72 32.61	77.33	128.81 89.93	58.9 41.1	218.7	72.91
22	29.1	4.43	.0453	26.65 21.14	47.79	27.02 23.23	50.25	30.57 24.09	54.66	84.24 68.46	55.2 44.8	152.7	50.90
23	18.2	18.9	.2098	73.93 52.21	126.1	76.26 47.19	123.4	87.10 47.98	135.1	237.29 147.38	61.7 38.3	384.7	128.2
24	18.4	11.9	.1261	63.77 40.20	104.0	64.82 46.23	111.1	80.58 43.78	124.4	209.17 130.21	61.6 38.4	339.4	113.1
25	18.9	11.0	.1170	41.82 27.42	69.24	50.81 29.24	80.05	44.97 33.26	78.23	137.60 89.92	60.5 49.5	227.5	75.84
26*	10.5	16.8	.1834	68.47 43.65	112.1	76.79 45.50	122.3	69.94 46.78	116.7	215.20 135.93	61.3 38.7	351.1	117.1
27	10.7	24.6	.2824	79.03 35.84	114.9	86.74 52.61	139.4	81.52 39.84	121.4	247.29 128.29	65.8 34.2	375.6	125.2
28*	10.7	35.1	.4316	102.2 46.90	149.1	133.7 59.30	193.0	120.4 64.4	184.8	356.3 170.6	67.6 32.4	526.8	175.6

TABLE 6.10 MANDREL ROLLING (170 mm ROLLS)

For. - Forward Rev. - Reverse

TUBE NO.	$\left[\frac{D}{t}\right]_o$	RED. OF AREA	LONG. STRAIN	ROLL TORQUE (N m)									
				ROLL 1		ROLL 2		ROLL 3		TOTAL (1+2+3)			MEAN ROLL TORQUE
				For. / Rev.	For. + Rev.					For. / Rev.	% Ratio of Total	For. + Rev.	
30*	21.7	4.15	.0424	24.03 14.32	38.35	27.65 19.07	46.72	29.81 23.29	53.10	81.49 56.68	59.0 41.0	138.2	46.05
31	20.3	13.2	.1417	43.65 28.95	72.60	46.93 27.02	73.95	51.88 35.20	87.08	142.5 91.17	61.0 39.0	233.7	77.88
32	21.6	16.4	.1790	75.78 59.61	135.39	68.64 51.96	120.60	84.31 49.84	134.15	228.7 161.4	58.6 41.4	390.1	130.0
33/1*	10.6	8.68	.0908	52.97 43.21	96.18	65.19 39.31	104.5	69.32 50.59	119.91	187.5 133.1	58.5 41.5	320.6	106.9
33/2	10.5	12.2	.1305	64.24		59.70		59.84		183.8 120.0	60.5 39.5	303.8	101.3
34*	10.5	18.5	.2041	74.08 43.17	117.3	87.66 42.66	130.3	77.88 43.52	121.4	239.6 129.4	64.9 35.1	369.0	123.0
35*	10.1	28.8	.3394	97.06 40.10	137.2	107.6 58.29	165.9	108.9 48.69	157.6	313.6 147.1	68.1 31.9	460.7	153.6
36	16.8	10.1	.1061	47.52 29.70	77.22	56.09 33.00	89.09	51.13 35.93	87.06	154.8 98.63	61.1 38.9	253.4	84.46
37*	18.0	17.8	.1961	56.66 34.73	91.39	72.12 36.77	108.9	62.65 48.83	111.5	191.4 120.3	61.4 38.6	311.7	103.9
38	18.6	14.4	.1560	75.36 53.30	128.7	77.26 45.03	122.3	67.16 55.12	122.3	219.8 153.5	58.9 41.1	373.3	124.4

6. ADDENDUM I

Additional rolling tests employing the larger 255 mm and 340 mm shroud diameter rolls were conducted for both the sinking and mandrel rolling processes. A selection of these results and recorded data, classified in chronological order, with the test phase and roll diameter, are presented in the following tables:

TABLE 6.I. 1/2 (Sinking/Mandrel Rolling) (255mm dia. Rolls)	Peripheral and axial longitudinal tube strains; measured and calculated.
TABLE 6.I. 3/4 (Sinking/Mandrel Rolling) (255 mm dia Rolls)	Tube specimen condition, individual and total roll force for forward and reverse rolling, mean roll separating force.
TABLE 6.I. 5/6 (Sinking/Mandrel Rolling) (255 mm dia. Rolls)	Tube specimen condition, individual and total roll torque for forward and reverse rolling, mean roll torque.
TABLE 6.I. 7/8 (Sinking/Mandrel Rolling) (340 mm dia. Rolls)	Peripheral and axial longitudinal tube strains - measured and calculated.

TABLE 6.I.9 (Sinking/Mandrel Rolling) (340 mm dia. Rolls)	Tube specimen condition, individual and total roll force, mean roll separating force.
TABLE 6.I.10 (Sinking/Mandrel Rolling) (340 mm dia. Rolls)	Tube specimen condition, individual and total roll torque, mean roll torque.
TABLE 6.I.11	Tube specimen condition, tube entry and exit velocities, roll root velocities.

Tube Specimen Condition

Number:

50	to	58	Sunk (255mm dia. Rolls)
137	to	139	- [various tube $\frac{D}{t}$ ratios and reductions]
120	to	123	

60	to	62	Mandrel (lub.) rolled (255 mm dia.Rolls) - [Ditto]-
130	to	134	Mandrel (dry) rolled (255 mm dia Rolls) - [Ditto]-
135	to	136	Mandrel (lub.) rolled (255 mm dia. Rolls) - [Ditto]-

150	to	153	Sunk (340 mm dia. Rolls) -[various tube $\frac{D}{t}$ ratios and reductions]
160	to	162	Mandrel (lub.) rolled (340 mm dia. Rolls) -[Ditto]-
170	to	172	Mandrel (dry) rolled (340 mm dia. Rolls) -[Ditto]-

Supplementary Notation:

See Chapter 6, page 253-255.

Tube No.	LONGITUDINAL STRAIN ε_{zs}						$\bar{\varepsilon}_h$
	Per. Stat.	R.T.L. Station			Axial Mean	Surface $\bar{\varepsilon}_{zs}$	Mean $\bar{\varepsilon}_z$	
		III	II	I				
50	1	.0673	.0685	.0670				
	1-2	.0635	.0665	.0655				
	2	.0608	.0624	.0616				
	2-3	.0614	.0590	.0601				
	3	.0653	.0611	.0619				
	3-1	.0671	.0670	.0650				
		.0642	.0641	.0635		.0635(I)		
51	1	.1304	.1269	.1251				
	1-2	.1318	.1273	.1279				
	2	.1297	.1244	.1238				
	2-3	.1283	.1232	.1240				
	3	.1245	.1242	.1222				
	3-1	.1282	.1244	.1240				
		.1288	.1251	.1245		.1245(I)		
52	1	.1359	.1335	.1377				
	1-2	.1330	.1355	.1407				
	2	.1256	.1327	.1386				
	2-3	.1472	.1324	.1339				
	3	.1381	.1320	.1311				
	3-1	.1509	.1336	.1331				
		.1385	.1333	.1359		.1359(I)		
53	1	.0604	.0598	.0575				
	1-2	.0586	.0595	.0596				
	2	.0571	.0591	.0602				
	2-3	.0647	.0594	.0609				
	3	.0665	.0596	.0587				
	3-1	.0674	.0598	.0581				
		.0625	.0595	.0592		.0592(I)		
54	1	.1120	.0959	.0900				
	1-2	.0925	.0956					
	2	.0914	.0973	.0957				
	2-3	.0925	.0984	.0980				
	3	.1012	.0983	.0943				
	3-1	.1040	.0972	.0928				
		.0989	.0971	.0942		.0942(I)		
55	1	.1023	.1048	.1087				
	1-2		.1093	.1093				
	2	.1211	.1097	.1144				
	2-3	.1110	.1220	.1080				
	3	.0990	.1146	.1083				
	3-1	.0960	.1087	.1078				
		.1059	.1115	.1094		.1094(I)		
56	1	.0280	.0338	.0349				
	1-2	.0301	.0361	.0344				
	2	.0401	.0374	.0361				
	2-3	.0490	.0369	.0384				
	3	.0447	.0354	.0387				
	3-1	.0326	.0342	.0375				
		.0374	.0356	.0367		.0367(I)		

TABLE 6.1.1 (cont'd) SINKING (255 mm ROLLS)

Tube No.	LONGITUDINAL STRAIN ε_{zs}							$\bar{\varepsilon}_h$
	Per. Stat.	R.T.L. Station III	II	I	Axial Mean	Surface $\bar{\varepsilon}_{zs}$	Mean $\bar{\varepsilon}_z$	
57	1		.0672	.0672				
	1-2		.0654	.0689				
	2		.0651	.0688				
	2-3		.0682	.0694				
	3		.0699	.0673				
	3-1		.0699	.0675				
			.0676	.0682		.0682(I)		
58	1	.0898	.0946	.0948				
	1-2	.0885	.0953	.0971				
	2	.0950	.0985	.1002				
	2-3	.1096	.1015	.1016				
	3	.1064	.1015	.0985				
	3-1	.1028	.0980	.0954				
		.0987	.0982	.0979		.0979(I)		
137	1		.1080	.1156	.1118			
	1-2		.1055	.1077	.1066			
	2		.1156	.0935	.1045			
	2-3		.1046	.1135	.1090			
	3		.1069	.1016	.1042			
	3-1		.1078	.1012	.1045			
			.1081	.1055		.1055(I)	.1086	
138	1	.0657	.0684	.0821	.0721			
	1-2	.0794	.0512	.0692	.0666			
	2	.0638	.0653		.0645			
	2-3	.0644	.0654		.0649			
	3	.0643	.0671	.0629	.0648			
	3-1	.0830	.0526	.0731	.0695			
		.0701	.0617	.0716		.0716(I)	.0629	
139	1	.0737	.0706	.0781	.0741			
	1-2	.0528	.0695	.0800	.0675			
	2	.0704	.0760	.0785	.0750			
	2-3	.0833	.0756	.0828	.0806			
	3	.0893	.0887	.0616	.0799			
	3-1	.0695	.0699	.1015	.0803			
		.0732	.0751	.0804		.0804(I)	.0784	

TABLE 6.I.2

MANDREL ROLLING (255 mm ROLLS)
(lubricated)

Tube No.	LONGITUDINAL STRAIN ε_{zs}						$\bar{\varepsilon}_h$
	Per. Stat.	R.T.L. Station III	R.T.L. Station II	R.T.L. Station I	Axial Mean	Surface $\bar{\varepsilon}_{zs}$	Mean $\bar{\varepsilon}_z$	
60	1	.2980	.3017	.2945				
	1-2	.3008	.3015	.3258				
	2	.2998	.3058	.2943				
	2-3	.2997	.2999	.2910				
	3	.2980	.2958	.2950				
	3-1	.2994	.2980	.2915				
		.2993	.3006	.2987		.2987(I)		
61	1	.2080	.2228	.2046				
	1-2	.2230	.2111	.2045				
	2	.2248	.2104	.2078				
	2-3	.2235	.2116	.2044				
	3	.2245	.2082	.2033				
	3-1	.2222	.2109	.2045				
		.2210	.2125	.2049		.2049(I)		
62	1	.1320	.1141	.1042				
	1-2	.1332	.1137	.1030				
	2	.1327	.1132	.1016				
	2-3	.1327	.1133	.1029				
	3	.1290	.1118	.1029				
	3-1	.1331	.1130	.1031				
		.1321	.1132	.1030		.1030(I)		

MANDREL ROLLING (255 mm ROLLS)

(dry/lubricated)

Tube No.	LONGITUDINAL STRAIN ε_{zs}							$\bar{\varepsilon}_h$
	Per. Stat.	R.T.L. Station III	R.T.L. Station II	R.T.L. Station I	Axial Mean	Surface $\bar{\varepsilon}_{zs}$	Mean $\bar{\varepsilon}_z$	
130	1		.1052	.1124	.1088			
	1-2		.0989	.0998	.0994			
	2		.0966	.0966	.0966			
	2-3		.1220	.0949	.1085			
	3		.0993	.0906	.0950			
	3-1		.0981	.0948	.0964			
			.1033	.0982		.1033(II)	.0971	
131	1	.0448	.0490	.0362	.0433			
	1-2	.0298	.0518	.0597	.0471			
	2	.0427	.0484	.0451	.0454			
	2-3	.0450	.0491	.0643	.0528			
	3	.0298	.0657	.0237	.0397			
	3-1	.0448	.0514	.0492	.0485			
		.0395	.0527	.0464		.0527(II)	.0532	
132	1		.0879	.0804	.0841			
	1-2		.0874	.0856	.0865			
	2		.0806	.0837	.0822			
	2-3		.0622	.0823	.0722			
	3		.0822	.0846	.0834			
	3-1		.0822	.0798	.0810			
			.0804	.0827		.0804(II)	.1139	
133/1	1	.1913	.1697	.1779	.1797			
	1-2	.1824	.1806	.1886	.1839			
	2	.1888	.1834	.1685	.1802			
	2-3	.1585	.1829	.1645	.1686			
	3	.1754	.1836	.1782	.1791			
	3-1	.1736	.1773	.1801	.1770			
		.1783	.1796	.1763		.1796(II)	.1906	
134	1	.1155	.1060	.1061	.1092			
	1-2	.1113	.1084	.1035	.1077			
	2	.1113	.1032	.1054	.1066			
	2-3	.1102	.1066	.1048	.1072			
	3	.1163	.0850	.1187	.1067			
	3-1	.1130	.1228	.0884	.1081			
		.1129	.1053	.1045		.1053(II)	.1344	
135	1	.0796	.0930	.0651	.0792			
	1-2	.0797	.0814	.0765	.0792			
	2	.0648	.0808	.0775	.0744			
	2-3	.0788	.0844	.0732	.0788			
	3	.0738	.0918	.0640	.0765			
	3-1	.0792	.0808	.0876	.0825			
		.0760	.0854	.0740		.0854(II)	.1078	
136	1	.0831	.0758	.0778	.0789			
	1-2	.0769	.0766	.0770	.0768			
	2	.0814	.0614	.0756	.0728			
	2-3	.0908	.0611	.0781	.0766			
	3	.0801	.0761	.0774	.0779			
	3-1	.0775	.0915	.0770	.0820			
		.0816	.0738	.0772		.0738(II)	.1742	

For. - Forward Rev. - Reverse

TUBE NO.	$\left[\frac{D}{t}\right]_o$	RED. OF AREA	LONG. STRAIN	ROLL FORCE (kN)									
				ROLL 1		ROLL 2		ROLL 3		TOTAL (1+2+3)			R.S.F.
				For. Rev.	For. + Rev.					For. Rev.	%Ratio of Total	For. + Rev.	
50	6.51		.0635	4.431 2.818	7.249	4.577 2.917	7.494	4.823 2.746	7.569	13.83 8.481	62.0 38.0	22.31	7.437
51	6.19		.1245	7.634 3.975	11.61	7.274 3.698	10.97	7.871 3.575	11.45	22.78 11.25	66.9 33.1	34.03	11.34
52	6.94		.1359	8.461 3.809	12.27	7.698 3.122	10.82	8.373 3.935	12.31	24.53 10.87	69.3 30.7	35.40	11.80
53	10.70		.0592	.827 .473	1.300	1.516 1.062	2.578	1.257 1.005	2.262	3.600 2.540	58.6 41.4	6.139	2.046
54*	10.70		.0942	2.637 .323	2.960	2.388 .857	3.245	3.066 .737	3.803	8.091 1.917	80.8 19.2	10.01	3.336
55*	11.27		.1094	4.236 .984	5.220	3.972 .993	4.965	4.732 1.198	5.930	12.94 3.175	80.3 19.7	16.12	5.372
56	17.80		.0367	.512 .079	.591	.910 .303	1.213	.628 .209	.837	2.050 .591	77.6 22.4	2.641	.880
57*	17.67		.0682	.811 .055	.866	1.326 .152	1.478	1.130 .177	1.307	3.267 .384	89.5 10.5	3.651	1.217
58	17.75		.0979	2.645 .449	3.094	3.032 .591	3.623	2.580 .645	3.225	8.257 1.685	83.1 16.9	9.942	3.314

STRIKING (255 mm ROLLS)

TABLE 6.1.3 (cont'd) SINKING (255 mm ROLLS)

For. - Forward Rev. - Reverse

TUBE NO.	$\left[\frac{D}{t}\right]_o$	RED. OF AREA	LONG. STRAIN	ROLL FORCE (kN)									
				ROLL 1		ROLL 2		ROLL 3		TOTAL (1+2+3)			
				For. Rev.	For. + Rev.					For. Rev.	%Ratio of Total	For. + Rev.	R.S.F.
137	6.99	10.29	1055	3.520 1.200	4.720	3.587 1.709	5.296	3.813 1.354	5.167	10.92 4.263	71.9 28.1	15.18	5.061
138	10.64	6.10	.0629	1.102 .826	1.928	1.728	3.103 1.375	1.423	2.553 1.130	4.253 3.331	56.1 43.9	7.584	2.528
139	17.53	7.54	.0784	.622 .236	.858	1.137 .440	1.577	1.420 .486	1.906	3.179 1.162	73.2 26.8	4.341	1.447
120	6.88	3.79		2.686	2.686	2.521	2.521	2.920	2.920	8.127		8.127	2.709
121	6.54	11.4		9.912	9.912	9.292	9.292	10.05	10.05	29.26		29.26	9.752
123	6.90	9.95		4.675	4.675	4.357	4.357	5.041	5.041	14.07		14.07	4.691

TABLE 6.I.4 MANDREL ROLLING (255mm ROLLS)

For. - Forward Rev. - Reverse

TUBE NO.	$\left[\frac{D}{t}\right]_o$	RED. of AREA	LONG. STRAIN	ROLL FORCE (kN)									
				ROLL 1		ROLL 2		ROLL 3		TOTAL (1+2+3)			
				For. Rev.	For. + Rev.					For. Rev.	%Ratio of Total	For. + Rev.	R.S.F.
60	10.60		.3006	14.53 10.89	25.42	13.54 9.88	23.42	13.88 10.12	24.00	72.84 24.28	57.6 42.4	72.84	24.28
61	10.61		.2125	12.25 9.645	21.90	11.09 8.739	19.83	11.68 8.925	20.61	35.02 27.31	56.2 43.8	62.33	20.78
62	10.78		.1132	9.180 7.840	17.02	9.030 7.670	16.70	8.890	16.03 7.140	27.10	54.5 22.65	49.75 45.5	16.58

TABLE 6.I.4 MANDREL ROLLING (255 mm ROLLS)
(Cont'd)

For. - Forward Rev. - Reverse

TUBE NO.	$\left[\frac{D}{t}\right]_o$	RED. OF AREA	LONG. STRN	ROLL FORCE (kN)									R.S.F.
				ROLL 1		ROLL 2		ROLL 3		TOTAL (1+2+3)			
				For. Rev.	For. + Rev.					For. Rev.	% Rat of Total	For. + Rev.	
130	18.07	9.25	.0971	12.47	12.47	11.45	11.45	12.38	12.38	36.30		36.30	12.10
131	17.65	5.18	.0532	9.41	9.41	8.37	8.37	9.10	9.10	26.88		26.88	8.96
132	22.04	10.76	.1139	9.86	9.86	8.53	8.53	9.23	9.23	27.62		27.62	9.21
133/1	10.57	17.36	.1906	14.39	14.39	13.59	13.59	14.48	14.48	42.46		42.46	14.15
134	10.48	12.57	.1344	11.28	11.28	10.79	10.79	11.75	11.75	33.82		33.82	11.27
135	28.67	10.22	.1078	7.96	7.96	7.46	7.46	8.01	8.01	23.43		23.43	7.81
136	10.78	15.98		7.79	7.79	7.62	7.62	8.09	8.09	23.50		23.50	7.83

TABLE 6.I.5 SINKING (255 mm ROLLS)

For. - Forward Rev. - Reverse

TUBE NO.	$\left[\frac{D}{t}\right]_o$	RED OF AREA	LONG STR'N	ROLL TORQUE (N m)									
				ROLL 1		ROLL 2		ROLL 3		TOTAL (1+2+3)			MEAN ROLL TORQUE
				For. Rev.	For. + Rev.					For. Rev.	%Rat. of Total	For. + Rev.	
50	6.51		.0635	54.76 12.48	67.24	71.26 14.16	85.42	39.90 15.77	55.67	165.9 42.41	79.7 20.3	208.3	69.44
51	6.19		.1245	110.9 38.12	149.0	124.6 29.50	154.1	133.4 30.62	164.0	368.9 98.24	79.0 21.0	467.1	155.7
52	6.94		.1359	121.3 35.81	157.1	127.4 46.96	174.4	136.2 31.08	167.3	384.9 113.9	77.2 22.8	498.8	166.3
53	10.70		.0592	23.11 2.08	25.19	34.21 3.54	37.75	40.59 8.12	48.71	97.91 13.74	87.7 12.3	111.7	37.22
54*	10.70		.0942	82.03 11.55	93.58	84.00 9.91	93.91	84.20 4.64	88.84	250.2 26.10	90.6 9.4	276.3	92.11
55*	11.27		.1094	117.8 29.79	147.6	99.98 26.88	126.9	111.2 5.10	116.3	329.0 61.77	84.2 15.8	390.8	130.27
56	17.80		.0367	16.17 2.31	18.48	7.08 1.18	8.26	16.24 1.16	17.40	39.49 4.65	89.5 10.5	44.14	14.71
57*	17.67		.0682	34.66 16.17	50.83	43.65 0.00	43.65	38.27 4.64	42.91	116.6 20.81	84.9 15.1	137.4	45.80
58	17.75		.0979	77.41 18.49	95.90	90.85 4.72	95.57	68.19 1.16	69.35	236.5 24.37	90.7 9.3	260.8	86.94

TABLE 6.I.5 (Cont'd) SINKING (255 mm ROLLS)

For. - Forward Rev. - Reverse

TUBE NO.	$\left[\frac{D}{t}\right]_o$	RED. OF AREA	LONG. STRN	ROLL TORQUE (N m)									
				ROLL 1		ROLL 2		ROLL 3		TOTAL (1+2+3)			MEAN ROLL TORQUE
				For. Rev.	For. + Rev.					For. Rev.	% Rat of Total	For. + Rev.	
137	6.99	10.29	.1086	82.94 20.62	103.6	103.1 18.91	122.0	79.45 24.48	103.9	265.5 64.01	80.6 19.4	329.5	109.8
138	10.64	6.10	.0629	31.19 9.24	40.43	46.01 1.18	47.19	34.56 1.16	35.72	111.8 11.58	90.6 9.4	123.3	41.11
139	17.53	7.54	.0784	33.04 13.86	46.90	30.67 0.00	30.67	24.35 6.96	31.31	88.06 20.82	80.9 19.1	108.9	36.29
120	6.88	3.79		46.30	46.30	23.11	23.11	16.79	16.79	86.20		86.2	28.73
121	6.54	11.4		186.8	186.8	121.1	121.1	149.2	149.2	457.1		457.1	152.4
123	6.90	9.95		93.29	93.29	99.28	99.28	117.7	117.7	310.3		310.3	103.4

For. - Forward Rev. - Reverse

TUBE NO.	$\left[\frac{D}{t}\right]_o$	RED. OF AREA	LONG. STR'N	ROLL TORQUE (N m)									MEAN ROLL TORQUE
				ROLL 1		ROLL 2		ROLL 3		TOTAL (1+2+3)			
				For. / Rev.	For. + Rev.					For / Rev.	%Ratio of Total	For. + Rev.	
60	10.60		.3006	118.6 88.68	207.3	117.4 66.00	183.4	139.9 67.16	207.1	375.9 221.8	62.9 37.1	597.7	199.2
61	10.61		.2125	110.1 11.62	121.7	73.07 64.59	137.7	103.0 105.4	208.4	286.2 181.6	61.2 38.8	467.8	155.9
62	10.78		.1132	62.55 54.16	116.7	72.65 50.19	122.8	66.79 39.70	106.5	202.0 144.1	58.4 41.6	346.0	115.3

TABLE 6.1.6 MANDREL ROLLING (255 mm ROLLS)

TABLE 6.I.6 (cont'd) MANDREL ROLLING (255 mm ROLLS)

For. - Forward Rev. - Reverse

TUBE NO.	$\left[\frac{D}{t}\right]_o$	RED. OF AREA	LONG. STR'N	ROLL TORQUE (N m)									
				ROLL 1		ROLL 2		ROLL 3		TOTAL (1+2+3)			MEAN ROLL TORQUE
				For. Rev.	For. + Rev.					For. Rev.	%Ratio of Total	For. + Rev.	
130	18.07	9.25	.0971	90.98	90.98	101.2	101.2	82.22	82.22	274.4		274.4	91.47
131	17.65	5.18	.0532	56.13	56.13	57.90	57.90	60.05	60.05	174.1		174.1	58.03
132	22.04	10.76	.1139	79.53	79.53	65.27	65.27	73.30	73.30	218.1		218.1	72.70
133/1	10.57	17.36	.1906	105.8	105.8	135.8	135.8	152.8	152.8	394.4		394.4	131.5
134	10.48	12.57	.1344	80.41	80.41	76.31	76.31	105.6	105.6	262.3		262.3	87.43
135	28.67	10.22	.1078	54.91	54.91	51.67	51.67	57.90	57.90	164.5		164.5	54.83
136	10.78	15.98		6.85	6.85	110.2	110.2	45.83	45.83	162.9		162.9	54.28

TABLE 6.I.7

SINKING (340 mm ROLLS)

Tube No.	LONGITUDINAL STRAIN ε_{zs}						$\bar{\varepsilon}_h$
	Per. Stat.	R.T.L. Station			Axial	Surface	Mean	
		III	II	I	Mean	$\bar{\varepsilon}_{zs}$	$\bar{\varepsilon}_z$	
150*	1	.0684	.0675	.0617	.0659			
	1-2	.0676	.0680	.0640	.0660			
	2	.0671	.0661	.0692	.0675			
	2-3	.0669	.0648	.0643	.0653			
	3	.0652	.0633	.0611	.0632			
	3-1	.0660	.0635	.0577	.0624			
		.0669	.0655	.0630		.0655(II)	.1229	
151	1	.0766	.0839	.0876	.0827			
	1-2	.0777	.0846	.0880	.0835			
	2	.0819	.0850	.0848	.0839			
	2-3	.0861	.0869	.0767	.0832			
	3	.0889	.0866	.0783	.0846			
	3-1	.0960	.0847	.0818	.0875			
		.0845	.0853	.0829		.0853(II)	.0615	
152*	1	.0611	.0621	.0579	.0603			
	1-2	.0609	.0643	.0621	.0624			
	2	.0572	.0602	.0599	.0591			
	2-3	.0551	.0562	.0597	.0570			
	3	.0600	.0560	.0556	.0570			
	3-1	.0616	.0580	.0598	.0598			
		.0593	.0594	.0592		.0594(II)	.0631	
153	1	.0653	.0679	.0658	.0664			
	1-2	.0612	.0684	.0669	.0660			
	2	.0653	.0679	.0684	.0672			
	2-3	.0699	.0660	.0652	.0671			
	3	.0744	.0640	.0644	.0676			
	3-1	.0720	.0656	.0645	.0674			
		.0680	.0667	.0659		.0667(II)	.0580	

TABLE 6.1.8

MANDREL ROLLING (340 mm ROLLS)
(lubricated/dry)

Tube No.	LONGITUDINAL STRAIN ε_{zs}						$\bar{\varepsilon}_h$
	Per. Stat.	R.T.L. Station			Axial	Surface	Mean	
		III	II	I	Mean	$\bar{\varepsilon}_{zs}$	$\bar{\varepsilon}_z$	
160	1	.0837	.0886	.0824	0849			
	1-2	.0832	.0857	.0864	.0851			
	2	.1008	.0869	.0713	.0863			
	2-3	.0677	.1014	.0889	.0860			
	3	.1015	.0705	.0810	.0843			
	3-1	.0798	.0866	.0873	.0846			
		.0861	.0866	.0829		.0866(II)	.0599	
161	1	.0901	.0953	.0959	.0938			
	1-2	.0905	.0955	.0955	.0938			
	2	.0803	.1087	.0953	.0948			
	2-3	.0907	.0935	.0964	.0935			
	3	.1076	.0880	.0970	.0975			
	3-1	.0900	.0957	.0940	.0932			
		.0915	.0961	.0957		.0961(II)	.0709	
162	1	.0879	.0954	.0957	.0930			
	1-2	.0936	.0931	.0980	.0949			
	2	.0823	.1072	.0928	.0941			
	2-3	.0847	.0957	.0959	.0921			
	3	.0853	.1084	.0923	.0953			
	3-1	.0735	.1093	.0956	.0928			
		.0845	.1015	.0950		.1015(II)	.0811	
170	1		.0485	.0523	.0505			
	1-2		.0550	.0553	.0552			
	2		.0682	.0433	.0557			
	2-3		.0589	.0540	.0565			
	3		.0538	.0566	.0552			
	3-1		.0541	.0542	.0541			
			.0564	.0526		.0564(II)	.0365	
171	1	.0426	.0422	.0431	.0426			
	1-2	.0419	.0428	.0427	.0425			
	2	.0418	.0413	.0433	.0421			
	2-3	0418	.0420	.0438	.0426			
	3	.0425	.0427	.0425	.0426			
	3-1	.0423	.0424	.0429	.0425			
		.0421	.0422	.0431		.0422(II)	.0572	
172	1	.0523	.0499	.0560	.0527			
	1-2	.0502	.0517	.0519	.0512			
	2	.0569	.0671	.0313	.0620			
	2-3	.0544	.0517	.0522	.0528			
	3	.0490	.0522	.0526	.0522			
	3-1	.0509	.0504	.0528	.0514			
		.0521	.0543	.0531		.0543(II)	.0540	

TABLE 6.I.9 SINKING/MANDREL ROLLING (340 mm ROLLS)

For. - Forward Rev. - Reverse

Tube No.	$(\frac{D}{t})_o$	Red. of Area (J)%	LONG. STR'N ε_z	ROLL FORCE (kN)									
				ROLL 1		ROLL 2		ROLL 3		TOTAL (1+2+3)			R.S.F.
				For. Rev.	For. + Rev.					For. Rev.	%Ratio of Total	For. + Rev.	
150*	18.04	11.56	.1229	.862	.862	.924	.924	.515	.515	2.30		2.300	.767
151	12.33	5.96	.0615	4.396	4.396	4.092	4.092	3.069	3.069	11.56		11.56	3.852
152*	7.49	6.12	.0631	2.345	2.345	2.292	2.292	1.386	1.386	6.02		6.023	2.008
153	6.48	5.63	.0580	3.180	3.180	3.372	3.372	3.332	3.332	9.88		9.884	3.295
160	22.02	5.81	.0599	8.61	8.61	8.55	8.55	9.54	9.54	26.70		26.70	8.90
161	17.37	6.85	.0709	10.82	10.82	10.93	10.93	13.02	13.02	34.77		34.77	11.59
162	10.96	7.79	.0811	9.29	9.29	8.92	8.92	10.15	10.15	28.36		28.36	9.45
170	10.81	3.59	.0365	8.02	8.02	8.38	8.38	9.15	9.15	25.56		25.56	8.52
171	17.61	5.56	.0572	8.95	8.95	8.56	8.56	9.79	9.79	27.29		27.29	9.10
172	22.05	5.26	.0540	9.55	9.55	9.51	9.51	11.02	11.02	30.09		30.09	10.03

TABLE C.1.10 SINKING/MANDREL ROLLING (340 mm ROLLS)

For. - Forward Rev. - Reverse

TUBE NO.	$\left[\frac{D}{t}\right]_o$	RED. OF AREA	LONG. STR'N	ROLL TORQUE (N m)									
				ROLL 1		ROLL 2		ROLL 3		TOTAL (1+2+3)			MEAN ROLL TORQUE
				For. Rev.	For. + Rev.					For. Rev.	%Ratio of Total	For. + Rev.	
150*	18.04	11.56	.1229	60.30	60.30	32.80	32.80	48.70	48.70	141.8		141.8	47.30
151	12.33	5.96	.0615	128.8	128.8	89.00	89.00	122.4	122.4	340.1		340.1	113.4
152*	7.49	6.12	.0631	71.86	71.86	48.14	48.14	72.95	72.95	193.0		193.0	64.32
153	6.48	5.63	.0580	60.19	60.19	71.73	71.73	115.6	115.6	247.5		247.5	82.51
160	22.02	5.81	.0599	78.55	78.55	65.54	65.54	62.42	62.42	206.5		206.5	68.84
161	17.37	6.85	.0709	79.48	79.48	92.21	92.21	99.40	99.40	271.1		271.1	90.37
162	10.96	7.79	.0811	95.12	95.12	102.1	102.1	73.65	73.65	270.9		270.9	90.30
170	10.81	3.59	.0365	77.23	77.23	80.61	80.61	64.49	64.49	222.3		222.3	74.11
171	17.61	5.56	.0572	65.48	65.48	62.09	62.09	63.46	63.46	191.1		191.0	63.68
172	22.05	5.26	.0540	54.68	54.68	72.29	72.29	73.92	73.92	200.9		200.9	66.96

TABLE 6.I. 11 SINKING/MANDREL ROLLING

(255 mm ROLLS)

TUBE No.	$\left[\frac{D}{t}\right]$	Tube Velocity .(mm/s)		Roll Root Velocity (mm/s)	Reduction of Area (%)	
		U_o(entry)	U_1(exit)	$V_{(r)}$	J_u	J_w
52(S)	6.94	4.03	4.59	4.34	12.2	12.7
53(S)	10.70	4.25	4.55	4.40	6.60	5.75
55(S)	11.3	4.06	4.52	4.37	10.2	10.4
131(M)	17.7	4.26	4.46	4.33	4.48	5.18
134(M)	10.5	4.02	4.59	4.32	12.4	12.6
135(M)	28.7	4.12	4.51	4.34	8.65	10.2

(S) Sunk tube specimen

(M) Mandrel rolled tube specimen

J_u Tube reduction assessed from constancy of volume i.e. $A_oU_o = A_1U_1$

J_w Tube reduction assessed by weighing method.

CHAPTER SEVEN

DISCUSSION

7. DISCUSSION

7.1. INTRODUCTION

The discussion will be introduced with an assessment of the viability of the forward and reverse rolling tests and the attempted deductions of the tube velocities and allied deformation zones. Both sinking and mandrel rolling processes will be considered and for each process the extent of the worked tube surface and associated strains will be assessed. Finally the influence of tube reduction, tube $\frac{D}{t}$ ratio etc., on the roll separating force and torque will be discussed, followed by a comparison between the proposed theories and the experimental results.

Except where indicated, this Chapter considers the sinking and mandrel rolling processes for the 170 mm shroud diameter rolls.

In the majority of the tube rolling trials three tube reductions for each tube $\frac{D}{t}$ ratio were obtained, so a detailed interpretation of the series of results is not attempted.

7.1.1. Effect of Forward and Reverse Rolling the Tube Specimen.

As stated in Chapter 5 the absence of pin loadcells within the roll groove profile meant that no measurement of the

roll pressure and tube-roll contact area was obtained; consequently the tube specimens were partially forward and reverse rolled. Thus the required tube roll contact area and contact angle were retained for inspection. Although a large number of the specimens were rolled in this manner, for comparative purposes some were completely rolled as a single pass.

The forward and reverse rolling process inherently implies an overall increase in the contribution of friction and redundancy in achieving a specific tube reduction, i.e. the summation of the individual roll load and torques for the forward and reverse rolling conditions is always greater than the corresponding case for a single roll pass. For both sinking and mandrel rolling processes the friction effect was proportionally greater at low tube reductions and for thinner tubes. The sinking redundancy contribution is primarily due to bending and not shear. Shear redundancy for both the sinking and mandrel rolling processes was shown to be negligible by Haleem (40) and Labib (43) respectively. Thus, the roll force & torque graphs represent the summation of force & torque in the forward & reverse directions for the total reduction of area effected.

Compared with the equivalent single pass condition the friction contribution in the reverse rolling situation is likely to be smaller. This is as a result of the outer tube surface, now appreciably deformed to the roll gap profile after forward rolling, experiencing minimal relative shear velocity values at the tube-roll interface.

The forward and reverse roll force results (TABLE 6.7/8) show in general that as the tube reduction of area increases so does the ratio of the forward to the total roll force (see column 12). This is believed to be the result of the friction contribution being proportionally greater at lower reductions, i.e. as the overall reduction decreases then the forward and reverse roll separating forces approach equality. Furthermore, the increase of the forward to the total roll force is greater in sinking than in mandrel rolling i.e. from 67.5% to 80.7% for sinking and from 52.3% to 61.7% for mandrel rolling, even though greater reductions are present in the latter process. This condition also suggests that the friction contribution, which predominates in mandrel rolling, reduces the difference between the forward and reverse roll forces.

Likewise the forward and reverse roll torque results presented in TABLE 6.9/10., show a similar trend to that for the roll forces. However the contribution of the forward to the overall roll torque (see column 12) is greater for both sinking and mandrel rolling, possibly due to the cumulative effect of a reduced contact area and moment arm for reverse rolling. Irrespective of tube reduction, the sinking results show a greater uniformity for the forward to total torque ratio values. Here again it can be reasoned that this is probably due to the reduced influence of friction in sinking compared with mandrel rolling.

7.1.2. Tube Velocity and the Contact Surface Deformation Zones.

In general the tube velocity trials were only partially reliable, particularly for the forward and reverse rolling tests where the necessary requirement to record quickly four velocity measurements increased the experimental errors. This was immediately apparent for the larger rolls with the attendant higher tube velocities. Furthermore, random transverse movement of the tube specimen, particularly during sinking, created parallax error, making the timed runs less accurate. The roll speed, set at the minimum and assumed constant, also varied slightly with load, especially for mandrel rolling.

Only a few tube velocity measurements were satisfactory and these are shown in TABLE 6.I.11. Furthermore, some uncertainty was involved in the measurement of the maximum peripheral tube-roll contact angle ($2\theta_{c1}$). Consequently the experimental assessment of the deformation zones was, in many cases, inconclusive. However interpretation of these zones does illustrate how they are influenced by the tube reduction. FIGURE 7.1., shows some of the better measured tube velocities and the associated surface deformation zones. They are in most cases approximately of the same format to those assumed for the theoretical models shown in FIGURE 3. 21.

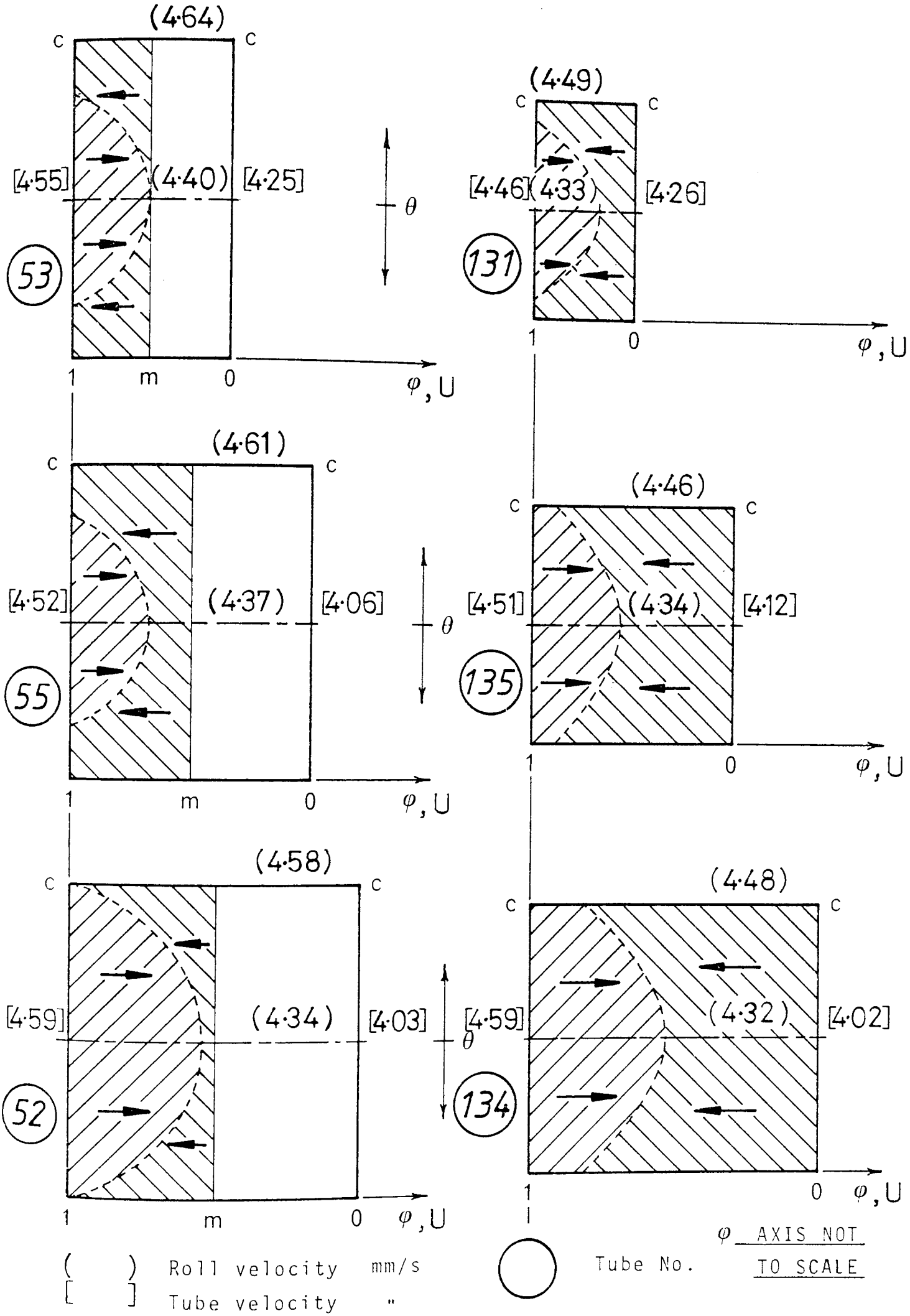
(4·64)
c
c
[4·55]
(4·40)
[4·25]
θ
53
1
m
0
φ, U
(4·49)
c
c
[4·46]
(4·33)
[4·26]
131
1
0
φ, U
(4·61)
c
c
[4·52]
(4·37)
[4·06]
θ
55
1
m
0
φ, U
(4·46)
c
c
[4·51]
(4·34)
[4·12]
135
1
0
φ, U
(4·58)
c
c
[4·59]
(4·34)
[4·03]
θ
52
1
m
0
φ, U
(4·48)
c
c
[4·59]
(4·32)
[4·02]
θ
134
1
0
φ, U
( ) Roll velocity mm/s
[ ] Tube velocity "
Velocity (Roll-tube)
Tube No.
φ AXIS NOT TO SCALE

FIGURE 7.1

7.1.3. Maximum Tube Reduction Within Roll Groove Depth.

The maximum tube reduction that can be accommodated with the depth of the roll groove profile i.e. root to shroud is shown in FIGURE 3. 21.b.

For constancy of volume:

$A_o U_o = A_n U_n = A_1 U_1$ where A and U are the respective tube cross sectional area and velocity at any stage in the deformation process,

The roll root velocity, $v_{(r)} = R_r \omega$

The roll shroud velocity, $v_{(s)} = R_s \omega$

where R_r and R_s are the respective roll root and shroud radii and ω is the roll angular velocity.

The limiting case for the total tube reduction to take place entirely within the roll groove depth is given by:

$A_s v_{(s)} = A_r v_{(r)}$ and when $v_{(s)} = U_s$ & $v_{(r)} = U_r$

This can also be written as:

$$A_1 U_s = A_o U_r$$

Then for the 170 mm diameter rolls:

$$\frac{Ao}{A_1} = \frac{78.308}{85,000} = 0.9213$$

$\therefore$ Jg = 0.0787 i.e. 7.87%

For the 255 mm diameter rolls:

$$\frac{Ao}{A_1} = \frac{120.81}{127.5} = 0.9475$$

$\therefore$ Jg = 0.0525 i.e. 5.25%

For the 340 mm diameter rolls:

$$\frac{Ao}{A_1} = \frac{163.31}{170.00} = 0.9606$$

$\therefore$ Jg = 0.0394 i.e. 3.94%

where Jg is the tube reduction taking place entirely within the roll groove depth.

7.2. SINKING, EXPERIMENTAL

7.2.1. Tube-Roll Contact Area.

PLATE 7.1., illustrates the shadowgraph projections of the tube profiles at the root and shroud contact regions for various tube reductions and $\frac{D}{t}$ ratios. The contact and free deformation zones are clearly visible and are approximately equal. Similar tube curvatures in these zones are apparent at the root section. However the shroud section appears to present a somewhat reduced curvature. The tube-roll "plan" contact areas displayed in PLATE 7.2., are associated with an increase in tube reduction from left to right i.e. tube numbers 14 to 16 to 11. They illustrate, for an increasing tube reduction, a transition from a shallow convex to a shallow concave peripheral contact line at tube entry. Therefore the assumption of a rectangular contact area appears to be justified. Cole (35) in his sinking trials observed a similar tube-roll "plan" contact area pattern. Furthermore, the relevant work of Haleem (40) indicated minimal change in the measured tube-roll arc contact length around the groove, i.e. endorsing the assumption of an approximate rectangular area of contact.

7.2.2 Measured Surface Longitudinal Strain Distribution.

The distribution of the measured longitudinal strains for the sinking process are shown in TABLE 6.5. (Chapter 6.

SOME SUNK TUBE PROFILES (LONGITUDINAL) x10

Tube $\frac{D}{t}$ ratio increasing from top to bottom.

Roll shroud contact on left.

Roll root contact on right.

PLATE 7.1

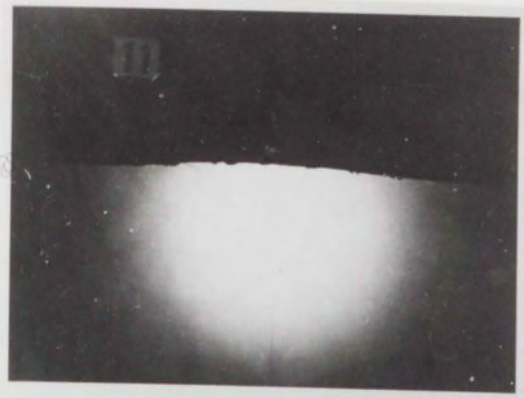

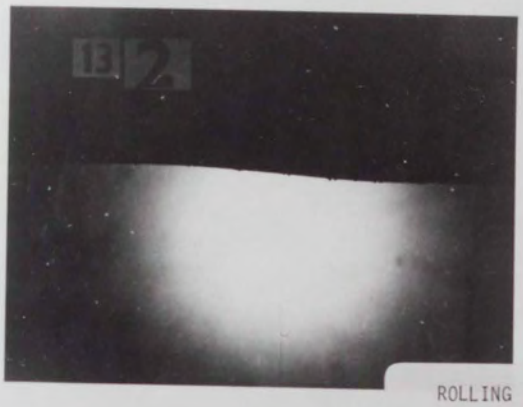

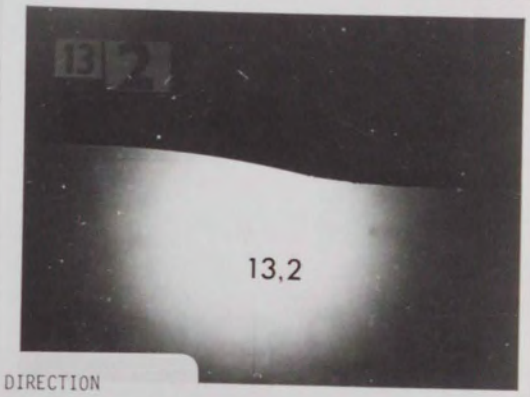

ROLLING DIRECTION
RIGHT TO LEFT

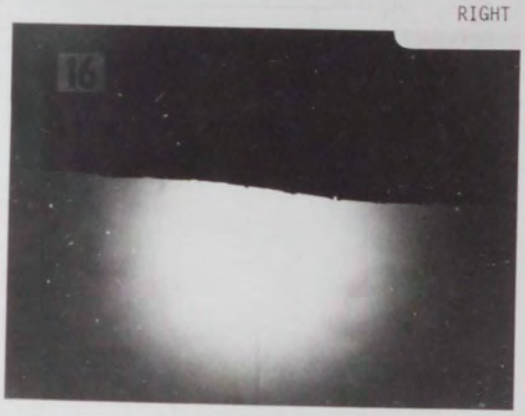

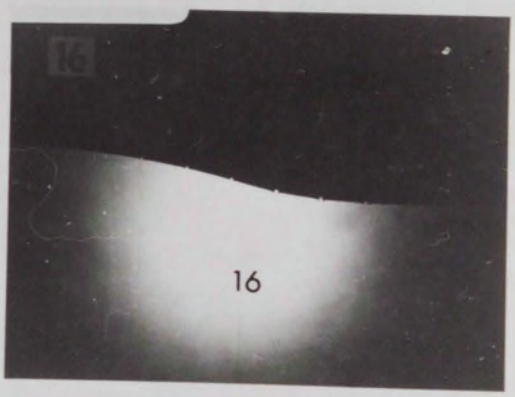

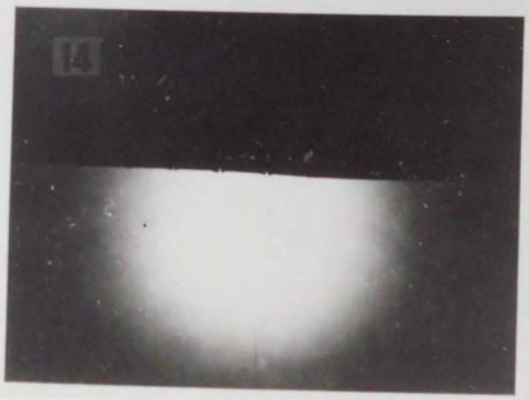

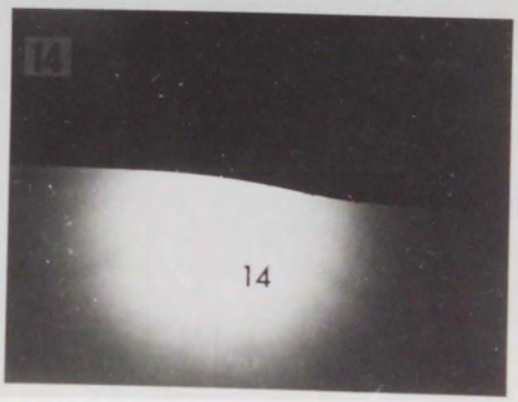

SOME EXAMPLES OF TUBE-ROLL

CONTACT AT ENTRY

Increasing reduction left to right, i e.

14 - 16 - 11 sunk,

30 - 25 - 32 - 27 - 35 mandrel rolled.

PLATE 7.2

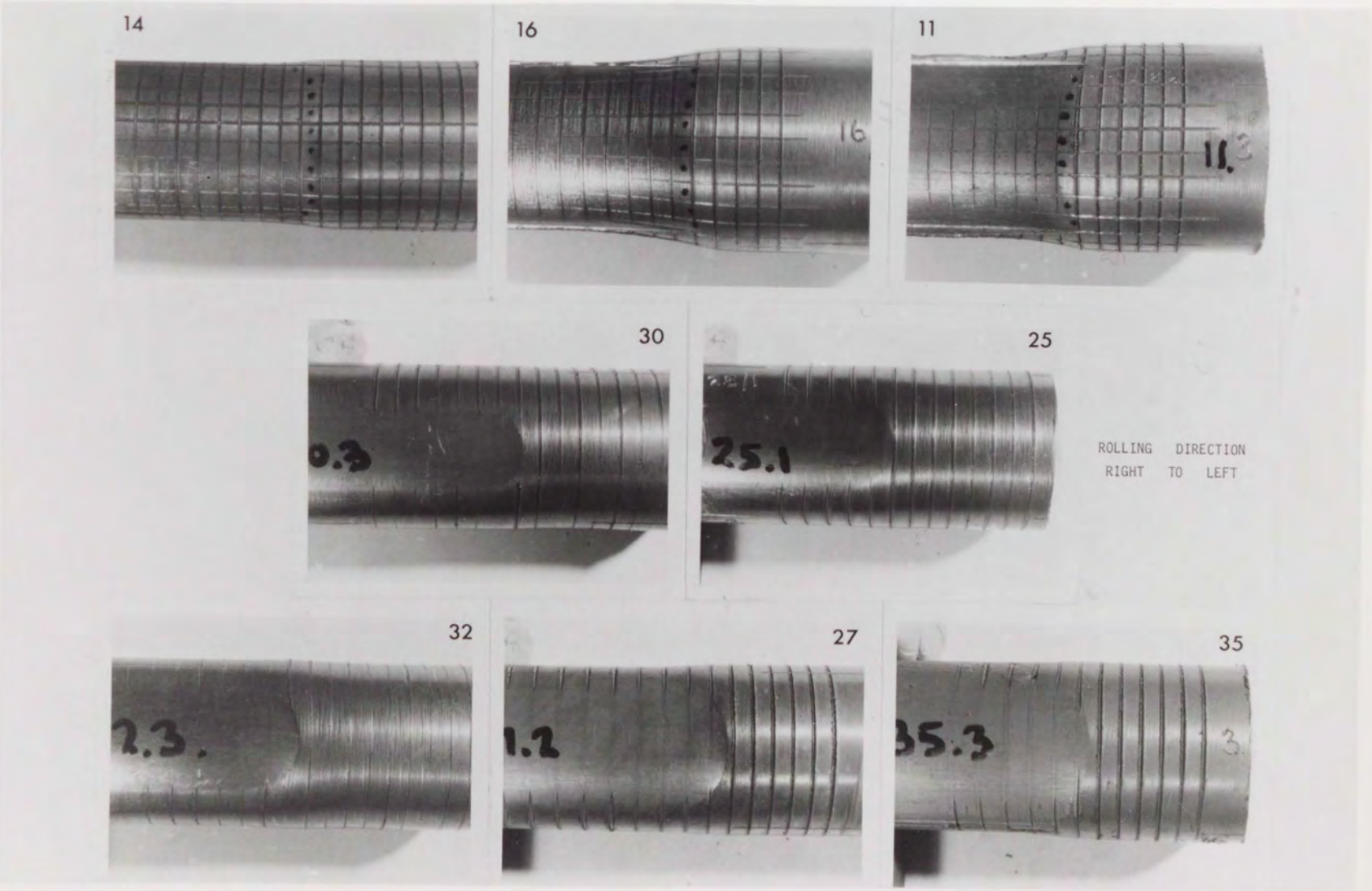
14
16
16
11
11
30
0.3
25
25.1
ROLLING DIRECTION
RIGHT TO LEFT
32
2.3.
27
1.2
35
35.3

indicated the relevant rolling condition.)

It was noted that the longitudinal strains at the shrouds are increased, particularly at high tube reductions. In some cases nascent or actual finning was detected. Almost all the specimens exhibit a consistent trend with regard to any change in this strain around the peripheral stations. However this change is small, and the net effect suggests equality of strains at the root and shroud positions; this is an indication perhaps of the relative efficiency of the three-roll process.

There is no discernible trend in the longitudinal strain pattern at the stations I, II and III.

7.2. 3. Tube Wall Thickness and Roll Peripheral Angle of Contact.

Shown in TABLE 6.1. are the tabulated tube wall thicknesses and the individual tube-roll peripheral angles of contact for the sinking condition. Forward and reversed rolled tubes are considered together with the completely rolled single pass tubes (numbers 1/1, 1/2, 1/3 and 13/1).

Apart from the smallest tube reductions all tests display the full peripheral roll contact angle of approximately 95^{o}.

The peripheral variation in the final tube wall thickness indicates little change in thickness at the roll root section for the thinner walled tube. However, the thicker walled tubes show a thinning at this position, presumably due to the tube material flowing away from this higher radially stressed region. A similar result was noted by Haleem (40) in his two-roll sinking tests. All the tubes show an appreciable thickening in the vicinity of the shrouds where the radial pressure is lowest.

In general the mean final tube wall thickness increases, except for a number of the thick walled tubes ($\frac{D}{t}$ ratio = 6.7) where overall thinning of the tube is present.

Further consideration of the tube wall thickness and the associated strains is discussed in the next section.

7.2.4 Mean Longitudinal and Thickness Strains

The variation of thickness strain with longitudinal strain for the considered tube $\frac{D}{t}$ ratios is depicted in FIGURE 7.2. All show the anticipated increase in thickness strain since the tube reduction is approximately equal to the longitudinal strain. Although there is a considerable scatter for the thick walled tubes ($\frac{D}{t}$ ratio of 6.7) a general thinning of the tube wall at low reductions is indicated. Several authors have noted this phenomenon in tube drawing without a mandrel. These

RELATIONSHIP BETWEEN

LONGITUDINAL AND THICKNESS STRAINS

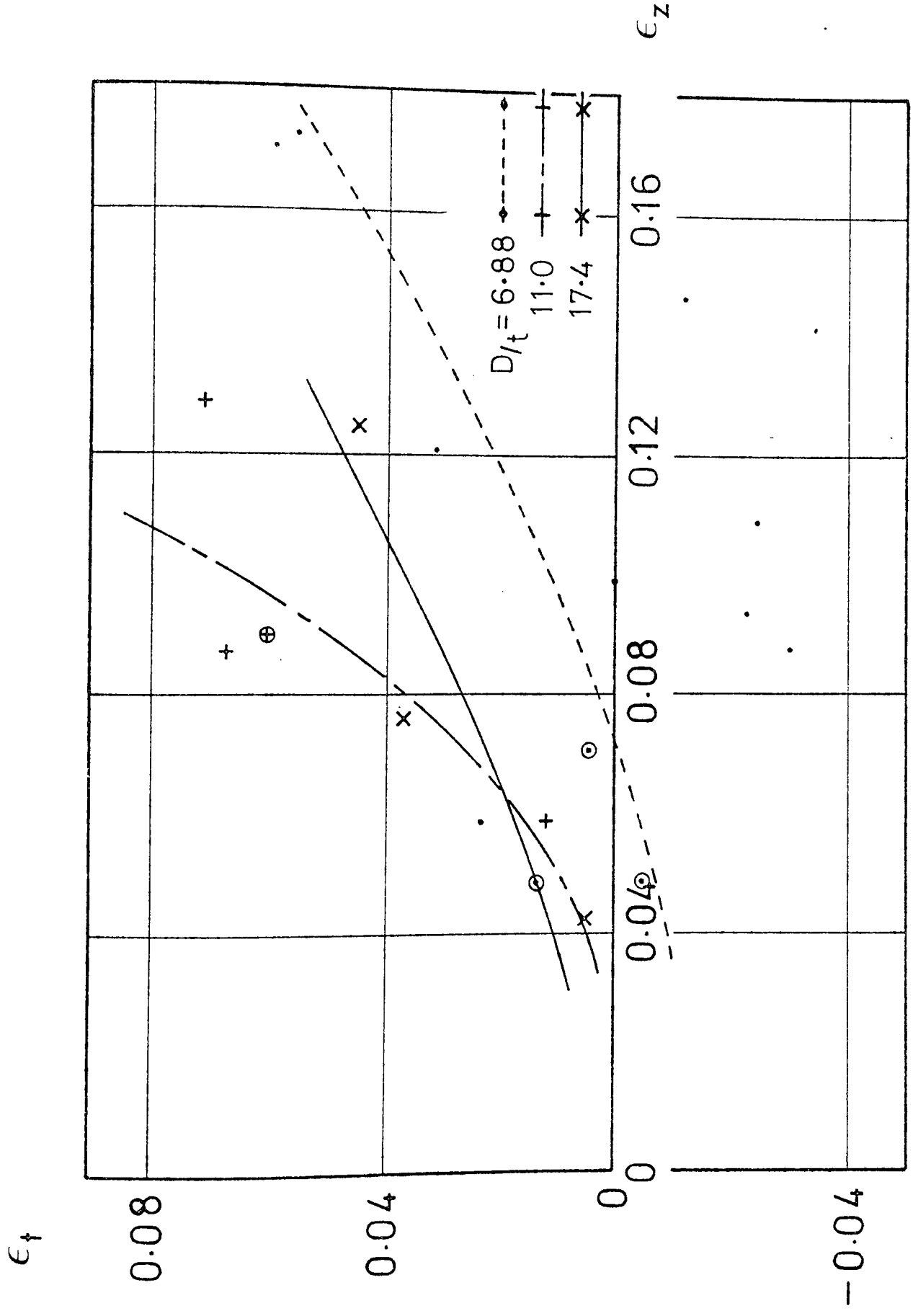

FIGURE 7.2

strain distributions suggest that at low reductions, where the thickness strains are negligible, the material flow is mainly longitudinal and circumferential.

The "ringed" results for the completely rolled single pass specimens show no significant difference from the forward-reverse roll results. This is to be expected since the homogeneous work on the tube and hence the strains can be considered as additive for the latter rolling conditions.

7.2.5. Roll Separating Force and Roll Torque

Various graphs have been constructed to demonstrate the experimental relationship obtained between roll loads, torques and tube deformation. All the graphs present the results for the forward and reverse rolling condition and where indicated "ringed" for a single complete pass. It will be remembered that the loads and torques plotted are the summed values for forward and reverse rolling.

The values of mean roll separating force against the reduction of area for the three tube $\frac{D}{t}$ ratios are shown in FIGURE 7.3, for the $\frac{D}{t}$ ratios of 11.0 and 17.4 approximate linear relationships are displayed. A curvilinear result however is indicated for the thicker walled tube i.e. $\frac{D}{t} = 6.53$. The single pass line (dotted) is also shown for this same tube $\frac{D}{t}$ ratio. Lower roll separating force values for these single passes presumably result from the absence of the additional

SINKING (170 mm ROLLS) INFLUENCE OF TUBE PARAMETERS ON MEAN R.S.F.

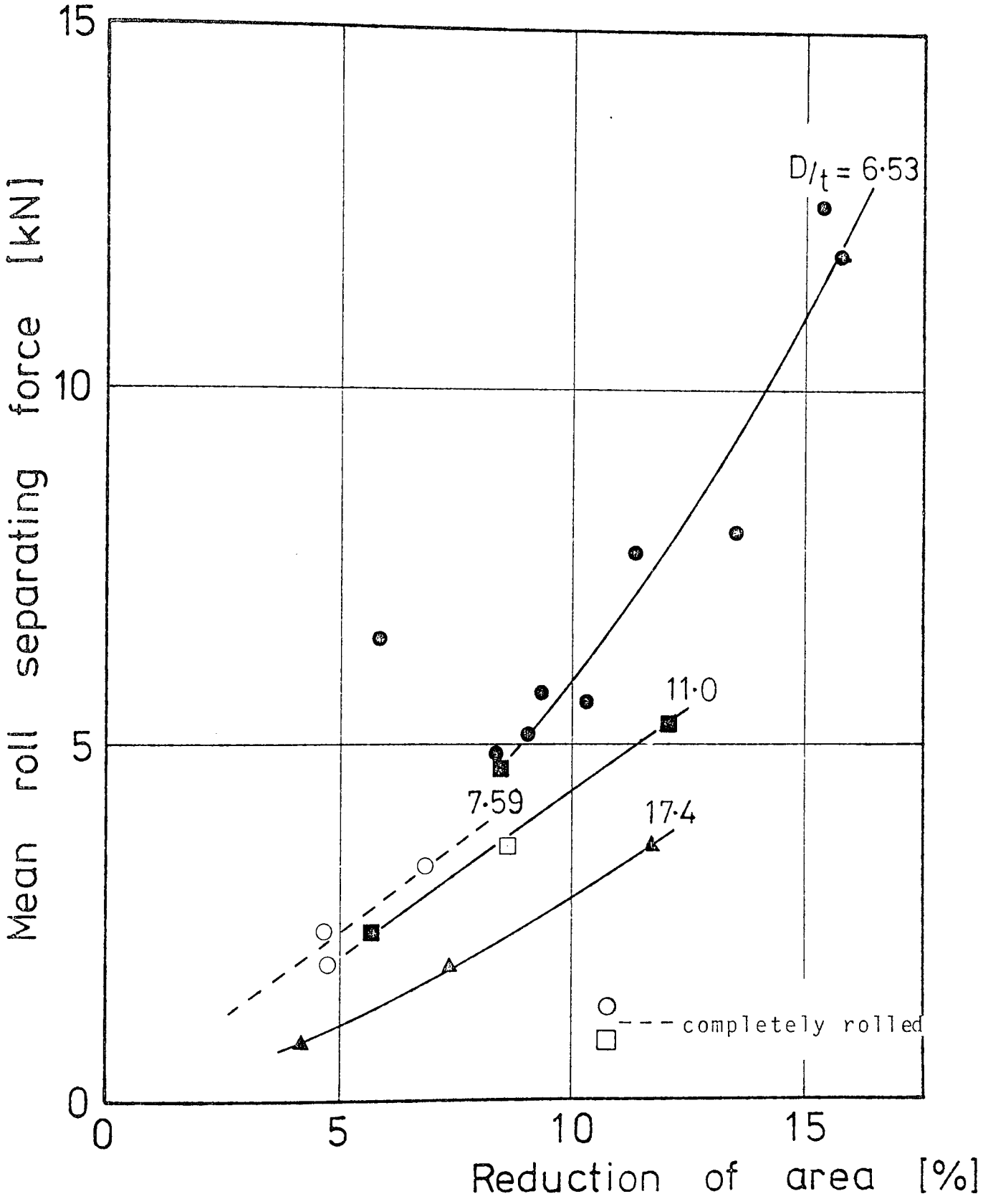

FIGURE 7.3

redundancy incurred in the reverse rolling process.

Linearity for these relationships has been confirmed by the results of Cole (35) and Haleem (40) for the two-roll arrangement. This linearity was anticipated since the tube reduction is approximately equal to the tube roll contact area, which itself is proportional to the roll separating force, assuming, for similar conditions, a constant mean roll pressure.

The total roll torque is a measure of the total external work done by the rolls on the tube and FIGURE 7.4, shows this plotted against the tube reduction of area for various tube $\frac{D}{t}$ ratios. Again an approximately linear relationship is observed, especially for the thinner tubes. This result was to be expected since the roll torque is approximately proportional to the square of the roll contact area, which is proportional to the tube reduction. Compared with the corresponding roll force graphs, the roll torque relationships appear to be a function of the tube reduction rather than tube $\frac{D}{t}$ ratio, i.e. the torque is influenced more by the tube-roll contact area than by the tube thickness; this indicates the greater influence of friction on the torque results. This behaviour was also observed, to a lesser degree, by the relevant experimental results of Haleem (40).

Finally, assuming that there is constancy of contact friction conditions, and great care was taken to maintain

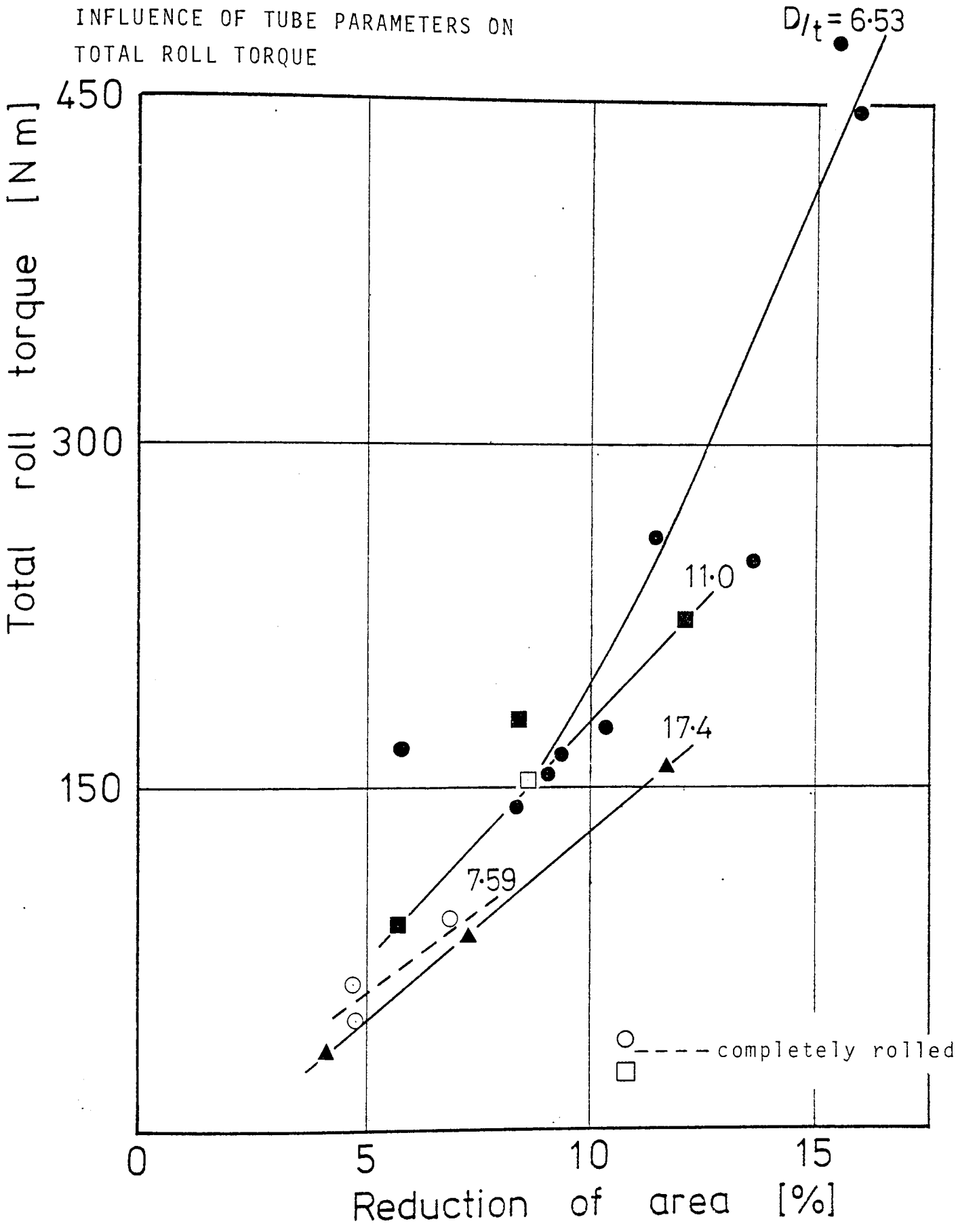
SINKING (170 mm ROLLS)
INFLUENCE OF TUBE PARAMETERS ON
TOTAL ROLL TORQUE
$D/t = 6{\cdot}53$
11·0
17·4
7·59
completely rolled
Total roll torque [N m]
450
300
150
0
5
10
15
Reduction of area [%]

FIGURE 7.4

this, the mean roll torque will be directly proportional to the mean roll separating force. FIGURE 7.5, shows this agreement, particularly for the thinner tubes, confirming in general the reliability of the load and torque cells.

7.3. SINKING, EXPERIMENTAL - THEORETICAL COMPARISONS

The lack of roll-groove pin load cells in this investigation has prevented a comprehensive assessment of the roll groove pressure distribution. Consequently no information was available relevant to the arcs of contact around the groove from which the tube-roll contact area can be deduced. This resulted in recourse having to be made tc part-rolled specimens and experimental pin loadcell evidence from other workers employing two-roll configurations.

The forward and reverse rolling tests yielded acceptable results with respect to the homogeneous deformation and hence the associated strain distributions. However these roll force and torque results should be treated with caution when considering the redundancy contribution.

7.3.1. Tube-Roll Arc of Contact

The comparison between the measured and calculated maximum tube-roll root contact angles at various tube reductions and specified tube $\frac{D}{t}$ ratios is shown in

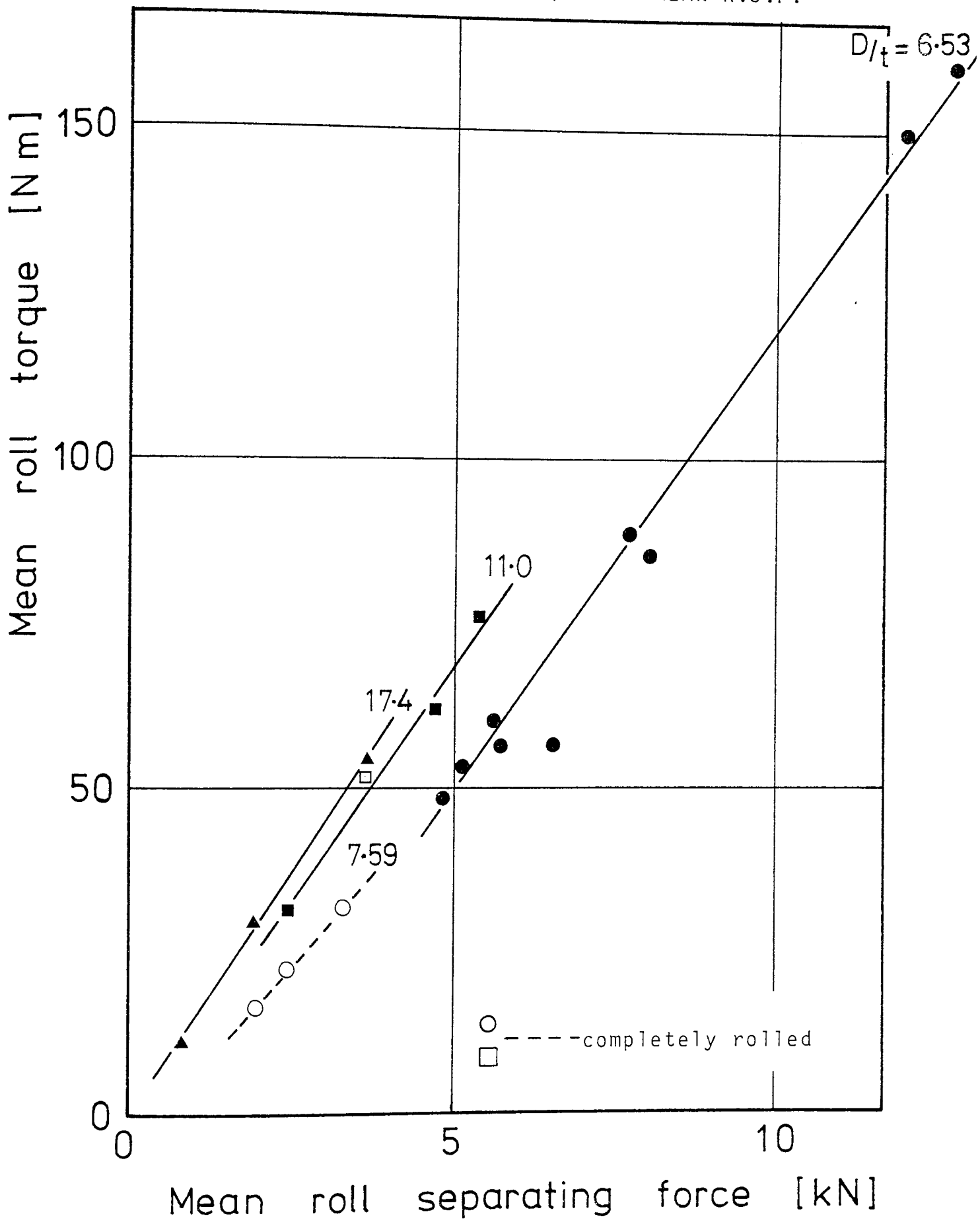
RELATIONSHIP BETWEEN MEAN ROLL TORQUE AND MEAN R.S.F.
Mean roll torque [N m]
Mean roll separating force [kN]
0
50
100
150
5
10
D/t = 6·53
11·0
17·4
7·59
completely rolled

FIGURE 7.5

FIGURE 7.6. They show an acceptable correlation, particularly for the thicker tubes and all indicate a measured value higher than the calculated value. A possible explanation for this effect is that further instantaneous static radial compression of the deformed tube occurs at the changeover from forward to reverse rolling.

The expression for calculating the tube-roll root contact angle is given in Appendix G.1.

7.3.2. Theoretical Sinking Pressure.

Compared with the completely rolled single pass specimens, additional frictional and redundant work is implied by the forward and reverse sinking tests. The additional frictional contribution is unlikely to be significant for reverse rolling. This, as previously argued is because after forward rolling, the tube now approximately rolled to the contour of the three-roll groove gap, will experience a small relative velocity vector at the tube-roll-interface. However, for the thicker walled tubes i.e. for the low tube $\frac{D}{t}$ ratios, the additional redundancy generated by the reverse rolling condition should make a modest work contribution. It should be noted that the redundancy contribution arises from bending and not from shear, which was shown by Haleem (40) to be negligible.

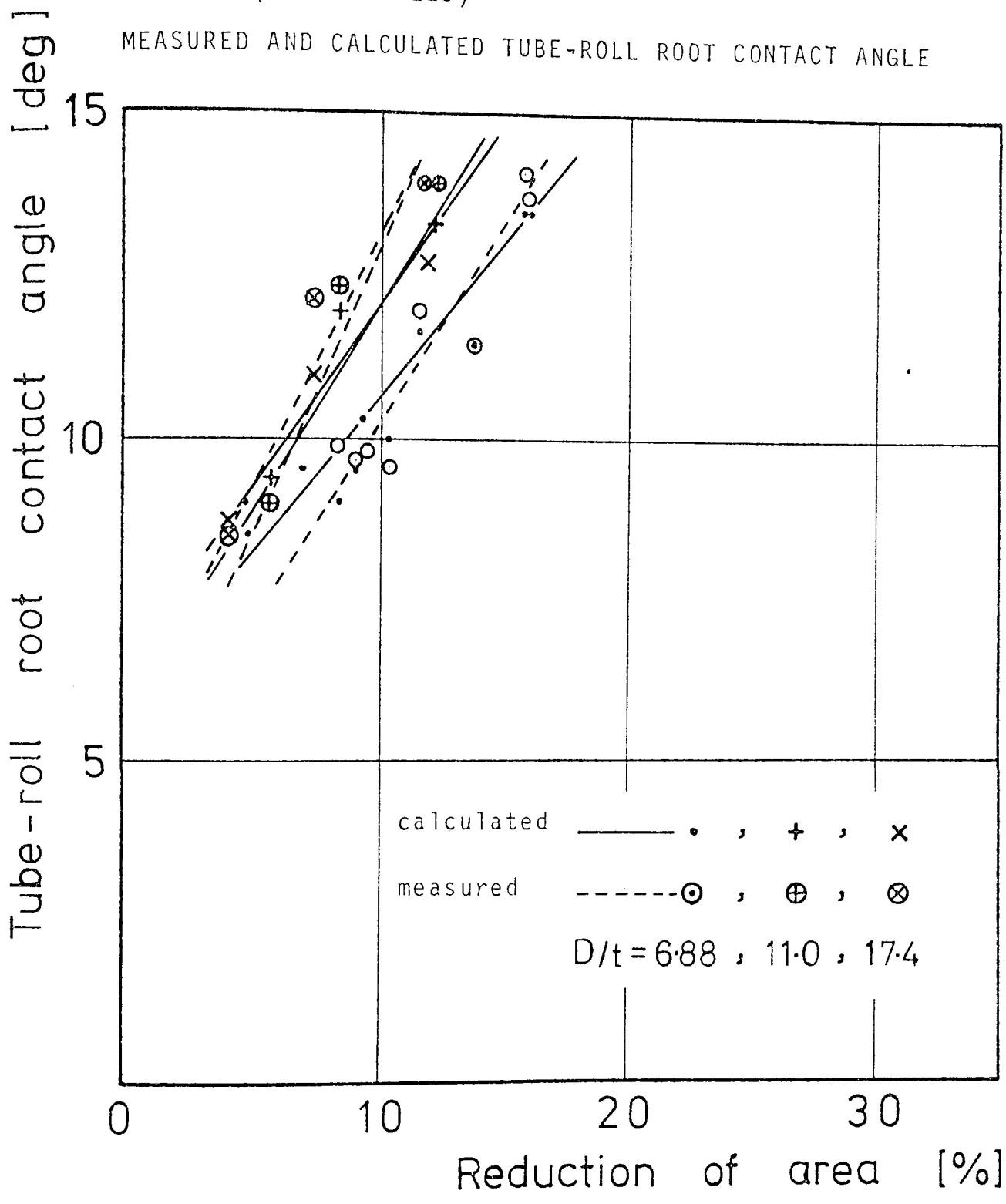
SINKING (170 mm ROLLS)
MEASURED AND CALCULATED TUBE-ROLL ROOT CONTACT ANGLE
Tube-roll root contact angle [deg]
15
10
5
0
10
20
30
Reduction of area [%]
calculated
measured
D/t = 6·88 , 11·0 , 17·4

FIGURE 7.6

Equilibrium (theoretical sinking pressure)

Since the equilibrium theory ignores circumferential friction only the stress situation in the tube at the root of the groove can be considered. This situation is acceptable provided it can be demonstrated that the pressure at the roll groove root is representative of the mean.

Haleem (40) utilising pin load cells in the groove of the upper roll showed that the maximum roll pressure existed at a groove angle, measured from the root, in the region of 45^{o} to 65^{o}. Furthermore, he noted that the mean roll pressure occurred at a groove angle of between 25^{o} and 40^{o}. FIGURE 7.7., illustrates a typical distribution map of roll pressure variation around the roll groove for various tube $\frac{D}{t}$ ratios as measured by Haleem (40). Since his two-roll groove profile and tube rolling conditions i.e. reducing round to oval tube, were similar to the current three-roll investigation, it can be surmised that the theoretical roll root pressure is likely to underestimate the mean.

Energy, (theoretical sinking pressure).

This approach estimates the mean roll pressure for a specific tube reduction. Hence no prior assumptions are required of either the circumferential or the longitudinal roll groove pressure distribution.

SINKING

DISTRIBUTION OF THE ROLL PRESSURE ROUND THE GROOVE - Haleem (40)

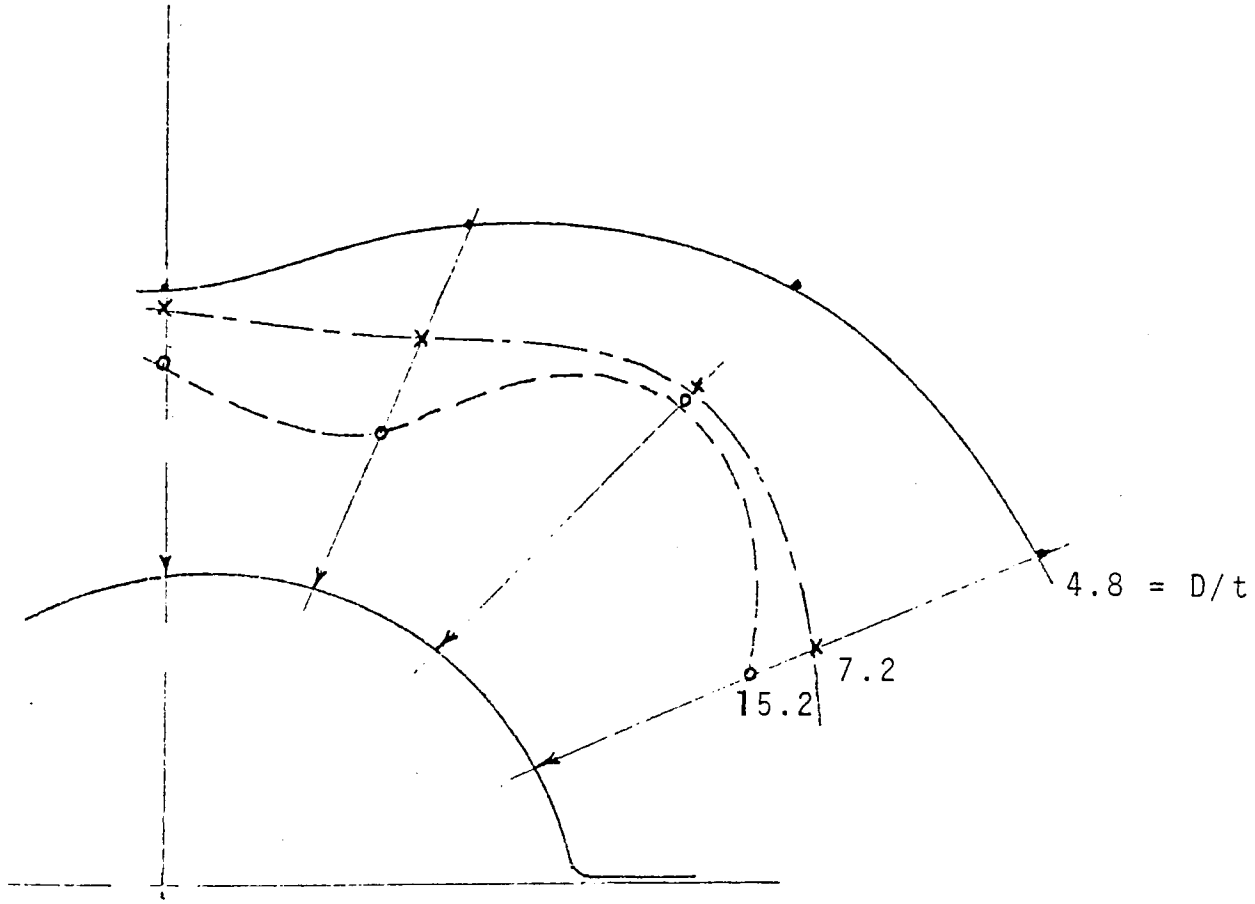

FIGURE 7.7

However this method does require a detailed knowledge of the relevant tube surface deformation zones, and, without the assistance of pin load cells only tentative deformation models can be assumed; these were discussed in Chapter 3.

In the assessment of the mean roll pressure, both theoretical analyses consider the extreme values of the shear friction factor m, that is, m = 0 and m = 1. As Haleem noted that m = 0.75 gave the best correlation, then for simplicity m was taken as unity i.e. full sticking conditions, for both the equilibrium and energy roll pressure analysis. These are displayed in FIGURE 7.8., together with Haleem's experimental results. Compared with his results the energy analysis appears to give better values at the higher tube reductions, suggesting that of the assumed deformation models, FIGURE 3.21.b is better than FIGURE 3.21a. Model FIGURE 3.21.a is applicable to near zero tube reduction, and is not really covered by the present sinking tests where around 4.5% was the minimum tube reduction.

The worked examples indicated in Appendix H.1 and 2, also suggests that the frictional contribution is relatively high for small reductions of area and thin tubes. This former condition is demonstrated in the final stands of a production tube rolling mill where the associated light reductions would require primarily a frictional roll

SINKING (170 mm ROLLS)

COMPARISON OF THEORETICAL ROLL PRESSURE WITH HALEEM'S EXPERIMENTAL VALUES

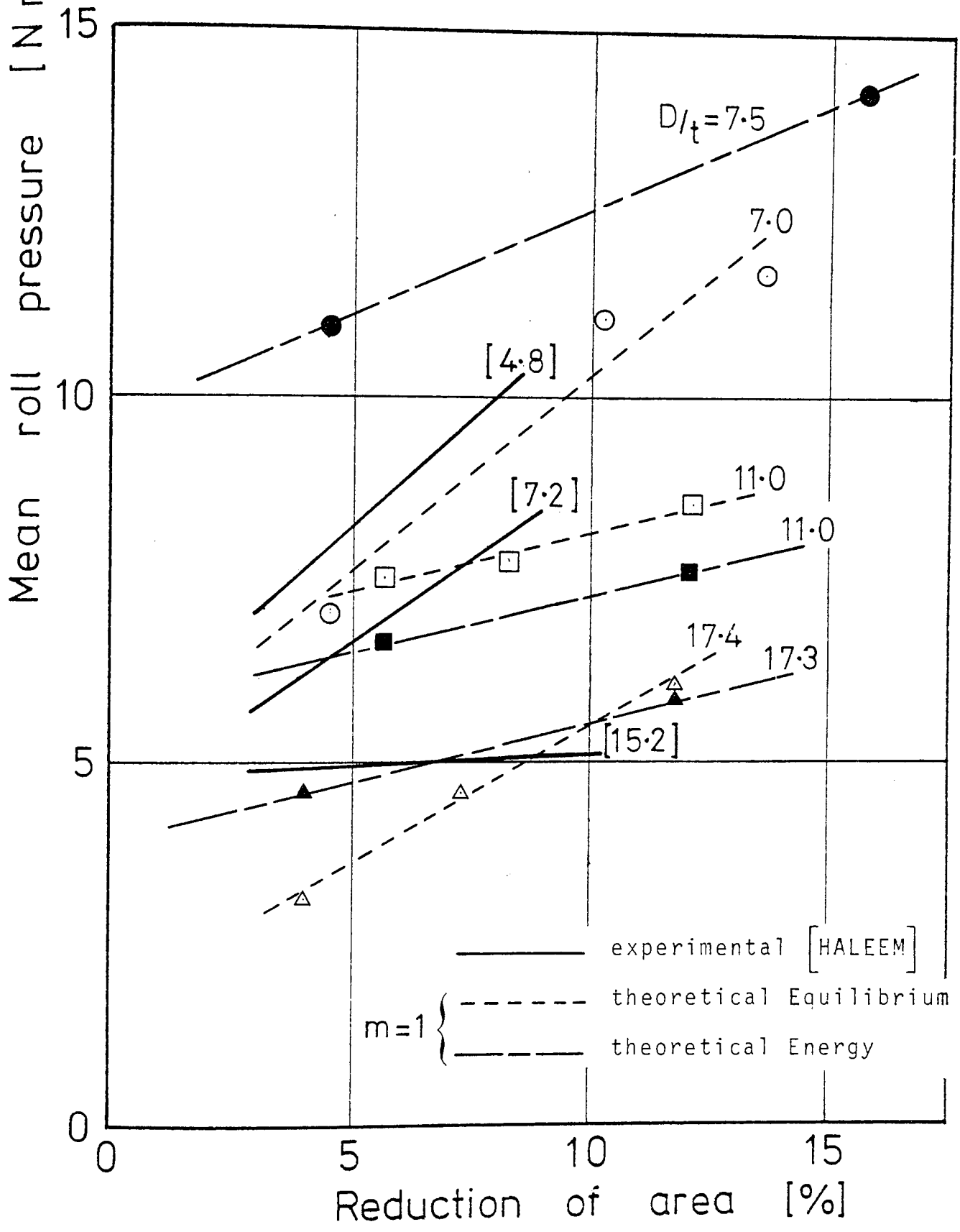

FIGURE 7.8

pressure.

All the sinking roll pressure results derived from both theoretical approaches are listed in the Appendix, TABLE H.1.

These theoretical sinking analyses, as discussed in Chapter 3, imply that the friction contribution occurs approximately in the latter half of the overall tube reduction process where the tube-roll contact is assumed present. This suggests that the friction assessment is likely to be an underestimate.

7.3.3. Theoretical Sinking Roll Separating Force and Torque

A further factor to note, is that the tube surface deformation models, FIGURE 3.21.a and 21.b, are only relevant to their associated tube reductions of nearly 0%, and 12%. In other words, it is only the tube specimens with these corresponding reduction figures that can be analysed sensibly. Consequently, this places a restriction on the number of specimens that can be considered for comparison purposes.

Since the calculated tube-roll contact area is directly deduced from the calculated maximum contact angle, the theoretical roll separating force graphs would be expected to show the same pattern as those for the theoretical mean roll pressure FIGURE 7.8., where full sticking friction was assumed i.e. m = 1. The graphs of FIGURE 7. 9, 10, and 11., of the theoretical roll separating force against reduction of tube area for the stated tube $\frac{D}{t}$ ratios and m = 0 and 1 confirm this behaviour. Furthermore, the theoretical and experimental assessments of the roll separating force show better comparisons for the full sticking friction case, and, where applicable, for the completely rolled single pass results.

In most series of tests only three tube specimens were rolled, consequently it would appear logical to pay

SINKING (170 mm ROLLS)

COMPARISON OF EXPERIMENTAL AND THEORETICAL R.S.F.

FOR TUBE D/t RATIO OF 7.06

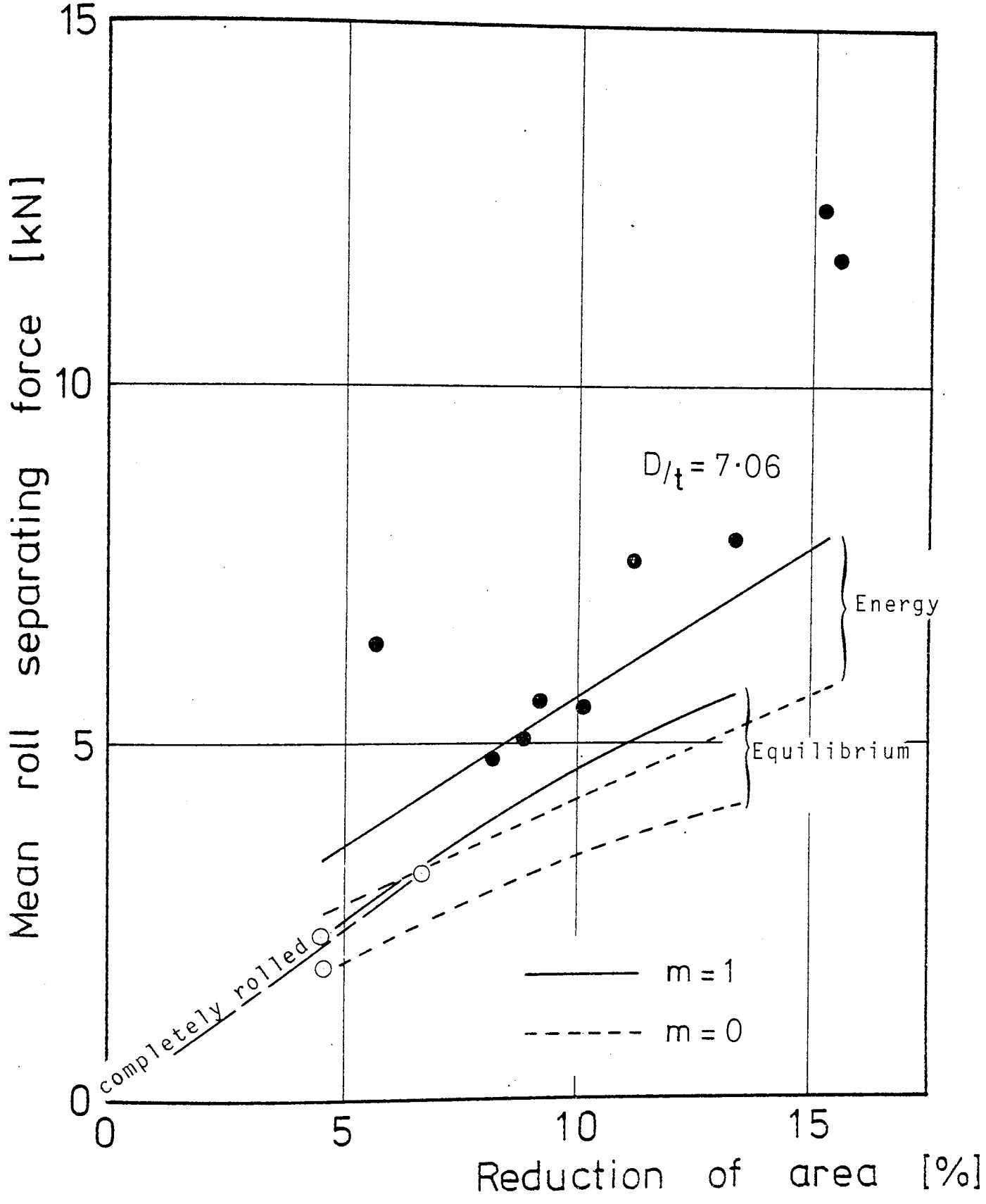

FIGURE 7.9

SINKING (170 mm ROLLS)

COMPARISON OF EXPERIMENTAL AND THEORETICAL R.S.F.

FOR TUBE D/t RATIO OF 11.0

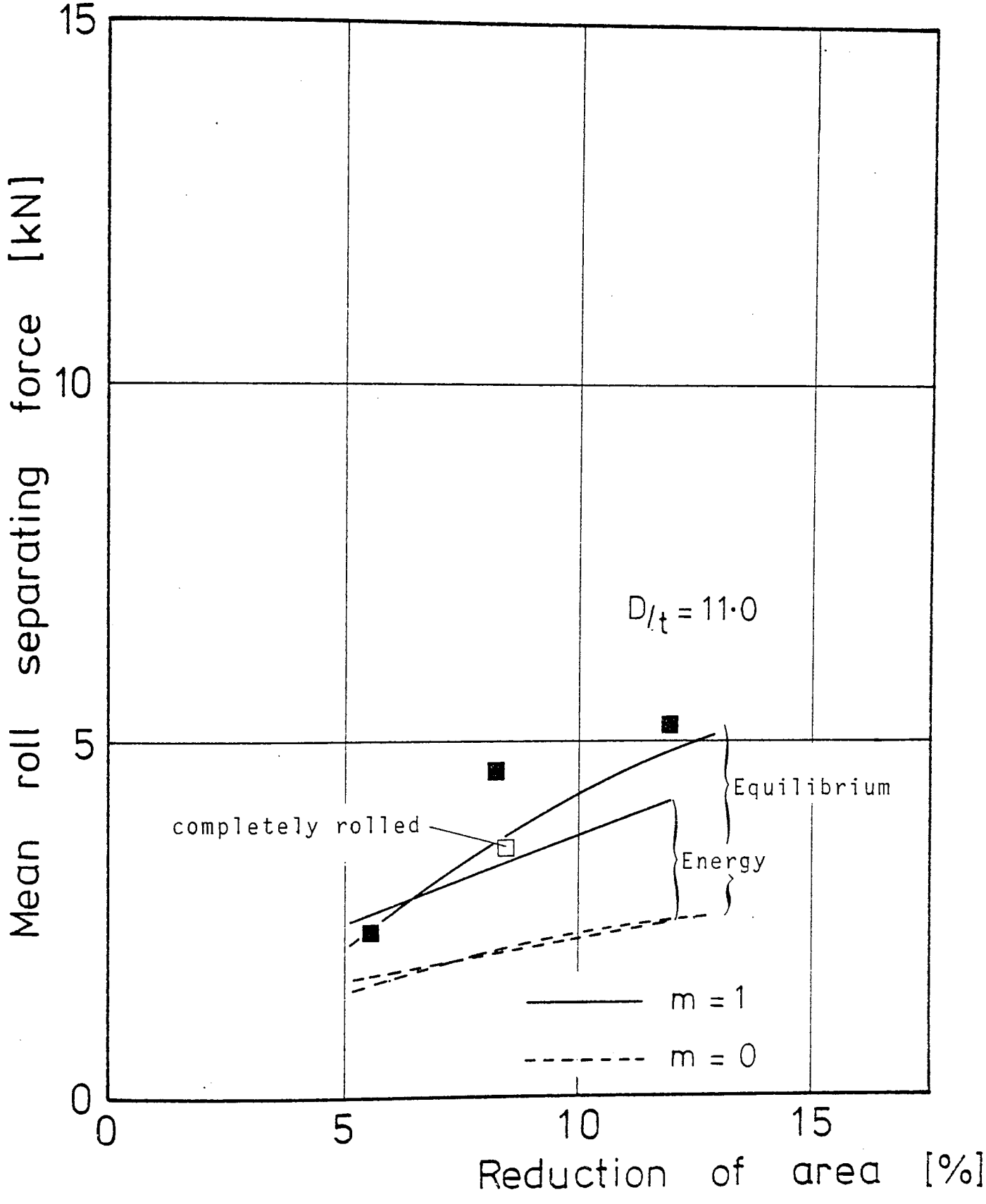

FIGURE 7.10

SINKING (170 mm ROLLS)

COMPARISON OF EXPERIMENTAL AND THEORETICAL R.S.F.

FOR TUBE D/t RATIO OF 17.4

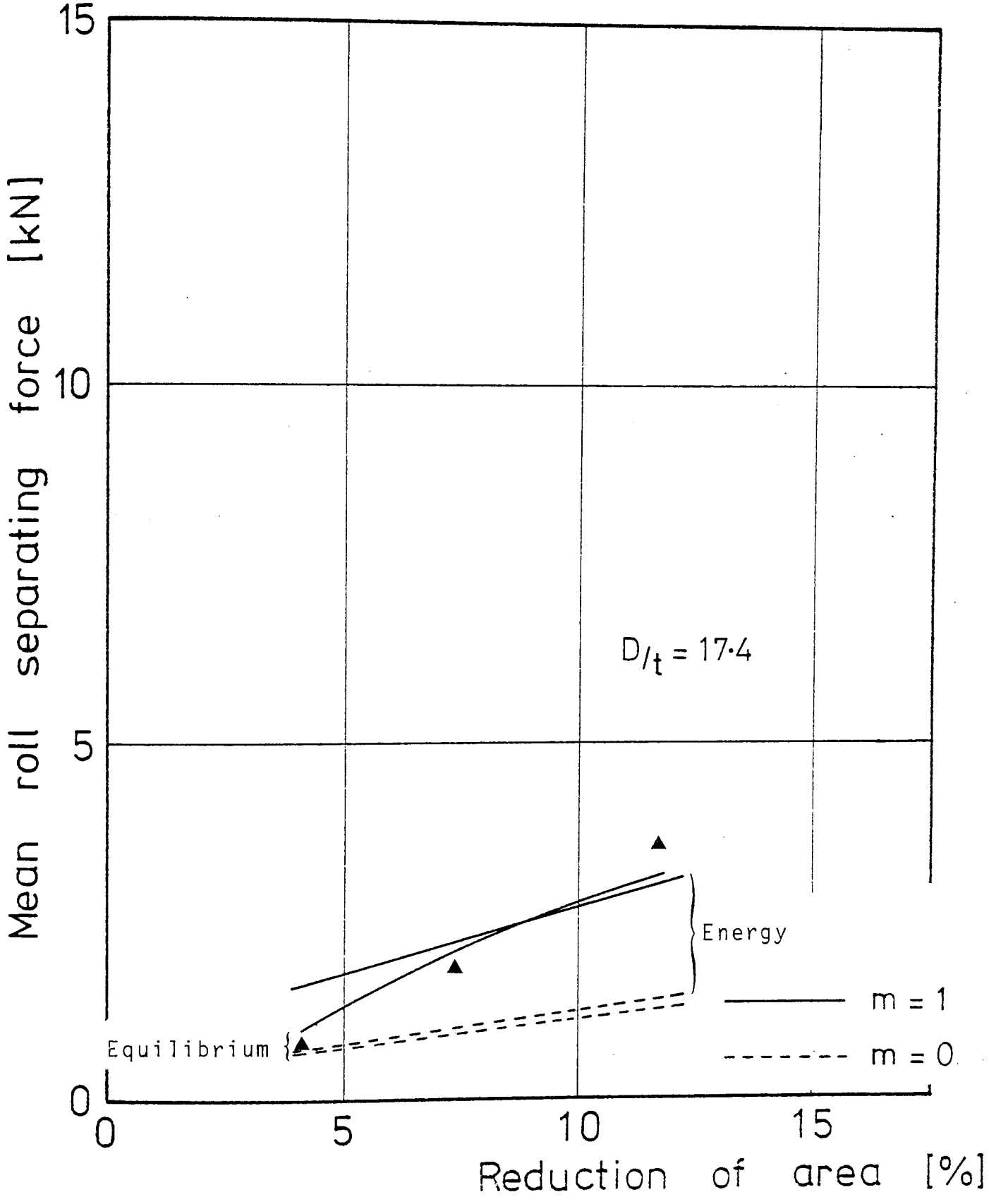

FIGURE 7.11

more attention to those tube $\frac{D}{t}$ ratios where a large number of tests was considered. Such a test series was conducted for the tube $\frac{D}{t}$ ratio of 6.88, (see FIGURE 7.9), where twelve specimens were rolled. These clearly show the underestimation of the equilibrium theory, which was implied in section 7.3.1. where the mean roll pressure was taken at the roll groove root. Also apparent is the improved correlation shown by the energy approach, which also hints at an optimum friction factor of about 0.75. As noted previously, a value of m = 0.75 was suggested by Haleem (40). These series of tests show a little more clearly the better correlation displayed by the three single pass rolled results.

In comparing the theoretical-experimental roll separating force, reference should be made to the assumed free-contact deformation model (page -127-) and the associated tube-roll contact angles. As already discussed these assumptions generally suggest an underestimation of the actual tube-roll contact areas and consequently of the theoretical roll separating force.

Since no direct measurements of the tube-roll arc lengths were available, it was felt inappropriate to assess theoretically the roll torque from the roll

separating force, using the concept of the roll moment or lever arm. Rather, noting the linearity relationships between the roll separating force and torque, as shown in FIGURE 7.5., it was decided to deduce the roll torque from the corresponding constant of proportionality.

It can be shown however that this direct proportionality does not exist for the partially rolled tubes of $\frac{D}{t}$ ratio 6.53. As observed in section 7.1.1. this is probably due to the greater effect of the forward and reverse rolling process on the thicker tube specimens.

The product of the derived equilibrium or energy mean roll pressure and the horizontal projected area of contact gives the roll separating force and these are presented in the Appendix, TABLE H.2.

7.4. MANDREL ROLLING, EXPERIMENTAL

7.4.1. Roll-Tube Contact Area

The shadowgraph profiles shown in PLATE 7.3 illustrate the root and shroud contact regions of the mandrel rolled tubes for various tube reductions and $\frac{D}{t}$ ratios. Since minimal circumferential strain is experienced in this process, these profiles, when compared with those for sinking, show the anticipated reduced roll contact arc and area. The photographic evidence in PLATE 7.3. also suggests some piling up of the tube at entry to the groove root. This implied increase in the tube-roll contact arc and contact area was also noted by Labib (43).

PLATE 7.2 Tube Numbers 30 to 25; 32 to 27; and 35: shows a selection of tube-roll contact areas for an increase in tube reduction from left to right. As a first approximation the theoretical assumption of a semi-ellipitical contact area appears to be acceptable. Similar photographic evidence was observed by Labib (43).

7.4.2. Surface Longitudinal Strain

Greater roll pressures is associated with the mandrel rolled specimens. This results in a tendency for the peripheral grid lines to be obliterated at the groove

SOME MANDREL ROLLED TUBE PROFILES x10

(LONGITUDINAL)

Tube $\frac{D}{t}$ ratio increasing from top to bottom.

Roll shroud contact on left.

Roll root contact on right.

PLATE 7.3

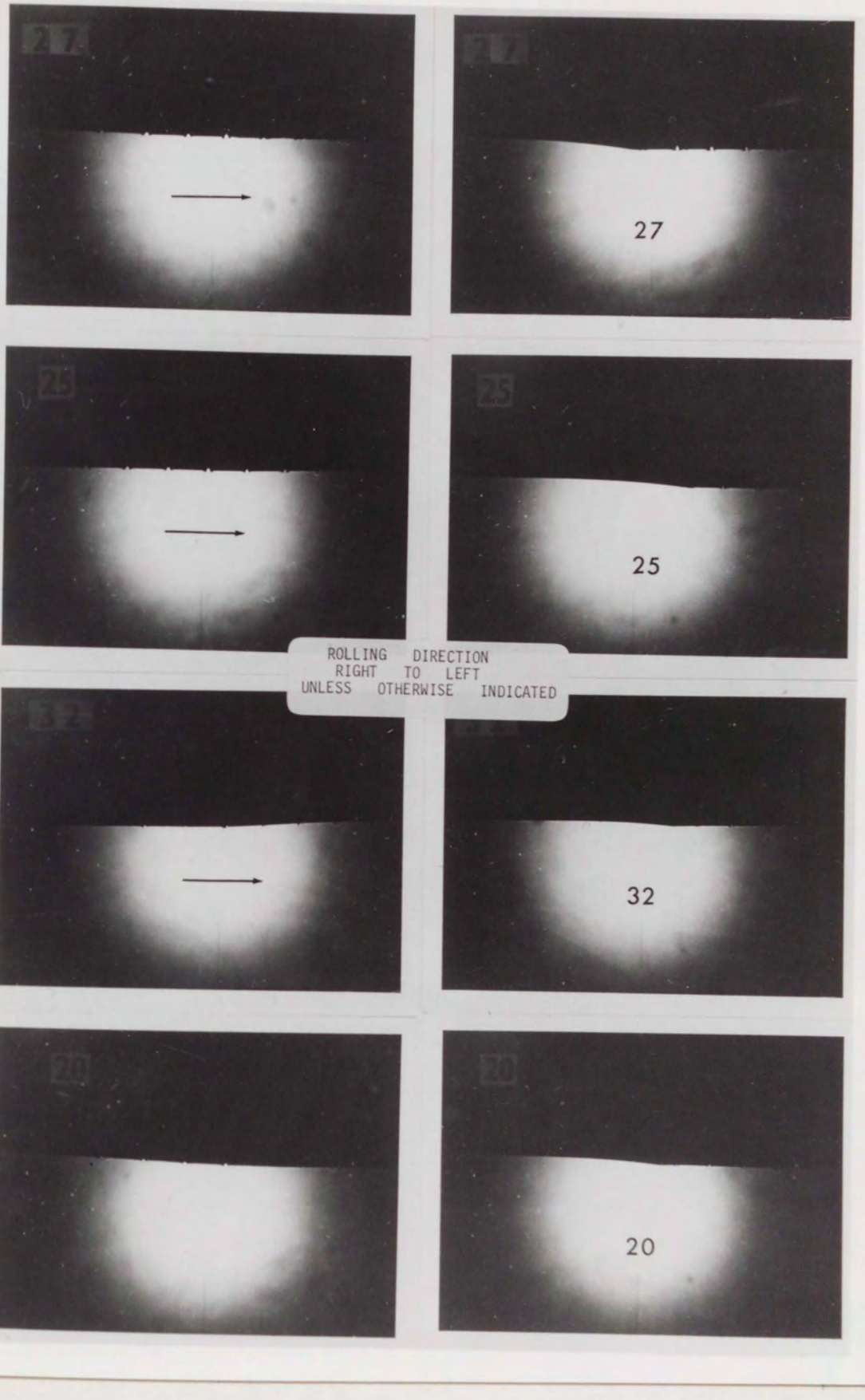
27
25
ROLLING DIRECTION
RIGHT TO LEFT
UNLESS OTHERWISE INDICATED
32
20

root region. Consequently these surface strains, shown in TABLE 6.6, should be treated with caution.

As for sinking there is no definite trend in the peripheral variation of the surface longitudinal strain for either dry or lubricated mandrel conditions. In general, the surface strains are greater than the mean, demonstrating a greater shear redundancy at the tube surface.

7.4.3. Tube Wall Thickness and Tube-Roll Peripheral Angle of Contact

As a result of the irregular contour of the mandrel rolled tube cross-section profiles, (see PLATE 7.4 lower two rows) an accurate, direct measurement of the mean final tube wall thickness was not possible. Furthermore, this problem was compounded by the high tube $\frac{D}{t}$ ratios employed in the mandrel rolling process having relatively thin final tube root wall thicknesses of from 0.76 mm to 2.90 mm. Consequently, this thickness had to be deduced indirectly from a knowledge of the mean tube diameter and the previously determined tube cross-sectional area at exit. Since some measurement errors were present, these inconsistencies were reduced graphically by constructing the 'best' straight lines. A better set of final mean tube wall thicknesses were obtained and are shown in TABLE 6.4.

SOME ROLLED TUBE CROSS-SECTIONS

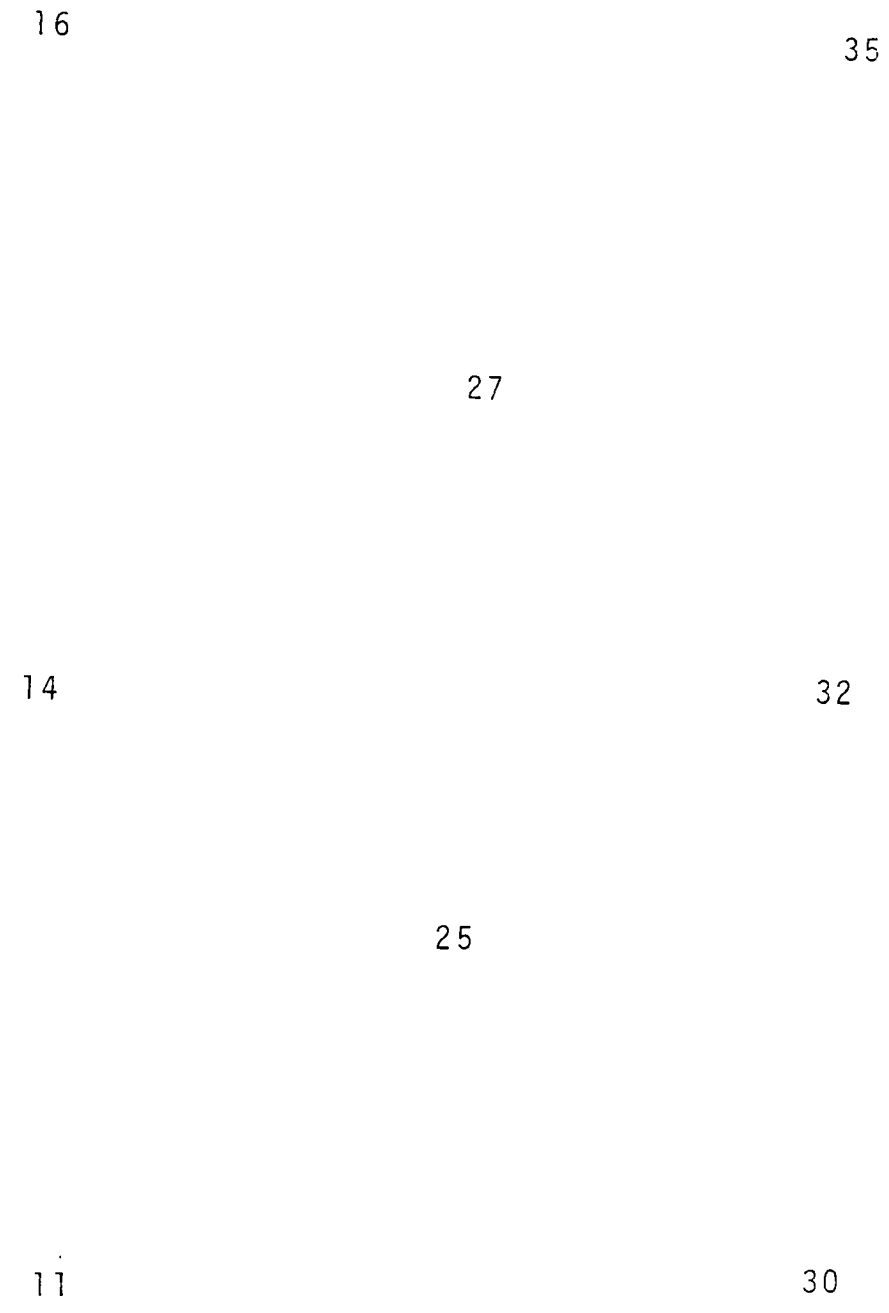

PLATE 7.4

With reference to FIGURE 3. 23 it can be seen that in the mandrel rolling process there are peripheral tube wall elements, which, whilst still remaining in contact with the rolls, no longer have contact with the mandrel. The measured final mean tube thicknesses in these regions ($t_{\theta\ -\gamma}$) are listed in TABLE 6.4., and very approximately equals the original tube wall thickness. This minimal thickness change, together with contact taking place only at the roll surface, suggests a sinking operation, with a consequential reduction in the roll pressure.

Shown in TABLE 6.2 are the final peripheral angles of contact per roll, for the tube-roll and tube-mandrel. Because of the imprecise nature of the extent of the peripheral roll contact on the tube, only the tube-mandrel contact angles (γ_c) were accurately measured.

Examination of the tube-mandrel contact angles (γ_c) for the dry and lubricated mandrel cases suggests a slight increase in γ_c for the dry mandrel rolled specimen. This result probably arises from the tube deformation, in this latter case, being restricted more longitudinally than circumferentially. This behaviour was also noted by Labib (43).

Comparisons of the final tube wall thickness indicate that for both dry and lubricated mandrel rolling the shroud contact wall thickness is closer to the mean for

thin tubes. Conversely for thick tubes it is the root section wall thickness which is nearer the mean. This result was expected, noting the increasing peripheral contact angle (θ and γ) for the lower tube $\frac{D}{t}$ ratios.

7.4.4. Mean Longitudinal and Thickness Strains

The previous section (7.4.3) discussed how the best straight line technique was employed to reduce these thickness irregularities to give a 'smoothed' final tube wall thickness. From a knowledge of this thickness the 'smoothed' thickness strains were determined. It is these thickness strains and the mean longitudinal strains which are shown in FIGURE 7.12 for mandrel rolling, dry and lubricated, and for the indicated tube $\frac{D}{t}$ ratios. All graphs show, in general, a numerical equality of longitudinal and thickness strains, implying negligible circumferential strain; this was an expected feature and it has been recognized also in the mandrel tube drawing process. These graphs also indicate that the longitudinal strains for the specimens rolled on a lubricated mandrel are somewhat greater than for the dry mandrel examples. The converse is obviously true for the thickness strains. As commented previously this result was anticipated, with higher tube reductions, and hence longitudinal strains being achieved with the mandrel lubricated.

MANDREL ROLLING (170 mm ROLLS)

RELATIONSHIP BETWEEN LONGITUDINAL

AND THICKNESS STRAINS

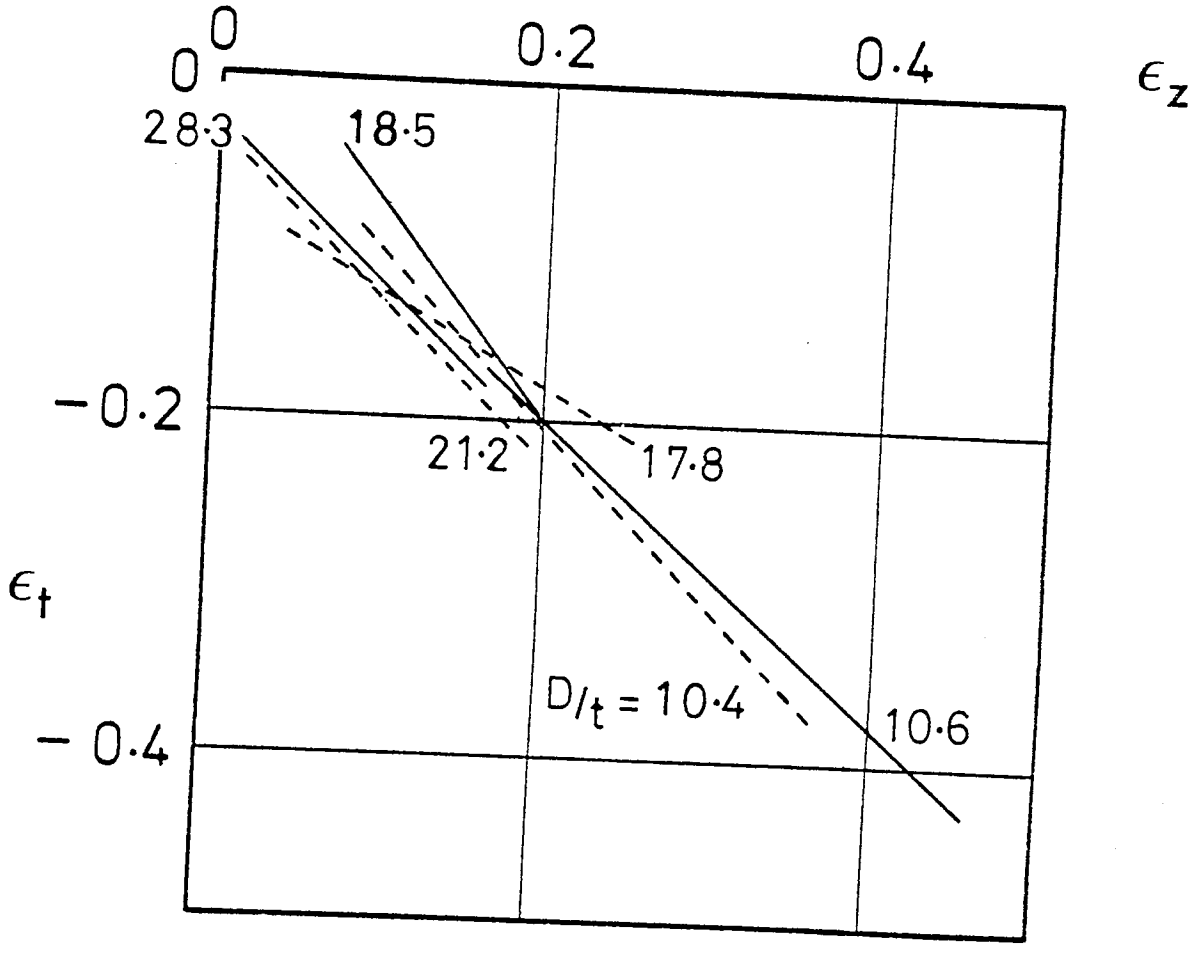

FIGURE 7.12

7.4.5. Roll Separating Force and Roll Torque

In order to assess the quality of the experimental mandrel rolling results, the mean roll separating force was plotted against the change in tube thickness at the roll groove root. For each tube $\frac{D}{t}$ ratio this linear relationship is shown in FIGURE 7.13 where lines of increasing slope with increase in the tube $\frac{D}{t}$ ratio differentiates the better from the poorer quality results.

The influence of changing the tube $\frac{D}{t}$ ratio on the mean roll separating force and tube reduction can be seen in FIGURE 7.14. Increasing the tube reduction of area was achieved by increasing the diameter of the tube specimen, thereby increasing the contact angle and area between tube and roll and between tube and mandrel. Furthermore, the shear redundant work, although small, increases with increasing contact angle. Consequently the resultant effect is one of increasing roll separating force with increasing reduction of area. For the same reduction of area, the mean roll separating force becomes greater for increasing tube $\frac{D}{t}$ ratios. This is due to the increase in the proportion of the frictional to the total work required in mandrel rolling. In other words, for high tube $\frac{D}{t}$ ratios "thin strip" was being rolled.

The influence of lower tube $\frac{D}{t}$ ratios on moderating the roll separating force is the principal reason why most

MANDREL ROLLING (170 mm ROLLS)

INFLUENCE OF "ROOT" TUBE WALL THICKNESS CHANGE ON MEAN R.S.F.

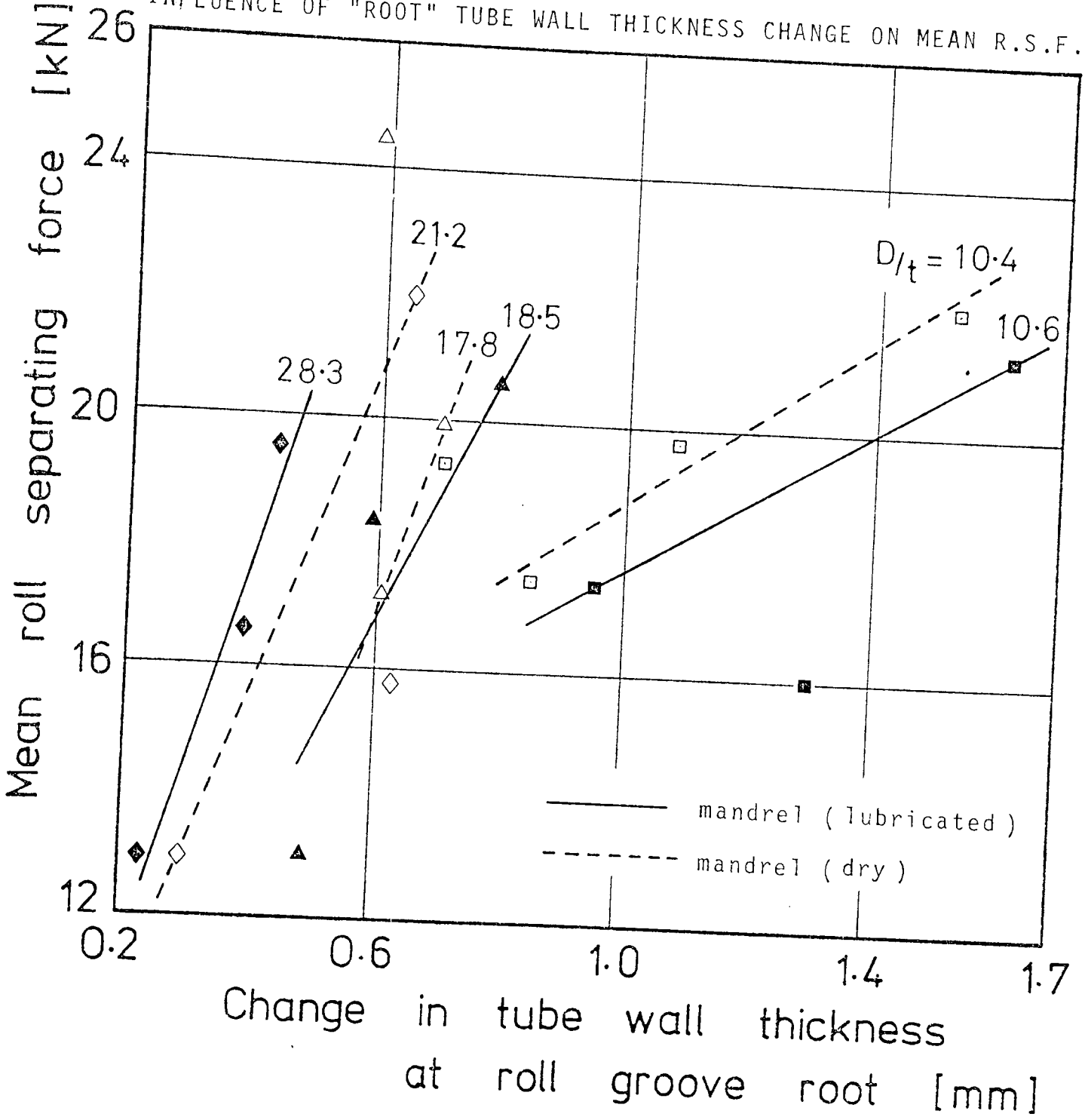

Notation:

D/t = 28·3 (◆), 21·2 (◇), 18·5 (▲), 17·8 (△),
10·6 (■), 10·4 (□).

FIGURE 7.13

MANDREL ROLLING (170 mm ROLLS)

INFLUENCE OF TUBE PARAMETERS ON MEAN R.S.F.

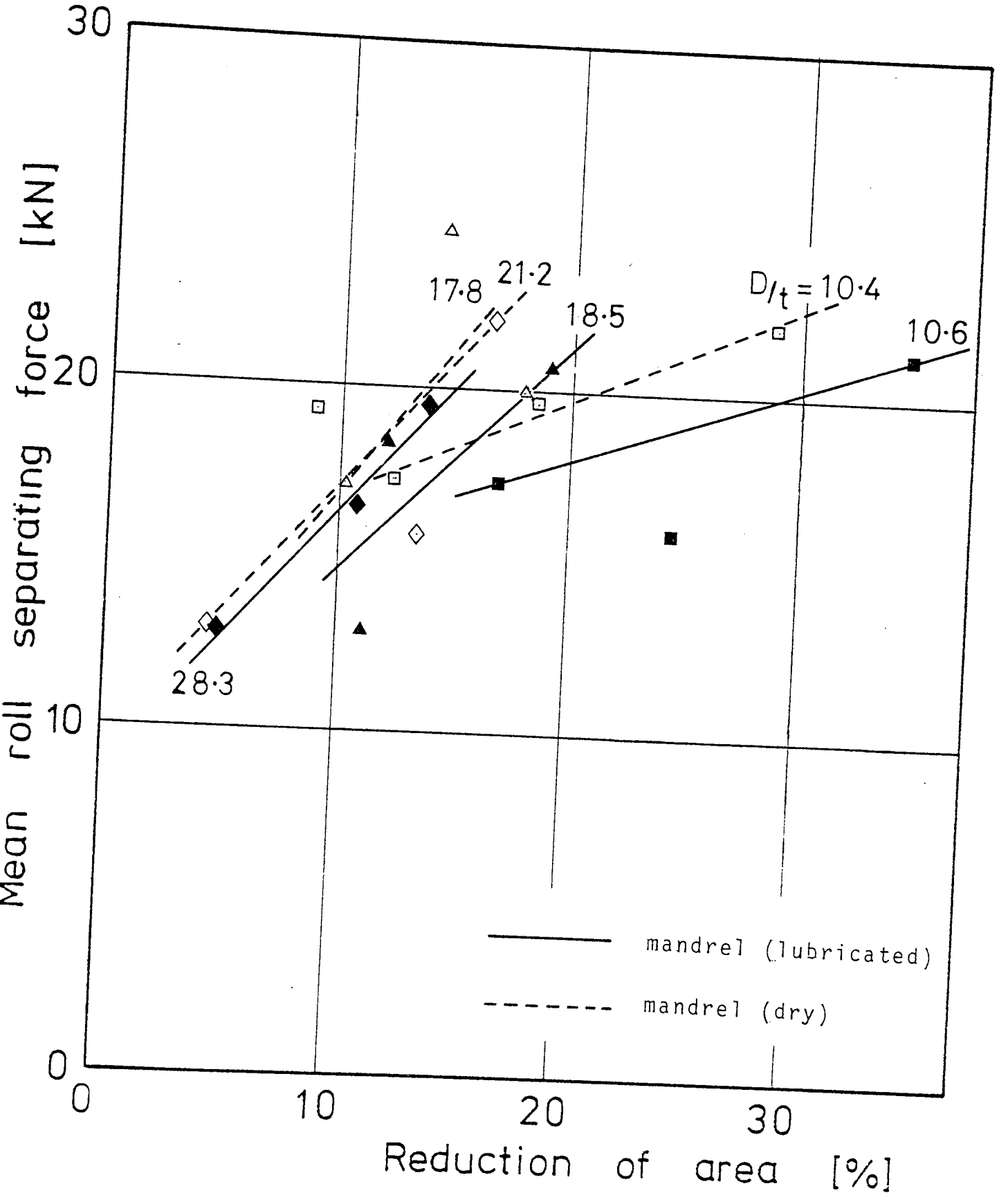

FIGURE 7.14

of the tube reduction in a production mill should be carried out in the initial stands, where the tube $\frac{D}{t}$ ratios are comparatively small.

FIGURE 7.15 shows the total roll torque plotted against the tube reduction of area for the stated tube $\frac{D}{t}$ ratios. They show the same trend as for the mean roll separating force graph FIGURE 7.14.

Both the roll separating force and torque, tube reduction relationships for mandrel rolling are in contrast to the corresponding graphs for sinking. For in the latter process the homogeneous work is greater in comparison with the friction work.

Provided the frictional conditions are constant, it may be reasoned, as for sinking, that the mean roll torque will be directly proportional to the mean roll separating force. The linearity between the roll load and torque shown in FIGURE 7.16 shows this relationship to be approximately correct.

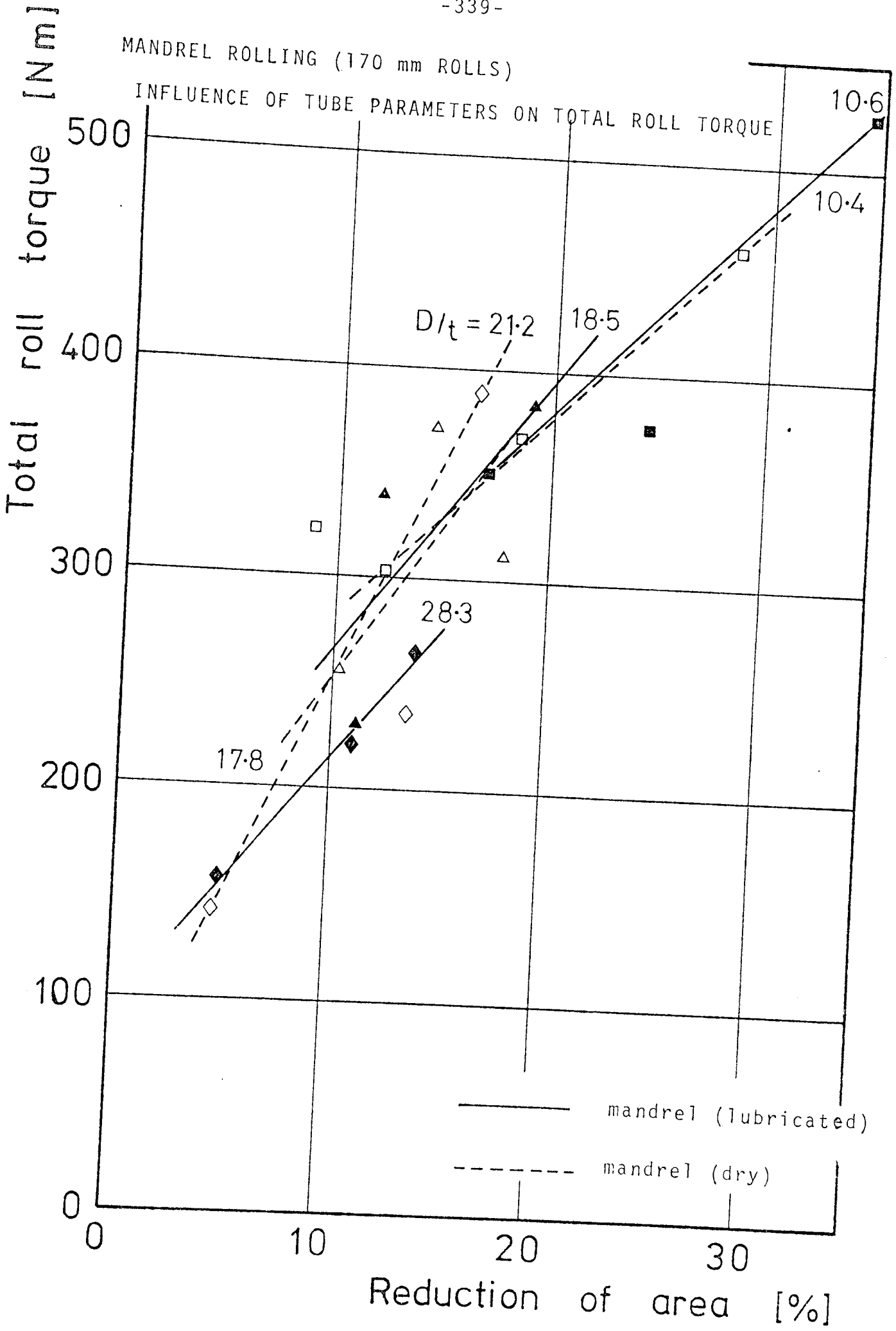
MANDREL ROLLING (170 mm ROLLS)
INFLUENCE OF TUBE PARAMETERS ON TOTAL ROLL TORQUE
Total roll torque [N m]
500
400
300
200
100
0
0
10
20
30
Reduction of area [%]
D/t = 21·2
18·5
10·6
10·4
28·3
17·8
mandrel (lubricated)
mandrel (dry)

FIGURE 7.15

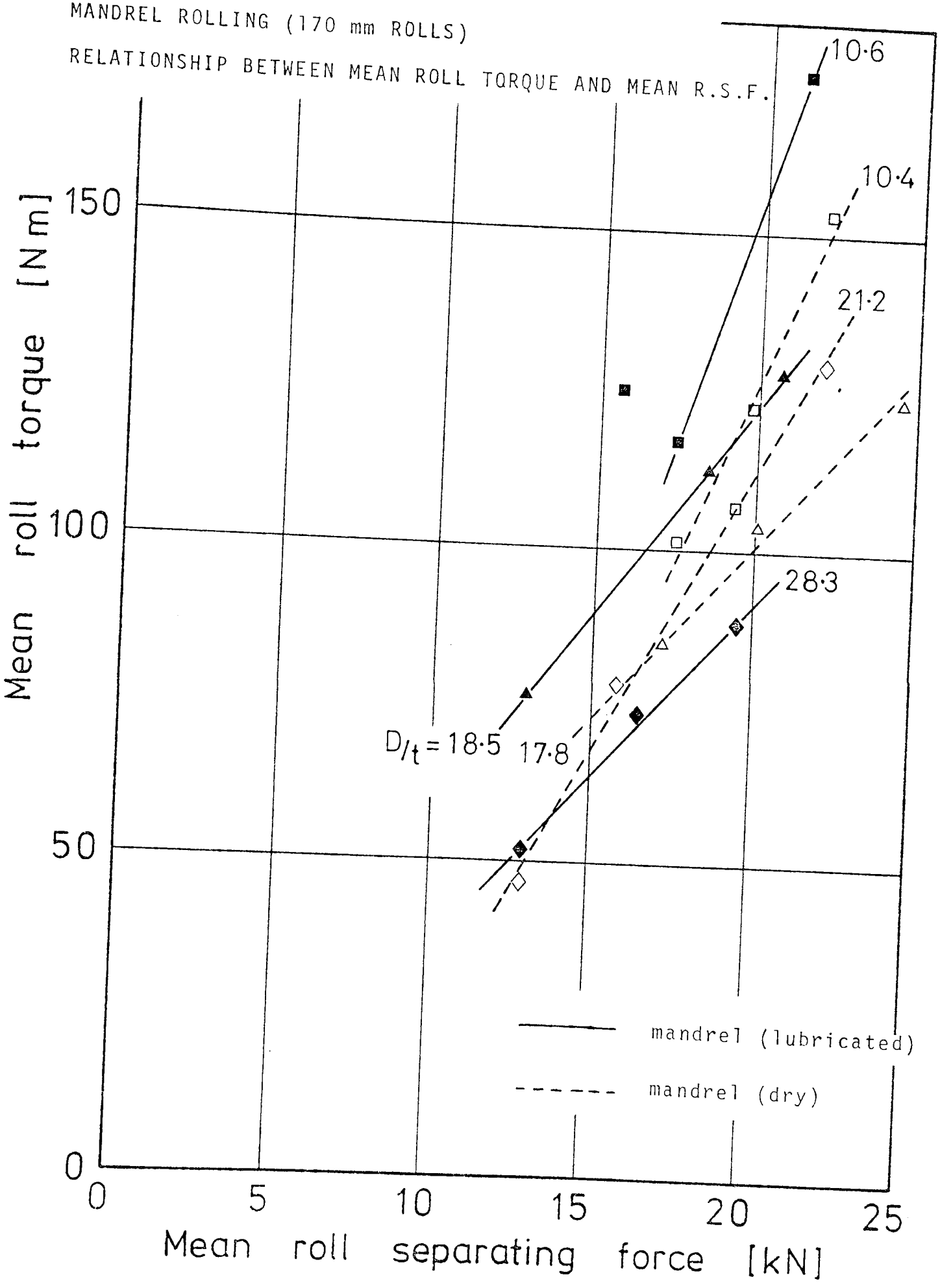
MANDREL ROLLING (170 mm ROLLS)
RELATIONSHIP BETWEEN MEAN ROLL TORQUE AND MEAN R.S.F.
Mean roll torque [N m]
150
100
50
0
0
5
10
15
20
25
Mean roll separating force [kN]
10·6
10·4
21·2
28·3
D/t = 18·5
17·8
mandrel (lubricated)
mandrel (dry)

FIGURE 7.16

Effect of Changing the Frictional Conditions at the Tube-Mandrel Surface.

Friction on the mandrel surface directly affects the roll loads and torques. The increase in the friction force, and consequently the work done at the tube-mandrel surface leads to an increase in the roll loads and torques.

The effect of friction on the roll separating force and torque for dry and lubricated mandrels are also shown in FIGURES 7.14 and 15 for the given tube $\frac{D}{t}$ ratios.

These graphs confirm the increasing contribution to the roll load and torques of friction at the tube-mandrel surface.

Again, as for sinking, the total roll torque seems to be primarily a function of tube reduction rather than the $\frac{D}{t}$ ratio.

7.5. MANDREL ROLLING, EXPERIMENTAL-THEORETICAL COMPARISONS

The problems which arose in the sinking tests from the absence of pin loadcells became even more relevant in the mandrel rolling process with the reduced tube-roll contact area. Although Labib's (43) two-roll mandrel rolling work did include substantial pin loadcell readings and corresponding roll groove loadings, only a sample set of these results was published. These results, relevant to thick and thin tube specimen are displayed in FIGURE 3.24. They suggest a "flat rolling" plane strain style deformation at the roll root groove, and, very approximately, parabolic roll groove pressure distribution longitudinally and peripherally. If the peak load points for each radially located pin are joined to give the neutral line, the resulting surface deformation model approaches that shown in FIGURE 3.21.c. In other words, as the tube reduction increases, the neutral line appears to approach a mid position between the tube entry and exit stations. This behaviour is particularly relevant to mandrel rolling, where, compared with the sinking process, higher tube reductions are employed. Therefore, the roll-tube surface deformation zone was assumed to be divided into equal areas. This assumption becomes more credible for the three-roll configuration with a reduced roll root to shroud depth which restricts the tube reduction within the roll profile. Consequently, the larger tube reductions associated with this process,

justifies, as a first approximation, the "flat" rolling concept.

Unfortunately, the uncertainties introduced into the results by the partially forward and reverse rolled test specimens became especially relevant in mandrel rolling, where the friction contribution is significant. Furthermore, since no completely rolled mandrel results were available for the 170 mm shroud diameter rolls, comparison of theory and experiment should be made cautiously. However, some specimens were completely mandrel rolled with the 255 mm and 340 mm diameter roll sets, as listed in Addendum I. The corresponding results are discussed in Addendum II.

7.5.1. Tube-Roll Arc of Contact

The measured tube-roll root contact angles for the lubricated and dry mandrel specimens are listed with the calculated values in TABLE 6.2.

To preserve clarity the individual values are not plotted; only the resultant lines are constructed and shown graphically in FIGURE 7.17.

Appendix G.2 gives the expression for calculating the tube-roll root contact angle.

For lubricated mandrel rolled tubes having $\frac{D}{t}$ ratios of 28.3, and 18.5 a satisfactory comparison can be seen, but the thick tubes $\frac{D}{t}$ = 10.6 show an underestimate of the measured value. For the dry mandrel rolled specimens the comparison is less good, possibly as a consequence of the deformation being more circumferential and radial, rather than longitudinal.

However, it may be remembered that these contact angles are relatively small and difficult to assess on the shadowgraph, as may be deduced from PLATE 7.3.

7.5.2. Theoretical Mandrel Roll Pressure

Although Labib's roll groove pressure measurements were

MANDREL ROLLING (170 mm ROLLS)

MEASURED AND CALCULATED TUBE-ROLL ROOT CONTACT ANGLES

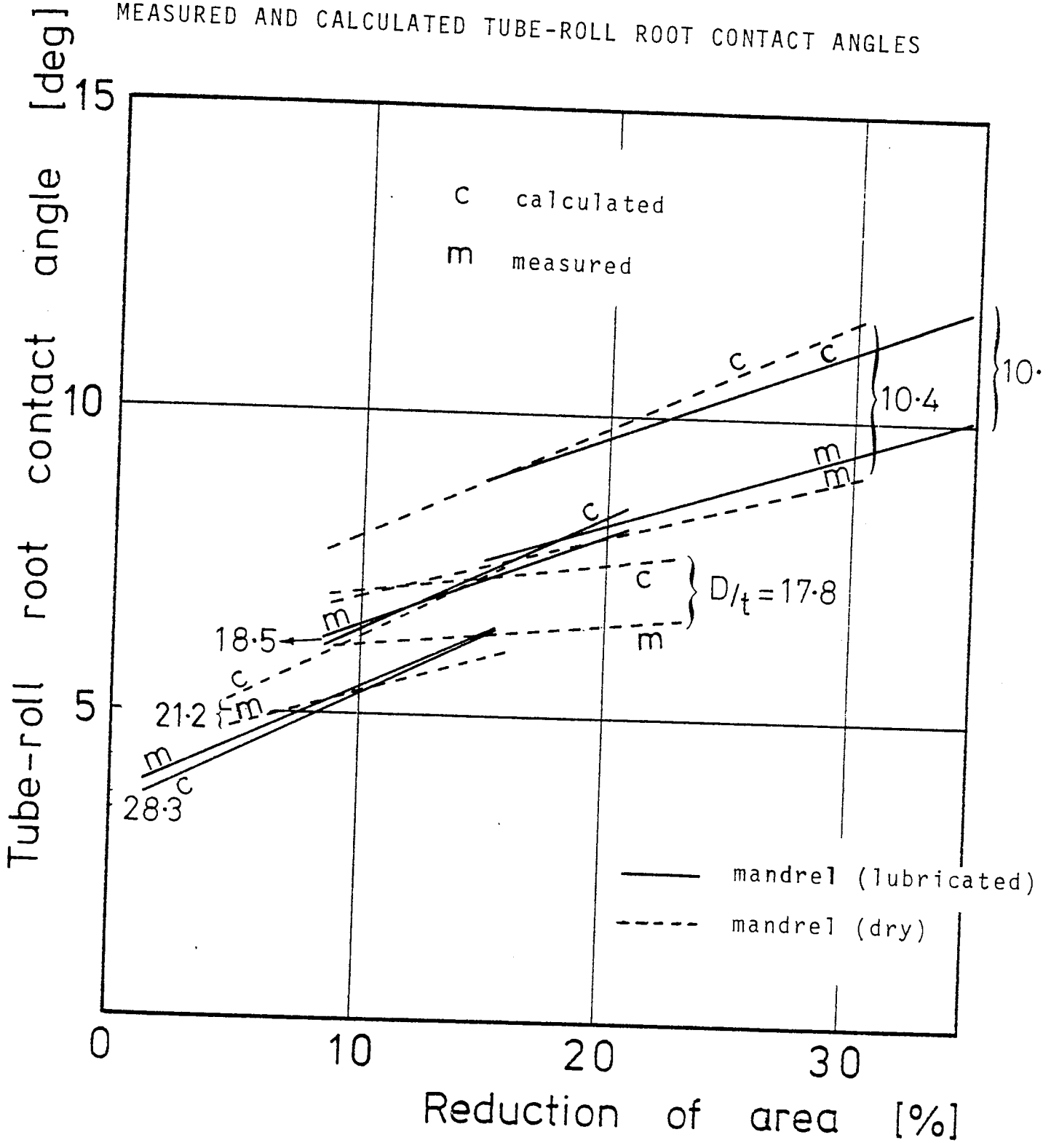

FIGURE 7.17

for the two-roll arrangement, and for smaller tube reductions, these are the only reliable results available, and therefore, it was felt advantageous to employ them as a basis for comparison.

Compared with the sinking process, the assessment of the theoretical mandrel roll pressure is a little unsure due to the smaller tube-roll arc contact angles, lengths and areas. A precise knowledge of these values of course was not available. This, understandably, affected the accuracy of the pressure calculations, particularly for the equilibrium approach. For reasons to be discussed in the next section, it was considered unrealistic to deduce the roll pressure for the 170 mm shroud diameter rolls utilising the equilibrium analysis. The only viable results were those realised by the energy method, and it is these results which are compared with the measured mean roll pressure values of Labib's (43) and shown together in FIGURE 7.18.

Equilibrium, (theoretical mandrel pressure)

The worked example Appendix H.2.1, presenting the equilibrium approach for determining the maximum roll pressure illustrates the sensitivity of these calculations to the roll diameter i.e. to the assessed value of the tube-roll contact angle at the groove root. As commented previously the contact angles in the mandrel rolling process are appreciably smaller than those occurring in

MANDREL ROLLING (170 mm ROLLS)

COMPARISON OF THEORETICAL MEAN ROLL PRESSURE WITH LABIB'S EXPERIMENTAL VALUES

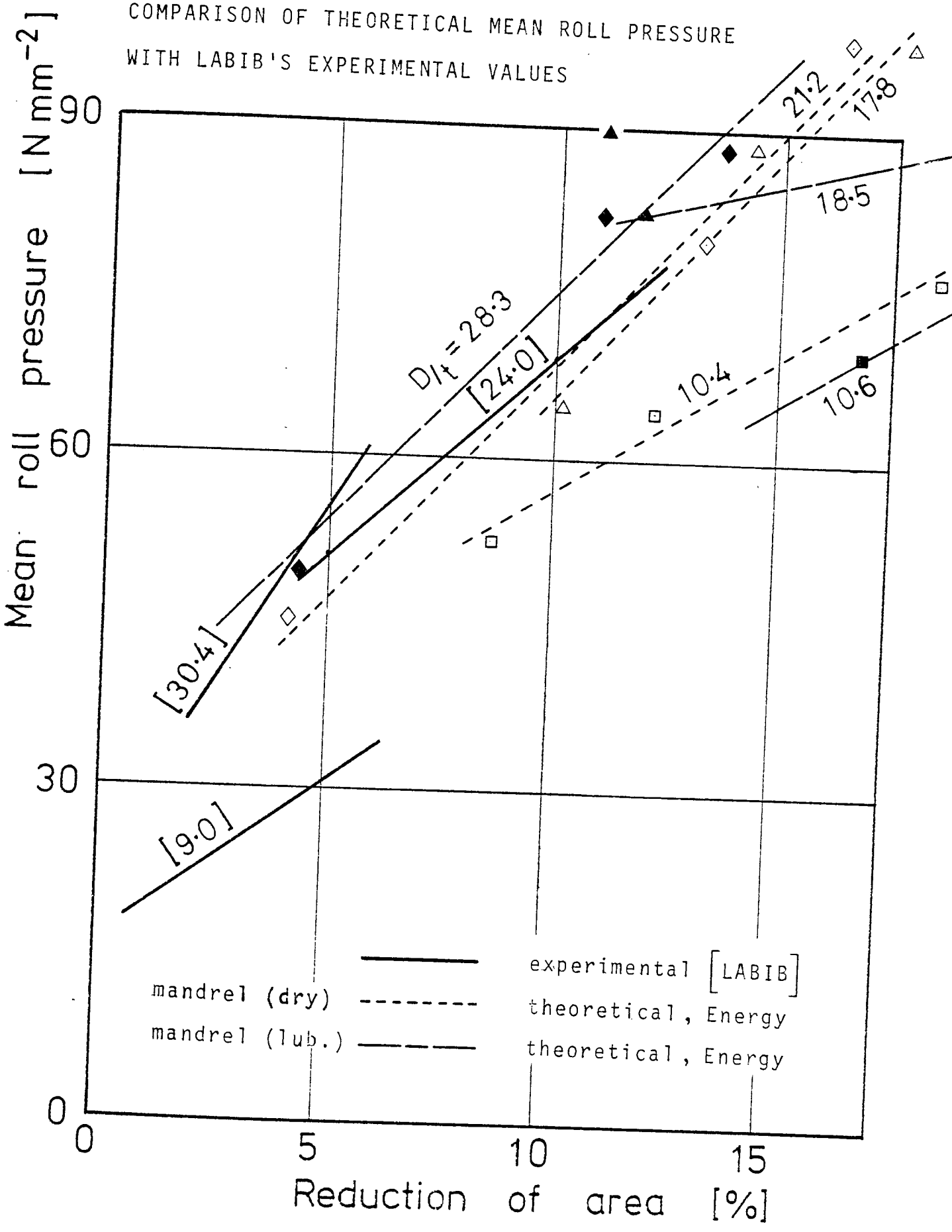

FIGURE 7.18

sinking and the subsequent errors in calculating this angle increases the discrepancy arising from the equilibrium based pressure calculations. This situation, together with the imprecise knowledge of the roll groove pressure distribution for the three-roll arrangement renders this analytical approach unreliable for the smallest diameter rolls. Furthermore, the probability of some roll flattening at the roll groove root, (the maximum pressure region) compounds this problem. All these adverse factors resulted in a decision being taken to discontinue the equilibrium analysis for the 170 mm diameter rolls. Appendix J discusses an alternative approach to this enigma.

However it was felt informative to utilise the results from the mandrel rolling trials employing the larger 255 mm shroud diameter rolls to evaluate the equilibrium approach. This example is shown in Appendix H.2.1.

Labib (43) in his mandrel rolling work presented an elastic roll flattening calculation based on Hitchcock's equation and the mean roll pressure. For a typical set of results, considering the mean roll separating force per unit roll width, he deduced, for the ratio of flattened to original roll radius, a maximum value of 1.06, with average values of 1.03 for thin walled tubes and 1.01 for thicker tubes. Although these ratios are negligible, they could become significant at the roll groove root and at the higher tube reductions considered

in the present work.

Energy, (theoretical mandrel pressure)

The theoretical energy analysis shown graphically in FIGURE 7.18 refer to two tube-mandrel interface conditions; dry and lubricated. For purposes of comparison with Labib's experimental results, the same mandrel surface conditions were assumed for the current theoretical investigation, i.e. the friction factor m for the dry mandrel case was taken to be 0.6 and for the lubricated mandrel as 0.4. In general, the comparisons displayed in FIGURE 7.18. are satisfactory if one can extrapolate some of Labib's measured results to the higher tube reduction ranges considered in the present investigation. For a particular tube $\frac{D}{t}$ ratio the dry mandrel analysis gives higher theoretical mean roll pressures than those for the lubricated mandrel, and, excepting the dry 17.8 tube $\frac{D}{t}$ case, fall within the corresponding envelopes displayed by Labib's figures. Furthermore, again ignoring the dry 17.8 tube $\frac{D}{t}$ ratio case, both the energy analysis and Labib's results show slight increases in slope with increase in the tube $\frac{D}{t}$ ratio.

A typical worked example applying the energy method for calculating the theoretical mandrel roll pressure is given in Appendix H.2.2.

All the theoretical mandrel roll pressure results are listed in the Appendix TABLE H1.

7.5.3. Theoretical Mandrel Rolling Roll Separating Force and Roll Torque

Labib also made a comparison between the calculated and measured values of the length of the arc of tube contact at the groove root. He detected in the cases relevant to this investigation, that the measured value was greater than the calculated value. For thick wall tubes the measured value of the root arc contact length was some 25% greater than the calculated, and for thin wall tubes 60% greater. This indicated a free deformation zone, where the oncoming tube rose or "piled up" as it approached the roll groove. PLATE 7.3 as noted earlier, gives some support to this tube behaviour in the present investigation. The implication, being an underestimation of the true tube-roll arc contact length and contact area.

The existence of a free zone or bulge formation has been observed in the drawing process by many investigators.

Both the roll separating force and roll torque require a detailed knowledge of the tube-roll contact arc length and area. This information, of course, was not directly available, and this, together with the reduced tube-roll contact associated with mandrel rolling resulted in the decision being taken not to pursue this particular issue.

A brief theoretical (equilibrium) roll separating force example of a single pass tube specimen ($\frac{D}{t}$ = 10.5), completely dry mandrel rolled with the 255 mm shroud diameter rolls is given in Appendix H.2.1 and shown in FIGURE 7.21. All the theoretical mandrel roll separating force results are listed in the Appendix, TABLE H2.

7.6. COMPARISON BETWEEN EXPERIMENTAL RESULTS AND OTHER THEORETICAL APPROACHES

As mentioned in Chapter 3 various sinking and mandrel rolling theories were examined. The theories evolved by Haleem (40) for sinking and Labib (43) for mandrel rolling were based on the energy method, and since reliable roll pressure measurements were also available these two analyses were considered in some detail. Any theoretical approach must account for the "free" deformation zone, which leads to a decrease in the roll arc contact length and area for sinking and an increase for mandrel rolling. Consequently, any modified theory must account for these actual contact area which implies a decrease in the work done against friction for sinking and an increase for mandrel rolling.

Both Haleem and Labib compared their two-grooved roll theories with those published by Russian and other workers. Consequently, noting their detailed commentaries, only a brief summary of their appraisals will be given here. Furthermore, the basic principles of any theory are independent of the number of rolls per stand, although the friction and redundancy contribution would be expected to be smaller for the three-roll configuration, confirming an increased rolling efficiency.

In conclusion, it was felt that a comparison of the three-roll theories, which are themselves scarce, would not be productive.

7.6.1 ·Sinking

In applying the energy method to two-roll tube sinking Haleem considered full sticking friction (m = 1) and frictionless (m = 0) conditions to calculate upper and lower values. These are displayed in FIGURE 7.19 and they compare his theoretical and measured values of the mean roll pressure with the Russian theories of Vatkin (8) and Shveikin & Gun (59) for various tube $\frac{D}{t}$ ratios. Haleem's results are relevant to rolling tube from round to oval (R-O pass), and for gap setting I, where the roll groove gap is essentially filled by the deformed tube. This particular sinking condition is the one most appropriate to the present three-roll investigation.

Comparisons, in FIGURE 7.19, also show that the two Russian theories, based on the equilibrium approach, are most unsatisfactory for real sinking conditions and even for moderate friction. Conversely, the energy method of Haleem shows good correlation with the upper bound (m = 1) solution; this is a situation which is most likely to correspond to actual mill practice.

SINKING

EXPERIMENTAL AND THEORETICAL MEAN ROLL PRESSURE

after HALEEM

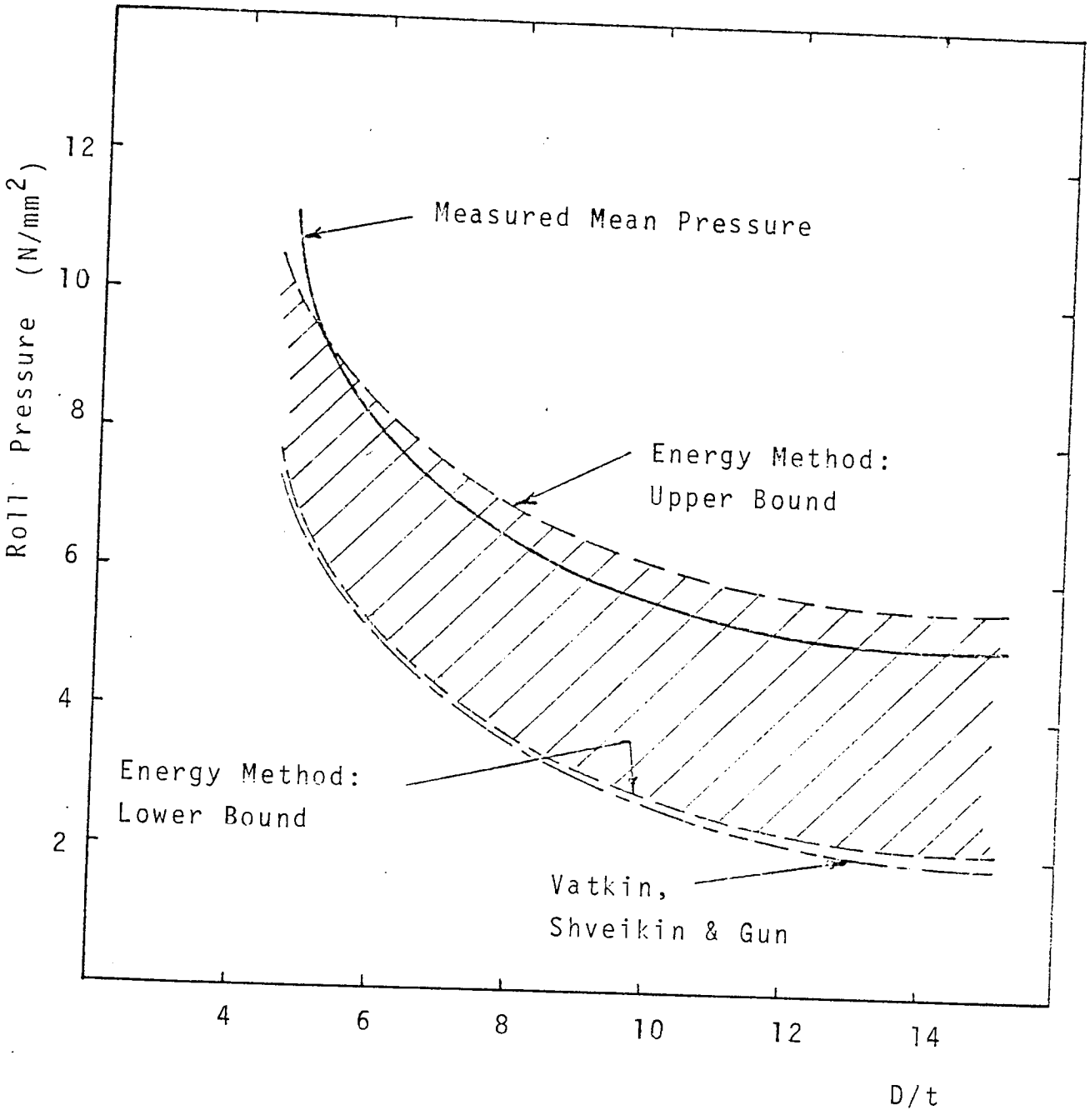

FIGURE 7.19

7.6.2. Mandrel Rolling

With the exception of Labib's work all the mandrel rolling theories considered in Chapter 3 involved the use of equilibrium approaches.

The theory of Okamoto and Hayashi (38) is only applicable to the particular case of complete filling of the tube around the roll groove perimeter; underfilling or overfilling was not accommodated. Consequently, underfilling, the situation in the present three-roll mandrel work is not applicable to Okamoto's and Hayashi's analysis. Additionally, they neglected friction. This is a serious omission in mandrel rolling and Labib expressed some doubt as to the correct interpretation of their theory.

Labib compared Vatkin's and Druyan's (33) prediction of average roll pressure and Fomichev's and Kirichenko's (62) theory for the root roll pressure with his corresponding measured pressure values. He noted that Fomichev's and Kirichenko's analysis seriously underestimated the measured roll root (maximum) pressure, whilst Vatkin's and Druyan's prediction of the mean roll pressure was somewhat better. Labib also commented on the incorrect dimensions in the Vatkin and Druyan equation for the average roll pressure.

7. ADDENDUM II Further Discussion Relevant to the Experimental results from Rolling Tests Employing the 255 mm and 340 mm dia. Rolls.

7. II. 1. INTRODUCTION

The major part of the current experimental investigation utilised the 170 mm shroud diameter rolls to sink and mandrel roll tube specimens of various sizes. For reasons already discussed, most of these specimens were partially forward and reverse rolled, with only a limited number completely sunk as a single pass. None were completely mandrel rolled. Consequently, bearing in mind the additional complexity introduced into the analysis by the partially forward and reverse mandrel rolled specimens, it was decided to include the additional test results procured from all tubes completely rolled as a single pass on the larger diameter roll sets. All such tube specimens were rolled by the larger roll sets i.e. the 255 mm and 340 mm shroud diameter rolls. This inclusion also complied with the original object of the investigation.

Since the roll separating force is more readily measured and utilised it is only this relationship with the stated tube rolling parameters which is considered in this section. Although a few tube specimens were sunk or mandrel rolled by the largest rolls (340 mm diameter), the roll load and

torque results, shown in TABLE 6.I. 9 & 10 were a little inconclusive and consequently were not incorporated in the graphs.

With reference to the range of roll diameters and tube diameters employed, it can be seen that the roll diameter to tube diameter ratio $(\frac{R_r}{D})$ is primarily a function of the roll diameter. Consequently, relationships between this ratio and the previously considered roll radius parameter will not yield any substantial additional information. This, and the lack of results from the 340 mm roll diameter tests, are the reasons why the effect of the ratio $\frac{R_r}{D}$ was not considered.

7.II.2. EXPERIMENTAL SINKING AND MANDREL ROLLING

7.II.2.1. Measured Surface Longitudinal Strain Distribution

The distribution of the longitudinal strains for the tube specimens rolled by the larger 255 mm and 340 mm roll diameters are presented in TABLE 6.I. 1/2 & 7/8 (Chapter 6.I. indicates the relevant rolling conditions).

These strain distributions show little longitudinal and peripheral variation and are of a similar pattern to those produced by the smaller 170 mm shroud diameter rolls. Again, in common with the mandrel specimens rolled with the smaller 170 mm diameter rolls, partial or complete obliteration of the tube grid lines, especially at the roll root region was observed. In general , a comparison between the surface and mean longitudinal strains in the majority of the sinking and mandrel rolling cases show a greater surface strain and hence a rudimentary indication of the shear redundancy level. However caution is expressed in drawing conclusions since it will be remembered that only three test specimens for each tube $\frac{D}{t}$ ratio were considered.

7.II.2.2. Roll Separating Force (Sinking)

Relationships between the mean roll separating force and tube reduction in area for the stated tube $\frac{D}{t}$ ratios are

shown in FIGURE 7.20 . The 255 mm diameter rolls were utilised for these sinking tests and as indicated in FIGURE 7.20 ., both complete and partially rolled tube specimens were employed. These graphs show a similar pattern to those displayed by the smallest roll diameter size of 170 mm. The anticipated higher roll loads result from the larger diameter rolls having an increased tube-roll contact area. One interesting comparative feature is the proximity of the completely and partially rolled specimen results for the thick tubes of $\frac{D}{t}$ ratio ≃6.6. Although only four test results were considered, it does appear that this behaviour may be due to a decrease in the bending redundancy level in reverse rolling. Reference to Chapter 3 (page 136) will show that for a given tube wall thickness the bending redundancy is inversely proportional to the roll radius, i.e. there is a reduction in redundancy as the roll size increases. Consequently, this results in a closer equality between the completely and partially rolled loads.

7.II.2.3. Roll Separating Force (Mandrel Rolling)

FIGURE 7.21 , shows the better quality results and relationships for the mean roll separating force tube reduction for various tube $\frac{D}{t}$ ratios and mandrel surface conditions. All the results were obtained utilising the 255 mm diameter rolls.

Comparison of the completely rolled results for the tube $\frac{D}{t}$ ratio of 10.6 clearly show an increase in roll loads

SINKING (255 mm ROLLS)

INFLUENCE OF TUBE PARAMETERS ON MEAN R.S.F.

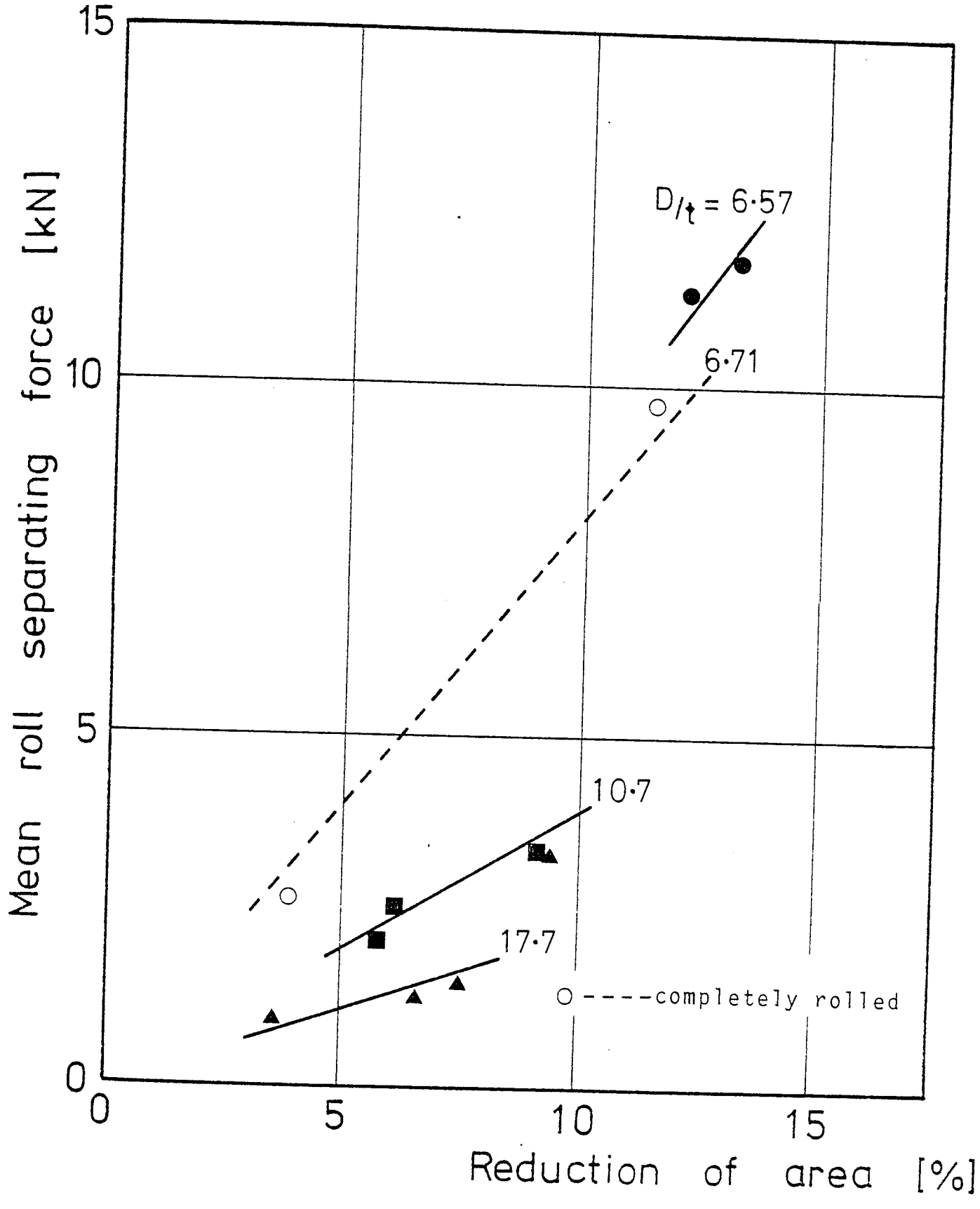

FIGURE 7.20

MANDREL ROLLING (255 mm ROLLS)

INFLUENCE OF TUBE PARAMETERS ON MEAN R.S.F.

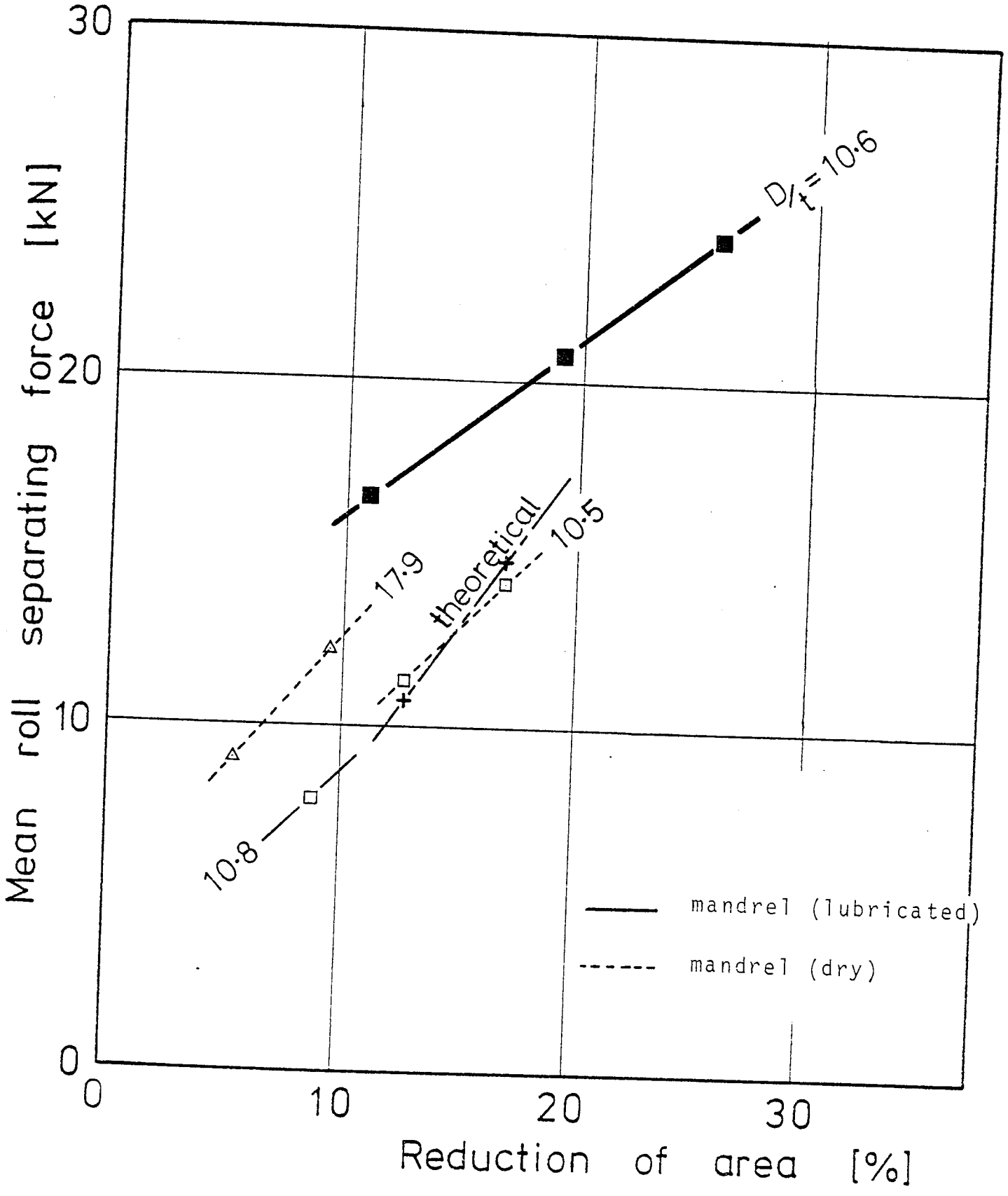

FIGURE 7.21

when the specimens were only partially rolled. This discrepancy must have also been present in the mandrel tests using the smaller 170 mm diameter rolls, where all specimens in this test series were partially rolled. This, obviously introduces a further complication into any attempted comparison between the experimental and theoretical test results obtained from the 170 mm rolls.

Generally, the somewhat limited results show an increase in the mean roll separating as the tube $\frac{D}{t}$ ratio increases and for the dry mandrel surface condition. This behaviour is in agreement with the corresponding mandrel rolling results from the 175 mm diameter roll tests and with those obtained by Labib (43).

7.II.3. MANDREL ROLLING EXPERIMENTAL-THEORETICAL COMPARISONS

7.II.3.1. Theoretical Mandrel Rolling Pressure and Roll Separating Force

The rudimentary mandrel roll pressure calculations shown in Appendix H.2.2 and results (see TABLE H1) are based on the determination of the average longitudinal roll pressure at the groove root and the assumption that this pressure is uniform around the roll groove circumference. This assumption undoubtedly gives an overestimation of the mean mandrel rolling pressure. Acceptable comparison

of the theoretical and experimental roll separating force for various tube reductions is shown in FIGURE 7.21 . This is probably due to the increased roll diameter (255 mm) producing a larger, and more readily assessed, tube-roll contact angle and area.

CHAPTER EIGHT

CONCLUSIONS

8. CONCLUSIONS

From this investigation of the longitudinal rolling of tube through three-grooved rolls the following conclusions have been reached.

The effect which the various tube parameters have on such variables as the roll force and torque have been studied for the sinking and mandrel rolling processes, and where relevant, presented in graphical form. Tubes were partially rolled to provide information relevant to the tube deformation pattern over the tube-roll contact surface. These specimens showed a disproportionate influence of friction and redundancy on the roll force and torque. For comparison purposes a number of tubes were completely rolled as a single pass.

Results from the sinking tests showed that the roll force and torque increased for higher tube reductions, larger roll diameters and for thicker tubes i.e. low tube $\frac{D}{t}$ ratios. Conversely, thinner tubes, when mandrel rolled, exhibited higher roll forces and torques, illustrating the greater influence of friction at the roll-tube-mandrel interfaces. The relative increased contribution of friction at lower reductions and higher tube $\frac{D}{t}$ ratios was confirmed by theory and experiments for both sinking and mandrel rolling. An increase in

friction between the tube and mandrel surface restricted the longitudinal strain of the tube, creating lower reductions and higher roll loads and torques. The way in which the roll force and torque was shared between the three-rolls for forward rolling, and where relevant, for reverse rolling, has been noted.

A rudimentary technique has confirmed the existence of two deformation zones for sinking, and tentatively, for mandrel rolling. The effect of these zones was to decrease the length of the tube-roll contact arc for sinking, whilst an increase in this length was suggested for mandrel rolling.

Assessment of the theoretical roll pressure by both the energy and equilibrium approaches suggests that the energy method is superior, especially for mandrel rolling. Furthermore, the correlation of the energy method improves with a discreet choice of the shear friction factor. For sinking, an elementary attempt was made to accommodate in the theory the two deformation zones i.e. the free and contact regions. Some success was observed in this approach.

The improved predictions of the energy theory for both sinking and mandrel rolling contrasted with the poor correlation obtained by the majority of the Russian theories utilising the equilibrium approach.

Comparisons between the surface and mean longitudinal tube strains confirmed a shear redundancy condition at the tube-roll contact surface. Minimal variation in the peripheral values of the surface longitudinal strain indicated an improved uniformity in the deformation process which is achieved by the three-roll arrangement.

CHAPTER NINE

SUGGESTIONS FOR FURTHER WORK

9. SUGGESTIONS FOR FURTHER WORK

The extensive nature of this investigation prompts the following headings for suggestions relating to improvements in mill design, and enhancement of experimental and theoretical techniques:

1. DESIGN

The lack of pin loadcells within the roll groove profile was a major hindrance in assessing the pressure distribution over the deformed surface of the tube. Attention must therefore be given to rebuilding one of the three rolls to accommodate these load cells. Experience gained within the Department in the design and operation of this type of loadcell and the availability of improved systems for collecting the loadcell signal should make this a straightforward exercise.

The cantilever design of the roll stand encouraged some elastic springback of the rolls. Reducing this effect could be readily achieved by incorporating a framework stiffener around the three-roll stand, taking particular care to maintain the roll separating force loadcells within the roll load path.

A design modification is also required to provide rapid radial retraction of one, or preferably two rolls. This would allow grided tube specimens to be quickly withdrawn

after being part-rolled, thus retaining the surface deformation pattern of the tube-roll contact zone.

The primitive visual technique utilised for the tube velocity measurements was only satisfactory for completely rolled tubes having long "timed" lengths. This, together with a detectable change in the roll speed, suggests the employment of photo electric cells and associated circuitry to measure the tube, roll and mandrel speeds.

2. Experimental

Although the application of longitudinal tension to the tube was considered by Haleem (40) and Labib (43) for two-roll tube rolling, its extension to the three-roll configuration should yield fruitful results.

Varying the operating environment of the mandrel by controlled changes in its surface condition and speed should be investigated. Also the effect where the mandrel is re-inserted in the tube specimen prior to rolling.

In this investigation, only the rolling of round to arcuate triangular tube was considered. This restricted the work to the simulation of tube rolling at the first stand of a tube production mill. Consequently, the scope of any further investigation could be considerably extended by rolling arcuate triangular tube with the apices at the

groove roots i.e. emulating the tube mill practice, where adjacent three-roll stands are orientated at 120^{o} to each other.

Consideration should be given to observing the influence of roll groove serrations on improving the tube behaviour in the roll gap.
Two serration patterns are available:

1. Longitudinal serrations - to alleviate the problem of tube twist in the rolling of arcuate triangular tube, (note previous paragraph).

2. Circumferential serrations - to increase the roll bite. This is particularly relevant to the initial stands of a production mill. However the pitch and depth would have to be judisciously applied, since too severe a serration depth may encourage premature shearing of the tube contact surface.

The effect of changes in the roll groove profile also merits inclusion in further work.

Ingham (65) shows that lead displays some strain hardening and strain rate effects, consequently further investigations may profit by a change in model material from lead to an aluminium alloy such as HE 30 WP. This alloy exhibits little strain hardening, is insensitive to strain rate at room temperature and is likely to be a

more precise and dependable model material.

The interpretation of the u.v. traces to assess the mean of each load and torque cell signal proved to be an onerous task. An immediate improvement would be for these analogue signals to be recorded and analysed, then to display in digital format the mean and peak values of each cell signal.

A consequence of the inclusion of roll groove pin loadcells would be the acquisition of a precise knowledge of the arc contact lengths within the deformation zone. For the sinking process this would enable a more exact specification to be made of the tube reduction taking place in the free and contact deformation zones. Likewise, in mandrel rolling, the "piling" up of the tube prior to roll contact could also be detailed for further analysis.

3. Theoretical

A more accurate assessment of the shear friction factor m is required, possibly as suggested by Kudo (66). He proposed that the shear stress of a Coulomb type of friction could be equated to that of a constant shear type of friction, i.e. $\mu_{av}\, p_{av} = m \frac{\sigma_y}{\sqrt{3}}$, where p_{av} is the average pressure. This would allow both the energy and equilibrium methods to be more precisely analysed.

Both theories should benefit from a more detailed knowledge of the tube deformation regions - a natural consequence of the roll groove pin loadcell work. The incorporation of circumferential friction could also improve the equilibrium approach.

It would also be helpful to include the roll mill modulus in any formulated theory, thereby yielding a better theoretical assessment of the final tube cross-section.

Finally, with the provision of roll groove pin loadcells enabling a more accurate assessment of the tube-roll contact area to be made, all further tube rolling tests should be conducted as a complete single pass.

CHAPTER TEN

ACKNOWLEDGEMENTS

ACKNOWLEDGEMENTS

The author is indebted to Professor Hugh Sansome for his critical guidance and encouragement throughout this protracted investigation. His continued support as mentor and colleague is much appreciated.

The financial support provided by Tube Investments Ltd., and the Mechanical Engineering Division for the construction of the experimental mill is gratefully acknowledged.

Thanks are due to Mr. Harry Pratt and Mr. Ken Apperley for their help with the experimental work.

The author also recognizes the time made available to him by the academic staff members of the Mechanical Engineering Division.

Finally, I wish to express sincere thanks to my wife Marjorie for typing the thesis and to her and my family for their sustained patience and interest.

CHAPTER ELEVEN

LIST OF REFERENCES

(1) EVANS, G. "Manufacture of Seamless Tubes, Ferrous and Non-Ferrous", London (1934).

(2) FINDLATER, S. "Iron Steel Eng." 87 (1947).

(3) HARTJENSTEIN, R. "Stahl Eisen." 69, 626 (1949).

(4) RODDER, W. "Iron Steel Engr," May (1949).

(5) YOUNG, J.L. "Iron Steel Engr," 53 April (1951).

(6) BLAIR, J.S. "Iron Coal Trades Rev." 150 63. 191, 305, 423 (1950).

(7) SHEVCHENKO, A.A. "Metallurgizdat" (1954).

(8) VATKIN, YA. L. "Davlenie metalla na valki pri prokatke trub bez opravki". (The pressure of the workpiece on the rolls for the rolling of tubes without a mandrel). Obrabokta Metallov Davleniem. Sbornik III. Moscow (1954).

(9) KAUFMAN, M.M.
GLEIBERG, A.Z.
NODEV, E.O.
SHANIN, P. K. "Stal'." 541 (1956)

(10) DANILOV, F.A.
GLEIBERG, A. Z.
BALAKIN, V. G.
"Metallurgizdat" 75, 282 (1962) (first published 1954).

(11) YAMADA, Y.
WATAKE, S.
INOUE, K.
TANI, H.
"7th Japan National Congr. Applied Mechanics" pp 63-66 (1957).

(12) SACHS, G.
KLINGER, L.J.
"J. appl. Mech." 69, A-88-A-98 (1947).

(13) CHEKMAREV, A.P.
GULYAEV, G.I.
"Stal' Rolling and Tube Manufacture (Suppl.) 276 (1958).

(14) GULYAEV, G.I.
YURGELENAS, V.A.
"Ferrous Metallurgy" 13, 120 (1958).

(15) SHVEIKIN, V.V.
GUN, G. YA.
"Ob izmenenii tolshchiny stenki truby pri redutsirovanii". (A study of the change in tube wall thickness during reducing). Nauch. Dokl. Vys. Shkoly, Metall. 140 (1958).

(16) HANTOS, R.
TORMA, N.
"Kohaszati Lapok" 4, 191 (1958).

(17) VATER, M. "Technische Mitteilungen." 500 (1958).

(18) GULYAEV, G.I.
YURGELENAS, V.A. "Stal' Sbornik Statei." 373 (1961).

(19) GLEIBERG, A.Z. "Byulleten' TsIIN ChM." 145 (1950).

(20) KRAEV, S.I. "Obrabotka Metallov Davlenien," Metallurgizdat, Vypusk 3 (1954).

(21) KOLMOGOROV, V.L.
GLEIBERG, A.Z. "Stal' Rolling and Tube Manufacture (Suppl.)" 180 (1959).

(22) KIRICHENKO, A. N. "Moment i moschchnost' prokatki sploshnykh zagotovok i trub bez opravki v kalibrakh" (Torque and power requirement for the rolling of solid billets and unsupported tubes in grooves). Proizvodstvo Trub. Vypusk 12, pp 24-29. Ukrainskii Nauchno-Issledovatel' skii Truonyi Institut, Moscow (1964).

(23) KIRICHENKO, A. N. "Proizvodstvo Trub." Vypusk 13, pp. 37-44. Ukrainskii Nauchno-Issledovatel'skii Trubnyi Institut, Moscow (1964).

(24) SHEVCHENKO A. A. CHEKNAREV, I. A. "Kompleksnoe issledovanie skorostnykh i silovykh parametrov pri nepreryvnoi prokatke trub na dlinnoi opravke" (Complex investigation of the velocity and force parameters for the continuous mandrel rolling of tubes). Proizvodstvo Trub. Vypusk 13, pp 28-37. Ukrainskii Nauchno-Issledovatel' skii Trubnyi Institut, Moscow (1964).

(25) MATVEEV, Yu. M. LAVROV, P. P. "Stal'" (in English), 51 (1964)

(26) FOMICHEV, N. A. KIRICHENKO, A. N. "Izvest, VUZ. Chern. Met." No. 10 (1965).

(27) SHEVCHENKO, A. A. CHEKMAREV, I. A. "Tekhnicheskii Progress v Trubnoi Proizvodstvo"(Developments in Tube manufacture). (Volume commemorating P. T. Emel'yananenko). Moscow (1965).

(28) IVSHIN, P. N.
SHVEIKIN, V. V.
"Tr. Uralsk. Politekhn. Inst." No. 142, 64 (1965).

(29) GULYAEV, G. I.
YURGELENAS, V. A.
"Trudy" UKRNITI, Vypusk 2, Metallurgizdat (1959).

(30) SHEVCHENKO, A. A.
ZIMIN, A. K.
"Proizvodstvo Trub." Vypusk 7, Metallurgizdat (1969).

(31) FOMICHEV, I. A.
KIRICHENKO, A. N.
"Invest. VUZ. Chern. Met." No. 4, 81 (1966).

(32) CHEKMAREV, A. P.
ONISHCHENKO, I. I.
et al.
"Izvest. VUZ. Chern. Met." No. 4, 77 (1966).

(33) VATKIN, YA. L.
DRUYAN, V. M.
"Izvest. VUZ. Chern. Met." No. 11, 72 (1966).

(34) FAZAN, B.
BLAIN, P.
"Rev. Metall." 209 (1967).

(35) COLE, I. M.
"An investigation of the rolling of cylindrical tube by grooved rolls" Ph.D. thesis 1969, University of Aston in Birmingham.

(36) NEUHOFF, K. W.
PFEIFFER, G.
"The Technology of deformation in the operation of a continuous tube mill." Stahl und Eisen, 90, 1970, No. 8, pp 406-412.

(37) OKAMOTO, T.
"The theory of deformation and stress of tubes by deformation factor." The Sumitomo Search No. 5, May 1971, pp 62-72.

(38) OKAMOTO, T.
HAYASHI, C.
"Theory of plasticity on mandrel rolling". The International Conference on the Science and Technology of Iron and Steel, Tokyo, 1971, vol. II, pp 655-658.

(39) GULYAEV, G. I.
IVSHIN, P. N.
EROKHIN, I. N.
KURILENKO, V. Kh.
"Metal spread and ovalization of the passes in reduction and sizing of tubes." Steel in the U.S.S.R. September 1971, pp 734-736.

(40) HALEEM, A. S.
"An investigation into the longitudinal rolling of tubes through two-grooved rolls." Ph.D. thesis, 1978, University of Aston in Birmingham.

(41) LOMACHENKO, A. N.
BLINOV, Yu. I.
et al.
"Transverse variations in wall thickness of tubes with reduction in two-and four roll stands. Stal, 1973, (10), pp 927-928.

(42) PFEIFFER, G.
"Causes of irregularities of material flow in the continuous tube rolling process and measures to improve the rolling conditions." Ph.D. thesis, Clausthal University, West Germany, 1973.

(43) LABIB, O. M.
"Mechanics of rolling tube on a mandrel through two-grooved rolls." Ph.D. thesis, 1982, University of Aston in Birmingham.

(44) BOETTCHER, W.
POMP, A.
"Stahl Eisen." 69, 615 (1949).

(45) NEUMANN, F. W.
HANCKE, D.
"Stahl u.Eisen." 75, 1452 (1955).

(46) GULYAEV,G. I.
et al.
"Stal' Rolling and Tube manufacture (Suppl.)." 180 (1959).

(47) GULYAEV, G. I.
YURGELENAS, V. A.
"Stal' Sbornik Statei." 335 (1961).

(48) VATER, M.
"Materialprüf." 3, 176 (1961).

(49) MISE, S.
TAKAI, I.
MATSUKI, N.
"Sumi, Met. (Japan)." 59 (1965).

(50) BILLER, H.
"Technische Mitteilungen." 60, 418 (1967).

(51) NEUMANN, F. W.
"BLECH." 6, 782 (1959).

(52) VALENTA, D.
"Hutnické Listy." 22, 756 (1967).

(53) GULAEV, G. I.
YURGELENAS, V. A.
ZIMIN, A. K.
"Stal' (in English)" 4, 332 (1968).

(54) SHVEIKIN, V. V.
et al.
"VUZ. Chern. Met." 4, 88 (1964).

(55) ANISIFOROV, V. P.
ZEL'DOVICH, L.S.
SHPIGEL'MAN, R. M.
LOKHOVININ, L. N.
NODEV, E. O.
"Stal' (in English)." 6, 505 (1968).

(56) BLAZYNSKI, T. Z. "Recent developments in seamless steel tube making." Metals and Materials (U.K.), April 1970, Metallugical Reviews, pp 27-45.

(57) PROCTOR, J.S.
JUBB, C. "The stretch mill". Journal of the Iron and Steel Institute, February 1973, pp 115-122.

(58) GRULAEV, G. I.
KUZNETSOV, E. D.
EROKHIN, I. N.
KORSHAKOV, A. N.
YANOVICH, V. K. "Effect of deformation on transverse wall-thickness variation in the hot reduction and cold rolling of tubes." Steel in the U.S.S.R. January 1974, pp 64-67.

(59) SHVEIKIN, V. V.
GUN, G. Ya. "Specific pressure for tube rolling without a mandrel." Nauchnye Doklady Vysshei Shkoly, Mettallurgiya, 1958, No. 2, pp 167-169.

(60) SACHS, G.
BALDWIN, W. M. "Stress analysis of tube-sinking." Trans. ASME, 1946 August, pp 655-661.

(61) AVITZUR, B. "Metal Forming Processes and Analysis." McGraw-Hill, 1968.

(62) FOMICHEV, I.A.
KIRICHENKO, A.N.
"The distribution of specific pressure in the zone of deformation for the rolling of tubes on a mandrel." "Izvest, VUZ Chern. Met. 1968, No. 4, pp 75-82.

(63) VATKIN, Ya. L.
et al
"The specific pressure of the workpiece on the rolls and the mandrel for the rolling of tubes on a long mandrel." Byull. Ts II N Ch.M. No. 20, 48, 1965.

(64) LOIZOU, N.
SIMS, R.B.
"The yield stress of pure lead in compression" J. Mech. Phys. Solids, Vol. 1, pp 234, 1953.

(65) INGHAM, P.M.
"The mechanics of thick slab rolling" Ph.D. thesis, 1980, University of Aston in Birmingham.

(66) KUDO, H.
"Some analytical and experimental studies of axi-symmetric cold forging and extrusion" Parts I & II, International Journal of Mechanical Sciences, Vol. 2, pp 102-127, 1960; Vol. 3, pp 91-177, 1961.

(67) HOFFMAN, O.
SACHS, G.
Introduction to the Theory of Plasticity for Engineers
McGraw-Hill, 1953.

(68) BASILY, B.B.
SANSOME, D.H.
JONES, G.M.
Ring beam load-cell
U.K. Patent No. 2036344B 1978.

APPENDICES

APPENDIX A

A.1. Fully Plastic Tube in Plane Stress Condition

The following analysis is based on that given by Hoffman and Sachs (67).

The state of complete plastic deformation of a short tube in plane stress when subjected to an applied external pressure p_b is given by the relationship:

$$\frac{b}{a} = \frac{e^{\frac{\sqrt{3}}{2}\sin^{-1}\left[\frac{\sqrt{3}}{2}\left(\frac{p_b}{\sigma_y}\right)\right]}}{\sqrt{1 - \frac{3}{4}\left(\frac{p_b}{\sigma_y}\right)^2} - \frac{1}{2}\left(\frac{p_b}{\sigma_y}\right)}$$

where a and b are the internal and external radii of the tube.

This relationship expresses $\left(\frac{p_b}{\sigma_y}\right)$ as an implicit function of $\frac{a}{b}$. Consequently a graphical solution is implied, where the required external pressure for a particular tube $\left(\frac{D}{t}\right)$ ratio can be determined, by noting that:

$$\frac{b}{a} = \frac{1}{1 - \frac{2t}{D}}$$

To this end assumed values of $(\frac{p_y}{\sigma_y})$ were substituted into this relationship and the deduced solutions for $\frac{b}{a}$ and hence $(\frac{D}{t})$ plotted graphically as shown in FIGURE A.A1. This enabled the required ratio $\frac{p}{\sigma_y}$ to be read off for a known tube $(\frac{D}{t})$ ratio.

Tabulated below are appropriate values of $\frac{b}{a}$ and $\frac{D}{t}$ from which the graphical solution (FIGURE A.A1) was constructed.

For convenience let $\frac{p_y}{\sigma_y} = C$

$(\frac{P}{\sigma_y}) = C$	$\frac{b}{a}$	$\frac{D}{t}$
0.40	1.58122	5.441
0.35	1.48029	6.164
0.30	1.39026	7.125
0.25	1.30931	8.466
0.20	1.23604	10.473
0.175	1.20191	11.905
0.150	1.16930	13.814
0.125	1.13809	16.484
0.100	1.10818	20.487

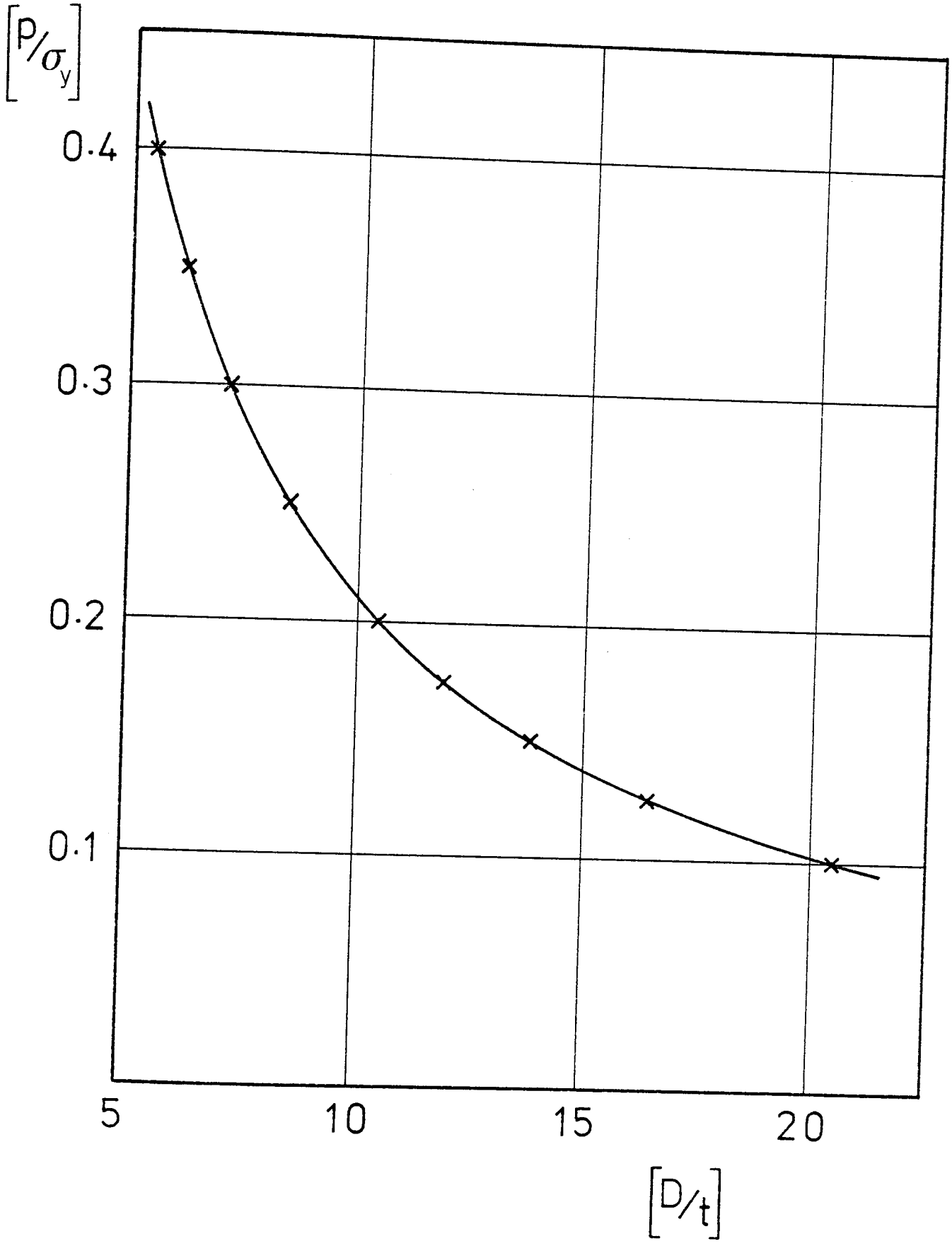

RELATIONSHIP BETWEEN $\left[\frac{p}{\sigma_y}\right]$ AND TUBE $\left[\frac{D}{t}\right]$ RATIO

FIGURE A.A1

APPENDIX B

B.1. Drawings of Complete Experimental Three-Roll Mill

The detailed drawings relevant to the experimental three-roll mill are inserted in the envelope at the rear of this thesis.

APPENDIX C

C.1. Design Calculations for the Axially Compact Load Cell

Although a rigorous theoretical analysis and design study was undertaken by Basily, Sansome and Jones (68), only a rudimentary analysis is given here. Reference to their work and further experimental evidence suggested a load cell ring cross section of breadth (b), 7.42 mm, depth (d) 11.66 mm, with sixteen sectorial mounting pads. To accommodate the loadcell within the roll support unit a mean diameter of 200 mm was indicated and further comparison with previous work finalised the design shown in FIGURE A.C1. To confirm the dimensions of the rectangular ring cross section a rudimentary deflection and stress analysis gave:

Axial deflection

From continuous beam theory, ignoring the ring curvature, the axial deflection (δ) is given by:

$$\delta = \frac{Wl^3}{192EI} = \frac{\frac{P}{8}\left(\frac{\pi D}{8}\right)^3}{192EI}$$

where P = max. total load (25kN)

D = mean load cell ring diameter = 200 mm

$$I = \frac{bd^3}{12} = \frac{7.42 \times (11.66)^3}{12} = 980 \text{ mm}^4$$

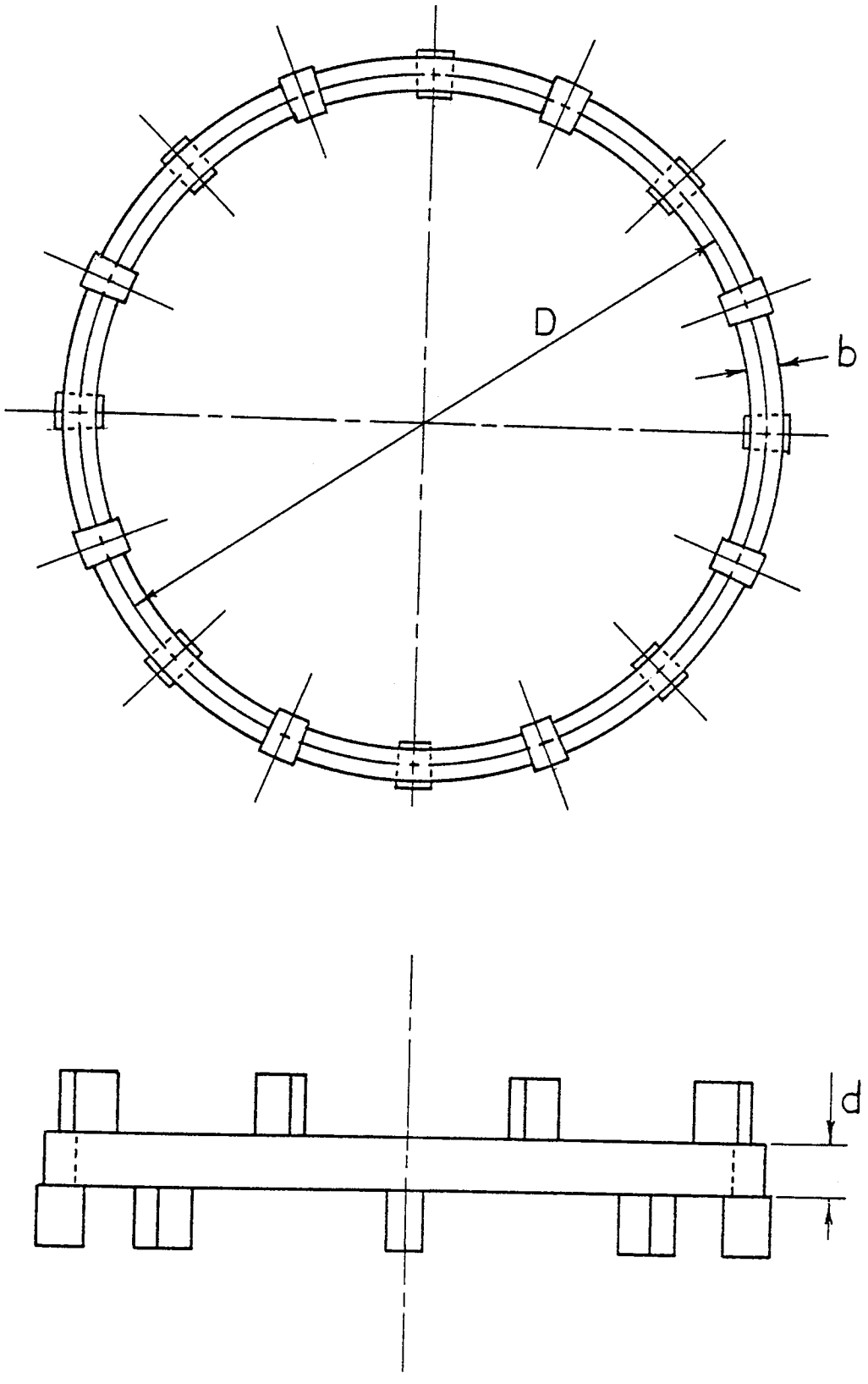

THE AXIALLY COMPACT RING BEAM LOAD CELL

FIGURE A.C 1

$E(\text{alloy steel}) = 207 \text{ kN mm}^{-2}$

$$\therefore \text{ Load cell stiffness } \left(\frac{P}{\delta}\right) = \frac{192\ EI \times 64^2}{(\pi D)^3}$$

$$\text{i.e. } \frac{P}{\delta} = 643 \text{ kN mm}^{-1}$$

Experimental calibration tests gave a measured stiffness of 639 kN mm^{-1} which compares favourably with the calculated value of 643 kN mm^{-1}.

Consequently the anticipated maximum R.S.F. of 25 kN implied a radial roll displacement of 0.039 mm.

Bending stress

The bending stress (σ_B) is the significant stress and from continuous beam theory, ignoring the ring curvature:

$$\text{Max. B.M.} = \frac{Wl}{8} = \frac{\frac{P}{8}\left(\frac{\pi D}{8}\right)}{8}$$

where P = max. load = 25 kN

and $\sigma_B = \frac{My}{I}$, where $y = \frac{d}{2} = \frac{11.66}{2}$ mm

i.e. $\sigma_B = 183 \text{ N mm}^{-2}$

For the medium alloy steel untilised in the loadcell construction (En 23), a yield stress of $\simeq$ 600 N mm^{-2} is quoted, giving a design factor of approximately 3. :

In conclusion, both the load cell ring deflection and stress are acceptable.

APPENDIX D

D.1. Voltage Level, Potentiometer Resistance and Galvanometer Characteristic for each Measuring Circuit.

These are tabulated below:

Load/Torque Cell	Voltage	Potentiometer Resistance (kΩ)	Galvanometer Characteristic		
			Type	Frequency (Hz)	D.C.Sensitivity μA/mm μV/mm
R.S.F. (10kN) (25kN)	30 / 12	100	SM1/Z	20	0.05 2.1
TORQUE (400 Nm) (800 Nm)	3.6 / 1.8	20	SM1/A	60	0.085 4.5

APPENDIX E

E.1. Specification of Mandrel and Tube Specimen Sizes

As referred to in Chapters 4 and 5 mandrels were utilised in the manufacture of all the tube specimens and for the mandrel rolling tests. The following is a brief summary of the calculations for the assessment of the mandrel diameters and associated tube outer diameters for a specific tube reduction of area. Reference should also be made to the roll groove profile shown in FIGURE 4.4.

SINKING

In the sinking process the experimental evidence suggests that very approximately the tube wall thickness remains constant. Then, for a particular tube $\frac{D}{t}$ ratio the associated mandrel and tube sizes for a specific tube reduction can be tentatively deduced as follows:

The anticipated tube reduction, $J \simeq 1 - \frac{(1.300-t_1)}{(D_o - t_o)}$

where t and D are the tube thickness and diameter respectively, and $t_o \simeq t_1$.

Then for the assumed tube $\frac{D}{t}$ ratios of 6.5, 10.7 and 17.6 and anticipated tube reductions J of 6%, 12% and 18%, the calculated mandrel diameters (tube inner diameter) dm and tube outer diameter D_o are:-

$(\frac{D}{t_o})$	Approx. J%	d_b (in)	D_o (in)
6.5	6	0.985	1.423
	12	1.037	1.498
	18	1.102	1.591
10.7	6	1.153	1.418
	12	1.220	1.500
	18	1.301	1.600
17.6	6	1.220	1.375
	12	1.301	1.468
	18	1.393	1.572

MANDREL ROLLING

For mandrel rolling the tube thickness is controlled by the roll groove and mandrel, consequently the final thickness of the tube specimen is more readily determined.

As in the previous section:

$$J \simeq 1 - \frac{(1.300^2 - dm^2)}{(D_o^2 - d^2_m)}$$

For the assumed tube $\frac{D}{t}$ ratios of 10.7, 17.6 and 22.6/28.9 the mandrel and tube diameters and associated anticipated

tube reductions are as follows:

$(\frac{D}{t})_o$	Approx. J%	dm(in)	Do(in)
10.7	23	1.102	1.354
	35	1.123	1.384
	47	1.153	1.418
17.6	22	1.181	1.332
	40	1.205	1.359
	50	1.220	1.376
22.6	12	1.198	1.314
	26	1.213	1.331
	36	1.220	1.344
28.9	3.5	1.213	1.303
	12	1.220	1.311
	30	1.235	1.327

APPENDIX F

F.1. Measurement Example of Shadowgraph Profile

In the majority of cases each tube specimen was sectioned before and after rolling. Each sectional length was then faced in the lathe and polished, thus enabling an assessment to be made of the cross-sectional area and the rolled tube profile. Each specimen cross-section was displayed on the shadowgraph and to illustrate the measurement procedure involved the following example of a mandrel rolled specimen is given:

Tube No. 21.

		Tube-Roll Contact Groove					
		1	2	3	1	2	3
$\bar{D}_1$ mm	(x10).	339.5	337.0	341.5	340.0	344.0	337.0
$\bar{d}_1$	(x10)	320.5	320.0	322.5	320.0	325.0	317.5
t_s	(x50)	57	53	58	58	51	60
t_r	(x50)	40	41	36	42	43	37
$t_{(\theta - \gamma)}$	(x10)	11.0	10.9	12.1	11.5	11.0	12.4
θc_1 deg.		(321-236)	(209-121)	(82-351)	(44-316)	(160-69)	(11-286)
		85	88	91	88	91	85
γ_{c1}		(305-247)	(195-131)	(70-6)	(298-240)	(236-173)	(90-25)
		58	64	64	58	63	65
$\hat{\phi}_{c1}$		(355.9-0.9)		(358.8-3.4)		(358.1-3.4)	
		5.0		4.6		5.3	

Each set of results was averaged and tabulated.

A similar procedure was involved for the sunk specimens apart from the $t_{(\theta-\gamma)}$, and γ_{cl} measurements which were not relevant to the process.

APPENDIX G

G.1. Tube-Roll Root Angle of Contact

The calculated tube-roll root contact angle ($\hat{\phi}_c$) can be readily determined from the roll groove geometry shown in FIGURE 4.4. as follows:

G.1.1. Sinking

From FIGURE . 3. 22 , indicating the calculated and measured arc contact lengths (Lg) and (Lm) respectively, Haleem (40) showed that, approximately:

$$l.m = \frac{1}{\sqrt{2}} Lg$$

Furthermore, reference to section 3.(ii).2.2., concerning the redundant work indicates that:

$$2\ Lm \simeq La$$

From the tube-roll root contact geometry:

$$Lg \simeq \sqrt{R_r\ (draft)}$$

$$\simeq \sqrt{R_r \left[\bar{D}_o - 2 \left(\frac{15.47}{33.02} \bar{D}_1 \right) \right]}$$

But $\sin\hat{\phi}_{c1} = \frac{Lm}{R_r} = \frac{Lg}{2R_r}$

i.e. $\sin \hat{\phi}_{c1} = \sqrt{\frac{\left[\bar{D}_o - 0.9369\ \bar{D}_1 \right]}{2R_r}}$

G.1.2. Mandrel Rolling

From FIGURE. 3. 23 , showing the mandrel rolled tube at the exit plane:

$$\sin \hat{\phi}_{cl} = \sqrt{\frac{2\ (t_o - t_r)}{R_r}}$$

APPENDIX H

Examples of Calculations of Mean Roll Pressure and R.S.F.

H.1. Theoretical Sinking Pressure

As previously discussed the approximate assumption will be made that the overall tube reduction is equally divided between the free and controlled deformation sections.

H.1.1. Equilibrium (tube no. 7/1) - 170 mm dia. Rolls.

Noting that:

$(\frac{D}{t})_o = 6.57$

$\bar{t} = \frac{1}{2}(5.73 + 5.66)$

$= 5.695$ mm

$\theta_{c1} = 47.4^o$

$\bar{\phi}_c = 5.735^o$

$J = 0.1366$

$A_o = 574.0$ mm^2

$\delta = 39.62 - 33.54$

$= 4.08$ mm

$r_g = 20.7$ mm

and $\bar{D}_1 = h_g + h_s$

and from former work:

$(\frac{D}{t})_1 = 5.926$ giving

$c = 0.3674$

i.e. $\frac{p_h}{\sigma_y} = 0.3674$

$\bar{\varepsilon}_h = 0.1630$

$\bar{\varepsilon}_r = \frac{2}{\sqrt{3}} \frac{5.695}{80.05} = 0.0821$

i.e. $\bar{\varepsilon}_h + \bar{\varepsilon}_r = 0.2451$

(& $\bar{\sigma}_y = 14.50$N mm^{-2})

With reference to Equation (3.(ii). 12 & 13), substituting, and considering the roll groove root :

$$A = 2 - \frac{1}{\cos 5.735} = 0.9950,$$

$$B = \frac{m\,\bar{\sigma}_y}{\sqrt{3}}\left(2 \tan 5.735 + \frac{1}{\sin 5.735}\right) = 5.894m\,\bar{\sigma}_y$$

$$\left[\frac{(r_1)}{(r_o)}\right]^A = \left[\frac{(27.88)}{(31.89)}\right]^{.9950} = 0.8748$$

for $m = 0$

$$\bar{p} = \bar{\sigma}_y\left[\left(\frac{1+0.8748}{2}\right)0.3674 + \frac{0.0821 \times 574.0}{3 \times 4.08 \times 20.7 \times 0.8273}\right]$$

$$\bar{p}_m \equiv 0.3444\,\bar{\sigma}_y$$

for $m = 1$, with $\left(\frac{\bar{r}_1}{r_i}\right) = \left(\frac{27.88}{29.885}\right)^{.9950} = 0.9332$

Assuming that $\bar{\sigma}_{fy}$ can be assessed at a strain of $\simeq \frac{3}{4}(0.2451)$:

$$\bar{p} = 0.3444\,\bar{\sigma}_y + \left[5.894\,\frac{(1-.9332)}{.9950 \times 2}\right]\bar{\sigma}_{fy}$$

$$\therefore\ \bar{p}_{m=1} = 0.3444\,\bar{\sigma}_y + 0.1978\,\bar{\sigma}_{fy}$$

From Equation (5.1) and FIGURE 5.1.

$$\bar{\sigma}_y = 14.50 \text{ N mm}^{-2} \text{ and } \bar{\sigma}_{fy} = 17.30 \text{ N mm}^{-2}$$

$$\therefore \quad \bar{p} = 8.254 \text{ N/mm}^2 \text{ and } \bar{p}_{m=1} = 11.68 \text{ N/mm}^2$$

Complementary assessment of the mean R.S.F.:

From Equation (3.(ii).27) and $(\overline{R.S.F.}) = \bar{p}\ (S_{ps})$ then:

For m=0 : $\overline{R.S.F.} = 3.92$ kN and for m = 1: $\overline{R.S.F.} = 5.55$kN

H.1.2. Energy (tube no. 10) - 170 mm dia. Rolls

Noting that:

$\left(\frac{D}{t}\right)_o = 6.40$

$\theta_{c1} = 47.4^o$

$\phi_m = 13.64$

$J = 0.1573$

$A_o = 660.4 \text{ mm}^2$

$A_m \simeq 608.5 \text{ mm}^2$

$\delta = 6.51 \text{ mm}$

$r_g = 20.7 \text{ mm}$

and from previous work:

$\bar{\varepsilon}_h = 0.2380$

$\bar{\varepsilon}_r \simeq \frac{\sqrt{3}}{2}\left(\frac{6.44}{78.308}\right) = 0.0950$

i.e. $\bar{\varepsilon}_h + \bar{\varepsilon}_r = 0.3330$

& $\bar{\sigma}_y = 15.88 \text{N mm}^{-2}$

From Equation (3.(ii).29), adjusted to account for $\bar{\varepsilon}_r$:

$$\bar{p} = \frac{A_o \sigma_y}{3 r_g \theta_c \delta}(\bar{\varepsilon}_h + \bar{\varepsilon}_r) \quad \text{ignoring friction}$$

i.e. for m = 0, $\bar{p}_{(m=0)} = \frac{660.4 \times 15.88 (0.3330)}{3 \times 20.7 \times 6.51 \times 0.8290}$

$$\bar{p}_{(m=o)} = 10.42 \text{ N mm}^{-2}$$

and $$\bar{p} = \frac{A_o}{3 r_g \theta_c \delta}\left[\sigma_y (\bar{\varepsilon}_h + \bar{\varepsilon}_r) + \sigma_{fy} 2\bar{\varepsilon}_f\right]$$ taking friction into account

and from Equation 3.(ii).16), substituting, and with m= 1:

$$\bar{\varepsilon}_f = \frac{6}{\sqrt{3}} \times 1 \times (20.7)^2 \times \frac{.8290}{608.5} \times .2381 \left[.0496 + 2.9099 - .8894 - 1.9660 \right] = 0.0502$$

i.e. for m = 1, and assuming that σ_{fy} can be assessed at a strain of $\simeq \frac{3}{4}$ (0.3330) i.e. σ_{fy} = 19.21 N mm^{-2}, then:

$$\bar{p}_{(m=1)} = \frac{660.4 \left[15.88 (0.3330) + 19.21 (2 \times 0.0502) \right]}{3 \times 20.7 \times 6.51 \times 0.8290}$$

$$\therefore \quad \bar{p}_{(m=1)} = 14.22 \text{ N mm}^{-2}$$

Complementary assessment of the mean R.S.F.

From Equation 3.(ii).27 and $\overline{(R.S.F.)} = \bar{p} (S_{ps})$ then:

For m = o : $\overline{(R.S.F.)} = 5.88$ kN

& for m=1: $\overline{(R.S.F.)} = 8.02$kN

H.2. Theoretical Mandrel Rolling Pressure

H.2.1. Equilibrium (tube no. 133/1) - 255 mm dia. Rolls

Noting that:

$\left(\frac{D}{t}\right)_o = 10.57$

$t_o = 3.45$ mm

$t_s = 3.40$ mm

$t_r = 2.40$ mm

$\bar{\phi} = 3.79^o$

From former work (at roll groove root):

$\varepsilon_t = -0.3629$

$\varepsilon_{zs} = 0.1789$

$\varepsilon_\theta = 0.1840$

$\bar{\varepsilon}_h = 0.3629$

$\bar{\sigma}_y = 16.29$ N mm^{-2}

Refering to the mandrel-tube-roll interface deformation region and in particular the roll groove root (which experiences the greatest roll pressures) the tube wall thickness (t_n) at the neutral angle (ϕ_n) can be deduced as follows:

Equating Equations (3.(ii).23 and 3.(ii).24) and deducing that:

$$F = \frac{\sigma_y\,(m_r + m_b)}{\sqrt{3}\,\tan\bar{\phi}} = \frac{\bar{\sigma}_y(1 + 0.8)}{\sqrt{3} \times 0.06624} = 15.688\,\bar{\sigma}_y$$

and $$\frac{\frac{\sqrt{3}}{2}\,\sigma_y + F}{\frac{\sqrt{3}}{2}\,\bar{\sigma}_y - F} = -1.1589$$

then,

$$t_n = \left[\frac{to}{t_r} \right]^{-1.1589} \left(\frac{1}{1 + 1.1589} \right) = 2.84 \text{ mm}$$

hence:

$$p_{(o-n)} = \bar{\sigma}_y \left(\frac{\sqrt{3}}{2} - 14.5331 \ln \frac{t_n}{t_o} \right)$$

$$p_{(n-1)} = \bar{\sigma}_y \left(\frac{\sqrt{3}}{2} + 16.8425 \ln \frac{t_n}{t_r} \right)$$

giving:

$\bar{p} = 2.5703 \bar{\sigma}_y = 41.9 \text{ N mm}^{-2}$ assuming uniform circumferential pressure:

From Equation (3.(ii).28): $S_{pm} = 353 \text{ mm}^2$

& $\overline{(R.S.F.)} = 41.87 \times 353$

$\simeq 14.8 \text{ kN}$

H.2.2. Energy (tube no. 31) - 170 mm dia. Rolls

Combining Equations 3.(ii).25 and 3. (ii).26 and assuming $k \simeq 0.5$ i.e. the roll-tube surface deformation zone divided into equal areas (see sections 3.(ii).4.2 and 7.5.), then:

$$\bar{\varepsilon}_f = \bar{\varepsilon}_{fr} + \bar{\varepsilon}_{fb} = \frac{3 \; r_g \; \phi_m R J}{A_o} \left[\frac{m_r \; \theta_{cl}}{(1 - \frac{J^2}{4}} + \right.$$

$$\left. + \frac{r_b}{r_g} \; m_b \; \frac{\gamma_{cl}}{2} \right]$$

furthermore, from Equation (3.(ii).30.):

$$p_m = \frac{\bar{\sigma}_y (\bar{\varepsilon}_h + \bar{\varepsilon}_f) A_o}{3 \; r_g \; \theta_c \; \Delta t} \quad \text{and} \quad \bar{\varepsilon}_A = \bar{\varepsilon}_h + \bar{\varepsilon}_f$$

and noting that:

$(\frac{D}{t})_o$	=	20.3
θ_{cl}	=	41.0^o
ϕ_m	=	7.17^o
γ_{cl}	=	34.0^o
J	=	.1320
A_o	=	151.4 mm^2
r_o	=	20.70 mm
r_b	=	15.22 mm
R_r	=	78.31 mm
t_o	=	1.58 mm
t_1	=	1.33 mm

and from previous work:

$\bar{\varepsilon}_h$	=	.1820
$\bar{\varepsilon}_r$	$\simeq$	0 hence $\bar{\sigma}_y$ = 13.27 N mm^{-2}
m_b	=	0.6
m_r	=	1

Substituting gives:

$$\bar{\varepsilon}_f = \frac{3 \times 20.7 \times 0.1251 \times 78.31 \times 0.1320}{151.4} \left[\frac{1 \times 0.7156}{1-.0044} + \right.$$

$$\left. + \frac{15.22 \times 0.6 \times 0.5934}{20.70 \times 2} \right] = 0.2602$$

$$\therefore \bar{\varepsilon}_A = 0.1820 + 0.2602 = 0.4422$$

$$\therefore p_m = \frac{13.27 \times 0.4422 \times 151.4}{3 \times 20.7 \times 0.7156 \times 0.25} = 80.0 \text{ N mm}^{-2}$$

For small tube reductions, where $k \simeq 0.25$; it can be shown that the subsequent insertion of this ratio into the analysis reduces $\bar{\varepsilon}_f$ by only 3.5%. Furthermore, for the lubricated mandrel case ($m_b = 0.4$) a reduction of around 5% in the roll pressure can be readily computed.

TABLES H1 and H2 lists all the theoretical roll pressure and force results for the sinking and mandrel rolling processes.

TABLE H1

TUBE NO.	$(D/t)_o$	J	THEORETICAL ROLL PRESSURE ($N\ mm^{-2}$)			
			Energy		Equilibrium	
			m=1	(m=o)	m=1	(m=0)
1/1	8.51	.0463	11.0	(8.69)		
1/2	8.04	.0457				
3	6.31	.0831			7.05	(5.47)
6*	6.46	.1032			11.8	(10.2)
7/1*	6.57	.1366			11.1	(8.82)
10*	6.40	.1555			11.7	(8.25)
13/2	10.8	.0830	14.2	(10.4)		
14*	18.0	.0402			7.77	(4.19)
15	17.6	.0726	4.62	(2.11)	3.09	(1.96)
16	16.5	.1174			4.60	(2.06)
17*	10.5	.0562	5.79	(2.71)	5.92	(2.33)
18*	11.5	.1212	6.79	(4.63)	7.54	(4.00)
			7.59	(4.51)	8.52	(4.04)
20*	28.4	.1360	88.3			
21	27.3	.1090	82.0			
22	29.1	.0443	49.3			
23	18.2	.1890	89.0			
24	18.4	.1190	82.5			
25	18.9	.1100	89.9			
26*	10.5	.1680	69.8			
27	10.7	.2460	84.3			
28*	10.7	.3510	114.0			
30*	21.7	.0415	45.2			
31	20.3	.1320	80.0			
32	21.6	.1640	98.0			
33/1*	10.6	.0868	52.5			
33/2	10.5	.1220	64.1			
34*	10.5	.1850	76.9			
35*	10.1	.2880	98.0			
36	16.8	.1010	60.5			
37*	18.0	.1780	98.2			
38	18.6	.1440	74.5			
131	17.7	.0468			36.8	
133/1	10.6	.1647			41.9	
134	10.5	.1245			35.8	

TABLE H2

TUBE NO.	$(D/t)_o$	J	S (mm^2)	THEORETICAL R.S.F.(kN)			
				Energy		Equilibrium	
				m=1	(m=0)	m=1	(m=0)
1/1	8.51	.0463	310	3.40	(2.69)		
1/2	8.04	.0457	346			2.44	(1.89)
3	6.31	.0831	375			4.43	(3.84)
6*	6.46	.1032	413			4.58	(3.64)
7/1*	6.57	.1366	475			5.55	(3.92)
10*	6.40	.1555	564	8.02	(5.88)		
13/2	10.8	.0830	497			3.86	(2.08)
14*	18.0	.0402	361	1.67	(0.76)	1.11	(0.70)
15	17.6	.0726	455			2.81	(2.09)
16	16.5	.1174	528	3.06	(1.43)	3.12	(1.23)
17*	10.5	.0562	388	2.63	(1.79)	2.93	(1.56)
18*	11.5	.1212	553	4.20	(2.49)	4.70	(2.23)
131	17.7	.0468	167			6.14	
133/1	10.6	.1647	353			14.8	
134	10.5	.1245	298			10.7	

APPENDIX J

Plane Strain Compression of Thin Strip between Parallel Platens.

Accepting the sensitivity of the mandrel equilibrium analysis to the mean tube-roll contact angle at the groove root, a partial solution to this dilemma would be to consider an extreme workface condition. In other words, to assume near complete roll flattening at the roll groove root. Then, to assess the associated mean roll pressure by applying the well known relationship for plane strain compression of thin strip between parallel platens. This relationship takes the form:

$$\bar{p} = \frac{2}{\sqrt{3}} \sigma_y \left[1 + \frac{z}{4t} \right]$$

where, $\bar{p}$ is the mean roll pressure along the groove root,

z is the longitudinal length of tube between "platens" i.e. roll-mandrel,

t is the thickness of tube wall between the "platens".

The difficulty here of course, is the accurate assessment of the tube-roll arc contact length at the roll groove root i.e. z and the peripheral roll pressure variation. Again,

lack of pin loadcell results prevented this assessment, and noting the other impendiments to a solution it was concluded not to pursue this particular analysis.